Charles University

Faculty of Science

Study programme: Developmental and Cell Biology

Mgr. Romana Weissová

Multi-level regulation of microtubules in neurons by microtubule-associated proteins, phosphorylation, and conformational changes

Víceúrovňová regulace mikrotubulů v neuronech pomocí mikrotubuly-vázajících proteinů, fosforylace a konformačních změn

Doctoral thesis

Supervisor: Mgr. Martin Balaštík, Ph.D.

Prague, 2024

Declaration:

I declare that I have written the thesis independently and I have listed all the sources and literature used. Neither the thesis nor its significant part has been used to get another or the same academic degree.

Prohlášení:

Prohlašuji, že jsem práci zpracovala samostatně a uvedla jsem veškeré použité informační zdroje a literaturu. Práce ani její podstatná část nebyla předložena k získání jiného nebo stejného akademického titulu.

Romana Weissová

Prague, 2024

Acknowledgements

I would like to thank to my supervisor Martin Balaštík for teaching me many laboratory methods, for discussions, and for advice. I thank to all members of his laboratory for creating a pleasant, friendly and productive working environment. Especially, I thank Jakub Žiak for his help and support.

I also would like to mention the whole Institute of Physiology with many helpful people and to thank for providing the facilities. Great thanks to the members of the IPHYS Bioimaging facility.

I would like to thank all our collaborators, mainly all coauthors of the presented papers and manuscripts, with special thanks to Carsten Janke, Eran Perlson, Roy Maimon, Zdeněk Lánský, Marcus Braun, Ján Sabó, and Valerie Siahaan and to the Imaging Methods Core Facility and Biophysical Core Facility of the Centre of Molecular Structure at BIOCEV.

I would like to thank to Charles University Grant Agency for partial financial support of this work (GA UK no. 524218).

Last but not least, I would like to thank to my parents for their support and to my husband Jan Kudláček for endless discussions about my project and my studies.

I am grateful for having the opportunity to study the doctoral study programme, which gave me a lot of experience.

Abstract

Microtubules are crucial components of cytoskeleton in neurons, play important roles in neural development, and are indispensable for intracellular transport. The dysregulation of the microtubule dynamics is neurotoxic and can result in neurodegeneration or various neurodevelopmental disorders. Microtubule dynamics is regulated by several mechanisms, one of which are interactions with microtubule-associated proteins. The activity of microtubule-associated proteins is itself tightly controlled. Even though the dysregulation of many microtubule-associated proteins has been linked to human conditions, the precise regulation of their function is not completely understood. Microtubule-associated proteins CRMP2 and tau have been shown to control microtubule dynamics and stability and both have been associated with the pathogenesis of Alzheimer's disease.

Here we show that CRMP2 function is regulated on the level of isoforms proportion, Cdk5-mediated phosphorylation, and conformational changes catalyzed by prolyl isomerases PIN1 and FKBP12. All of these have a direct impact on microtubule dynamics. We also show that Cdk5-mediated phosphorylation has a negative impact on the formation and maintenance of tau envelopes - patches of cooperatively bound tau with microtubule-protecting function. Disruption of tau envelopes results in microtubule destabilization in cells. Together, we demonstrate that microtubule dynamics and stability, essential for neural development and defective in neurodevelopmental or neurodegenerative disorders, is tightly controlled by tau and CRMP2A and their multi-level regulation.

Keywords: Microtubule-associated proteins, Collapsin Response Mediator Protein 2 (CRMP2), tau, phosphorylation, Cdk5, prolyl isomerases, FKBP12, PIN1

Abstrakt

Mikrotubuly jsou významnou složkou cytoskeletu neuronů, hrají důležité role ve vývoji nervové soustavy a jsou také nepostradatelné pro buněčný transport. Poruchy regulace mikrotubulů jsou pro neurony toxické a mohou vyústit v degeneraci neuronů nebo v některé neurovývojové poruchy. Dynamika mikrotubulů je regulována několika způsoby, mezi které patří interakce s proteiny vážícími mikrotubuly. Aktivita těchto regulačních proteinů je rovněž přísně kontrolována. Přestože byla popsána souvislost mezi narušenou regulací funkce některých mikrotubuly-vazebných proteinů a neurodegenerací, přesná regulace fungování těchto proteinů není zcela objasněna. Mezi proteiny vážící mikrotubuly patří CRMP2 a tau, které upravují dynamiku a stabilitu mikrotubulů a byly oba spojeny s patogenezí Alzheimerovy choroby.

V této práci je popsána regulace funkce proteinu CRMP2 nastavením hladin CRMP2 isoforem, fosforylací zprostředkovanou kinázou Cdk5 a konformačními změnami katalyzovanými prolyl isomerázami PIN1 a FKBP12. Tyto regulační mechanismy mají přímý vliv na dynamiku mikrotubulů. Dále ukazujeme, že fosforylace kinázou Cdk5 má negativní dopad na utváření a stabilitu tau obálek (shluků tau proteinu spojených kooperativní vazbou a obalujících mikrotubuly), což vede ke snížení stability mikrotubulů v buňce. Naše výsledky ukazují, že dynamika a stabilita mikrotubulů, děje nezbytné při vývoji nervové soustavy a narušené při neurovývojových či neurodegenerativních procesech, jsou kontrolovány pomocí proteinů tau a CRMP2 a jejich víceúrovňové regulace.

Klíčová slova: Proteiny vážící mikrotubuly, CRMP2, tau, fosforylace, Cdk5, prolyl isomerázy, FKBP12, PIN1

Abbreviations

AD	Alzheimer's disease
Ala	Alanine
ALS	Amyotrophic Lateral Sclerosis
AMV RT	Avian Myeloblastosis Virus Reverse Transcriptase
APP	Amyloid Precursor Protein
ASD	Autism spectrum disorder
Asp	Aspartic acid
ATP	Adenosine triphosphate
Cdk5	Cyclin-dependent kinase 5
cDNA	Complementary DNA
CIP	Calf intestinal alkaline phosphatase
coIP	Coimmunoprecipitation
CoV	Coefficient of variation
CRMP	Collapsin Response Mediator Protein
CRMP2 KO	Collapsin Response Mediator Protein2 knockout
CRMP2A KO	Collapsin Response Mediator Protein2A knockout
DAB	3,3′-Diaminobenzidine
DEPC	Diethyl pyrocarbonate
DIC	Dynein intermediate chain
DIV	Days *in vitro*
DMSO	Dimethyl sulfoxide
dNTPs	Deoxynucleotide triphosphates
DRG	Dorsal root ganglia
DTT	Dithiothreitol
EB1	End-binding protein 1

EB3	End-binding protein 3
ECL	Enhanced chemiluminescence
EDTA	Ethylenediaminetetraacetic Acid
EGF	Epidermal growth factor
EGTA	Ethylene glycol tetraacetic acid
ER	Endoplasmic reticulum
FBS	Fetal bovine serum
FKBP	FK506-Binding Protein
FKBP12	FK506-Binding Protein 12
FRAP	Fluorescence Recovery After Photobleaching
GAPDH	Glyceraldehyde 3-phosphate dehydrogenase
GDP	Guanosine diphosphate
GFP	green fluorescent protein
Glu	Glutamic acid
GMPCPP	Guanosine-5'-[(α,β)-methyleno]triphosphate
GSK3beta	Glycogen synthase kinase-3 beta
GST	Glutathione S-transferase
GTP	Guanosine triphosphate
HEK293T	Human embryonic kidney 293T cells
HEPES	4-(2-hydroxyethyl)-1-piperazineethanesulfonic acid
HRP	Horseradish Peroxidase
IMCD3	Mouse Inner Medullary Collecting Duct-3 cells
IP3R	Inositol 1,4,5-triphosphate receptor
LB	Luria-Bertani broth
Leu	Leucine
LTP	Long-term potentiation

MAPs	Microtubule-associated proteins
mTOR	Mammalian target of rapamycin
NFT	Neurofibrillary tangles
NGF	Nerve growth factor
NMDA	N-methyl-D-aspartate
NSC	Non-silencing control
OCD	Obsessive-compulsive disorder
ON	Overnight
PAGE	Polyacrylamide gel electrophoresis
PBS	Phosphate buffered saline
PCR	Polymerase Chain Reaction
PD	Parkinson's disease
PEI	Polyethyleneimine
PFA	Paraformaldehyde
PIN1	Peptidylprolyl *cis*/*trans* isomerase, NIMA-interacting 1
PIN1 KO	PIN1 knockout
PIPES	Piperazine-N,N′-bis(2-ethanesulfonic acid)
PKA	Protein kinase A
PKC	Protein kinase C
PP1	Protein phosphatase 1
PP2A	Protein phosphatase 2A
PPIs	Prolyl isomerases
Pro	Proline
PTMs	Post-translational modifications
PVDF	Polyvinylidene Fluoride
ROI	Region of interest

RT	Room temperature
RyR	Ryanodine receptor
SD	Standard deviation
SDS	Sodium dodecyl sulfate
SEM	Standard error of the mean
Sema3A	Semaphorin 3A
Ser	Serine
shRNA	Short hairpin RNA
SLIC	Sequence- and ligation-independent cloning
SOD1	Superoxide dismutase type 1
Suc-AAPF-pNA	Succinyl-Ala-Ala-Pro-Phe-p-nitroanilide
tau-ΔN	Tau with deleted N-terminus
TB	Terrific Broth
TBE	Ttris-borate-EDTA
TBS	Tris-buffered saline
TG	Thyroglobulin
TGFbeta	Transforming growth factor-β
Thr	Threonine
TIRF	Total internal reflection fluorescence
Trp (W)	Tryptophan
Tyr	Tyrosine
WT	Wild type
Xaa	Any amino acid

1. Table of Contents

1 Introduction

The cytoskeleton is a crucial structural and functional component of every cell. It is responsible for forming and maintaining the cell shape and for connecting the distant parts of the cell to the cell body. This is mainly important in neurons, cells with a specific shape involving long projections (neurites). Microtubules, polymers composed of tubulin dimers and the largest type of cytoskeletal fibers, play a significant role in reinforcing the neurites as well as enabling cellular transport through them and keeping the communication between the cell compartments. The importance of microtubules in neurons is supported by the observation that their deregulation is tightly connected to neurodegeneration (Sferra et al., 2020). Various microtubule-associated proteins regulate function of microtubules, their polymerization, stability, or microtubule-based transport. As regulators of microtubule dynamics, the microtubule-associated proteins and their activity must be also tightly controlled. One of the critical means to quickly and efficiently regulate the activity of proteins is through posttranslational modifications. Among the posttranslational modifications, phosphorylation seems to be one of the most important and widespread - regulating virtually all cellular processes. Recently, conformational regulation by prolyl isomerases was identified as another important regulator of protein activity, stability, and cell signaling.

Even though the function of microtubule-associated proteins has been extensively studied in neurons, their precise regulations and their role in neural development and neurodegeneration are not well understood.

This work aims to characterize the function of some microtubule-associated proteins important in neurons, to reveal their regulation and its involvement in neural development and in neurodegenerative diseases. The thesis focuses on how microtubule-associated proteins are regulated by phosphorylation mainly by Cdk5 kinase and how this regulation affects their accessibility for another regulatory mechanism – conformational changes catalyzed by prolyl-isomerases. I have focused on two families of microtubule-associated proteins important in neuron growth and neural development – Collapsin response mediator proteins (CRMPs) and tau.

1.1 Cytoskeleton

Cytoskeleton represents all prokaryotic and eukaryotic cells' leading structural and organizational network consisting of filamentous structures that support the cell's mechanical resistance, help maintain internal organization, and are crucial for cellular division and movement. Cytoskeletal fibers are long polymers composed of protein subunits whose assembly and disassembly provide dynamic properties which are necessary for the cytoskeletal functions. In eukaryotic cells, three types of cytoskeletal fibers exist – microfilaments, intermediate filaments, and microtubules (reviewed in Fletcher and Mullins, 2010; Hohmann and Dehghani, 2019).

Microfilaments (also called actin filaments) are thin filamentous structures (7 nm in diameter) composed of globular protein units of actin. Generally, actin fibers can be found on the cytoplasmic side of the plasma membrane creating a mesh-like network providing mechanical support and allowing movement of the cell surface (reviewed in Fletcher and Mullins, 2010; Hohmann and Dehghani, 2019).

Intermediate filaments are composed of a variety of related proteins sharing one structure – coiled-coil structure – a pair of two intertwined proteins bound by hydrophobic interactions. Intermediate filaments are less dynamic than microfilaments or microtubules and due to their high stability provide mechanical support to cells (reviewed in Fletcher and Mullins, 2010; Hohmann and Dehghani, 2019).

1.1.1 Microtubules

Microtubules are the thickest type of cytoskeletal fibers with a diameter of approx. 25 nm. The building blocks – heterodimers of alpha- and beta-tubulin bind together in a head-to-tail fashion resulting in structurally polarized linear protofilaments, which then associate laterally to form a hollow tube. Microtubules are not just rigid skeleton of the cell, they switch between the phases of growth and disassembly in a process called dynamic instability. The instability of microtubules is intrinsic given by the GTP/GDP state of tubulin dimers - free tubulin binds GTP which is in beta-tubulin hydrolyzed after the incorporation into microtubule to GDP, which then tends to destabilize the microtubule lattice. A cap of GTP tubulin is therefore important for stable growth. As microtubules are polarized, the two microtubule ends have different properties - the plus end (terminated by beta-tubulin) is usually more dynamic – it grows faster and undergoes more depolymerization events (catastrophes), which can be

replaced by the polymerization phase again (rescue; Figure 1; reviewed in Fletcher and Mullins, 2010; Hohmann and Dehghani, 2019).

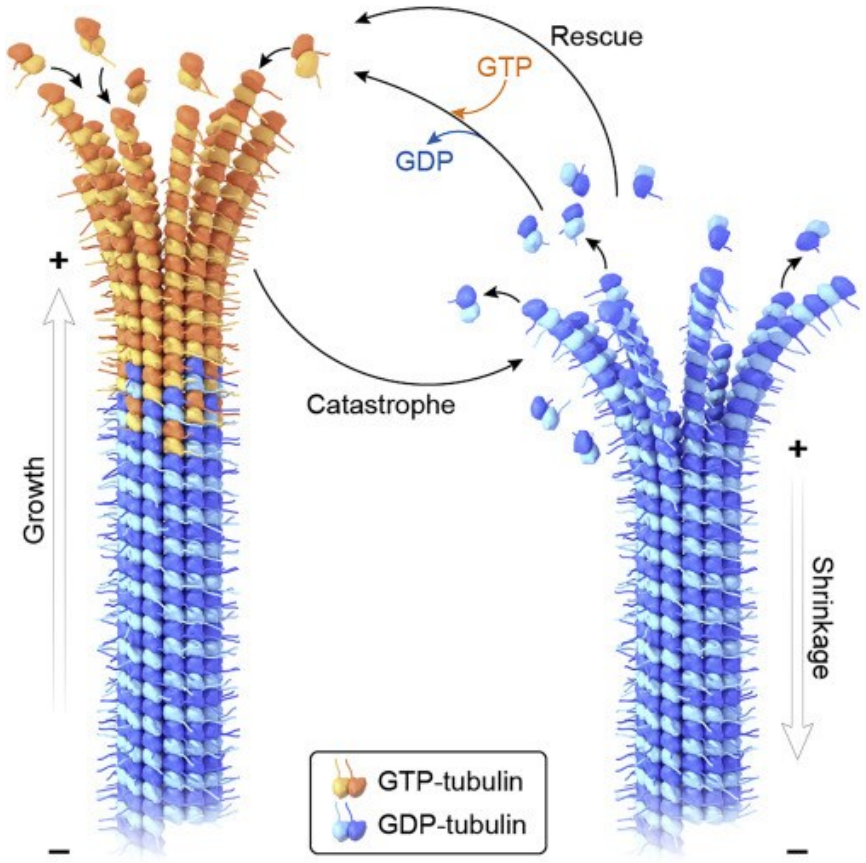

Figure 1:Microtubules and their dynamic instability.

Microtubules are polymers of alpha- and beta-tubulin dimers. They grow by the addition of GTP-tubulin dimers at the growing (termed +) end. After the dimer incorporation, GTP is hydrolyzed to GDP which could destabilize the growing end. The switch from polymerization to depolymerization is called catastrophe while the switch from depolymerization to polymerization phase is called rescue. C-terminal tails of tubulin proteins rise from the surface of the microtubule and are the main place for posttranslational modifications and interactions with microtubule-associated proteins (adapted from Roll-Mecak, 2020).

The regulation of microtubules and their dynamics happens on many levels. There are specific tubulin isotypes – in most eukaryotes both alpha- and beta-tubulin subunits are encoded by multiple genes giving rise to different tubulin isotypes exhibiting different characteristics and different cellular and tissue distributions (reviewed in Gasic, 2022; Janke and Magiera, 2020). Alpha- or beta-tubulin subunits can be also subjected to a broad range of posttranslational modifications (covalent biochemical modification of one or more amino acids following the protein biosynthesis) placed mainly in the C-terminal tails of tubulins which are

exposed on the surface of the microtubule (Figure 1; reviewed in Janke and Magiera, 2020). Yet another way of affecting microtubules and their dynamics are various microtubule-associated proteins (MAPs), which can bind to microtubules and regulate their dynamics as well as other features (reviewed in Bodakuntla et al., 2019). All these mechanisms must work together to maintain microtubule dynamics, which is crucial for cells and whose disruption can lead to the cell death (reviewed in Fanale et al., 2015).

1.1.2 Microtubule-associated proteins (MAPs)

MAPs are proteins that bind to microtubules and affect the microtubule cytoskeleton. According to their function, MAPs can be divided into several groups – structural MAPs (promoting polymerization, stabilizing, bundling), nucleators, destabilizers and severing proteins (e.g. katanin or spastin), capping proteins (or end-binding proteins e.g. EB1 or EB3), motile MAPs (motor proteins e.g. kinesines and dynein), and crosslinkers (connecting different components of the cytoskeleton; reviewed in Bodakuntla et al., 2019). Many other proteins can occasionally bind to microtubules - proteins involved in signal transduction, translation, and metabolism. MAPs themselves also interact with a plethora of proteins and thus might link the microtubule cytoskeleton to many other cellular functions, such as signal transduction pathways and synaptic function (reviewed in Goodson and Jonasson, 2018). Even though they are usually connected with specific functions, one microtubule-binding protein can have different effects on microtubules (for example stabilizers can also affect cellular transport along the microtubules) and the effects of MAPs on microtubules can also depend on the conditions (reviewed in Goodson and Jonasson, 2018). A large number of MAPs can potentially coexist on a microtubule because several different MAP binding sites are present on the microtubule surface but at the same time, some MAPs can compete for similar sites on the microtubule or effectively regulate the access of other MAPs (reviewed in Bodakuntla et al., 2019).

Generally, it is considered that MAPs are highly (but not exclusively) interacting with acidic C-terminals of tubulin molecules which are decorating the surface of microtubules. C-termini are also the main place for posttranslational modifications so it is not surprising that posttranslational modifications of tubulin can regulate the selectivity of the microtubule for special MAPs (reviewed in Janke and Magiera, 2020). MAPs are important regulators of microtubule dynamics and function therefore their deregulation is involved in various pathological conditions (reviewed in Bodakuntla et al., 2019).

1.2 Cytoskeleton in neurons

Neurons are cell type displaying an extremely polarized morphology with structurally and functionally distinct compartments – usually a long axonal process responsible for transmitting electrical signals to efferent neurons and several branched dendrites receiving afferent information. The neuronal cytoskeleton provides not only a mechanical support important for neural development (migration, extensions of neurites, guidance of the neurites, and formation of functional synapses) and maintenance of the special neuronal structures, but is also critical for long-distance transport, which is essential for neuronal function. The neuronal cytoskeleton has to be flexible and dynamic to maintain the functioning throughout the life of an organism (reviewed in Muñoz-Lasso et al., 2020).

Microfilaments in neurons are enriched in the regions near the plasmatic membrane and are particularly concentrated in presynaptic terminals, dendritic spines, and growth cones (the structure at the end of the developing or regenerating axon) where they create membrane protrusions called lamellipodia or filopodia. Neuronal intermediate filaments, collectively referred to as neurofilaments, provide mechanical strength and stabilize the cytoskeletal network. Intermediate filaments are mostly abundant in the axons of neurons where they can modulate the axonal diameter. Neuronal microtubules are present throughout the neurons, are important for protrusion growth and guidance, and possess a special function in providing continuous transport tracks for the active transport of mitochondria, vesicles, and mRNA throughout the compartments (Figure 2; reviewed in Muñoz-Lasso et al., 2020).

These three groups of cytoskeletal fibers are highly connected and work together to achieve the development as well as maintenance of neurons. For example, in the central core of the growth cone, the microfilaments interact with axonal microtubules. In long motor axons, intermediate filaments are anchored to actin filaments and microtubules (Figure 2reviewed in Muñoz-Lasso et al., 2020).

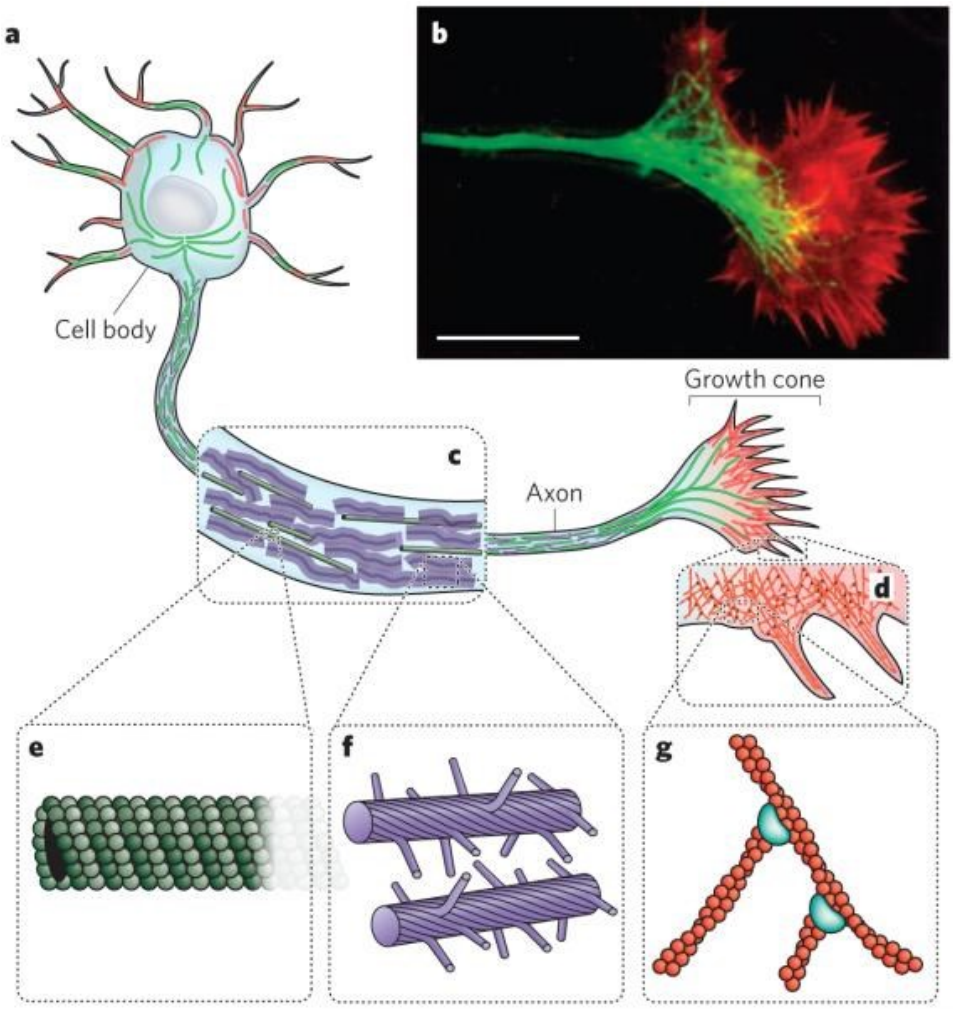

Figure 2: Neuronal cytoskeleton.

Cytoskeleton in neurons (a) is composed of microfilaments, microtubules and intermediate filaments (neurofilaments). Microfilaments (in red; g) are enriched in the regions near the plasmatic membrane and particularly in the growth cones where they create mesh-like structure (b, d). Neurofilaments (in purple; f) stabilize the cytoskeletal network and are mostly abundant in the axons of neurons (c). Neuronal microtubules (in green; e) are present in the cell body, dendrites and axons, they regulate neurite outgrowth and provide tracks for the active transport throughout the neuron. b) Fluorescence staining of the neuronal growth cone with microtubules in green and microfilaments in red. Scale bar 20µm (adapted from Fletcher and Mullins, 2010).

1.2.1 Microtubules in neurons

Microtubules are an essential component of the neuronal cytoskeleton. The organization of microtubules in neurons is different in several aspects from that in non-neuronal cells. Microtubules in axons and dendrites are usually arranged in bundles and are not continuous to the cell body to be associated with the microtubule-organizing center (centrosome) as in other cell types (reviewed in Muñoz-Lasso et al., 2020). As mentioned above, microtubules have intrinsic polarity and in neurons, they are tightly organized. In mammalian neurons, axonal

microtubuless are all of the same orientation facing all minus ends to the cell body (parallel plus-end out orientation) while dendritic microtubules are usually shorter with mixed polarity. The orientation of microtubules is relevant for the function of neurites as well as for the transport properties as the molecular motors displays a specificity in the terms of directions (reviewed in Muñoz-Lasso et al., 2020).

Neuronal microtubules are heterogeneous not only in regards to their orientation, there is also a mixture of multiple tubulin isotypes (mainly βII and βIII, with the latter being almost exclusively neuronal), microtubules in different parts of the cell can differ in posttranslational modifications as well as in MAPs bound. For example, axonal microtubules are usually acetylated and detyrosinated while more dynamic microtubules in the growth cone contain mainly tyrosinated tubulin. Given this heterogeneity, microtubules in different parts of the neurons possess different features which are important for special functions of neuronal compartments (reviewed in Janke and Magiera, 2020).

Microtubules play important roles in neurite formation, polarization, migration, or axon guidance during neuronal development. In adult neurons, microtubules are important for cellular maintenance, synaptic plasticity, localized cell signaling, and cellular transport. The special function of microtubules is providing not only structural support, but also main long-distance tracks for cellular transport, which is especially important in neurites because of the long distances that different cellular components have to travel. So-called molecular motors connected to microtubules transport for example organelles, vesicles, cell signaling molecules, and RNAs throughout the neuronal processes (reviewed in Muñoz-Lasso et al., 2020).

The importance of microtubules for neuron function is supported by the fact that deregulation of microtubule dynamics or transport given by mutations of tubulin proteins, disrupted posttranslational modifications, or deregulated MAPs is linked to many neurodevelopmental and neurodegenerative disorders (reviewed in Muñoz-Lasso et al., 2020).

1.2.2 MAPs in neurons

Besides the ubiquitously expressed MAPs, several structural MAPs are expressed mainly in neurons. Typical neuronal MAPs are tau (mainly in axons) and MAP2 (mainly in dendrites). Other important neuronal MAPs are the family of CRMP proteins which are expressed mainly during neuronal development.

Even though the deregulation of neuronal MAPs is connected to neurodevelopmental and neurodegenerative disorders, the mechanism by which these structural MAPs are regulated is not fully understood.

1.2.2.1 Tau

Tau protein (τ, tubulin-associated unit) was first described in 1975 as a heat-stable protein essential for microtubule assembly (Weingarten et al., 1975). Tau is able to promote microtubule growth, to stabilize microtubules against depolymerization or bundle microtubules (Drubin and Kirschner, 1986; Kanai et al., 1989). Those effects of tau are the question of concentration and other conditions, and nowadays, tau is not considered a simple stabilizer but a microtubule-associated protein whose main function is to modulate the stability and growth of microtubules (Qiang et al., 2018).

Tau protein is widely expressed with the highest expression in the brain where it constitutes over 80% of neuronal MAPs and is localized mainly in axons (Dugger et al., 2016; Gu et al., 1996). Through its interaction with microtubules, tau supports axonal differentiation, morphogenesis, outgrowth, and maintenance (Dawson et al., 2001; Esmaeliazad et al., 1994; Kempf et al., 1996). Tau also has other, not so well-known roles, e.g. regulation of microtubule spacing (Frappier et al., 1994; Chen et al., 1992), involvement in signaling pathways (reviewed in Mueller et al., 2021), or regulation of intracellular transport (Vershinin et al., 2007).

Full-length adult tau is an intrinsically disordered protein consisting of a projection domain that includes two N-terminal inserts, proline-rich domains, four imperfect repeats of the microtubule-binding domain, and a C-terminal flanking region (Figure 3; Mandelkow et al., 1995). In humans, tau exists in six protein isoforms created from one gene (*MAPT*, microtubule-associated protein tau) by alternative splicing. These isoforms have different numbers of N-terminal inserts (0N, 1N, 2N) and repeat domains (3R or 4R). The expression of different isoforms is cell-type- as well as developmental stage-dependent and it was shown that imbalances in their ratios may lead to pathological conditions (Hutton et al., 1998; Spillantini et al., 1998). *In vitro* studies described a reduced microtubule-binding affinity and assembly for 3R-tau isoforms (Goedert and Jakes, 1990; Goode et al., 2000; Panda et al., 2003).

Structurally, tau protein is considered an intrinsically disordered, flexible, and elastic protein with dynamic local secondary structure elements and intra-molecular interactions (Mukrasch et al., 2009; Schweers et al., 1994) and it was suggested that phosphorylation makes tau stiffer and extended (Hagestedt et al., 1989).

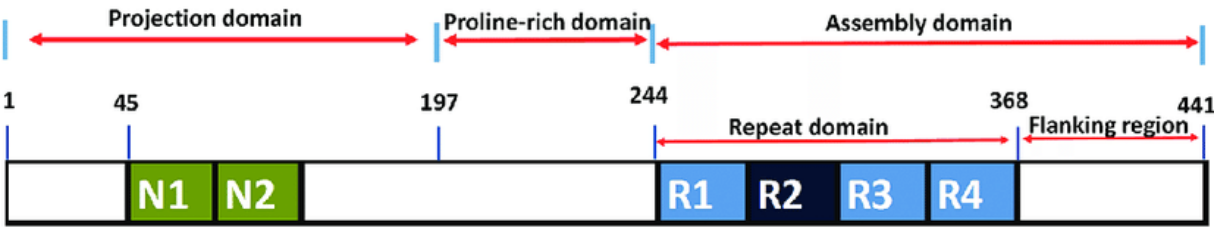

Figure 3: Microtubule-associated protein tau.

Tau consists of several structural and functional domains. The full-length isoform consists of projection domain containing two N-terminal inserts (N1-N2; green), proline-rich domain, and assembly domain including four imperfect repeats of the microtubule-binding regions (R1-R4; blue) and a C-terminal flanking region. The repeat 2 (R2; dark blue) in the repeat microtubule binding domain is the subject of alternative splicing and is missing in 3R-tau isoforms (adapted from Wu et al., 2017).

Tau protein is connected to several neurodegenerative diseases collectively termed tauopathies. Tauopathies are characterized by the inhibition of tau binding to microtubules, inhibiting the stabilizing or polymerization-promoting function, or by the presence of pathological fibrillar tau aggregates. Many tau mutations are connected to frontotemporal dementia and parkinsonism linked to chromosome 17 (FTDP-17). Interestingly, the pathological mutations include also those affecting splicing and thus changing the ratio between tau isoforms (Goedert, 2005). Eventhough the tau aggregation is connected mainly to pathological conditions of neurodegeneration, non-toxic aggregation of tau was described during neural development (Hefti et al., 2019). Moreover, it was shown that tau can form droplet-like assemblies under physiological conditions *in vitro* or in cells by the process of liquid-liquid phase separation which could happen regardless of the phosphorylation of tau molecules (Boyko et al., 2019; Wegmann et al., 2018). The role of the droplets is not fully understood as it was suggested that it has a physiological role in bundling microtubules but it can also evolve into pathologic tau aggregates (Hernández-Vega et al., 2017; Wegmann et al., 2018). Tau is a subject of many posttranslational modifications, among them phosphorylation is one of the most analyzed. As aggregated tau is often hyperphosphorylated, and some phosphorylations decrease the binding of tau to microtubules, it was suggested that tau

unbinding and the higher concentration of unbound tau in the cytoplasm can be the prerequisite for aggregates formation. However, it was shown *in vitro* that some specific phosphorylation sites promote tau aggregation (Despres et al., 2017). Thus, the relationship between phosphorylation, physiological tau droplets, and pathological tau aggregates has not been well understood so far.

1.2.2.1.1 Tau binding to microtubules and tau envelopes

The binding of tau to microtubules is provided by the microtubule-binding domain consisting of the repeat domains and the flanking regions (Figure 3; Mandelkow et al., 1995). In *in vitro* experiments, bound tau adopts an extended conformation along the crest of the protofilament tethering tubulin dimers together (Al-Bassam et al., 2002; Kellogg et al., 2018). On the other hand, in cells, the model of microtubule-induced folding of tau leading to the convergence of N- and C-terminus was proposed (Di Primio et al., 2017). It was suggested that at very high concentrations, tau molecules can even aggregate on top of each other on the microtubule surface (Ackmann et al., 2000). Other authors are suggesting two different modes of tau binding. The one described above occurs when a microtubule has already been assembled and stabilized either by taxol (in the experimental conditions), or by a sufficient number of other MAP molecules, as may occur *in vivo*, and the second one occurs if tau is present during microtubule polymerization. In the case of co-polymerization, tau was bound also to the inner surface of the microtubules (Kar et al., 2003). Tau binds differently to different tubulin isoforms (Bhandare et al., 2019), and the binding of tau to microtubule is affected also by posttranslational modifications such as phosphorylation or acetylation (reviewed in Alquezar et al., 2020).

Even though tau has been extensively studied for decades, there are still many questions regarding its binding to microtubules including the kinetics. Tau was first discovered in 1975 as a factor binding to tubulin tightly and almost irreversibly (Weingarten et al., 1975). Later, the affinity of tau to microtubules was described as moderate consisting of several weak interaction sites allowing a flexible and regulated binding (Butner and Kirschner, 1991). Another study showed that tau binding can be either reversible (when it is bound to preassembled microtubules) or partially irreversible if incorporated into microtubules during polymerization (Makrides et al., 2004).

It was shown several times independently that there is more than one way, tau can bind to microtubules. In 2012, it was shown that approximately half of the tau bound on microtubules is stationary while the second half of the tau molecules are moving bidirectionally along microtubules and the diffusing population is sensitive to pH (Hinrichs et al., 2012). The observed diffusion is independent of tau concentration but dependent on the presence of C-termini of tubulin (Hinrichs et al., 2012). It was shown that 4R tau isoform is on microtubule equally distributed between the static and diffusing populations while on GMPCPP-stabilized microtubules (non-hydrolyzable analog of GTP) diffusing conformation is preferred (McVicker et al., 2014).

Other authors suggested two-phase binding of tau depending on tau concentration showing that tau binds first as individual molecules which is followed by accumulation of tau on microtubules creating tau aggregates (Ackmann et al., 2000). It was shown that tau can create oligomers after binding to microtubules even in a low tau-to-tubulin molar ratio. Those oligomers encircled microtubules in ring-like structures possibly strengthen lateral interactions. Interestingly in saturating tau to tubulin ratios, tau covered the microtubules fully in a regular structural pattern (Makrides et al., 2003). Another study shows that tau can form patches consisting of multiple tau molecules on taxol-stabilized microtubules and that it affects molecular transport (Dixit et al., 2008). Similar results were obtained using *in vitro* reconstitution and single-molecule imaging, showing tau self-association on the microtubule surface resulting in localized and reversible condensation of tau molecules creating cohesive tau envelopes (Figure 4; Siahaan et al., 2019; Tan et al., 2019). These envelopes differ in binding kinetics and regulate the accessibility and thus activity of microtubule severing enzymes as well as the movement of molecular motors, which could be an important mechanism regulating microtubule dynamics and neuronal function (Siahaan et al., 2019; Tan et al., 2019). The tau molecules in the condensates are bound cooperatively locally altering the spacing of tubulin dimers within the microtubule lattice and the formation of the envelopes is dependent on the termini of tubulin (Siahaan et al., 2022). Even though it was suggested that the patches are visible in neurons at least in some developmental stages (Tan et al., 2019), it is expected that in cells where the majority of microtubules consist of GDP-tubulin, to which tau has higher affinity (Castle et al., 2020), tau covers the whole microtubules and visualization of the envelopes in cells needs the destabilization of tau binding - e.g. using taxol (Siahaan et al., 2022).

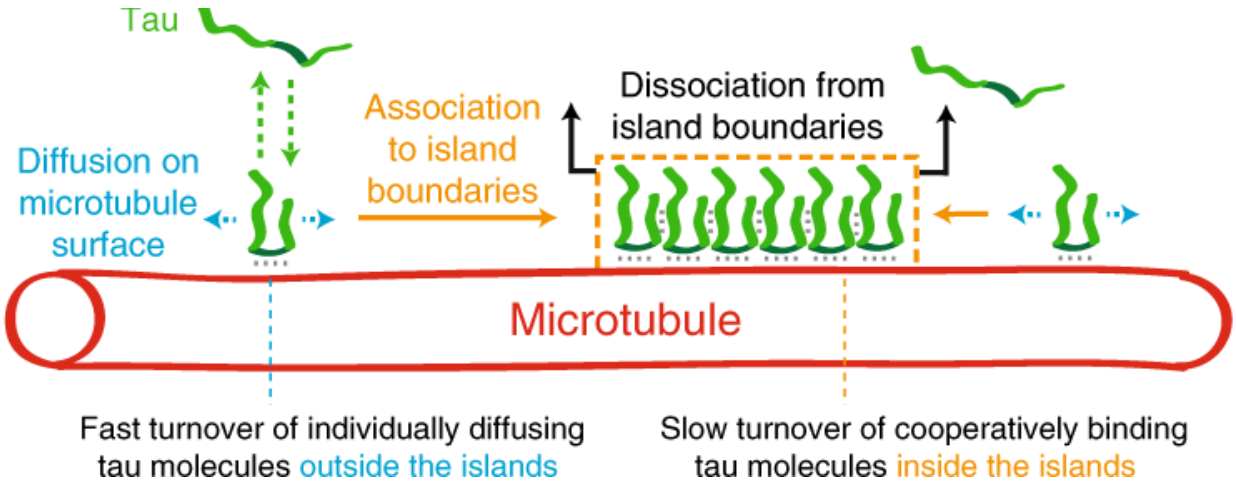

Figure 4: Tau envelopes.

Tau (green) can be bound to microtubules (red) either as individual diffusing molecules or as cooperatively bound tau making envelopes (also named islands). Cooperatively bound tau has slower turnover and dissociates usually only from envelope (island) boundaries (adapted from Siahaan et al., 2019).

1.2.2.1.2 Tau phosphorylation

Tau undergoes a variety of posttranslational modifications e.g. phosphorylation, acetylation, ubiquitination, methylation, or oxidation. These modifications can regulate tau-microtubule interaction, localization of tau, degradation, or aggregation (reviewed in Alquezar et al., 2020; Ye et al., 2022). The modifications may be influenced by each other and the pattern of posttranslational modifications may represent the functional state of tau (reviewed in Ye et al., 2022).

The most studied posttranslational modification of tau is phosphorylation. Human full-length tau contains more than 80 potential phosphorylation sites with the majority of them located in the proline-rich domain (Kimura et al., 2018). Phosphorylation affects the physiological functions of tau, but is also highly connected to tau pathologies. The main studied effect of phosphorylation is the regulation of tau binding to microtubules and tau aggregation.

The most notable phosphorylation site examined for its ability to abolish tau-microtubules binding is Ser262 which is located within the microtubule-binding repeats and in a non-phosphorylated state forms a hydrogen bond with alpha-tubulin (Biernat et al., 1993; Kellogg et al., 2018). Another phosphorylation decreasing microtubule binding is Thr231 in the proline-rich domain (Cho and Johnson, 2004). On the other hand, some phosphorylation, mainly on

the C-terminus, promotes tau binding to microtubules as well as its assembly-promoting function (Deancos et al., 1993; Cho and Johnson, 2003; Liu et al., 2007). Physiological increase in phosphorylation was observed during human neural development where it plays an important role in axonogenesis and interestingly, some phosphorylated sites overlap with phosphorylation observed in neurodegenerative diseases (Biernat and Mandelkow, 1999; Brion et al., 1993; Goedert et al., 1993; Hefti et al., 2019; Kenessey and Yen, 1993). It was also suggested that hyperphosphorylation predisposes tau to liquid-liquid phase separation and aggregation (Ambadipudi et al., 2017; Despres et al., 2017). Indeed, tau aggregates were described even in the fetal brain, where higher phosphorylation was also described (Hefti et al., 2019).

Several kinases can phosphorylate tau, but the two main studied are Glycogen synthase kinase-3 beta (GSK3beta) and cyclin-dependent kinase 5 (Cdk5), which provide both physiological phosphorylations as well as the abnormal hyperphosphorylation of tau in Alzheimer's disease (AD; reviewed in Hanger and Noble, 2011; Kimura et al., 2014). The phosphorylation status of tau is the result of the balance between kinases and phosphatases activity, with the main phosphatase for tau in the human brain being protein phosphatase 2A (PP2A; Liu et al., 2005). Yet another mechanism regulating the phosphorylation status of tau is isomerization provided by prolyl isomerase PIN1. PIN1 binds to all main Cdk5-phosphorylated sites on tau and allows its dephosphorylation (Kimura et al., 2013).

Although aggregates of hyperphosphorylated tau in AD brains were observed decades ago, the relationship between phosphorylation and aggregation is still elusive (reviewed in Wegmann et al., 2021).

1.2.2.1.2.1 Phosphorylation of tau by Cdk5

Cdk5 is a proline-directed Ser/Thr kinase, which means that it phosphorylates specifically Ser/Thr-Pro motifs. Although Cdk5 is a member of the cyclin-dependent kinase family, members of which are important regulators of the cell cycle, Cdk5 is not involved in cell cycle regulation and it is active particularly in post-mitotic neurons. Although Cdk5 is expressed in many cell types, the activity of this kinase is determined by the availability of its regulatory subunits which are present mainly in neurons. Cdk5 is active especially in axon shafts and growth cones where it is involved in the regulation of cytoskeleton dynamics. Cdk5 is essential

for neural development, it is involved in processes of axon growth and guidance, neuronal migration, vesicular transport, and synaptic function (reviewed in Pao and Tsai, 2021).

Cdk5 was purified from brain microtubule fraction as one of two first-discovered tau protein kinases together with GSK3beta (Ishiguro et al., 1992). Cdk5 is able to phosphorylate tau at several sites *in vitro*, but four main Cdk5-dependent phosphorylation sites were described after *in vitro* phosphorylation as well as in cells. Those sites are Ser202, Thr205, Ser235, and Ser404 (Figure 5; reviewed in Kimura et al., 2014).

Some Cdk5 phosphorylation sites serve as priming for following phosphorylation by kinase GSK3beta, for example, Thr231 and Ser396 are primed by phosphorylation at Ser235 and Ser404 by Cdk5, respectively (Figure 5; Li et al., 2006). Thus, increased phosphorylation of tau by Cdk5 could potentiate subsequent phosphorylation by GSK3beta but at the same time, high Cdk5 activity inhibits the activity of GSK3beta (Plattner et al., 2006; Wen et al., 2008).

Cdk5 needs to be activated by its activator (p35 or p39 which have different spatial and temporal expression; Zheng et al., 1998). Cdk5's activator p35 can be cleaved by calpains (Ca^{2+}-dependent proteases) giving rise to shorter version of p35 named p25. This N-terminally truncated protein has longer turnover and lacks the myristoylation site changing the localization of active Cdk5 within the cell. Cdk5 activated by p25 could localize for example to the nucleus where it can activate cell cycle machinery (reviewed in Pao and Tsai, 2021). The cleavage of p35 can happen as a consequence of treatment of cells by H_2O_2, NMDA, glutamate, or Amyloid beta (1-42), models of neuronal stress or overexcitation (reviewed in Shelton and Johnson, 2004). Even though p25 was considered to be a pathological product and a potential cause of neurodegeneration (Patrick et al., 1999), recently, it was connected to physiological memory formation while its role in neurodegenerative diseases is rather controversial (Engmann et al., 2011; Giese, 2014; Tandon et al., 2003).

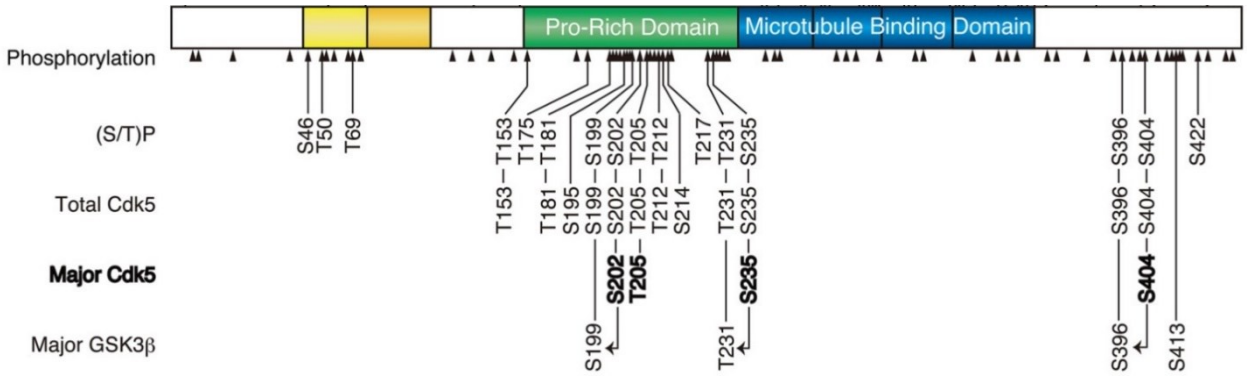

Figure 5: Tau phosphorylation sites.

Schematic illustration of tau molecule (N-terminal inserts in yellow, proline-rich domain in green and microtubule binding repeats in blue) and its phosphorylation sites (shown by arrowheads bellow). Ser/Thr-Pro motifs ((S/T)P), sites described to be phosphorylated by Cdk5 in vitro (total Cdk5), sites described repeatedly to be phosphorylated by Cdk5 (major Cdk5) and major GSK3beta phosphorylation sites are listed below. The arrows between major Cdk5 and major GSK3beta sites show priming phosphorylation (adapted from Kimura et al., 2014).

Many groups studied the effect of Cdk5 activity on tau phosphorylation, but the results are rather inconsistent. It was shown that phosphorylation of tau is not decreased but even increased in some phosphorylation sites in mice lacking p35 (Hallows et al., 2003). On the other hand, Cdk5 knockdown showed reduced tau phosphorylation at specific phosphorylation sites (Piedrahita et al., 2010). Overexpression of p25 *in vivo* is able to hyperphosphorylate tau (Ahlijanian et al., 2000; Cruz et al., 2003) or at least increase the phosphorylation of specific phosphorylation sites while other sites are not affected (Noble et al., 2003; Takashima et al., 2001; Wen et al., 2008).

It is widely accepted that p35 provides physiological phosphorylation while p25 mainly pathological phosphorylation of tau, but evidences of the different p25 versus p35 activation of Cdk5 and tau phosphorylation are not clear. *In vitro* studies showed increased activation of Cdk5 by p25 in comparison to p35 and higher tau phosphorylation on specific phosphorylation sites (Hashiguchi et al., 2002) while other authors did not observe any differences in the activation of Cdk5 by the two regulatory proteins and the same tau phosphorylation (Peterson et al., 2010). However, in cells, p25 acquires a longer half-life and is, in contrast to p35, not attached to the membrane which could lead to aberrantly activated Cdk5 leading to higher phosphorylation of tau which could be in cells followed by subsequent phosphorylation by other kinases (reviewed in Kimura et al., 2014).

Although both tau and Cdk5 kinase are deeply studied proteins, there are still conflicting results about the effect of Cdk5-phosphorylation on tau, and till now the effect of Cdk5 phosphorylation on tau protein *in vivo* is not completely understood. Also, most of the studies focus on pathological tau phosphorylation but the physiological role of Cdk5-mediated phosphorylation of tau is under-explored. Considering tau is one of the most studied MAPs, the effect of Cdk5 phosphorylation on other MAPs (e.g. CRMPs) is even less understood.

1.2.2.2 Collapsin response mediator proteins (CRMPs)

Collapsin response mediator proteins (CRMPs) are a family of 5 cytosolic proteins predominantly expressed in the nervous system and highly conserved between species (about 95% similarity between mice and humans; reviewed in Charrier et al., 2003). CRMPs are microtubule-associated proteins that bind to tubulin heterodimer and facilitate microtubule polymerization. CRMPs are expressed mainly during neural development regulating axonal growth and guidance through affecting microtubule polymerization but some CRMPs are present in several brain regions also in adulthood (reviewed in Charrier et al., 2003). CRMP2 is the one that keeps a relatively high level of expression while CRMP4 is the least expressed in the adult brain (Wang and Strittmatter, 1996). Nevertheless, CRMP4 is expressed in the adult neuromuscular junctions (Byk et al., 1996) and its role in adult mice was described in the regeneration of peripheral nerves (Girouard et al., 2020).

CRMPs were originally identified as mediators of Semaphorin 3A (Sema3A) signaling. Semaphorins are mainly repulsive axon guidance cues that regulates axon guidance in the peripheral as well as central nervous system. Sema3A signaling activates Cdk5 and GSK3beta kinases which phosphorylate CRMPs, this phosphorylation inhibits the binding of CRMP to tubulin and together with other events leads to axonal growth cone collapse (reviewed in Schmidt and Strittmatter, 2007). CRMPs can regulate also cellular events other than neurite dynamics, they were described as molecules transducing signals leading to apoptosis or as ligands of the extracellular matrix in the neonatal brain and are involved in synaptic plasticity (reviewed in Hou, 2020; Charrier et al., 2003).

CRMPs create hetero-tetrameric complexes *in vivo* (Wang and Strittmatter, 1997). Each CRMP displays a different precisely regulated spatiotemporal expression pattern which could result in the presence of spatiotemporally different types of tetramers and different CRMPs may play distinct but complementary physiological roles during ontogenesis (reviewed in Charrier et al., 2003).

The levels of CRMPs and their activity are altered in several neurological diseases. For example, CRMP4 is connected to Amyotrophic lateral sclerosis (ALS), a fatal motor neuron disease (Duplan et al., 2010), hyperphosphorylated CRMP2 is (similarly to tau) present in neurofibrillary tangles in Alzheimer's disease, and altered expression of CRMP2 was described in several psychiatric disorders, mainly schizophrenia (reviewed in Hensley et al., 2011).

1.2.2.2.1 CRMP2

CRMP2 was discovered in 1995 (Goshima et al., 1995) and it is the best-studied member of the CRMP family. CRMP2 binds to tubulin dimers, promotes microtubule growth, and mediates Sema3A signaling (Goshima et al., 1995; Niwa et al., 2017). In neurons, CRMP2 brings tubulin dimers to growing microtubules in axons promoting axonal branching and growth (Fukata et al., 2002; Kimura et al., 2005) and is also involved in axon specification as it was shown that CRMP2 accumulates in the future axon tip during neuron polarization and overexpression of CRMP2 induces multiple axons (Inagaki et al., 2001). CRMP2 is also connected to axonal regeneration (Suzuki et al., 2003). and autophagy (reviewed in Hensley and Kursula, 2016).

CRMP2 works not only as a microtubule-associated protein, it regulates axon formation and growth also by interactions with other proteins e.g. actin and actin cytoskeleton regulators (Arimura et al., 2005; Kawano et al., 2005). CRMP2 has been also shown to serve as an adaptor protein and to regulate axonal transport and vesicle trafficking (reviewed in Khanna et al., 2012). CRMP2 affects endocytosis (Nishimura et al., 2003) and synaptic transmission (reviewed in Stratton et al., 2020). CRMP2 expression is not restricted only to neurons, it is expressed in oligodendrocytes and also in peripheral tissues where CRMPs are connected to several types of cancer (reviewed in Moutal et al., 2019; Tan et al., 2014).

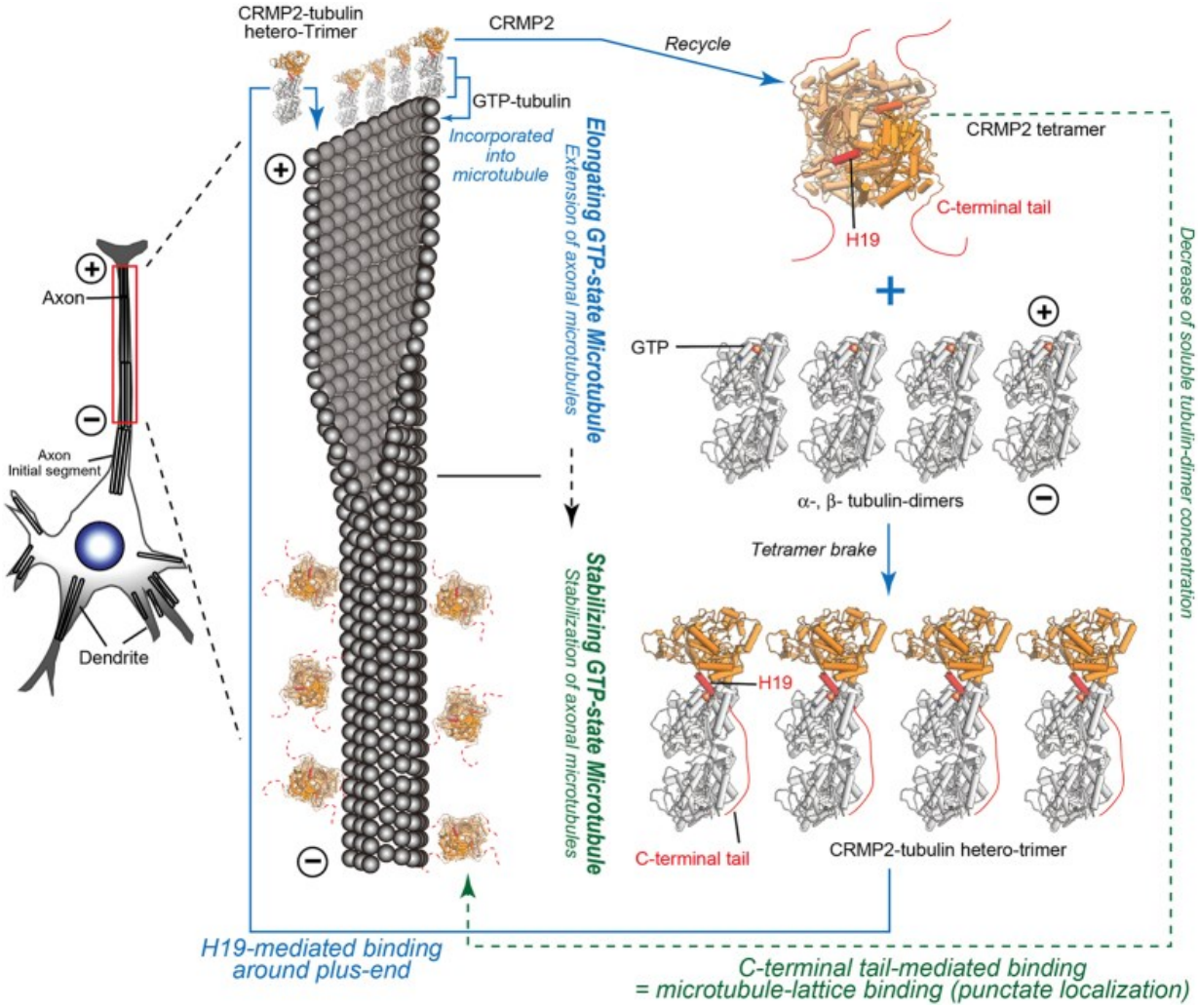

Figure 6: Microtubule-associated protein CRMP2.

CRMP2 (orange) forms tetramers, which bind to and stabilize GTP-state microtubule. C-terminal flexible tail of CRMP2 (red) tethers the wall of the microtubule. In the presence of tubulin dimers (gray), CRMP2 tetramers disintegrate and form heterotrimers (CRMP2 and alpha/beta-tubulin dimer) utilizing helix H19. CRMP2 promotes microtubule assembly by bringing the tubulin heterodimer closer to growing microtubule tip, where tubulin dimer is incorporated (adapted from Niwa et al., 2017).

CRMP2 molecule folds into a globular domain with a flexible unstructured C-terminus. The globular part interacts with beta-tubulin to form a CRMP2-tubulin heterotrimeric complex which could be incorporated into the growing end of microtubule. CRMP2 can also form homotetramers or heterotetramers with other members of the CRMP family. The globular parts assemble into tetramers with the C-termini probably creating unfolded chains extending from the tetramer and tethering the tetramer to microtubule GTP-state lattice leading to its stabilization (Figure 6; Lin et al., 2011; Niwa et al., 2017). Indeed, the function of CRMP2 is regulated by many posttranslational modifications and the majority of them are located at the

C-terminus (reviewed in Moutal et al., 2019). CRMP2 exists in two isoforms produced by alternative splicing. A shorter CRMP2B isoform is more abundant and more studied. CRMP2A isoform is less expressed and is localized mainly to axonal growth cones (Balastik et al., 2015; described in more detail below).

1.2.2.2.1.1 CRMP2 phosphorylation

CRMP2 is subject to many posttranslational modifications, the most studied of which is phosphorylation. Several kinases can phosphorylate CRMP2, e.g. upon Sema3A signaling, CRMP2 is phosphorylated at Ser522 by Cdk5 kinase. This phosphorylation allows phosphorylation by another kinase GSK3beta, which phosphorylates CRMP2 on Thr509/Thr514/Thr518 (Figure 7; Uchida et al., 2005). Another well-known phosphorylation of CRMP2 is phosphorylation by Rho-kinase, which phosphorylates CRMP2 on Thr555 as a consequence of lysophosphatidic acid treatment or Ephrin-A5 signaling (Figure 7; (Arimura et al., 2005). The described phosphorylations have similar consequences on CRMP2 function, i.e. decrease of its affinity to tubulin dimer resulting in an impaired tubulin polymerization and neurite outgrowth (Arimura et al., 2005; Uchida et al., 2005)Figure 7. In accordance with this, it was shown that deletion of GSK3beta promotes microtubule growth and axon regeneration and this effect can be reversed by overexpression of phospho-mimetic CRMP2 (Liz et al., 2014). CRMP2 can be phosphorylated also by FER kinase, which phosphorylates Tyr479 and Tyr499 residues. This phosphorylation regulates microtubule bundling and polymerization by affecting CRMP2 tetramerization (Tyr479) and microtubule binding (Tyr499) (Figure 7; Zheng et al., 2018Figure 7).

Dephosphorylation of CRMP2 on GSK3beta phosphorylation sites is provided mainly by protein phosphatase 1 (PP1) and PP2A while the Cdk5-phosphorylation site was described as rather resistant to dephosphorylation (Cole et al., 2008; Zhu et al., 2010).

In pathological conditions, CRMP2 can be phosphorylated by other kinases such as Protein kinase A (PKA), Protein kinase C (PKC), or Calmodulin kinase II (CaMKII) (reviewed in Nakamura et al., 2020). Hyperphosphorylation of CRMP2 is connected to Alzheimer's disease (Cole et al., 2007).

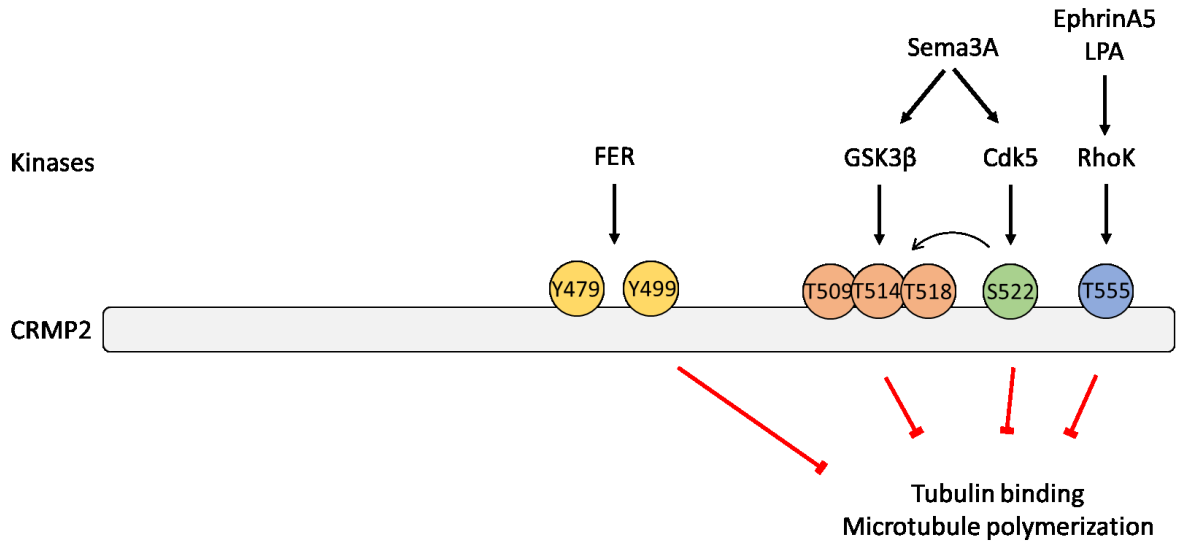

Figure 7: Main kinases and phosphorylation sites on CRMP2.

In Sema3A signaling, CRMP2 is phosphorylated by Cdk5 kinase on Ser522 and by GSK3beta on Thr509/Thr514/Thr518. Ser522 serves as a priming site for phosphorylation by GSK3beta. CRMP2 can by phosphorylated by Rho-kinase (RhoK) on Thr555 as a consequence of Lysophosphatidic acid (LPA) treatment or EphrinA5 signaling. FER kinase phosphorylates Tyr479 and Tyr499. All these phosphorylations have negative effect on CRMP2-promoted microtubule polymerization or stability (adapted and modified from Nakamura et al., 2020).

1.2.2.2.1.2 CRMP2 isoforms

As mentioned above, CRMP2 exists in two isoforms produced by alternative splicing. CRMP2A (75 kDa) is longer, containing an alternative N-terminal exon, and it is less expressed than CRMP2B (64 kDa; Figure 8). Overexpression of each CRMP2 isoform in fibroblast affects microtubule patterns but, interestingly, not the same way. While CRMP2A makes the microtubules long and oriented (resembling axonal microtubules), CRMP2B makes microtubules rather short and disoriented (Yuasa-Kawada et al., 2003). In neurons, CRMP2B overexpression promotes axon branching and suppresses axon elongation. CRMP2A expression does not affect axon branching or elongation, but it is able to abolish the effect of CRMP2B overexpression, suggesting that the two isoforms are regulating microtubule pattern in opposite ways and each can reverse the effect of the another one (Yuasa-Kawada et al., 2003). These data show that the ratio of the two isoforms plays an important role in regulating microtubule growth and neural development.

Moreover, it was shown that the distribution of the two CRMP2 isoforms in the neuron is not the same. While the expression of CRMP2B is observed in the whole neuron, CRMP2A is

localized mainly to the somatic and axonal part and is increased in distal axons and axonal growth cones (Balastik et al., 2015; Bretin et al., 2005; Yuasa-Kawada et al., 2003). In accordance with this, it was shown that CRMP2B knockout neurons have reduced length of dendrites, and specifically CRMP2B isoform is connected to proper dendritic development and was connected to mental disorders such as schizophrenia (Feuer et al., 2023). The different localization of CRMP2 isoforms was shown also in non-neuronal cells, where CRMP2B is found only in the cytoplasm, while CRMP2A was detected also in the nuclear fraction and was suggested to be the isoform connected to cancer (Grant et al., 2015) regulating carcinoma cell invasion and migration (Morgan-Fisher et al., 2013).

CRMP2 isoforms are differentially expressed also during development. In rat brains, CRMP2A isoform was observed mainly in early postnatal stages and diminishes in adulthood while CRMP2B expression lasts (Quinn et al., 2003; Rogemond et al., 2008). Another study showed isoforms levels during embryonic development in the chick retina showing the highest expression of both of them between E10 and E16 and the earlier reduction of the level of CRMP2A isoform (Yuasa-Kawada et al., 2003).

Besides the two isoforms produced by the alternative splicing, it was shown that specifically CRMP2B can be in cells cleaved by calpain producing the truncated CRMP2B form (58 kDa) which has also a specific temporal pattern and probably specific function (Rogemond et al., 2008). In adults, this truncation is connected mainly to axonal degeneration (Zhang et al., 2016), but it was suggested that the calpain-cleaved CRMP2B can play a role in synaptic plasticity (Bretin et al., 2006). It was suggested that also CRMP2A isoform could be a target of calpain cleavage but it was not studied in more detail (Bretin et al., 2006).

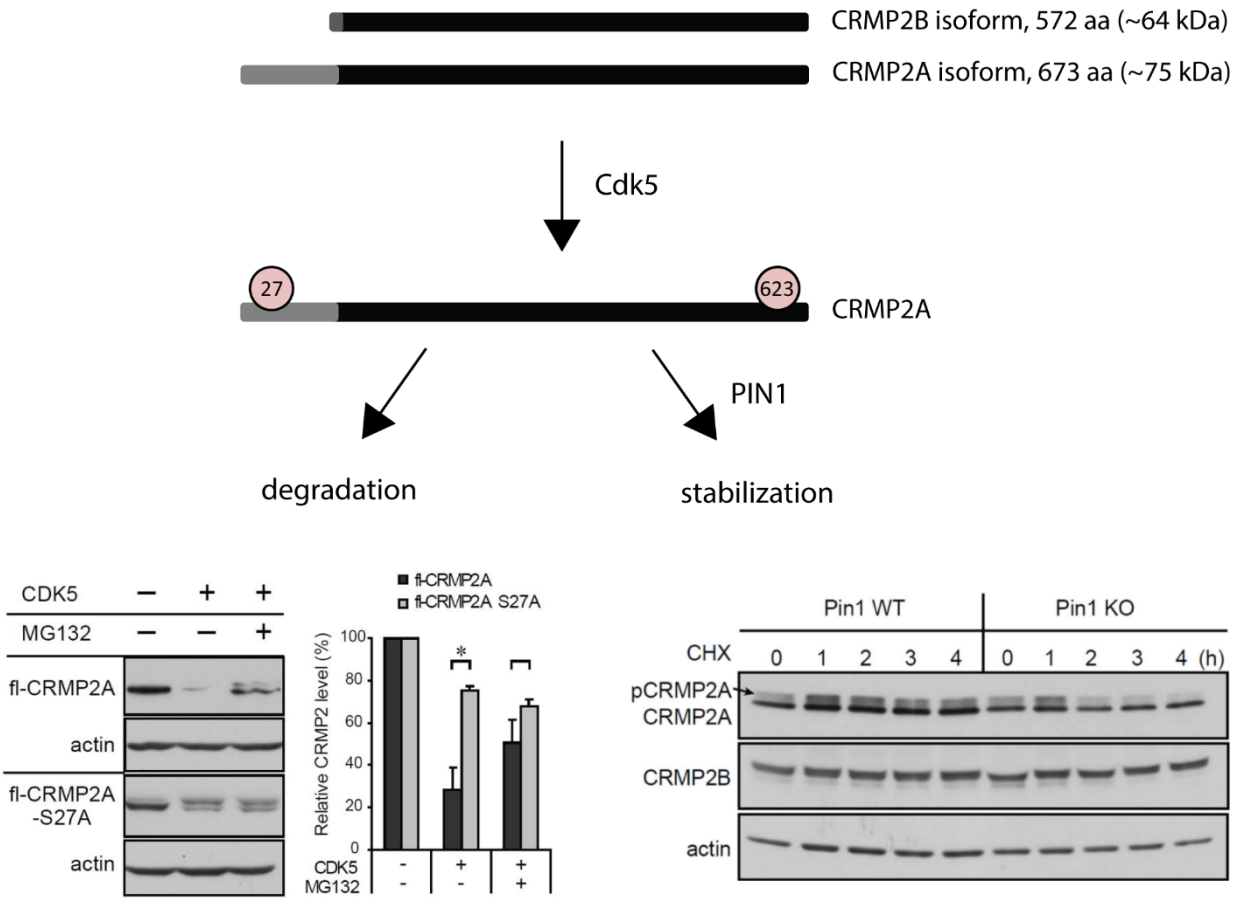

Figure 8: CRMP2A isoform and its stabilization by PIN1.

CRMP2 exists in two isoforms produced by alternative splicing - shorter isoform (CRMP2B) and longer isoform (CRMP2A). CRMP2A isoform possess alternative N-terminal exon in which is located a unique Cdk5-phosphorylation site (Ser27). Another Cdk5-phosphorylation site is located at the C-terminus (Ser623) and corresponds to Ser522 in CRMP2B. Cdk5-mediated phosphorylation directs CRMP2A towards degradation, which can be prevented by treatment with MG132 (proteasome inhibitor) or by the de-phospho-mimetic mutation of CRMP2A (CRMP2A S27A). Prolyl isomerase PIN1 which binds specifically CRMP2A isoform phosphorylated by Cdk5 can stabilize CRMP2A against degradation. The stability of CRMP2A is higher in WT neurons than in neurons lacking PIN1 (PIN1 KO), which was demonstrated in the presence of cycloheximide (CHX) inhibiting protein synthesis and thus showing protein stability (modified from Balastik et al., 2015).

We have shown that specifically CRMP2A isoform can be bound and regulated by prolyl isomerase PIN1. PIN1 binds to CRMP2A phosphorylated by Cdk5 (on phosphorylation sites Ser27 and Ser623 - corresponding to Ser522 on CRMP2B) and protects phosphorylated CRMP2A from degradation (Figure 8; Balastik et al., 2015). Phosphorylated CRMP2A is directed towards proteasomal degradation, which can be rescued by the inhibitor of preoteasome (MG132) or by the de-phospho-mimetic mutation of Ser27 (CRMP2A S27A). Moreover, the prolyl isomerase PIN1 can bind to phosphorylated CRMP2A and prevet its

degradation, which makes CRMP2A more stable in WT than in PIN1 KO neurons (Figure 8). Thus, PIN1 can protect CRMP2A keeping the stable amount of CRMP2A and thus stabilizing axons in low concentrations of the repulsing signals of Sema3A. By this mechanism, PIN1 regulates axon guidance (Balastik et al., 2015)Figure 8.

The distinct regulation of CRMP2 isoforms suggests their different functions and emphasizes the importance of studying them separately.

1.2.2.3 CRMP2 and tau similarities and their role in Alzheimer's disease

Microtubule-associated proteins CRMP2 and tau share some similarities. Both tau and CRMP2 are regulators of microtubule stability although tau binds to the microtubule lattice and prefers its GDP state, while CRMP2 binds to growing microtubule ends which are in the GTP state. Both CRMP2 and tau are localized to axons and their growth cones and both of these proteins are connected to neurodegeneration (reviewed in Hensley and Kursula, 2016).

Even though CRMP2 and tau do not share the same domains, the C-terminal tail of CRMP2 and the proline-rich domain of tau show considerable sequence homology, both are highly basic and share a high concentration of proline-directed phosphorylation sites (reviewed in Hensley and Kursula, 2016).

The same main kinases regulate the function of CRMP2 and tau. Both tau and CRMP2 are phosphorylated by GSK3beta which is primed by phosphorylation by Cdk5 and this phosphorylation affects the binding of tau and CRMP2 to microtubules and thus stability of microtubules. Both Cdk5 and GSK3beta as well as CRMP2 and tau were connected to neurodegeneration, mainly to Alzheimer's disease pathology (reviewed in Giese, 2009; Liu et al., 2016).

Alzheimer's disease is a progressive neurodegenerative disorder accompanied by memory loss progressing to dementia caused by loss of neurons, dendritic spines, and synapses (reviewed in Yu and Lu, 2012). Alzheimer's disease is characterized by the accumulation of amyloid-beta-rich extracellular plaques (senile plaques; amyloid-beta is a cleavage product of amyloid precursor protein (APP)) and intracellular aggregates of hyperphosphorylated proteins, mainly tau, called neurofibrillary tangles (NFT). In Alzheimer's disease, tau is abnormally posttranslationally modified (mainly hyperphosphorylated), it detaches from microtubules and is prone to form fibrillary aggregates called paired helical filaments which

are a predominant part of NFT. However, it was shown that the pathologic phenotype is more correlated to the accumulation of soluble aggregated tau (pre-filamentous tau), oligomeric intermediates preceding tangles formation (reviewed in Brunden et al., 2008). Moreover, tau protein can be secreted and internalized by other cells which gave rise to the theory of spreading the pathogenic misfolded tau through the brain and providing cells with toxic "seeds" that could recruit endogenous tau and other MAPs (reviewed in Zhang et al., 2021). Alzheimer's disease phosphorylation of tau is considered to be provided mainly by Cdk5 and GSK3beta (Flaherty et al., 2000) both of which are also associated with NFT (Yamaguchi et al., 1996). Tau first oligomerizes in AD early stages and it is a consequence of Thr231 phosphorylation (Lasagna-Reeves et al., 2012).

Even though NFT observed in Alzheimer's disease are usually described as hyperphosphorylated aggregates of tau protein, tau is not the only component of the tangles. Proteomic analysis of NFT revealed more than 150 proteins, the majority of them were proteins of energy and metabolism and cytoskeletal or structural proteins (Wang et al., 2005). CRMP2 is also associated with NFT, and moreover, one of the first antibodies raised against NFT (3F4 antibody) recognizes phosphorylated CRMP2 (Yoshida et al., 1998). Phosphorylation of CRMP2 is increased in Alzheimer's disease and also in the triple transgenic mouse model of Alzheimer's disease where CRMP2's hyperphosphorylation is evident before plaques or tangles formation (Cole et al., 2007). It was shown that both CRMP2 isoforms are hyperphosphorylated in Alzheimer's disease and to some lesser extent also in other neurodegenerative diseases mainly on sites Thr555, Thr514, and Ser522 (Mokhtar et al., 2018). Interestingly, CRMP2 can play a role also as an extracellular component (Moutal and Khanna, 2018), and phosphorylated CRMP2 was found also in senile plaque neurites (Yoshida et al., 1998). Moreover, CRMP2's function was described also in regulating the actin network or in vesicle transport and autophagy, processes which are affected in AD (reviewed in Hensley and Kursula, 2016).

So, even though tau and its phosphorylation are more studied in connection to Alzheimer's disease, CRMP2 and its regulation is also disturbed in the early stages of this disorder and could be similarly important for the pathology. Notably, not only are tau and CRMP2 regulated by similar kinases, but upon phosphorylation they both have been shown to be conformationally regulated by prolyl isomerase PIN1.

1.3 Prolyl isomerases

Prolyl isomerases (Peptidyl-prolyl *cis*/*trans* isomerases; PPIs) are ubiquitous enzymes expressed in prokaryotic and eukaryotic cells that are able to catalyze the conformational change of peptide bond N-terminal to proline residue. The majority of peptide bonds in the cells (99.95 %) are in *trans* conformation because of the steric hindrance applying in the *cis* conformation. However, peptide bonds in front of the proline are more likely to adopt *cis* conformation (around 6.5 % of Xaa-Pro bonds in proteins) because of the special ring structure of the proline molecule (Stewart et al., 1990). The structure of proline affects by itself protein features and in addition, it allows switching between *cis* and *trans* conformations, two distinct structures of the peptide bond. Proline-isomerization occurs spontaneously, but the process is very slow and can be accelerated by enzymes called prolyl isomerases. Isomerization may regulate protein folding but importantly, it may also serve as a unique type of posttranslational modification (non-covalent structural change of peptide backbone in contrast to classical posttranslational modifications) regulating protein functions and through it many cellular processes (Figure 9; reviewed in Gurung et al., 2023).

The conformation changes can regulate catalytic activities, phosphorylation status, protein interactions, localization, or protein stability. The importance of prolyl isomerases in cellular processes is illustrated by the fact that there are many examples of proteins specifically recognizing *trans* or *cis* conformation. Besides kinases and phosphatases, many proteases have been shown to be isoform-specific (Fischer et al., 1984; Weiwad et al., 2000; Zhou et al., 2000). For example, chymotrypsin is well known to digest specifically *trans*-conformation peptide bonds, which is exploited in prolyl isomerase assay for determination of PPIase activity (Fischer et al., 1984). Prolyl isomerases themselves show stereospecificity for recognizing their substrates (Schiene et al., 1998).

Prolyl isomerases were first discovered for their connection to immunosuppressive drugs (cyclosporin A in the case of cyclophilins and FK506 in the case of FKBPs). Nowadays, prolyl isomerases are classified into three groups – cyclophilins, FKBPs (FK506 binding proteins), and parvulins and are known as regulators of many signal transduction pathways, e.g. regulation of DNA repair, cell cycle, apoptosis, or immune response. Because of their regulatory roles, expression, localization and activity of prolyl isomerases have to be tightly regulated. Dysregulation of these enzymes is connected to various diseases such as

autoimmune diseases, cancer, or neurodegenerative disorders (reviewed in Gurung et al., 2023).

In the following chapters, I introduce FKBP12, a prototype member of the FKBP family containing only one prolyl isomerase domain, and PIN1, a member of the parvulin family and the only known phospho-specific prolyl isomerase.

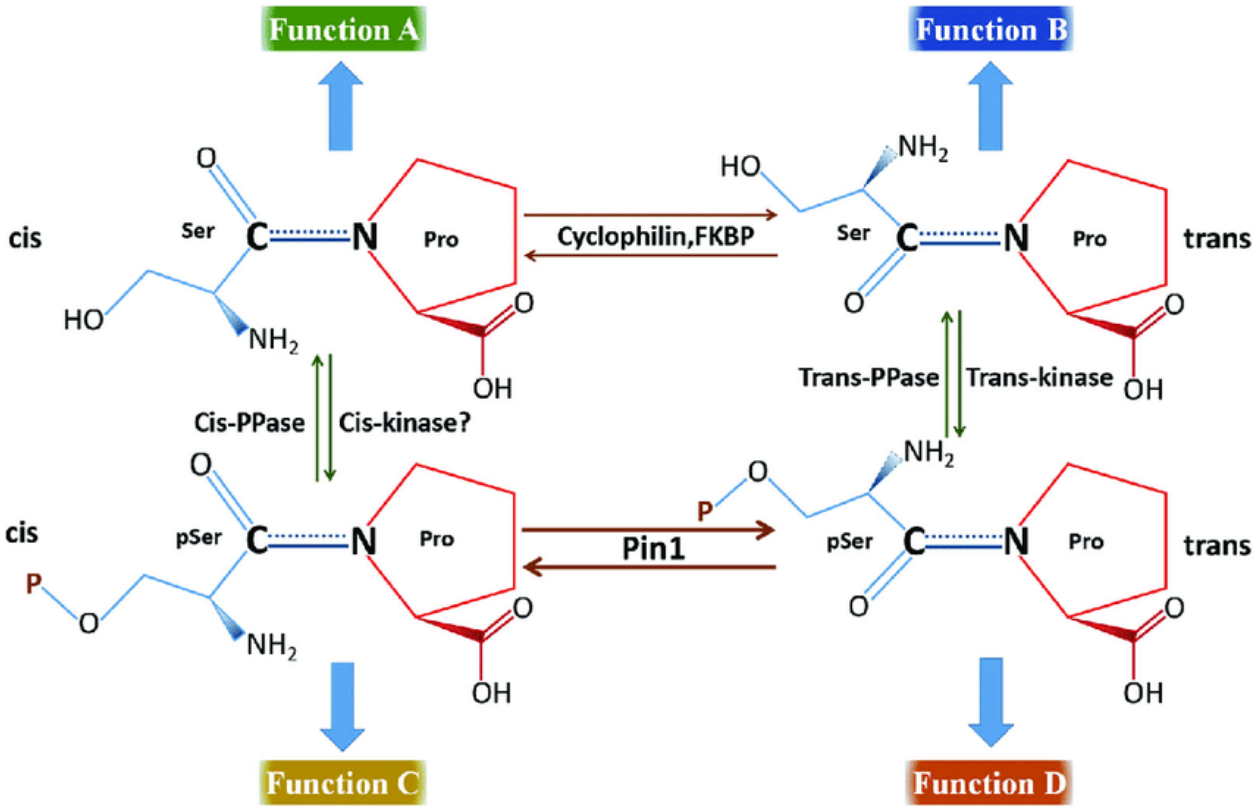

Figure 9: Peptidyl-prolyl cis/trans isomerases.

Peptidyl-prolyl isomerization is a process of switching between cis and trans isomers of the peptide bond preceding proline (Pro; in red). This process can be in cells facilitated by enzymes called prolyl isomerases – cyclophilins and FKBP, which isomerize non-phosphorylated substrates and parvulins with the most studied member PIN1, which is the only known phospho-specific prolyl isomerase. Prolyl isomerization could be considered a type of posttranslational modification that can serve as another level of regulation of protein function on top of phosphorylation. The combination of phosphorylation/dephosphorylation together with prolyl isomerization could produce up to 4 forms of the same motif which could possess different functions (Adapted from Chen et al., 2018).

1.3.1 FKBP12

FKBP12 is the smallest (and archetypical) member of the FKBP family. Mammalian FKBPs are ubiquitously expressed proteins that can be divided according to their cellular localization

to cytoplasmic, endoplasmic reticulum-localized, and nuclear. Humans have at least 15 members of the FKBP family. The role of FKBPs was described in protein folding, signaling, transcription control, regulation of apoptosis, or T-cell activation (reviewed in Tong and Jiang, 2016).

FKBP12 is a 12 kDa globular cytosolic protein consisting of one prolyl isomerase domain with a hydrophobic binding pocket. Even though there are many members of the FKBP family, deletion of the murine FKBP12 gene leads to a lethal phenotype mainly due to heart defects (Shou et al., 1998). FKBP12 was first discovered as a target of the immunosuppressive drug FK506 also known as tacrolimus (Harding et al., 1989; Siekierka et al., 1989). Later, it was shown that FKBP12 binds also another immunosuppressive drug rapamycin (sirolimus). Both drugs bind to FKBP12 and inhibit its PPIase activity, even though it is not the cause of their immunosuppressive functions (Bierer et al., 1990). The immunosuppressive effect of FK506 is accomplished through binding of FKBP12-FK506 to calcineurin which is affecting T-cell activation and thus blocking the adaptive response of the immune system (Liu et al., 1992). Rapamycin in complex with FKBP12 inhibits proliferation of T cells through its association with mTOR, a kinase involved in regulating cellular metabolism and proliferation (Sabatini et al., 1994).

The physiological roles of FKBP12 are not completely understood. FKBP12 was shown to associate with several membrane receptors in different cell types – with ryanodine receptors (RyR; the major Ca^{2+} channels in the sarcoplasmic reticulum releasing Ca^{2+} to the cytoplasm during muscle contraction), inositol triphosphate receptor (IP3R; which control release of Ca^{2+} from ER after inositol 1,4,5-triphosphate exposition), or transforming growth factor beta (TGFbeta) receptors. FKBP12 stabilizes the receptors or regulates their phosphorylation but the role of prolyl isomerase activity in these processes has not been documented (Brillantes et al., 1994; Cameron et al., 1997; Wang et al., 1994).

FKBP12 is enriched in the central and peripheral nervous system but the role of FKBP12 in neurons is not fully understood (Steiner et al., 1992). FKBP12 is present in cell bodies as well as neurites of neurons (Sugata et al., 2009), and it was shown that FK506 (FKBP12 inhibitor) stimulates neurite outgrowth, reduces ischemic brain damage, and promotes regeneration (reviewed in Hausch, 2015). Later, it was shown that non-immunosuppressive analogs of FK506 show similar neuroprotective and regeneration-promoting effects (Gold et al., 1997), but the dependency of the neuroprotective effect of these drugs on the FKBP12 has been questioned and it was suggested that another member of the FKBP family could also mediate

the effect (Gold et al., 2005). However, it was shown that brain-specific FKBP12 deletion in mice leads to an increase in mTOR activity, enhanced hippocampal long-term potentiation (LTP – one of the key mechanisms in memory formation), and some aspects of autism (Hoeffer et al., 2008).

FKBP12 binds to neuronal microtubule-associated protein tau and prevents tau from pathological aggregation (Ikura and Ito, 2013; Jiang et al., 2023). FKBP12 also colocalizes with phosphorylated neurofilament protein in axons (Sugata et al., 2009). However, the physiological role of FKBP12 in neurons is not well understood.

1.3.2 PIN1

PIN1 (Protein interacting with NIMA1 (never in mitosis A-1)) is the best-known member of the parvulin family of prolyl isomerases in mammals. PIN1 was discovered in connection to cell cycle regulation (Lu et al., 1996), but was shown to play roles also in DNA damage response, transcription and RNA processing, immune response, or the development of the germ cells (reviewed in Lu, 2004).

PIN1 consists of the WW (Trp-Trp) domain, which determines the substrate specificity of PIN1 and the C-terminal PPIase domain connected by a flexible linker (reviewed in Lu and Zhou, 2007). PIN1 has a strict specificity for its substrates binding exclusively to pSer/pThr-Pro bond in contrast to other prolyl isomerases which can not act on these phosphorylated motifs (Ranganathan et al., 1997; Yaffe et al., 1997). The Ser/Thr-Pro bond's spontaneous isomerization is even slower after its phosphorylation (Schutkowski et al., 1998), making PIN1 a special and important regulator of many processes which works in tandem with "proline-directed" kinases and phosphatases (reviewed in Lu and Zhou, 2007).

Although PIN1 homolog in budding yeast (Ess1) is essential (Hani et al., 1995), PIN1 knockout mice are viable (Fujimori et al., 1999) suggesting that some mammalian PPIases could substitute PIN1's function.

In contrast to many constitutively active PPIases, the activity of PIN1 is in cells tightly regulated by transcriptional regulation (regulated by transcription factors E2F and NOTCH), the level of mRNA (regulated by microRNAs), and many posttranslational modifications such as phosphorylation, sumoylation, ubiquitylation, or oxidation (reviewed in Chen et al., 2018; Lu, 2004). This tight regulation is important mainly for the regulation of the cell cycle but also

for other processes regulated by PIN1 and the deregulation of PIN1‘s activity is connected to many pathological conditions such as cancer or neurodegenerative disorders. In many types of cancer, PIN1 is overexpressed and the amount of PIN1 correlates with poor prognosis (reviewed in Chen et al., 2018).

PIN1 expression is induced during neuronal differentiation and neurons maintain high levels of PIN1 in the cytoplasm and the nucleus (Hamdane et al., 2006). PIN1 regulates neural development (Nakamura et al., 2012b), neuronal apoptosis (Becker and Bonni, 2006), or synaptic activity (reviewed in Fagiani et al., 2021). During the development, PIN1 regulates axonal growth (Balastik et al., 2015) and growth cone motility (Sosa et al., 2016). PIN1 knockout mice develop age-dependent neuropathy, showing markers of premature aging phenotype and degeneration, and inhibition of PIN1 in adult neurons is connected to neurodegenerative disorders (Liou et al., 2002; Liou et al., 2003). However, the role of PIN1 in neurons is not fully understood.

1.3.3 Prolyl isomerases in neurodegeneration

Several neurodegenerative disorders are characterized by protein aggregates composed of proteins that are normally completely or partially unfolded (intrinsically disordered), but are prone to aggregation into fibrillary structures. Because the proteins adopt in aggregates an alternative conformation, these neurodegenerative disorders are classified as “conformational disorders” (reviewed in Carrell and Lomas, 1997). Amino acid proline is usually avoided from regions with secondary structure, is more often found in turn or coil regions, and is considered to be the most disordered-regions promoting amino acid (Theillet et al., 2013).

The most known examples of conformational disorders are Parkinson’s disease (PD; defined by aggregates of alpha-synuclein called Lewy bodies), and Alzheimer’s disease (AD; defined by aggregates of hyperphosphorylated tau and amyloid-beta), neurological disorders characterized by the progressive loss of neurons leading to progressive irreversible dementia and physical impairment of the aged population worldwide.

Prolyl isomerase PIN1 is deficient in many neurodegenerative disorders including PD and AD. PIN1 accumulates in Lewy bodies and enhances the formation of alpha–synuclein aggregates (Ryo et al., 2006). PIN1 is downregulated and its activity can be inhibited by oxidation in AD brains (Butterfield et al., 2006; Chen et al., 2015; Sultana et al., 2006). It was even shown that expression of PIN1 inversely correlates with degeneration in AD (Liou et al.,

2002; Liou et al., 2003). PIN1 colocalizes with NFT and PIN1-dependent isomerization of the pThr231-Pro232 motif in tau was suggested as crucial in the progression of AD (Lu et al., 1999). It was shown that the *cis*-isomer of tau is the one prone to pathological aggregation (Nakamura et al., 2012a). PIN1 can restore the function of tau directly (Lu et al., 1999) or indirectly through its isomer-specific dephosphorylation (Zhou et al., 2000). PIN1 also protects against AD by regulation of APP turnover via regulation of GSK3beta activity (Ma et al., 2012). Moreover, PIN1 can bind to phosphorylated APP (Thr668-Pro motif) and accelerate its isomerization which determines APP's non-amyloidogenic (*trans*) or amyloidogenic (*cis*) processing (Pastorino et al., 2006).

FKBP12 is also connected to neurodegenerative diseases including AD and PD. Expression of FKBP12 is increased in the brains of PD patients and FKBP12 co-localizes with alpha-synuclein in Lewy bodies (reviewed in Avramut and Achim, 2002). FKBP12 accelerates aggregation of alpha-synuclein *in vitro* and in cells, leading to the production of fibrillary aggregates found in PD. This effect can be abolished by FK506 treatment (Deleersnijder et al., 2011; Gerard et al., 2006). FKBP12 levels are downregulated in AD brains and FKBP12 colocalizes with NFT (Sugata et al., 2009). FKBP12 prevents aggregation of tau peptide which is dependent on PPIase activity (Ikura and Ito, 2013). FKBP12 binds also to the intracellular domain of APP and overexpression of FKBP12 enhances the processing of APP to amyloidogenic peptide which can be blocked by FK506 (Liu et al., 2014). AD was also connected to Ca^{2+} deregulation – elevated Ca^{2+} release from RyR can contribute to neurotoxicity and cell death in which FKBP12 could potentially play a role (reviewed in Thibault et al., 2007).

As several neurodegenerative disorders are connected to pathological protein aggregates, the role of prolyl isomerases in their development can not be overlooked. Several prolyl isomerases are shown to be deregulated in these pathologies but the precise mechanism of their function in the development of the disease is not fully understood.

2 Aims and hypotheses

This study aims to characterize the regulation of neuronal microtubules by microtubule-associated proteins and to analyze the effect of phosphorylation and conformational changes of microtubule-associated proteins on microtubule dynamics and axon growth.

The goal of the thesis can be divided into three aims:

1.) Characterization of collapsin response mediator proteins and their isoforms in neural development and neurodegeneration

We hypothesize that the different CRMP2 isoforms play distinctive roles during ontogenesis and in Sema3A signaling during neural development. In addition, we hypothesize that CRMP4a isoform's transport is contributing to neurodegeneration in motor neurons.

2.) Prolyl isomerases and their role in the regulation of CRMP2A function, microtubule dynamics, and axon growth

We hypothesize that not only prolyl isomerase PIN1, but also FKBP12 regulate CRMP2A and its function and that their effect is phosphorylation-dependent. We will explore the effect of FKBP12 on CRMP2A function in the regulation of microtubule dynamics and test the effect of FKBP12 on neural development.

3.) Uncovering the role of tau phosphorylation in formation of tau envelopes and protection of microtubules

We hypothesize that Cdk5-phosphorylation of tau affects tau envelopes' stability and their microtubule-protective function in cells.

3 Materials and methods

3.1 Mouse lines

All animal work was performed in compliance with European directive 2010/63/EU and experiments were approved by the Czech Central Commission for Animal Welfare. Mice (C57BL6/N background) were housed and handled according to the institutional committee guidelines and had free access to food and water. We used WT, CRMP2 knockout (CRMP2 KO; Ziak et al., 2020), CRMP2A knockout (CRMP2A KO; produced in our laboratory; Ziak et al., in preparation), or PIN1 knockout (PIN1 KO; Fujimori et al., 1999) mice.

Mice were used for primary neurons isolation, in utero electroporations, and for isolations of brains. The age of the embryos was calculated from the date of a positive vaginal plug (=E0.5).

3.1.1 Mouse genotyping

Mice were genotyped from genomic DNA isolated from tail biopsy. The tissue sample was incubated overnight at 55°C in the lysis buffer with proteinase K (100mM Tris pH 8.5, 5mM EDTA, 0.2% SDS, 200mM NaCl, 100 µg/ml Proteinase K), DNA was precipitated using sodium acetate and isopropanol, washed in 70% EtOH, dissolved in sterile water and used for genotyping by PCR reaction with the primers listed in Table 1.

Table 1: Primers used for mouse genotyping

Mouse line	**primers**
CRMP2 KO	F-TCACCCTCCCGGGACGAT R-TCTACCAATGTTACAACACAGA R-ACTTACCGTGATGCGTGGAA
CRMP2A KO	F-TCCCTCAACCCTCAGCTCT R-GCTCGATTCAACAGATGGCT R-TCCACCCCCAGGATGGAG
PIN1 KO	F-CCGATCCTGTTCTGCAAACT

	R-GGATTAGAAGCAAGATTCGACT R-CCACTTGTGTAGCGCCAAGTGC

3.2 Brain lysates

Mice were sacrificed at desired age by cervical dislocation (or by decapitation in case of embryos and early postnatal pups), brains were isolated and homogenized in the lysis buffer (50mM HEPES pH 7.4, 150mM NaCl, 10% glycerol, 1% Triton X-100, 1.5mM $MgCl_2$, 1mM EGTA, 100mM NaF, 1mM Na_3VO_4, 1mM DTT, cOmplete™ EDTA-free Protease Inhibitor Cocktail (Merck)) using ultraturrax. The samples were sonicated and centrifuged. Total protein concentration in the supernatant was determined by Bradford assay (using BSA standards), samples were diluted in the sample buffer (final concentration: 50mM TrisCl pH 6.8, 2% SDS, 2% beta-mercaptoethanol, 10% glycerol, 0.1% Bromphenol Blue) to required concentration (usually 2 µg/µl) and incubated at 98°C for 10 minutes.

3.3 Western blot

Samples (usually 10-20 µg of the total protein) were loaded on polyacrylamide gels (7.5%, 12% or 15%) and after the electrophoresis (100 V) were transfered to a PVDF membrane (Merck, IPVH00010) using wet (40 mA, 4°C, overnight) or semi-dry transfer (Trans-Blot SD Semi-Dry Transfer Cell, Bio-Rad, according to the provider instructions). Proteins were stained by coomassie staining (2.5 g/l Coomassie briliant blue R250, 50% MetOH, 10% Acetic acid) and washed in TBS-T (100mM Tris, 0.9% (w/v) NaCl, 0.1% (w/v) Tween). The membranes were blocked in 5% milk/TBS-T (Lowfat powdered milk (Roth)). After blocking, the membranes were incubated with appropriate primary antibodies (the antibodies used are listed in Table 2) diluted in the blocking solution overnight at 4°C. After washing (TBS-T), the membranes were incubated with HRP-conjugated secondary antibodies (1.5 hour, RT). Membranes were washed and chemiluminiscence reaction was performed using ECL substrate solution (0.1M Tris, pH 8.8, 1.25mM luminol, 0.2mM p-coumaric acid, 0.006% H_2O_2). Films (AGFA CP-BU NEW) were exposed to membranes in a dark room and developed in a FUJI film developer. Films were scanned (EPSON Perfection V 700 photo) and signal density was analyzed in FIJI.

Table 2: List of antibodies used

Primary antibodies Targeted protein	**Provider**	**Identifier**	**Application**
Beta tubulin	DSHB Iowa	E7 (deposited to the DSHB by Klymkowsky, M.)	Immunocytochemistry
Beta-III-tubulin	Exbio	11-264-C100	immunocytochemistry
Cleaved Caspase-3 (Asp175)	Cell signaling	9661	Western blot
CRMP2	FUJIFILM Wako chemicals	014-24821 (9F)	Western blot, immunocytochemistry
CRMP2 pS522 (recognizing also CRMP2A pS623)	MRC PPU Reagents	S761B	Western blot
CRMP2A	(Balastik et al., 2015)		Western blot, immunoprecipitation
CRMP2A pS27	produced in rabbit against CNLGSG(Sp)PKPRQK and affinity purified using the same peptide; antibodies against non-phosphorylated peptide were removed by affinity purification with the non-phosphorylated peptide		Western blot
CRMP4 (TUC4)	Merck	AB5454	Western blot, immunocytochemistry
FKBP12	Abcam	ab2918	Western blot
FKBP12	Abcam	ab58072	immunocytochemistry

Flag	Merck	F7425	Western blot
GAPDH	Merck	G9545	Western blot
GFP	ThermoFisher Scientific	A11120	Western blot
Neurofilament (NF-M)	DSHB Iowa	2H3 (deposited to the DSHB by Jessell, T.M./ Dodd, J.)	Whole-mount staining
PIN1	R&D systems	MAB2294	Western blot, immunocytochemistry
Secondary antibodies	**Provider**	**Identifier**	**Application**
anti-Mouse A488	ThermoFisher Scientific	A-11029	immunocytochemistry
anti-Rabbit A594	ThermoFisher Scientific	A-11037	immunocytochemistry
anti-Mouse A647	ThermoFisher Scientific	A21236	immunocytochemistry
anti-Rabbit A488	ThermoFisher Scientific	A-11029	immunocytochemistry
anti-mouse HRP	ThermoFisher Scientific	31432	Western blot, whole-mount staining
anti-rabbit HRP	ThermoFisher Scientific	31462	Western blot
anti-sheep HRP	Merck	12-342	Western blot

3.4 Primary neuron cultures, DRG, microfluidic chambers

Brains were isolated (in HBSS media - ThermoFisher Scientific 14065-049; with 20mM HEPES, pH 7.3) from murine embryos (E15.5-E17.5), homogenized in Neurobasal media supplemented with B27 supplement, 2mM glutamine, and Penicillin/Streptomycin (ThermoFisher Scientific), filtered using cell strainer (40 μm; Biologix) and spun down. The cell pellet was resuspended in fresh media, counted, and cultured in Neurobasal media supplemented with B27 supplement, glutamine, and Penicillin/Streptomycin in the density 80000 - 100000 cells/well in 24-well plate and 3000000 cells/60mm dish.

Dorsal root ganglia (DRG) were isolated from mouse embryos (E11.5-E12.5) and cultivated in the chambered coverslips (pretreated with Laminin and Poly-D-lysine - 2 μg/ml and 50 μg/ml respectively; Merck - L2020 and Millipore - A-003-E respectively) in Neurobasal media supplemented with B27 supplement, glutamine, Penicillin/Streptomycin and 25 ng/ml NGF (R&D systems).

If not stated otherwise, half of the media was replaced by fresh media every other day.

3.4.1 Neuronal transfection and transduction

Neuronal transfection was done at DIV1 (unless stated otherwise) using Lipofectamine 2000 (1.5-2 μg of DNA and 2 μl of Lipofectamine for 1 well in 24-well plate; Invitrogen) in OptiMEM medium (ThermoFisher Scientific). Before the transfection, cells were washed 3x with OptiMEM. Four hours after the transfection the media was replaced by Neurobasal media supplemented with B27 supplement, 2mM glutamine, and Penicillin/Streptomycin (conditioned medium).

Transduction of neurons or DRG was done 5 or 24 hours after the plating (unless stated otherwise). Lentiviral particles were added to the media at desired concentration. In case that the ratio between amount of lentiviral particles solution and the media was higher than 1:1, the media was replaced in 3 hours, otherwise, the media was replaced in 24 hours. For the transduction of neurons in the microfluidic chambers, the lentiviral particles were added without dilution for one hour, after that they were replaced by the conditioned media.

3.4.2 Neuronal samples for western blot analysis

For western blot analysis, neurons were plated on cell culture dishes (35 or 60 mm) pretreated with Laminin and Poly-D-lysine (2 µg/ml and 30 µg/ml respectively). Neurons at required DIV were washed (PBS) and incubated with the lysis buffer (50mM HEPES pH 7.4, 150mM NaCl, 10% glycerol, 1% Triton X-100, 1.5mM $MgCl_2$, 1mM EGTA, 100mM NaF, 1mM Na_3VO_4, 1mM DTT, cOmplete™ EDTA-free Protease Inhibitor Cocktail) on ice for one minute. The cells in the lysis buffer were harvested with the cell lifter, sonicated, and centrifuged. The protein concentration was measured by Bradford assay and samples were diluted in the sample buffer (final concentration: 50mM TrisCl pH 6.8, 2% SDS, 2% beta-mercaptoethanol, 10% glycerol, 0.1% Bromphenol Blue) to required concentration (usually 1-2 µg/µl) and incubated at 98°C for 10 minutes.

3.4.3 Immunocytochemistry

For immunocytochemistry, neurons were plated on glass coverslips (12 mm No. 1.5H; 0117520 – Paul Marienfeld; placed in 24-well plate) pretreated with Laminin and Poly-D-lysine (2 µg/ml and 50 µg/ml respectively). Cells were fixed at the required DIV with 4% PFA/PBS for 15 minutes and subsequently with 100% MetOH (-20°C). After washing (PBS), cells were blocked with 0.1% BSA/PBS and incubated with selected primary antibodies diluted in the blocking solution overnight at 4°C. After washing, cells were incubated with secondary antibodies conjugated with Alexa Fluor of required excitation and emission for 1.5 hour at RT. Cells were washed and samples were mounted with mowiol. Cells were captured using confocal scanning microscope Leica SP8 or Leica Stellaris 8 (PL FLUOTAR 25x/0.75 IMM or HC PL APO CS2 63x/1.40 OIL).

For correlation between CRMP2A and prolyl isomerase intensities, intensities of 100 pixels/cell (n=5) were measured and normalized (mean subtracted and divided by SD). Pearson correlation coefficient for CRMP2A and FKBP12/PIN1 signal was calculated. Differences between correlations were calculated according to (Lenhard, 2014).

3.4.4 Microfluidic chambers

Microfluidic chambers were prepared from Sylgard 184 silicone (Dow) as described previously (Ionescu et al., 2016; Maimon et al., 2018). Sylgard 184 elastomer base (41 g) and

Sylgard 184 elastomer curing agent (4 g) were mixed and casted to the molds. The bubbles were removed using vacuum desiccator and silicone was cured on heating plate 70°C overnight. Four 7mm-diameter wells (2 on the axonal part and 2 on the cell-body part) for the cultivation media were introduced and chambers were UV-sterilized and placed into 6-well glass bottom plate (Cellvis - P06-1.5H-N) pretreated with Laminin and Poly-D-lysine (2 μg/ml and 50 μg/ml respectively). Neurons were plated on the cell-body part of the chamber and transduced 5 hours after the plating. Four days after the plating, neurons were stained using Alexa 647-conjugated Cholera toxin Subunit B (1:1000; ThermoFisher Scientific) for 1 hour. After washing, axonal part of the chamber was captured for 40 hours (20-minute timeframe) using confocal microscope Leica TCS SP8 (10×/0.3 dry objective). Videos were analyzed using FIJI plugin MTrackJ and average velocity was quantified. Kymographs were produced using FIJI plugin Multi Kymograph.

3.5 Cell lines, lentiviral particles production, transfection, transduction

HEK293T cells were cultured in DMEM media (Sigma - D6429) supplemented with 10% fetal bovine serum (ThermoFisher Scientific - 10270106) and 1% penicillin/streptomycin (ThermoFisher Scientific - 15240122). IMCD3 cells were cultured in DMEM/F12 (ThermoFisher Scientific – 31330038) supplemented with 10% fetal bovine serum and 1% penicillin/streptomycin. Cell passaging was done by trypsinization, cells were cultured in a humidified 5% CO_2 atmosphere at 37 °C.

3.5.1 Cell lysates for western blot

For western blot analysis, cells were washed and harvested using cell lifter. After centrifugation, the cell pellet was lysed in the lysis buffer (50mM HEPES pH 7.4, 150mM NaCl, 10% glycerol, 1% Triton X-100, 1.5mM $MgCl_2$, 1mM EGTA, 100mM NaF, 1mM Na_3VO_4, 1mM DTT, cOmplete™ EDTA-free Protease Inhibitor Cocktail), sonicated and centrifuged. The protein concentration of the supernatant was measured by Bradford assay and samples were diluted in the sample buffer (final concentration: 50mM TrisCl pH 6.8, 2% SDS, 2% beta-mercaptoethanol, 10% glycerol, 0.1% Bromphenol Blue) to required concentration (usually 1-2 μg/μl) and incubated at 98°C for 10 minutes.

3.5.2 HEK293T transfection

HEK293T cells were split 24 hours before transfection to get about 70% confluency. The mixture of DNA and PEI (polyethylenimine; Polysciences, Inc. – 23966) was prepared (15 µg of DNA and 45 µl PEI/p10 dish) in OptiMEM buffer (ThermoFisher Scientific) and added to cells in DMEM with 1% FBS. Four hours after the transfection, the medium was replaced by a conventional culture medium (DMEM, 10% FBS, Pen/Strep). Cells were collected 48 hours after transfection (if not stated otherwise).

3.5.3 Lentiviral particles production

Lentiviral particles were produced by co-transfection of HEK293T cells with lentiviral vector carrying the sequence coding the protein of interest or shRNA together with the packaging plasmid (delta8.9) and envelope plasmid (vsv-g) in the ratio 1:0.9:0.1. The medium containing lentiviral particles was collected 48 hours after the transfection, filtered (0.45 µm pores) and used for transduction or stored at -80°C. To apply lentiviral particles to neurons, HEK293T cells were after the transfection cultivated in Neurobasal media supplemented with 0.5xB27 supplement, glutamine, and Penicillin/Streptomycin.

3.5.4 IMCD3 cells transfection and transduction

IMCD3 cells were transfected 24 hours after splitting using Lipofectamine 2000 according to the manufacturers instructions. The transfection was done in Optimem in 12-well plate or in 8-well coverslips (Ibidi; 0.5 µg of DNA + 0.9 µl Lipofectamine/well). The medium was changed 3 hours after transfection.

For lentiviral transduction, the medium containing the lentiviral particles was added to the cells and the efficiency of the transduction was checked 48 hours after the transduction (with the fluorescent microscope in case of fluorescent marker in the vector).

For katanin experiments, IMCD3 cells were transfected with vectors for overexpression of mCherry-tau or mCherry, katanin subunit p60, katanin subunit p80-GFP, and Cdk5 and p25 or empty pCDNA3 vector (in the ratio: 1: 0.375: 0.375: 0.375: 0.375). Cells were fixed 12 hours after transfection and stained with anti-β-tubulin antibody. We analyzed the mean intensity of tubulin signal in transfected cell relative to the intensity of surrounding non-transfected cells using FIJI. These values were either correlated to the intensity of the katanin signal (correlation

plot with the linear regression) or plotted in a bar graph (in this case only cells with the relative intensity of katanin between 0.5-3 were plotted).

3.5.5 IMCD3 cells – elevated pH treatment, FRAP

IMCD3 cells were transduced by lentiviral particles for mScarlet-tubulin production and transfected with vectors producing GFP-tau, GFP-tauΔN in the presence or absence of Cdk5 and p25 expression (tau:Cdk5:p25 vectors ratio = 1:0.85:0.15). The imaging was done 24 hours after the transfection.

For elevated pH treatment, cells were imaged every 20 seconds for 10 minutes. After 1 minute of imaging, the media was changed for the regular media with pH adjusted to 8.4 with NaOH. Imaging was performed using TIRF microscope (Apo TIRF 60x Oil DIC N2) using OKO-lab chamber (37°C, 5% CO_2). Cells were analyzed using FIJI. The mean intensity of the GFP signal was measured in random circular regions of the cytoplasm before elevated pH treatment. The mean intensity of tau on the microtubule was measured before elevated pH treatment and divided by the mean intensity of the same-size region in the cytoplasm next to the measured microtubule. microtubule coefficient of variation (CoV) was determined using FIJI from the standard deviation of the tau fluorescent signal within the ROI (a line drawn on a single microtubule), divided by the mean. Three random microtubules were measured in each cell and the CoV was averaged. The intensity of tau signal in the tau patches at 5 different timepoints after elevated pH treatment was analyzed (for tau-ΔN the intensity over the random regions of the microtubule was analyzed), and subtracted by the intensity of the same-size region next to the microtubule. All timepoints were normalized to the intensity of tau before the elevated pH treatment. To analyze the recovery of tau signal after the pH treatment, the mean tau intensity in the cell (ROI comprising most of the cell) was measured at all time points and subtracted by the intensity of the GFP signal in the cytoplasm (next to the microtubules). The intensity in each time point was normalized to the intensity before elevated pH treatment.

For FRAP experiments, cells were captured using a spinning-disk confocal microscope (Nikon CSU-W1; CF Plan Apo VC 60XC WI objective; 37°C and 5% CO_2) equiped with FRAP/photoactivation module. Imaging was done for 17 frames (100 ms exposure time, 500 ms interval) before FRAP, then FRAP was performed on a circular region of 0.5 μm diameter, after which the cell was imaged for 22 seconds to visualize the recovery. The analysis

of the FRAP data was done using FIJI and Matlab. The intensity of the GFP signal in a small ROI on the microtubule in the bleached region of the cell was analyzed, the same-size region on the microtubule in the same cell but outside the bleached area was used as a reference (ref) and the same-size region outside the cell was used as a background (bg). The curves were double-normalized according to the equation $F_{frap\text{-}normalized}(t) = (F_{ref\text{-}pre}/[F_{ref}(t) - F_{bg}(t)])([F_{frap}(t) - F_{bg}(t)]/F_{frap\text{-}pre})$, where $F_{ref\text{-}pre} = \Sigma_{(t=0;t=17)} ([F_{ref}(t) - F_{bg}(t)]/f_{prebleach})$; $F_{frap\text{-}pre} = \Sigma_{(t=0;t=17)} ([F_{frap}(t) - F_{bg}(t)]/f_{prebleach})$; $f_{prebleach} = 17$; $F_{ref}(t)$ is the reference fluorescence intensity on the microtubule in the same cell but not in the bleached region; $F_{frap}(t)$ is the fluorescence intensity on the microtubule in the bleached ROI; $F_{bg}(t)$ is the fluorescence intensity in a background ROI outside the cells; $F_{ref\text{-}pre}$ is the mean fluorescence intensity of the reference ROI before the bleaching after background subtraction; $F_{frap\text{-}pre}$ is the mean fluorescence intensity of the bleached ROI before the bleaching after background subtraction (Breuzard et al., 2013). The normalized data was fitted using the Matlab fitting tool using the equation: $y = a*exp(-b*x)+c$; where b = rate constant and c = asymptote. For the analysis of the immobile fraction, we used the equation: Immob = $[1-(c-F_0)/(1-F_0)]*100$; where c is the asymptote (of the fitted curve), and F_0 is the normalized intensity immediately after the bleaching (Breuzard et al., 2013).

3.6 Vectors, Cloning, Mutagenesis

We used the pCDNA3 vector for the expression of flag-tagged proteins in HEK293T cells. Vector pCDNA3.1 was used for the expression of CRMP2 proteins fused to mCherry in neurons or IMCD3 cells. Vector pCDNA3.1 expressing flag-tagged GFP-CRMP2 was used for the purification of proteins used in *in vitro* assays. pCDNA3 or pLL3.7 vectors expressing CRMP4a or its truncated or mutated forms were used for immunoprecipitation experiments. Vector pGEX-KG was used for protein purification from bacteria. Lentiviral expression of FKBP12 was provided by pWCC19 or pTRIP vectors. Experiments with GFP-EB3 expression combined with CRMP2A or FKBP12 were done using pTRIP vector and the two proteins were separated by 2A cleavage site. Experiments with GFP-EB3 in DRG was performed using pTRIP GFP-EB3 combined with either CRMP2A expression or FKBP12 knockdown. For in utero electroporation of GFP or CRMP2A, we used pCAGGS vector. For the expression of tau or its truncated form fused to GFP, pCDNA4 vector was used. Katanin was expressed by co-transfection of two katanin subunits in pLL vector. For tubulin visualization in live cells,

lentiviral vector expressing mScarlet-tubulin was used. To get phosphorylated CRMP2A or phosphorylated tau, we did co-transfection of the expression vector together with pCDNA3-Cdk5 and pCDNA3-p25 (in the ratio 1: 0.6: 0.13). Created and used vectors together with the cloning information are listed in Table 3. For the preparation of some vectors, the SLIC cloning method was used (Jeong et al., 2012). Mutations or deletions were introduced using the classical QuikChange protocol or by one-step site-directed mutagenesis protocol (Liu and Naismith, 2008).

Knockdown of proteins was performed using pLKO.1, pGhU6 (Radomska et al., 2012) or mCherry-pGhU6, knockdown in in utero electroporations was done using pSUPER (OligoEngine) vector. Silencing sequences and the hairpin sequences inserted into the relevant vector are listed in Table 4.

All insertions or manipulations with the sequences were confirmed by DNA sequencing (provided by SEQme company). Vectors were amplified using RbCl competent E. Coli TOP10.

Table 3: Expression vectors used

Expressed protein	**Vector**	**Source or preparation**
flag-CRMP2A flag-CRMP2B flag-CRMP2B S522A flag-CRMP2A S27A flag-CRMP2A S623A flag-CRMP2A S27A,S623A	pCDNA3	(Balastik et al., 2015)
flag-CRMP2AΔ604 flag-CRMP2BΔ503	pCDNA3	Truncated forms of CRMP2A (1-604) and CRMP2B (1-503) were prepared from full-length sequences and cloned into pCDNA3, primers: CRMP2A-F-ACCTCGAGATGGCCGAGAGAAAGCAATC CRMP2B-F-ACCTCGAGATGTCTTATCAGGGGAAGA R-TATCTAGACTATACCGGTCCGTCATACAGG
mCherry-CRMP2A	pCDNA3.1	mCherry (from pEmCherry vector) inserted in front of CRMP2A using KpnI and EcoRI; primers: F- AATGGTACCGCCACCATGGTGAGCAA R- CTCAGAATTCTAACTTGTACAGCTCGTCCA

mCherry-CRMP2A S27A,S623A	pCDNA3.1	CRMP2A in mCherry-CRMP2A-pCDNA3.1 replaced by CRMP2A S27A, S623A from pCDNA3 using XhoI and XbaI
flag-GFP-CRMP2B flag-GFP-CRMP2A	pCDNA3.1	Produced from GFP-CRMP2B and GFP-CRMP2A by my colleague; GFP-CRMP2 vectors were produced by insertion of GFP (from pEGFP vector) in front of CRMP2 using KpnI and EcoRI; primers: F- AATGGTACCGCCACCATGGTGAGCAA R- TCAGAATTCGGACTTGTACAGCTCGTC
flag-GFP-CRMP2B Y479E flag-GFP-CRMP2A Y580E	pCDNA3.1	Produced from flag-GFP-CRMP2B and flag-GFP-CRMP2A by my colleague
flag-CRMP4a	pCDNA3	Sequence of CRMP4a (gene 22240; NP_033494.1) was amplified from cDNA library prepared from mouse brain and inserted using XhoI and XbaI, primers: F-ATACTCGAGATGTCCTACCAGGGCAAGAA R- TCTTCTAGATTAACTCAGGGATGTGATGTTA
GFP-CRMP4a	pLL3.7	Sequence of CRMP4a was transferred into pLL3.7 to get GFP-fused protein using EcoRI; primers: F-TGAGAATTCATGTCCTACCAGGGCAAGA R-GCCGAATTCCTTAACTCAGGGATGTGATGT
GFP-CRMP4aΔ100-150	pLL3.7	primers F-GCGGGAGGCGAGGTACAGAGCCTCAGCAAGGAAAAAGGCGT R-CTGTACCTCGCCTCCCGCTAAGGCAGCCTTTGTCCCTTGGAA using site-directed deletion protocol (Liu and Naismith, 2008).
GFP-50aa (TTMIIDHVVPEPESSLTE	pLL3.7	Amplified from GFP-CRMP4a, primers: F-CTCGAATTCACCACCATGATCATTGACCAC

AYEKWREWADGKSCCD YALHVDITHWNDSVKQ)		R-GTCGAATTCTTACTGCTTGACGCTGTCATTCC and inserted into pLL3.7 with EcoRI
flag-CRMP4a I141V	pCDNA3	The point mutation I141V was generated in flag-CRMP4a vector according to the protocol described (Liu and Naismith, 2008), primers: F-ATGTGGACGTCACCCACTGGAATGACAGCGTCAAG CAG R-AGTGGGTGACGTCCACATGCAAAGCATAGTCACA GCAGC
GST GST-PIN1	pGEX-KG	(Balastik et al., 2015)
GST-FKBP12	pGEX-KG	FKBP12 sequence (gene 14225; NP_032045.1) was prepared from mouse brain cDNA library and inserted into pGEX-KG-GST by XbaI and XhoI, primers: F-TACTCTAGAGATGGGAGTGCAGGTGG R-GACTCGAGCTGTCATTCCAGTTTTAGAAG
Cdk5 p25	pCDNA3	(Balastik et al., 2015; Patrick et al., 1999)
FKBP12 (mutated)	pWCC19	FKBP12 was first inserted into pWCC19 by SalI and SmaI and because the expression was very low, QuikChange mutation was used to introduce Kozak sequence, primers: F-CCACCTGCACTCCCATGGTGAGGGGGATCCGATTC R-GAATCGGATCCCCCTCACCATGGGAGTGCAGGTGG The vector expressing FKBP12 with seven silent mutations which should abolish its recognition by the target sequence used in shFKBP12 construct was prepared by QuikChange mutation protocol, primers: F-GGGGATGCTTGAAGATGGAAAGAAATTTGATTCTT

		CGAGAGATCGGAACAAGCCTTTTAAGTTTACACTAG GCAAGC R-GCTTGCCTAGTGTAAACTTAAAAGGCTTGTTCCGA TCTCTCGAAGAATCAAATTTCTTTCCATCTTCAAGCA TCCCC
GFP-EB3 GFP-EB3, CRMP2A GFP-EB3, CRMP2A, shluciferase GFP-EB3, shluciferase GFP-EB3, shFKBP12	pTRIP	The vectors were prepared by our collaborators (Carsten Janke lab, Institut Curie)
GFP-EB3, CRMP2A S27A	pTRIP	CRMP2A S27A was inserted into pTRIP-GFP-EB3 opened by XhoI using SLIC cloning, primers: F-ACCTGGATCCACTAGTGTCGACATGGCCGAGAGAA AGCAATC R-CCATGTTTTTCTAGGTCTCGAGTTAGCCCAGGCTG GTGATG
GFP-EB3, FKBP12	pTRIP	FKBP12 sequence was inserted into pTRIP-GFP-EB3 opened by XhoI using SLIC cloning, primers: F-ACCTGGATCCACTAGTGTCGACATGGGAGTGCAGG TGGAGACCA R-CCATGTTTTTCTAGGTCTCGAGTCATTCCAGTTTTA GAAGCTCCACA
FKBP12	pTRIP	EB3 was removed from pTRIP GFP-EB3, FKBP12 using NheI
GFP	pCAGGS	(Ziak et al., 2020)
CRMP2A	pCAGGS	The CRMP2A sequence was inserted into pCAGGS vector by my colleagues

GFP-tau	pCDNA4	Human full-length tau sequence fused to eGFP; the vector was provided by our collaborators
GFP-tau-ΔN	pCDNA4	Tau sequence with deleted N terminus (tau 242-441) was created from control tau using one-step site-directed deletion, primers: F-CGGCCGCACGCCTGCAGACAGCCCCCGTGCCCAT R-GCAGGCGTGCGGCCGCGGCTCCGAATTCTTTGTATAGT
mCherry-tau	pCDNA4	GFP in vector GFP-tau was replaced by mCherry using KpnI and EcoRI
mScarlet-tubulin		Human tubulin sequence (TUBA1B) fused with mScarlet for lentiviral particles production provided by our collaborators (Carsten Janke lab, Institut Curie)
katanin p60 subunit GFP-katanin p80 subunit	pLL	Vectors were provided by our collaborators (Lansky and Braun lab)
mCherry	pGhU6	The reporter gene in pGhU6 (GFP) was replaced by mCherry sequence using BamHI and EcoRI (followed by treatment with Klenow fragment); the vector was then used for knockdown of proteins

Table 4: Vectors used for knockdown and shRNA sequences

Targeted protein	**TRC library database number** https://www.broadinstitute.org/rnai-consortium/trc-shrna-design-process	**Targeting sequence**	**Cloning details** (Hairpin sequence for insertion into the vector - Forward oligonucleotide)
			pLKO.1
PIN1 (mouse)			(Balastik et al., 2015)
CRMP2A (mouse)			(Balastik et al., 2015)
CRMP2 (mouse)	TRCN0000032641	CCAGTCCTTCTATGCAGACAT	Prepared by my colleague
scrambled (non-silencing control)			(Balastik et al., 2015)
			pGhU6 (HpaI, XhoI)
CRMP4 (mouse)	TRCN0000032673	CCATTCTCTGACTATGTCTAT	AACCCCCCATTCTCTGACTATGTCTATTCAAGAGATAGACATAGTCAGAGAATGGTTTTTGGAA
FKBP12 (mouse)	TRCN0000012492	TGATTCCTCTCGGGACAGAAA	AACCCCTGATTCCTCTCGGGACAGAAATCAAGAGTTTCTG

			TCCCGAGAGGAATCATTTTT GGAA
FKBP12 (mouse)	TRCN0000012489	CCAGGCATCATCCCACCACAT	AACCCCCCAGGCATCATCCC ACCACATTCAAGAGATGTGG TGGGATGATGCCTGGTTTTT GGAA
FKBP12 (mouse)	TRCN0000012491	GCCAAACTGATAATCTCCTCA	AACCCCGCCAAACTGATAAT CTCCTCATCAAGAGTGAGGA GATTATCAGTTTGGCTTTTT GGAA
FKBP12 (mouse)	TRCN0000416982	ACAGCACAAGCGATGGGTTAA	AACCCCACAGCACAAGCGA TGGGTTAATCAAGAGTTAAC CCATCGCTTGTGCTGTTTTTT GGAA
PIN1 (mouse)		CCGGGTGTACTACTTCAATCA	AACCCCCCGGGTGTACTACT TCAATCATCAAGAGTGATTG AAGTAGTACACCCGGTTTTT GGAA (prepared by my colleague)
NSC (non-silencing control)		ATCTCGCTTGGGCGAGAGTAAG	AACCCCATCTCGCTTGGGCG AGAGTAAGTCAAGAGCTTA CTCTCGCCCAAGCGAGATTT TTTGGAA
			pSUPER (BglII, HindIII)
FKBP12	TRCN0000012492	TGATTCCTCTCGGGACAGAAA	GATCCCCTGATTCCTCTCGG GACAGAAATTCAAGAGATTT CTGTCCCGAGAGGAATCATT TTTA
NSC		ATCTCGCTTGGGCGAGAGTAAG	GATCCCCATCTCGCTTGGGC GAGAGTAAGTTCAAGAGAC TTACTCTCGCCCAAGCGAGA TTTTTTA

3.6.1 cDNA library preparation

3.6.1.1 RNA isolation

cDNA library was prepared from WT mouse brain (1-month-old) using Tri-reagent (Sigma – T9424) according to the manufacturer‘s protocol. Briefly, the tissue was homogenized in Tri-reagent (10 µl/mg of tissue) using ultraturrax. After 5 minutes of incubation (RT), chloroform was added (0.2 µl/µl of Tri-reagent) and shaken vigorously (around 15 seconds). After 2 minutes of incubation (RT), the sample was centrifuged (4°C, 15 minutes, 12000 g), the upper (aqueous phase) was transferred to a new tube, and 100% Isopropanol (0.5 µl/µl of Tri-reagent) was added. After 10 minutes incubation (RT), the sample was centrifuged again (10 minutes) and the pellet was washed with 75% ethanol (1 µl/µl of Tri-reagent), mixed well, and centrifuged again (4°C, 5 minutes, 7500 g). The pellet was then air-dried for 5 minutes, resuspended in RNAse-free water, and incubated at 55°C for 10 minutes. Obtained RNA was stored at -80°C, and used for RNA-quality testing and cDNA preparation. The concentration and $A_{260/280}$, $A_{260/230}$ ratios were measured by nanodrop, and the quality of RNA was checked by gel analysis. The electrophoresis was performed using 1% agarose gel (the TBE used was prepared from 0.1% DEPC (Sigma – D5758)) around 1 µg of RNA was loaded.

3.6.1.2 Reverse transcription (cDNA synthesis)

Two µg of the RNA isolated from mouse brain, 4 µl of random hexamers (50µM), 8 µl of dNTPs mix (10mM), and RNAse-free water (final volume 32 µl) were incubated at 65°C for 3 minutes, spun down, and placed on ice. AMV RT buffer was added together with 80 U of RNAse inhibitor (murine, New England Biolabs - M0314S) and 20 U of AMV reverse transcriptase (New England Biolabs – M0277S) getting the final volume of 40 µl. The mixture was incubated at 25°C for 15 minutes, 42°C for 40 minutes, 90°C for 5 minutes, and on ice for 5 minutes. After this, RNAse-free water was added up to 200 µl. The cDNA library was stored at -20°C, and 5 µl was used for the PCR reactions.

3.6.2 PCR

3.6.2.1 Insert amplification

For amplification of desired suquence by PCR, we used primers listed in the Table 3, and 5 µl of cDNA or 500 ng of template vector. The sequence was amplified by 1.25 U Phusion polymerase (with its buffer; New England Biolabs M0530S), 25 pmol of Fwd and Rev primers and 0.2mM dNTPs mix in a final volume of 50 µl. The amplification was done by 30-35 cycles consisted of denaturation at 95°C for 1 minute, annealing for 30 s (the temperature was set according to the primers‘ melting temperature), extension phase at 72°C (the duration was set according to the length of the sequence).

3.6.2.2 QuikChange mutagenesis

The mutagenesis by the QuikChange protocol was performed by PCR using the primers listed in Table 3. We used 20 ng of the template vector, 50 pmol of Fwd and Rev primers, 0.6mM dNTPs mix, 2 U Phusion polymerase (with its buffer), in a final volume of 50 µl. The amplification was done by 18 cycles consisted of denaturation at 95°C for 30 s, annealing for 1 minute (the temperature was set according to the primers‘ melting temperature), extension phase at 72°C (the duration was set according to the length of the sequence). After the PCR, the product was treated with 1µl of DpnI (New England Biolabs) at 37°C overnight.

3.6.2.3 One-step site-directed mutagenesis or deletion

One-step site-directed mutagenesis or deletion was done according to the published protocol (Liu and Naismith, 2008). We used 5-10 ng of the template vector, 50 pmol of Fwd and Rev primers (primers listed in Table 3), 0.6mM dNTPs, 2 U Phusion polymerase (with its buffer), in a final volume of 50 µl. The amplification was done by 12 cycles consisted of denaturation at 95°C for 1 minute, annealing for 1 minute (the temperature was set according to the primers‘ melting temperature), extension phase at 72°C (the duration was set according to the length of the sequence). The PCR was finished with an additional annealing step (the temperature was set according to the primers‘ melting temperature) for 1 minute and an extension step at 72°C for 30 minutes. The PCR product was treated with 1 µl DpnI at 37°C overnight.

All PCR products were analyzed by agarose gel electrophoresis. If needed, the products were subjected to restriction cleavage and/or are purified using GeneJET PCR Purification Kit

(ThermoFisher Scientific - K0702) or GeneJET Gel extraction Kit (ThermoFisher Scientific - K0692). DNA concentration was estimated from the band intensity on the gel or measured using NanoDrop One (ThermoFisher Scientific).

3.6.3 Restriction cleavage and ligation

The vector or insert for DNA cloning were digested using restriction endonucleases from New England Biolabs according to manufacturer‘s instructions. Digested vector was dephosphorylated (Alkaline Phosphatase, Calf Intestinal (CIP), New England Biolabs). Prepared insert and vector were purified using GeneJET PCR Purification Kit (ThermoFisher Scientific - K0702) or GeneJET Gel extraction Kit (ThermoFisher Scientific - K0692). DNA concentration was estimated from the band intensity on the agarose gel or measured using NanoDrop One (ThermoFisher Scientific).

Ligation of insert and vector (usually at the molar ratio of 6:1) was done in the final volume of 10 µl using T4 DNA ligase (New England Biolabs) according to manufacturer protocol at 16°C overnight. The ligation mixture was then transformed into competent bacteria.

3.6.4 SLIC (One-step sequence- and ligation-independent cloning)

SLIC cloning was performed according to the published protocol (Jeong et al., 2012). The insert was prepared using primers with overhangs (15-20 nucleotides overhangs, Table 3) and the vector was opened by restriction cleavage and dephosphorylated. Insert and vector were mixed at a molar ratio of 1:2 in the NEB buffer 2.1 (New England Biolabs) in the final volume of 10 µl. T4 DNA polymerase (0.2 µl, New England Biolabs) was added and the mixture was incubated at RT for 2.5 minutes and then 10 minutes on ice. The mixture was then transformed into competent bacteria.

3.6.5 Knockdown-vectors cloning

For preparation of vectors used for production of shRNA, the oligonucleotides (the hairpin sequence containing the targeting sequence) were ordered (according to the Table 4; only the Fwd sequences are listed). Forward and reverse oligonucleotides (50µM) were annealed in the annealing buffer (10x annealing buffer: 100mM Tris-HCl, pH 8, 10mM EDTA, pH 8, 1M

NaCl) in the final volume of 20 µl. The reaction was incubated at 95°C for 4 minutes and allowed to cool down to RT. The double-stranded oligonucleotides were checked by the gel analysis using 6% agarose gel and 6 µl of them were phosphorylated using T4 DNA kinase (in the T4 buffer, final volume 50 µl; New England Biolabs) at 37°C for 30 minutes, and purified with the PCR purification kit. The prepared inserts (phosphorylated double stranded oligonucleotides) were then ligated into the vector (opened by restriction cleavage and dephosphorylated) in the ratio of 11:1.

3.6.6 Bacterial transformation

The vector for amplification (0.2 µl), the ligation mixture (5 µl), the mixture after SLIC cloning (5 µl), or the PCR product in the mutagenesis treated with DpnI (2 µl) was transformed into RbCl competent E. Coli TOP10 bacteria. The bacteria were cultivated on the agar plate with the relevant antibiotic overnight at 37°C. Several colonies were grown in 5 ml of LB media with the appropriate antibiotic, the vectors were purified (GeneJET Plasmid Miniprep Kit, Thermo - K0503) and the insertion or mutation was verified by control restriction digestion and DNA sequencing (provided by SEQme company).

3.7 Bacterial protein production and purification

Vector pGEX-KG with GST or fused proteins GST-PIN1/GST-FKBP12 was transformed to E. Coli BL-21 (several colonies were tested for protein expression level and one clone for each vector was used for final protein expression), and 100 ml of LB (containing 100 µg/ml Ampicillin - Sigma A9518) was inoculated with transformed bacteria and incubated overnight at 37°C, shaking. The overnight culture was diluted 1:20 into 1l of TB (1.2% tryptone, 2.4% yeast extract, 0.5% glycerol, 0.017M KH2PO4, 0.072M K2HPO4 with 100 µg/ml Ampicillin). The culture was grown up to OD_{600} = 0.5-0.7 and IPTG was added to a final concentration of 0.5mM. After 3 hours (OD_{600} around 1.2), the cells were harvested by centrifugation (4000 g, 20 minutes, 4°C). Bacterial pellet was resuspended in 25 ml of lysis buffer (50mM TrisCl pH 8.0, 500mM NaCl, 1mM EDTA, 1mM EGTA, 5% glycerol, 1mM DTT, 1% Triton X-100, cOmplete™, EDTA-free Protease Inhibitor Cocktail). Bacterial lysis was promoted by incubation with lysozyme (final concentration 0.2 mg/ml, 20 minutes, RT; Sigma, L6876). The lysate was sonicated (5x 1 minute, 60%, 1s ON + 1s OFF) and centrifuged (28000 g, 60

minutes). The supernatant was incubated with glutathione-agarose beads (sigma G4510; swelled before overnight in water and washed 3x with water and 1x with lysis buffer) for 3 hours and then washed (4x with the lysis buffer and 2x with the lysis buffer without triton X-100) and then eluted using 30mM glutathione (Merck, G4251). Eluted protein was dialysed overnight and subsequently 2x for 3 hours (dialysis buffer: 25mM Tris pH 7.4, 150mM NaCl, 5% glycerol, 1mM DTT, 50 µg/ml PMSF; SnakeSkin dialysis tubing, 10K MWCO – 88245 ThermoScientific). The dialysed protein was aliquoted, flash-frozen and stored at -80°C. Purified protein was analyzed by polyacrylamide gel electrophoresis (PAGE) and staining of the gel by coomassie staining. The concentration of the protein was determined using Bradford assay and/or measured by NanoDrop One (ThermoFisher Scientific). Purified proteins were used for pull-down assays and for *in vitro* assays.

3.8 Flag-tagged protein production and purification

Flag-tagged proteins were purified from transfected HEK293T cells. Two days after the transfection, cells were washed with BRB40 (40mM HEPES, 150mM KCl, 1mM EGTA, 2mM $MgCl_2$, pH 6.8) and harvested using a cell lifter. Cell pellet was resuspended in ice-cold lysis buffer (BRB40, 0.1% Tween, 5% glycerol, 1mM DTT, 10 µg/ml Cytochalasin D (Merck - C2618), Benzonase (5U; Merck - 70664), cOmplete™ EDTA-free Protease Inhibitor Cocktail + 10mM ATP (Merck – 797189)). The samples were sonicated (30%, 20 s, 4x) and centrifuged. The supernatant was incubated with anti-flag agarose beads (Anti-DYKDDDDK Tag (L5) Affinity Gel Antibody; BioLegend) overnight at 4°C. After washing (BRB40 + 1mM DTT), the protein was eluted by 3x DYKDDDDK Peptide (ThermoFisher Scientific, A36805), dialyzed against the dialysis buffer (BRB80, 1mM DTT), and flash-frozen. Purified protein was analyzed by PAGE and gel staining. The concentration of the protein was measured by NanoDrop One (ThermoFisher Scientific). Purified proteins were used for *in vitro* assays.

3.9 Whole-mount staining of mouse embryos

Mouse embryos (E10.5-E12.5) were isolated (from heterocrosses of CRMP2 or CRMP2A knockout strains) in PBS and fixed overnight in 4% PFA/PBS at 4°C. After washing with PBS (several times for at least 8 hours), the epitopes were unmasked (4 minutes of boiling in unmasking solution (Antigen Unmasking Solution, Citric Acid Based; Vector - H-3300)). After

washing with PBS, the embryos were incubated in Dent's fix (20% DMSO in Methanol) for 30 minutes at 4°C and bleached overnight (5% H_2O_2 in 20% Dent's fix; 4°C). After washing in Dent's fix (at least 4 hours) and in PBS (3x 30 minutes), blocking was performed (5% FBS, 20% DMSO/PBS, overnight, 4°C) and embryos were incubated with primary antibodies (anti-neurofilament; 1:100 in blocking solution) for 3-4 days at RT. After washing with PBS (overnight, 4°C) and 20% DMSO/PBS (overnight, 4°C), embryos were incubated with secondary antibodies (anti-mouse IgG, HRP-conjugated; 1:1000) for 24 hours, 4°C. After washing (20% DMSO/PBS, 2x 4 hours), the embryos were permeabilized (0.6% Tween/PBS; overnight, 4°C) and washed in PBS (3x 10 minutes, 4°C). Embryos were incubated in DAB solution (0.05% DAB/PBS (3,3'-Diaminobenzidine; Sigma - D8001) for 2 hours, 4°C and the signal was developed using H_2O_2 in the final concentration of 0.03%. After the washing with PBS, embryos were cleared in increasing concentrations of glycerol and stored at 80% glycerol at 4°C. Embryos were captured using Nikon SMZ18 stereomicroscope, the images were processed with Helicon focus and analyzed using FIJI or Neurolucida.

3.10 CRMP2A immunoprecipitation

Immunoprecipitation was performed as described (Balastik et al., 2015). One half of the mouse brain (WT or CRMP2 KO, 1-3 months old) was homogenized using ultraturrax (in the lysis buffer; 50mM HEPES pH 7.4, 150mM NaCl, 10% glycerol, 1% Triton X-100, 1.5mM $MgCl_2$, 1mM EGTA, 100mM NaF, 1mM Na_3VO_4, 1mM DTT, cOmplete™, EDTA-free Protease Inhibitor Cocktail (Roche)), sonicated (30 s, 30%) and centrifuged (20 minutes, 20000 g, 4°C). The supernatant was incubated with Protein A Sepharose beads (10:1; CL-4B; Merck) for 1 hour at 4°C (preclearing). After the preclearing, the supernatant was incubated with the Protein A Sepharose beads preincubated overnight with antibodies (Anti-CRMP2A antibody affinity purified; Balastik et al., 2015) for 24 hours at 4°C. The beads were washed (4x with the lysis buffer) and boiled (98°C, 12 minutes) in 2x Sample Buffer (1:1; 100mM TrisCl pH6.8, 4% SDS, 4% beta-mercaptoethanol, 20% glycerol, 0.2% Bromphenol Blue). The samples were centrifuged and the supernatant (or the diluted lysate as in Input) was loaded on 15% or 7.5% gel for Western blot analysis. Bands were visualized using antibodies anti-FKBP12 and anti-CRMP2 (Table 2).

3.11 Pull-down

HEK293T cells were transfected with pCDNA3 vector expressing proteins of interest tagged with flag-tag. Two days after transfection, cells were washed with PBS and harvested using cell lifter. After centrifugation, cell pellets were homogenized in the lysis buffer (50mM HEPES pH 7.4, 150mM NaCl, 10% glycerol, 0.5% Triton X-100, 1.5mM $MgCl_2$, 1mM EGTA, 1mM NaF, 1mM Na_3VO_4, 1mM DTT, cOmplete™ EDTA-free Protease Inhibitor Cocktail). The lysate was incubated with glutathione-agarose beads (Merck - G4510) pre-incubated with the purified GST-fused protein (1µM protein incubated with the beads for 3 hours at 4°C, washed 2x with the lysis buffer) for 4 hours at 4°C. The beads were washed 5x with the lysis buffer (with 0.1% Triton X-100). Washed beads were boiled in the 2x sample buffer (1:1; 100mM TrisCl pH6.8, 4% SDS, 4% beta-mercaptoethanol, 20% glycerol, 0.2% Bromphenol Blue) and the supernatant was subjected to western blot. The bands were visualized using anti-flag antibody (Table 2).

In the pull-down experiment using FK506, the beads with the GST-FKBP12 bound were incubated with 20µM FK506 (InvivoGen, tlrl-fk5) for 1 hour at 4°C and after washing were used for the incubation with the lysate.

3.12 Mass photometry

Purified proteins were subjected to Mass photometry (TwoMP – Refeyn Ltd., Oxford, UK, Biophysical CF of Centre of Molecular Structure BIOCEV) according to the protocol (Wu and Piszczek, 2021). The proteins were diluted in BRB80 buffer (80mM PIPES, 1mM EGTA, 1mM $MgCl_2$, pH 6.8), 15 µl of the diluted sample was injected into the well of the silikon gasket placed on the cleaned microscope coverslip, and movies of 60 s duration were recorded. The raw data were converted to molecular mass using three-point calibration curve (BSA and TG proteins). The number of events of each size was visualized in the form of histogram with 10 kDa bin width. Mass photometry data acquisition was performed using AcquireMP (Refeyn Ltd.) and the data were processed and analyzed using DiscoverMP (Refeyn Ltd.).

3.13 EB3 assay

Vectors pTRIP expressing GFP-EB3 were used for tracking the growing ends of microtubules in IMCD3 cells. For FKBP12 overexpression, we transduced the cells with EB3 or EB3+FKBP12 and transfected the cells with mCherry-CRMP2A, mCherry-CRMP2A S27A, or mCherry. Cells were captured 48 hours after the transfection. For FKBP12 knockdown, cells were transduced with GFP-EB3, GFP-EB3-CRMP2, or GFP-EB3-CRMP2 S27A and then with pGhU6-mCherry shFKBP12 or NSC. The efficiency of the knockdown/overexpression was checked by western blot. For EB3 tracking in axons of DRG, we used pTRIP expressing GFP-EB3 in combination with CRMP2A or knockdown of FKBP12 (GFP-EB3-CRMP2A-shluciferase; GFP-EB3-shluciferase; GFP-EB3-shFKBP12). DRG were transduced 5 or 24 hours after plating and captured at DIV 3-5.

Cells were captured for 1 minute (every 2 s) in 8-well coverslips (Ibidi – 80827 - µ-Slide 8 Well Glass Bottom) using Nikon Ti-E fluorescence microscope (CFI Plan Apo VC 100X Oil; 37°C, 5% CO_2). Only cells positive for both GFP and mCherry were analyzed. GFP signal was analyzed using FIJI plugin MTrackJ. The mean velocity of the growing microtubules on the periphery of the cell with no contact with other cells was counted. The data are represented in the form of kymographs using FIJI plugin Multi Kymograph.

3.14 In utero electroporation

In utero electroporation was done as previously described (Haddad-Tvólli et al., 2013). Anesthetized mouse (induction by isoflurane 2.5%, maintenance 2% isoflurane) was shaved and the skin was disinfected with ethanol. The incision (around 2 cm long) of the abdominal wall was made and the embryos were pulled out and kept wett (PBS, 37°C). DNA solution (1-3 µl) was injected into the brain lateral ventricle of the embryos using pulled and grinded (30°) borosilicate glass capillaries (Science products – GB100TF-10P). Electric pulses introduced by 5mm electrodes (Electroporator NEPA21-Nepa Gene) were used for DNA delivery into the cells (35 V, 50 msec transfer pulse + 950 msec pause, 5 pulses, impedance must be below 500 kΩ). Abdominal cavity was filled with PBS (37°C) and the ebryos were put back inside. Muscles and skin were sutured and 200 µl of 1% Rimadyl/PBS was injected subcutaneously. Mouse was placed for two hours into the cage on top of a heating pad (37°C) with food and water ad libitum.

For in utero electroporations, vector pSUPER was used for knockdown and pCAGGS was used for overexpression, pCAGGS-GFP was used for visualization of electroporated cells. All vectors used for in utero electroporation were endotoxine-free (NA0410 GenElute™ HP Endotoxin-Free Plasmid Maxiprep Kit; according to the manual) and were diluted to the final concentration of 2 μg/μl in sterile PBS with 0.1% Fastgreen (Merck-F7252).

Embryos were electroporated at E15.5 and analyzed 3 days later (E18.5). Isolated embryos were fixed (overnight, 4°C, 4% PFA/PBS) and sliced using vibratome (150 μm; Leica). The sections were captured in propyl gallate (0.5% N-propyl gallate/90% glycerol/PBS; Merck-P3130) using confocal microscope (Leica TCS SP8).

The amount of cells in the upper third of the cortical plate was analyzed and related to total amount of cells in the whole cortical plate. The analysis was done manually using FIJI or semi-automaticly using TRON software (Taylor et al., 2020).

3.15 Tubulin turbidity assay

Porcine brain tubulin (final concentration 25 μM), flag-tagged GFP-CRMP2A purified from HEK293T cells (final concentration 1.25 μM) and GST-FKBP12 purified from bacteria (final concentration 4.5 μM) were used for tubulin turbidity assay. FKBP12 inhibitor - FK506 (final concentration 40 μM; InvivoGen, tlrl-fk5) was preincubated with FKBP12 for 5 minutes on ice. The assay was performed in 96-well plates with glass bottom (Invitrogen, M33089) in a final volume of 100 μl. All reagents were mixed on ice in BRB80 buffer (80mM PIPES, 1mM EGTA, 1mM $MgCl_2$, pH 6.8) with 25% glycerol, 1mM DTT. After adding 1mM GTP, the absorbance at 350 nm was measured every 15 seconds (for 1 hour, 37°C) using BioTek Cytation3. For quantification of the absorbance in the plateau phase, 20 values at the end of the measurement were averaged.

3.16 Peptidyl-prolyl *cis/trans* isomerase assay

Prolyl isomerase activity was assayed in a chymotrypsin-coupled assay as described previously (Fischer et al., 1984). Chymotrypsin (Merck; 60 mg/ml in 1mM HCl) was incubated with FKBP12 in the reaction buffer (buffer: 50mM HEPES, 100mM NaCl, pH 8) on ice for 10 minutes, the peptide (Suc-AAPF-pNA - Santa Cruz; 3mM, dissolved in 20 mg/ml LiCl in trifluoroethanol) was added and the absorption at 390 nm was measured (every 3 s for 5

minutes). The measurement was performed in 96-well plates with glass bottom (Invitrogen, M33089) in a final volume of 200 µl using BioTek Cytation3.

3.17 *In vitro* tubulin polymerization assay

For *in vitro* tubulin polymerization assay, we used GST-FKBP12 protein purified from bacteria and flag-GFP-CRMP2A protein purified from HEK293T cells. GMPCPP seeds were prepared and the *in vitro* assay was performed. The microtubules were captured using total internal reflection (TIRF) mode of an inverted widefield microscope Nikon Eclipse Ti-E equipped with 100x HP Apo TIRF objective, H-TIRF module (for detailed description of the methods, see the manuscript in the Supplement). The data were analyzed using FIJI NanoJ-Core and Multi Kymograph plugins. The polymerization velocity, the depolymerization velocity, the frequency of catastrophes and the frequency of rescues were analyzed (Zwetsloot et al., 2018). We also analyzed the GFP-positive signal on the growing microtubules as the average length of GFP-possitive ends or as a persistence of GFP signal on growing microtubules.

3.18 Microscopy

The imaging was performed using the microscopes provided by IPHYS Bioimaging facility and Imaging Methods Core Facility at BIOCEV.

3.19 Data analysis and presentation

The analysis were performed using FIJI (ImageJ) if not stated otherwise. GraphPad Prism was used for statistical analysis and graph illustration. For comparison of two independent groups, Welch's t-test or Mann-Whitney test was used according to the data normality unless stated otherwise. The figures were prepared using Adobe Illustrator.

4 Results

4.1 Collapsin response mediator proteins and their isoforms in neural development and neurodegeneration

4.1.1 The amount of CRMP2 isoforms is developmentally regulated

CRMP2 is a microtubule-associated protein important in the processes of neural development. Two isoforms of CRMP2 are produced by alternative splicing (Figure 8) and even though the longer isoform of CRMP2 (CRMP2A) has been not much studied, some differences between CRMP2A and CRMP2B isoforms regarding their effects on microtubules were described (for more details see the introduction; Yuasa-Kawada et al., 2003). We have shown that specifically CRMP2A isoform is enriched in distal axons and it contains a unique phosphorylation site on its N terminus (Ser27; Figure 8) whose phosphorylation promotes the binding of this isoform to prolyl isomerase PIN1 (Balastik et al., 2015) supporting that these two isoforms are differentially regulated and could play different roles in cells. To follow up on this study, we tested the differences between the isoforms and the phosphorylation status of CRMP2A in more detail. As CRMPs were linked mainly to neural development, we first focused on the regulation of the CRMP2 isoforms expression in the development of the murine model. Using the antibody against CRMP2 (both isoforms) and western blotting, we noticed that the ratio between CRMP2A and CRMP2B isoforms seems to be increased in primary embryonic neurons, compared to early postnatal brains (Figure 10A). To verify the specificity of the detected western blot bands, we tested the antibody using CRMP2A KO (mice lacking the CRMP2A isoform; Ziak et al., in preparation) and CRMP2 KO (mice lacking both CRMP2 isoforms; Ziak et al., 2020; Figure 10B) brain lysates showing that the upper band corresponds to CRMP2A. In both isoforms, we detected on Western blots two bands (at least in primary neurons samples) corresponding to the different phosphorylation statuses as described before (Balastik et al., 2015; Yoshimura et al., 2005). We also detected a lower band (around 58 kDa) corresponding to the described cleavage product of CRMP2 (Rogemond et al., 2008). As the brain lysates samples consist of different cell types and CRMP2 was detected also in non-neuronal cells in the brain, mainly oligodendrocytes (Ricard et al., 2000), the difference observed between brain lysates and primary neurons could be the consequence of different type of the sample.

We decided to analyze the relative amount of CRMP2 isoforms during the development in more detail and we characterized CRMP2A and CRMP2B levels in samples of murine brains from embryos to aged mice. Using embryonic brains (E16), young brains (2 months old), adult (6 months old), and aged brains (21 months old), we performed western blotting using antibodies against CRMP2A isoform, phospho-specific CRMP2A antibodies (against CRMP2A phosphorylated on Ser27), and CRMP2 antibodies (used for visualization of CRMP2B). Our results show that the ratio between the two isoforms (CRMP2A/CRMP2B) decreases during life (Figure 10C, D; $p<0.0001$; Kruskal-Wallis test). As the CRMP2A isoform seems to be more temporally regulated, we focused also on its specific phosphorylation (unique site Ser27). The results showed that phosphorylation of Ser27 is significantly decreasing in postnatal and aged brains (Figure 10C, E; $p<0.0001$; Kruskal-Wallis test). These results suggest that CRMP2A isoform is not only more specifically regulated than CRMP2B but also that the phosphorylation of this isoform on its N-terminus is temporally regulated.

Because the phosphorylation on the C-terminus (Ser522 for CRMP2B and Ser623 for CRMP2A) was described as an important regulatory site for CRMP2 function and it was shown that it functions as a priming site for other phosphorylations (Brown et al., 2004; Cole et al., 2006; Yoshimura et al., 2005), we tested if the phosphorylation of Ser27 is dependent on the phosphorylation of Ser623 or vice versa. For this purpose, we used CRMP2A with Alanine (de-phospho-mimetic) mutations (S27A, S623A, S27A S623A). We showed that CRMP2A which can not be phosphorylated on Ser27 is still phosphorylated on Ser623 and vice versa (Figure 10F). The experiment also show the specificity of the phospho-specific antibodies, as the de-phospho-mimetic mutations did not stain positive.

Together, we show that the two CRMP2 isoforms are differently regulated during mouse development and aging. While the amount of CRMP2B is more stable, high levels of CRMP2A isoform, especially its phosphorylated form, are more restricted to earlier developmental stages.

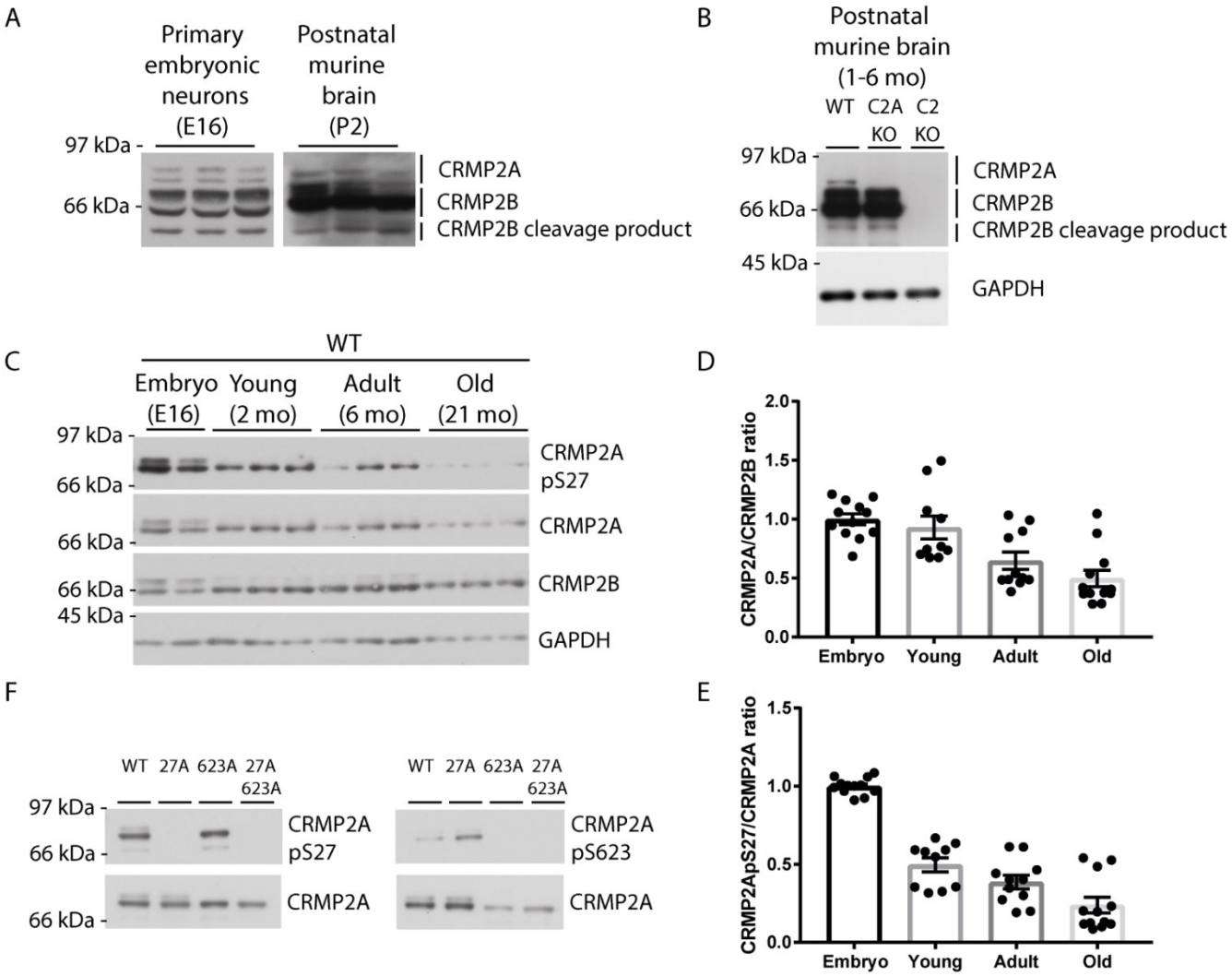

Figure 10: CRMP2A isoform levels and its phosphorylation are regulated in development and aging.

A) The representative images of the western blot showing the two CRMP2 isoforms (with the antibody against the C terminus recognizing both isoforms) in the primary embryonic (E16) neurons culture and in the lysates of postnatal (P2) murine brains. Upper bands correspond to longer CRMP2A isoform (expected size 75 kDa) while lower bands correspond to CRMP2B (expected size 64 kDa). The cleavage product of CRMP2 was also detected. B) Brain lysates of 1-6 months old wild-type (WT), CRMP2A KO (CRMP2A knockout, denoted as C2A KO) and CRMP2 KO (CRMP2 knockout, denoted as C2 KO) mice. Upper bands correspond to longer CRMP2A isoform (expected size 75 kDa) while lower bands correspond to CRMP2B (expected size 64 kDa). The cleavage product of CRMP2 was also detected. GAPDH was used as a loading control. C) Representative images of western blot analysis of murine brain lysates from different age groups (embryo (E16), young (2 months old), adult (6 months old), and old (21 months old)). Antibodies against phosphorylated CRMP2A on Ser27 (CRMP2A pS27), CRMP2A, and CRMP2 (only the band corresponding to CRMP2B was analyzed) were used. GAPDH was used as a loading control. D) Quantification of the relative ratio between the CRMP2 isoforms (CRMP2A/CRMP2B ratio) in the different age groups (embryo = 1 ± 0.05, young = 0.93 ± 0.10, adult = 0.65 ± 0.07, old = 0.50 ± 0.07). Represented as mean ± SEM. 3 brain lysates were analyzed in 3-4

western blots in each group. E) Quantification of the relative ratio between the phosphorylated CRMP2A and total CRMP2A (CRMP2ApS27/CRMP2A ratio) in the different age groups (embryo = 1 ± 0.02, young = 0.50 ± 0.04, adult = 0.39 ± 0.04, old = 0.24 ± 0.05). Represented as mean ± SEM. 3 brain lysates were analyzed in 3-4 western blots in each group. F) Representative images of western blot analysis of mutated forms of CRMP2A protein expressed in HEK293T cells (wild-type (denoted as WT), CRMP2A S27A (denoted as 27A), CRMP2A S623A (denoted as 623A) and CRMP2A S27AS623A (denoted as 27A623A)). Antibodies against phosphorylated CRMP2A proteins (CRMP2A pS27 and CRMP2A pS623) and the antibody against CRMP2A were used.

Some of the data are a part of the manuscript in preparation (Ziak et al., in preparation).

4.1.2 Both CRMP2 isoforms form oligomers *in vitro*

It was suggested before, that CRMP2 in its monomeric form binds to tubulin dimers, while CRMP2 tetramers can bind and stabilize polymerized microtubules (Niwa et al., 2017). To test if there is a difference between the two isoforms in the probability of tetramer formation, we compared the tetramerization of CRMP2 isoforms using mass photometry. As a control, we prepared the mutated CRMP2 proteins (CRMP2B Y479E and CRMP2A Y580E) which are not able to form tetramers (Zheng et al., 2018). As expected, the mutated CRMP2 molecules exhibit peaks corresponding to the CRMP2 monomer (94 kDa for CRMP2B and 105 kDa for CRMP2A) and dimer (188 kDa for CRMP2B and 210 kDa for CRMP2A), but no peak was detected in the expected size of tetramers. In contrast, both WT CRMP isoforms exhibited a peak corresponding to the size of CRMP2 tetramers (376 kDa for CRMP2B and 420 kDa for CRMP2A; Figure 11).

Thus, our *in vitro* data show that both isoforms CRMP2A and CRMP2B form tetramers in solution similarly and that the described phospho-mimetic point mutation is able to abolish the tetramerization (while retaining the ability to form dimers as it was described in the case of CRMP2B; Niwa et al., 2017). Thus, our data indicate that the described different effects of CRMP2A and CRMP2B on microtubules (Yuasa-Kawada et al., 2003) are not due to the different preferred oligomerization states of the two isoforms.

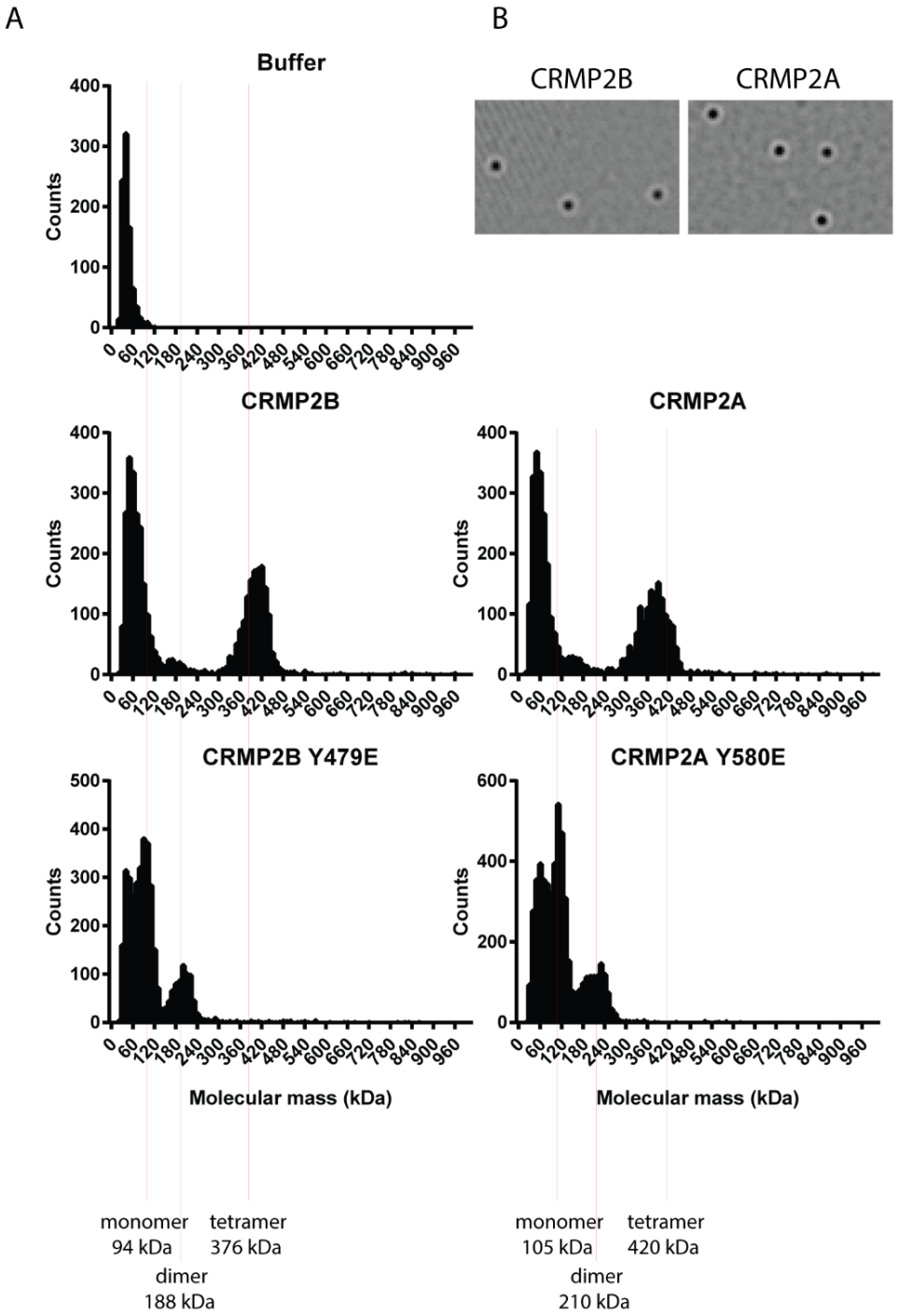

Figure 11: Both CRMP2 isoforms oligomerize in vitro.

A) Distributions of particles of different sizes in the sample presented as histograms (x-axis showing molecular mass, y-axis the number of events) measured by mass photometry. The buffer used for the sample dilution was measured as a control. Orange lines are showing peaks according to the expected molecular masses for the monomeric, dimeric, and tetrameric forms of CRMP2B (94, 188 and 376 kDa respectively) and CRMP2A (105, 210 and 420kDa respectively). Mutated forms of CRMP2 unable to form tetramers (CRMP2B Y479E, CRMP2A Y580E) were used as controls. C) Representative single ratiometric frames (for CRMP2B and CRMP2A samples) obtained by Mass Photometry.

The constructs for the purification of proteins used for Mass photometry were prepared by my colleague Djamel Eddine Chafai under my supervision. I performed the Mass Photometry experiments in the Biophysical CF of the Centre of Molecular Structure BIOCEV.

4.1.3 CRMP2, but not CRMP2A deficiency affects the growth of peripheral nerves

CRMP2 has been identified as a downstream factor in Sema3A signaling (Goshima et al., 1995). We have shown that CRMP2A isoform is enriched in the growth cones of axons and that PIN1 stabilizes specifically CRMP2A isoform and buffers low-level Sema3A stimulation (Balastik et al., 2015). We have also shown that decreased levels of PIN1 lead to inhibited axon growth which can be rescued by CRMP2A overexpression (Balastik et al., 2015). Moreover, PIN1 KO embryos display shorter and less branched processes in cranial nerves, the opposite of what was described for Sema3A (or its downstream targets) knockouts (Kitsukawa et al., 1997; Taniguchi et al., 1997). This suggests a specific role of CRMP2A isoform in mediating Sema3A signaling.

To test this hypothesis, we stained the embryos of CRMP2 KO mice (lacking both CRMP2 isoforms) and CRMP2A KO mice (lacking specifically CRMP2A isoform) and analyzed the growth and branching of the trigeminal nerve (which is regulated by Sema3A and overgrowth of this nerve was found in Sema3A KO mice; Kitsukawa et al., 1997). The growth and branching of the ophthalmic branch of the trigeminal nerve were significantly increased in CRMP2 KO mice at E10.5-E12.5 (the growth of the spinal nerves was increased as well; Figure 12A-B; Ziak et al., 2020). The observed phenotype suggests that the growth-promoting function of CRMP2 can be compensated by other factors (at least in the tested areas) while its function as a mediator of repulsive guidance signals is not substituted. Interestingly, the isoform-specific knockout (CRMP2A KO) did not show any significant difference in the peripheral nerves in the developing embryos (Figure 12C-D) which suggests that CRMP2B isoform can substitute the function of CRMP2A in mediating Sema3A signaling in peripheral nerves in CRMP2A deficient mice. We did not see an increase of CRMP2B expression in CRMP2A KO mice in brain lysates by western blotting though (Figure 10B), and we have shown that deficiency of PIN1 (which regulates specifically CRMP2A isoform) is able to affect the peripheral nerves growth in the development. However, there could be changes of CRMP2B levels in distal parts of axons (where we found the CRMP2A-PIN1 regulation; Balastik et al., 2015) which may not be detectable by western blotting in brain lysates. The compensation can also be due to other members of the CRMP family as several of them have

been connected to Sema3A signaling (Deo et al., 2004; Uchida et al., 2005) and may be substrates of PIN1 via another phosphorylation site (the phosphorylation site regulating the binding of PIN1 to CRMP2A is unique for this isoform; Balastik et al., 2015).

Together, our data show that while CRMP2 is critical for the development of the peripheral nervous system, the function of CRMP2A in this area is redundant.

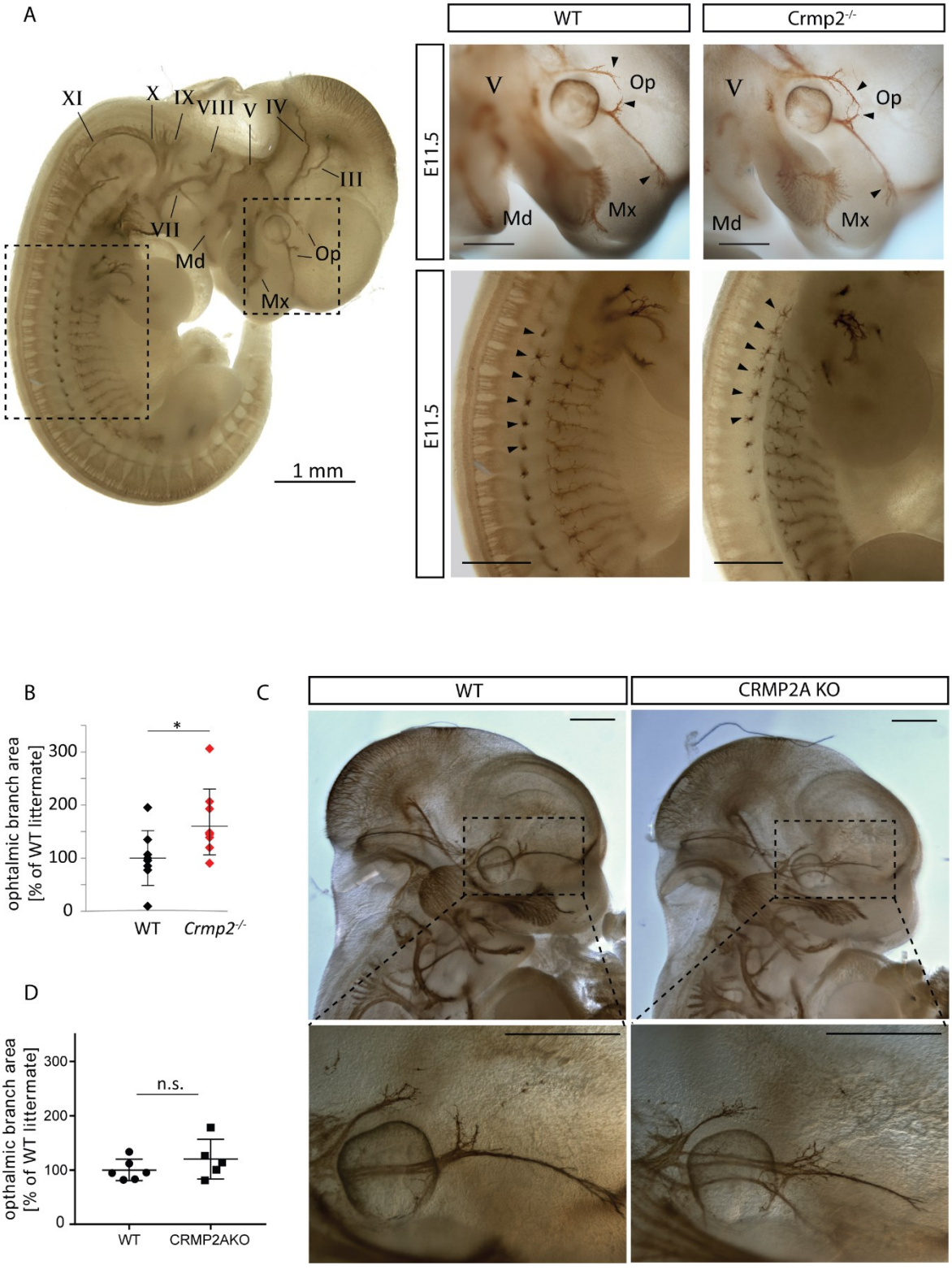

Figure 12: CRMP2, but not CRMP2A regulates the growth of peripheral axons.

*A) Mouse embryo (E11.5) stained with the antibody against neurofilaments to label peripheral nerves (III—oculomotor, IV—trochlear, V—trigeminal, VII—facial, VIII—vestibulocochlear, IX—glossopharyngeal, X—vagal, and XI—accessory nerve. Op—ophthalmic branch, Mx—maxillar branch, and Md—mandibular branch of the trigeminal nerve). Dashed rectangles marking the zoom-in regions (in the right panels) showing the comparison of wild-type (WT) and CRMP2 KO mouse (Crmp2$^{-/-}$) focusing on the ophthalmic branch of the trigeminal nerve (upper panels) and the spinal nerves (lower panels). Both regions show increased growth and branching in CRMP2 KO embryos (indicated by the arrows). The quantification of the spine nerves is not shown here but it is shown in the attached publication (Ziak et al., 2020) B) Quantification of the area innervated by the ophthalmic branch of the trigeminal nerve in CRMP2 KO (Crmp2$^{-/-}$) mice normalized to wild-type (WT) littermates. The innervated area is increased by 66% in CRMP2 KO mice (*p<0.05, n=10). C) Heads of mouse embryos (E11.5) stained with the antibody against neurofilaments of wild type (WT) and CRMP2A knockout mouse (CRMP2A KO) with the dashed rectangles marking the zoom-in regions shown in lower panels focusing on the ophthalmic branch of the trigeminal nerve. D) Quantification of area innervated by the ophthalmic branch of the trigeminal nerve in CRMP2A KO mice normalized to wild-type (WT) littermates. The innervated area is increased by 20% in CRMP2 KO mice (n.s.=not significant; p=0.2772 (unpaired t-test), n=6 and 5 for WT and CRMP2A KO respectively. Scale bars: 500 µm (if not marked otherwise).*

The final pictures and the final analysis were done by Jakub Žiak and are part of a publication (Ziak et al., 2020) or of a manuscript in preparation (Ziak et al., in preparation).

4.1.4 CRMP4 mediates motor neuron loss in Amyotrophic lateral sclerosis

CRMP protein family members have been shown to form heterotetramers, the composition of which may modulate their function. CRMP2 was shown to interact with one of its sequentially closest family member - CRMP4 (Quach et al., 2020; Tan et al., 2015) and we and others have shown that CRMP2 KO mice have increased levels of CRMP4 protein (Figure 13A; Nakamura et al., 2016; Ziak et al., 2020). CRMP4 is spliced into two isoforms and a correlation was found between the degree of damage to the neuromuscular junctions and changes in CRMP4a (the shorter CRMP4 isoform) expression (Duplan et al., 2010). The upregulation of CRMP4a is sufficient to trigger muscle denervation and motor neuron degeneration *in vivo*, and specific mutations in the N-terminus of CRMP4 were associated with Amyotrophic lateral sclerosis (ALS) in patients (Duplan et al., 2010; Valdez et al., 2012). ALS is a degenerative motor neuron disease and it is the most common motor neuron disease in adults. Interestingly, Sema3A is involved in the pathobiology of the SOD1 ALS mouse model (Venkova et al., 2014) and CRMP4a was shown to be elevated in the neuromuscular junctions of the SOD1 mouse model of ALS (Duplan et al., 2010; Valdez et al., 2012). However, the mechanism of the toxicity mediated by CRMP4 is not clear.

Considering the changes of CRMP4 in CRMP2 KO mice, we chose to test its effect on neurons in more detail in a collaborative project with the laboratory of Prof. Eran Perlson

(University of Tel Aviv, Israel) focusing on the role of CRMP4 in motor neurons and in the ALS. First, we prepared the constructs for lentiviral knockdown of CRMP4 protein and tested their efficiency (and the specificity of anti-CRMP4 antibody: Millipore AB5454) in primary neuron cultures using western blot (Figure 13B) and immunocytochemistry (Figure 13C). Using the tested antibody, we demonstrated that CRMP4 is not only increased in motor neurons of ALS but also mislocalized (Maimon et al., 2021). Moreover, the mislocalization in the ALS-diseased neurons was reinforced by Sema3A exposition and was dependent on molecular motor dynein (Maimon et al., 2021).

It was shown that CRMP2 binds to dynein and that the binding is mediated by two specific domains (Arimura et al., 2009). To test if the interaction between CRMP4 and dynein is mediated by the homologous domains as in CRMP2, we cloned the sequence of CRMP4 isoforms into expression vectors (pCDNA3 vector for production of flag-tagged protein and pLL3.7 for GFP-CRMP4a; Figure 13D, E). Subsequently, we deleted the part corresponding to the dynein binding domains in CRMP2 in the GFP-CRMP4a sequence (deletion of amino acids 100-150; denoted as GFP-CRMP4Δ100-150; Figure 13E). Those constructs were used for immunoprecipitation of endogenous dynein intermediate chain in COS7 cells. The results show the interaction of the dynein intermediate chain with the full-length CRMP4 but not with the truncated CRMP4 (Maimon et al., 2021; Figure 14A, B). The binding of the full-length CRMP4 was also reduced by the presence of blocking peptides (the mixture of four peptides designed to bind to the proposed dynein binding domain; Maimon et al., 2021; Figure 14A, B).

Using the flag-tagged CRMP4a in the pCDNA3 vector, we also tested the interaction between CRMP4 and dynactin (a dynein activator) showing that CRMP4 co-immunoprecipitates with dynactin and this interaction decreases in the presence of blocking peptides (Maimon et al., 2021; Figure 14C, D) further supporting the interaction between CRMP4 and the dynein/dynactin complex. Next, we prepared a plasmid for expression of CRMP4-dynein-binding motif sequence (amino acids 100-150; denoted as GFP-50aa; Figure 13E) and used it (instead of the mixture of blocking peptides) for dominant-negative inhibition of co-immunoprecipitation of CRMP4 with the dynein intermediate chain. The results showed lower binding of CRMP4 to dynein in the presence of GFP-50aa supporting the importance of this domain (amino acids 100-150) for CRMP4/dynein/dynactin binding (Maimon et al., 2021).

Finally, we prepared a vector expressing CRMP4a with I141V mutation identified in ALS patients (Blasco et al., 2013). This mutation is located in the dynein-binding motif suggesting that its toxicity in ALS patients can be due to altered CRMP4a-dynein interaction. Indeed, the

immunoprecipitation experiments show the enhanced formation of the CRMP4 I141V-dynein complex (Maimon et al., 2021; Figure 14E, F).

Together, the experiments show that CRMP4a is mislocalized in ALS neurons because of the formation of a complex with dynein mediated by the amino acids 100-150 in CRMP4a, and suggest that altered CRMP4a-dynein interaction may promote motor neuron death in ALS patients (Maimon et al., 2021).

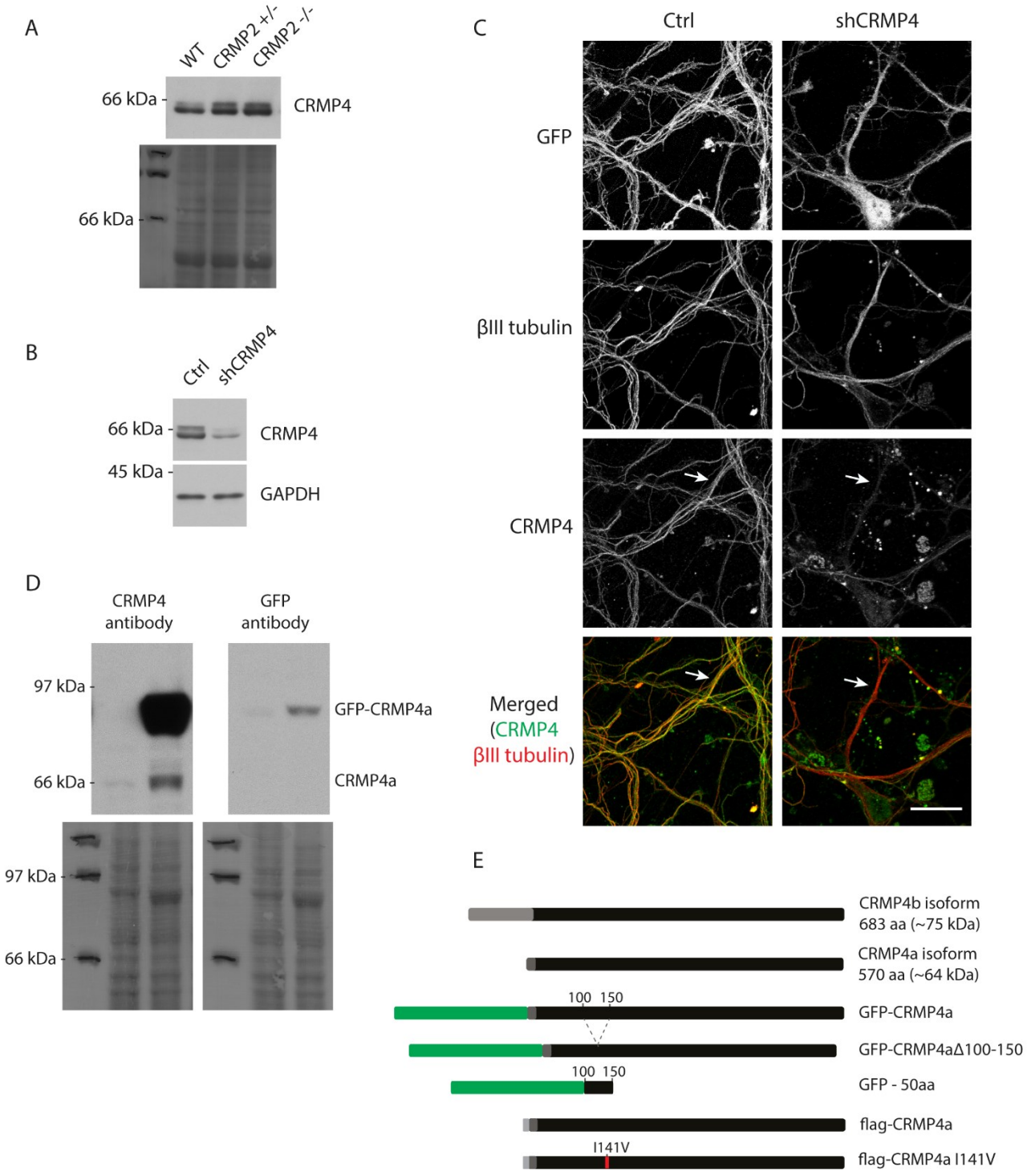

Figure 13: CRMP4 constructs for studying motor neuron loss in Amyotrophic lateral sclerosis.

A) Representative western blot of brain lysates of wild-type (WT), CRMP2 heterozygote (CRMP2 +/-), and CRMP2 knockout (CRMP2 -/-) mice (1-month-old). Antibody against CRMP4 was used. Coomassie staining of the membrane serves as a loading control. B) Representative images of western blot of lysates of primary neurons culture transduced with CRMP4 knockdown (shCRMP4) or non-silencing control (Ctrl). Anti-CRMP4 and anti-GAPDH (loading control) antibodies were used. C)

Primary cortical neurons transduced with CRMP4-silencing lentiviral vector (shCRMP4) and control cells (Ctrl; transduced with the vector carrying non-silencing control sequence). Cells carrying the vector are GFP-positive. Cells were fixed and immunostained using antibodies against CRMP4 and βIII-tubulin (neuronal marker). Scale bar: 20 μm. D) Representative western blot showing the expression of GFP-tagged CRMP4a inserted into pLL3.7 vector in HEK293T cells. Antibodies against CRMP4 and GFP were used. Coomassie staining of the membrane serves as a loading control. E) Schematic representation of CRMP4 isoforms and prepared variants of the protein-expressing vectors with GFP indicated in green and flag in light gray.

I prepared and tested the constructs used. Results obtained using the vectors are a part of the publication (Maimon et al., 2021).

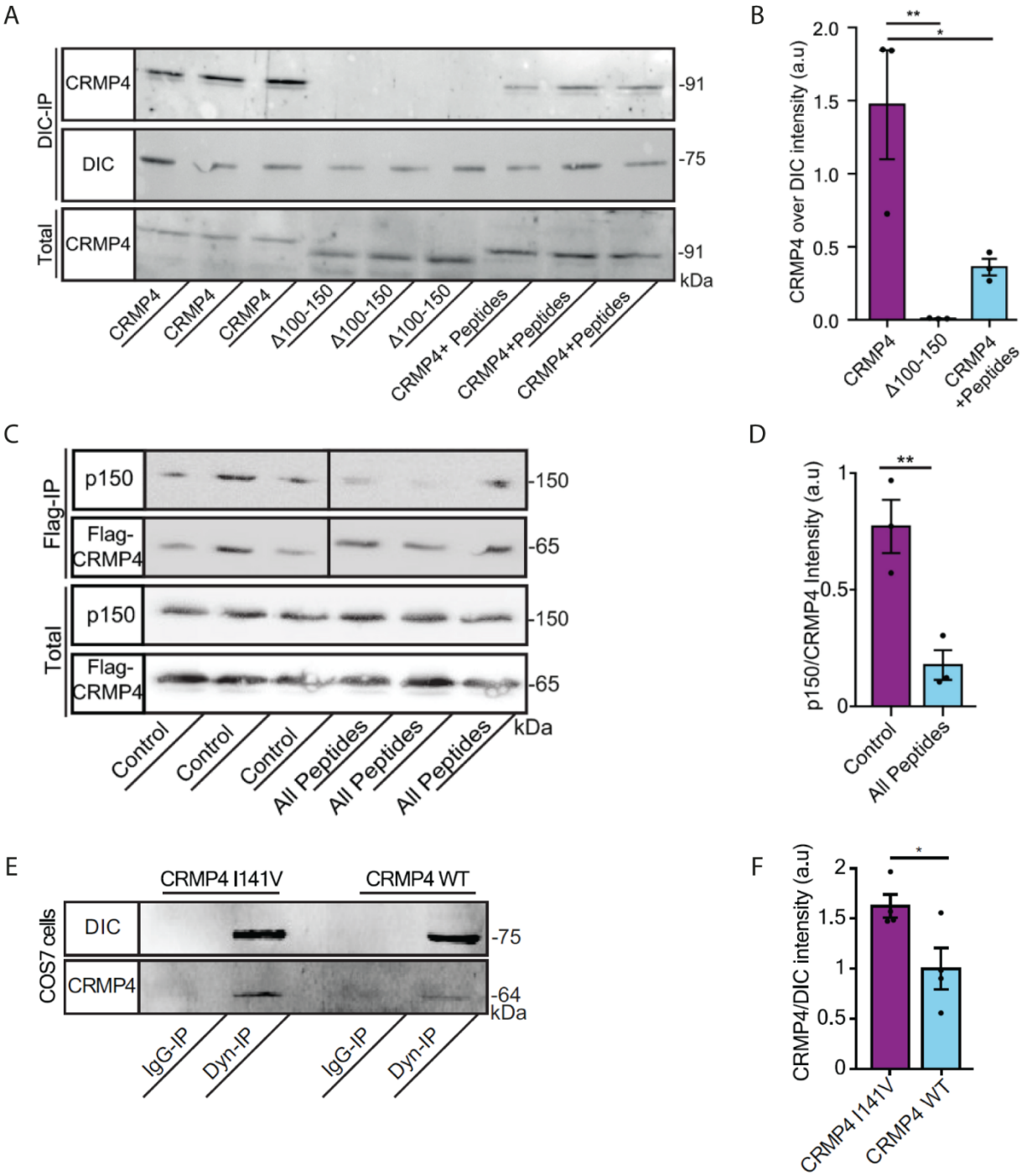

Figure 14: CRMP4 interacts with dynein through domain located between amino acids 100-150.

*A) Co-immunoprecipitation of dynein intermediate chain (DIC) and CRMP4 from COS7 cells overexpressing GFP-CRMP4a or GFP-CRMP4aΔ100-150. In the CRMP4+peptides group, GFP-CRMP4a overexpressing cells were preincubated with a 10μM mixture of 4 peptides homologous to the deleted region in CRMP4 (100-150). Immunoprecipitated samples were analyzed using western blot. The lower panel shows the amount of overexpressed proteins in the input. B) Quantification of the co-immunoprecipitation experiment shown in A). Data are presented as mean ± SEM; One-way ANOVA, Tukey's multiple comparisons test; **p<0.01; * p< 0.05; n = 3 experiments. C) Co-immunoprecipitation of flag-CRMP4 and dynactin (denoted as p150) from COS7 cells overexpressing flag-CRMP4a in the presence or absence of four blocking peptides (peptides homologous to the region*

*100-150 of CRMP4a). Immunoprecipitated samples were analyzed using western blot. Lower panels show the amount of proteins in the input. D) Quantification of the co-immunoprecipitation experiment shown in C). The intensity of the dynactin band was normalized to the flag-CRMP4 band in each repeat. Data are presented as mean ± SEM; Student's t-test; **p=0.01; n = 3 repeats. E) Co-immunoprecipitation of dynein intermediate chain (DIC) and CRMP4 from COS7 cells overexpressing WT or mutant CRMP4 (I141V). Control IgG antibody was used as a negative control. F) Quantification of the co-immunoprecipitation experiment shown in E). The intensity of the CRMP4 band was normalized to the intensity of the DIC band in each repeat. Data are presented as mean ± SEM; Student's t-test; * p<0.05; n = 4 experiments.*

I prepared the vectors used in these experiments. The experiments, analysis, and final pictures were done by our collaborators from the laboratory of Prof. Eran Perlson (University of Tel Aviv, Israel) and are a part of the publication (Maimon et al., 2021).

4.2 Prolyl isomerases and their role in the regulation of CRMP2A function, microtubule dynamics, and axon growth

4.2.1 PIN1 knockout mice have similar temporal CRMP2A regulation as WT

We have previously shown that prolyl isomerase PIN1 can stabilize Cdk5-phosphorylated CRMP2A isoform (Balastik et al., 2015; Figure 8). Since we found that the levels of the two CRMP2 isoforms are differentially regulated during life and that phosphorylation of CRMP2A is also temporally regulated (Figure 10C-E), we hypothesized that this could be the effect of temporal regulation of PIN1 prolyl isomerase. To test this, we analyzed the time profile of PIN1 expression in our samples of mouse brains of different ages (the samples analyzed in Figure 10C-E). PIN1 amount decreased significantly with age ($p<0.0001$; one-way ANOVA; Figure 15A-B) which is consistent with previously published data (Nakamura et al., 2012b) and also with the premature-aging-like phenotype observed in PIN1 knockout mice (Liou et al., 2002).

The decrease of PIN1 amount (and thus lower stabilization of CRMP2A) in time, could be the reason for decreasing levels of CRMP2A (and particularly phosphorylated CRMP2A) observed during the time in Figure 10C-E. To test this hypothesis, we analyzed the levels of CRMP2 isoforms and CRMP2A phosphorylation in developing, adult, and aged PIN1 KO brains. The profiles as well as the amounts of studied proteins show no apparent differences compared to the results observed with WT brains (Figure 15C, D, E) which could be explained by the adaptation of PIN1 KO mice to the absence of PIN1 via genetic compensation (Rossi et al., 2015). The role of PIN1 in regulating CRMP2A could be substituted by other prolyl isomerases even though PIN1 is the only known phospho-specific prolyl isomerase. It was discussed that PIN1 regulates many cellular processes (including cell cycle) but the phenotype of PIN1 KO mice is rather mild, so the existence of a compensation mechanism has already been speculated (Liou et al., 2002).

Together, we show that there are no apparent differences in the amount and phosphorylation of CRMP2A in the PIN1 KO mouse brains even though we have shown that knockdown of PIN1 leads to decrease of CRMP2A level and phosphorylation in primary neurons (Balastik et al., 2015; Figure 18B, C, D).

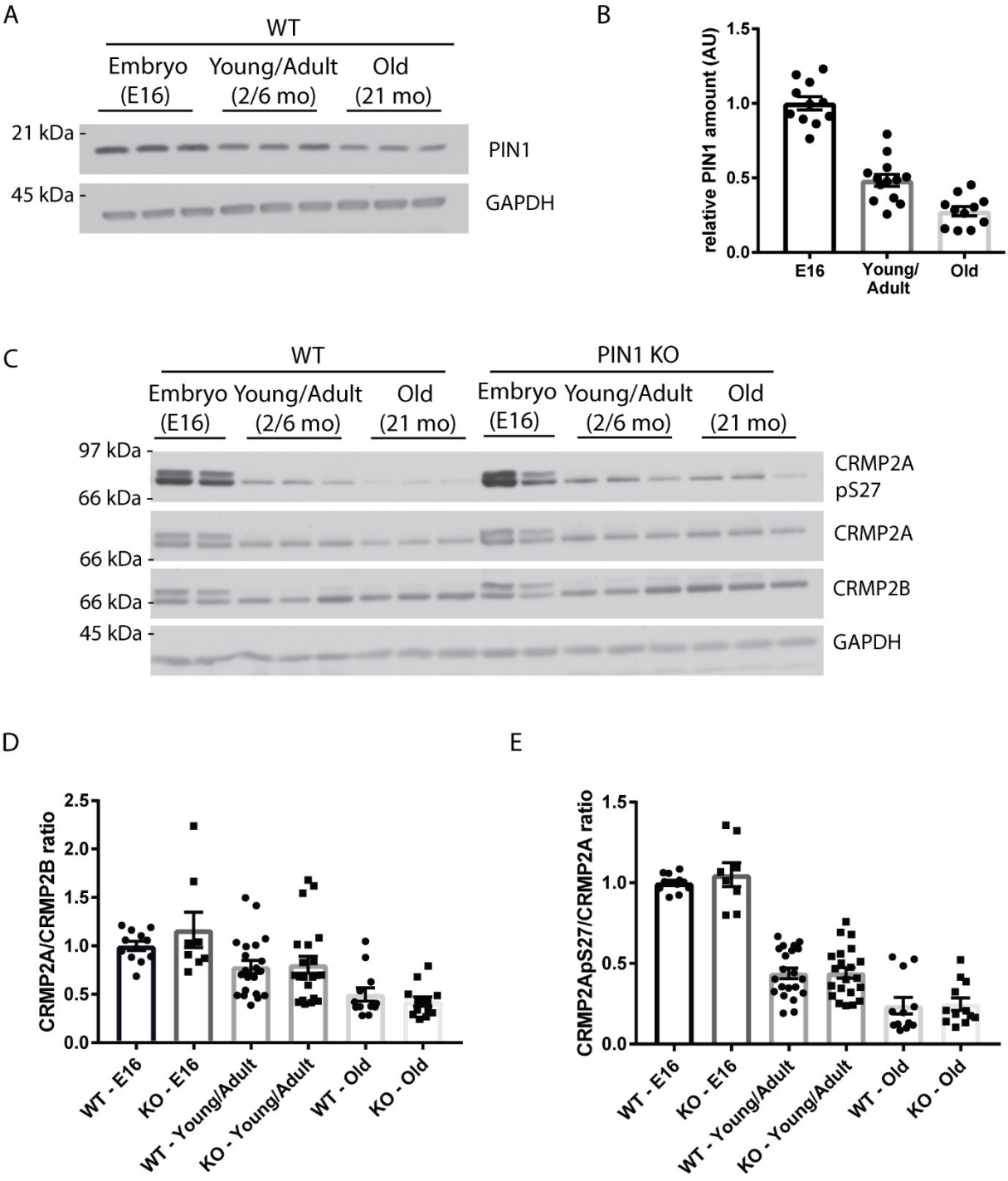

Figure 15: PIN1 knockout mice have similar temporal CRMP2A regulation as WT.

A) Representative western blot showing the amount of PIN1 protein in lysates of mouse brains of different ages (embryos at embryonic day 16 (E16), Young/Adult mice (2-6 months old), and Old mice (21 months old)). Antibodies against PIN1 were used, GAPDH was used as a loading control. B) Quantification of the relative amount of PIN1during the studied time points (embryo = 1 ± 0.04, Young/Adult = 0.48 ± 0.04, Old = 0.28 ± 0.03. Represented as mean ± SEM. 3 brain lysates were analyzed in 4 western blots in each group. C) Representative western blot showing the amount of CRMP2 isoforms and CRMP2A Ser27 phosphorylation in brain lysates of different age groups.

Antibodies against phosphorylated CRMP2A on Ser27 (CRMP2A pS27), CRMP2A, and CRMP2 (only the band corresponding to CRMP2B was analyzed). GAPDH was used as a loading control. D) Quantification of the relative ratio between the CRMP2 isoforms (CRMP2A/CRMP2B ratio) in the different age groups (WT embryo (denoted as WT-E16) = 1 ± 0.046, WT-Young/Adult = 0.78 ± 0.067, WT-Old = 0.50 ± 0.070, PIN1KO embryo (denoted as KO-E16) = 1.17 ± 0.18, PIN1KO Young/Adult (denoted as KO-Young/Adult) = 0.80 ± 0.09, PIN1KO Old (denoted as KO-Old) = 0.43 ± 0.05). Represented as mean ± SEM. 3 brain lysates (2 brain lysates in the PIN1KO – embryo group) were analyzed in 3-4 western blots in each group (the Young and Adult groups were merged). E) Quantification of the relative ratio between the phosphorylated CRMP2A and total CRMP2A (CRMP2ApS27/CRMP2A ratio) in the different age groups (WT embryo (denoted as WT-E16) = 1 ± 0.02, WT-Young/Adult = 0.44 ± 0.03, WT-Old = 0.24 ± 0.05, PIN1KO embryo (denoted as KO-E16) = 1.05 ± 0.07, PIN1KO young/adult (denoted as KO-Young/Adult) = 0.44 ± 0.03, PIN1KO old (denoted as KO-Old) = 0.25 ± 0.04). Represented as mean ± SEM. 3 brain lysates (2 brain lysates in the PIN1KO – embryo group) were analyzed in 3-4 western blots in each group (the Young and Adult groups were merged).

The data from WT brains (the part of the experiment shown in C-E is also presented in Figure 10C-E).

4.2.2 Prolyl isomerase FKBP12 binds CRMP2A isoform

Prolyl isomerase PIN1 regulates phosphorylated CRMP2A isoform (Balastik et al., 2015). Whether other prolyl isomerases regulate conformation of CRMP2A and may partially compensate for PIN1 deficiency in PIN1 KO mice is so far not known. To address this question, we have first investigated if other prolyl isomerases can bind to CRMP2 and regulate its function. We focused first on FKBP12, a member of the FKBP family of prolyl isomerases containing a single prolyl isomerase domain. Even though FKBP12 was first described in connection with immune reaction, FKBP12 is highly expressed in the brain and its level, like that of PIN1, is altered in the brains of patients with neurodegenerative diseases and it was hypothesized that FKBP12 might play a role in axonal transport (Avramut and Achim, 2002).

To test if FKBP12 binds to CRMP2, we first performed an immunoprecipitation experiment using antibodies against CRMP2A protein. The results show that FKBP12 is indeed co-immunoprecipitated together with CRMP2A from the WT murine brain lysate, but not from the CRMP2 KO brain lysate which was used as a negative control (Figure 16A). There is also a significant amount of immunoprecipitated CRMP2B which is consistent with the published data showing that the CRMP members can form heterotetramers (Stenmark et al., 2007; Wang and Strittmatter, 1997).

Hence, to test if there is a specific binding of FKBP12 to only one of the CRMP2 isoforms, we performed a pull-down experiment using HEK293T cells which have low endogenous expression of CRMP proteins (The human protein atlas; Karlsson et al., 2021). We

overexpressed flag-tagged CRMP2A, CRMP2B, or C-terminally truncated CRMP2 isoforms (CRMP2AΔ604 and CRMP2BΔ503; Figure 16D), since the C-terminus is considered the main regulatory region of CRMP2 carrying most of the phosphorylation sites, and tested their binding to FKBP12. The results show that FKBP12, similar to PIN1, binds predominantly to CRMP2A isoform ($p=0.01$, Figure 16B, C). Interestingly, there is a non-significant trend of increased binding in the absence of the C-terminus ($p=0.16$, Figure 16B, C). These results suggest that the N-terminus extension which is present only in CRMP2A isoform is critical for FKBP12 binding while the regulatory C-terminus possibly has an inhibitory effect.

To test the binding in more detail and to verify the specificity of our pull-down assays, we performed the pull-down of CRMP2A in the absence or presence of FK506 (tacrolimus, FKBP12 inhibitor). Indeed, FK506 decreased the binding, suggesting competition of CRMP2A and FK506 for the FKBP12 hydrophobic binding site pocket (Figure 16E).

Finally, as it was shown that both CRMP2 and FKBP12 are abundant in neurons (Kamata et al., 1998; Steiner et al., 1992) and CRMP2A isoform is enriched in axonal growth cones (Balastik et al., 2015), we wanted to show that endogenous FKBP12 and CRMP2A can interact in neurons. We stained primary neuron cultures for FKBP12 and CRMP2A to show their co-localization. Indeed, we detected a partial co-localization of FKBP12 and CRMP2A in neurons, particularly in distal axons and axonal growth cones (Figure 16F).

Together, the results indicate that FKBP12 binds specifically to CRMP2A isoform in the distal parts of growing axons.

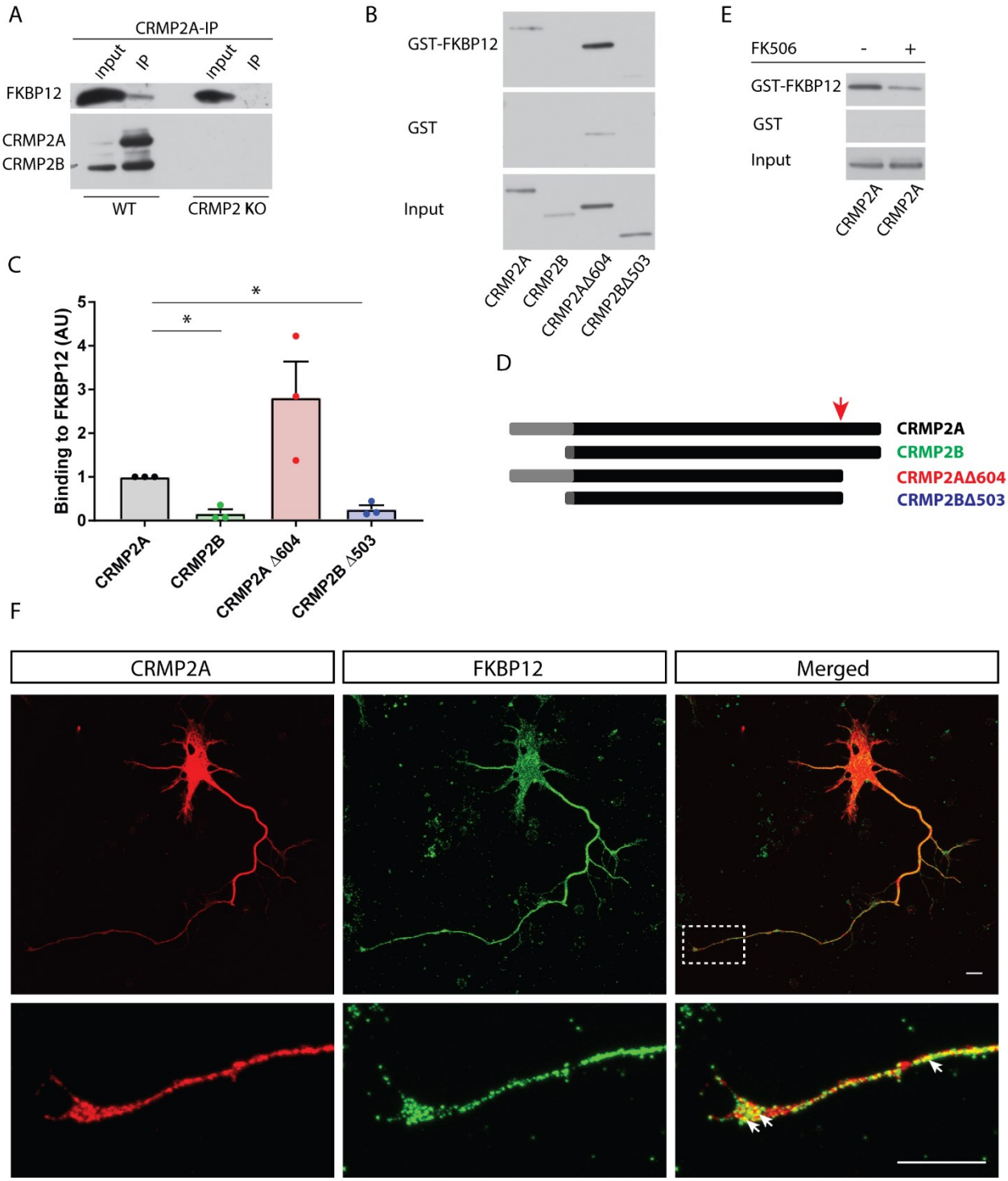

Figure 16: Prolyl isomerase FKBP12 interacts with CRMP2A in distal axons.

A) Co-immunoprecipitation experiment using antibody against CRMP2A. Brain lysates of either wild-type (WT) or CRMP2 knockout (CRMP2 KO) young mice (1-3 months old) were used. Immunoprecipitated proteins (IP) and the used lysate (Input) were visualized by western blot using antibodies against CRMP2 (both isoforms) and FKBP12. B) Pull-down experiment from HEK293T-cell lysates overexpressing flag-tagged CRMP2A, CRMP2B or their truncated forms CRMP2AΔ604 and

*CRMP2BΔ503 respectively. The proteins were pulled down using glutathione-agarose beads together with purified GST-FKBP12 or GST as a negative control. CRMPs were visualized using anti-flag antibody. C) Quantification of the pull-down experiment presented in B) normalized to the input and related to CRMP2A (CRMP2A = 1 ± 0; CRMP2B = 0.16 ± 0.10; CRMP2AΔ604 = 2.82 ± 0.82; CRMP2BΔ503 = 0.26 ± 0.09; mean ± SEM, Welsch's t-test; *p<0.05; n = 3 experiments). D) Schematic illustration of truncated isoforms used for the pull-down experiment presented in B) and C). E) Pull-down experiment from HEK293T cells overexpressing flag-CRMP2A in the absence (-) or the presence (+) of FK506. F) Double-immunostaining of primary neurons (DIV4) using antibodies against CRMP2A (red) and FKBP12 (green). The dashed rectangle marks the zoomed-in region shown in the lower panels. Arrows showing the co-localization of CRMP2A and FKBP12. Scale bar 10 µm.*

4.2.3 FKPB12 binds specifically to non-phosphorylated CRMP2A

We have previously shown that PIN1 binds specifically to Cdk5-phosphorylated CRMP2A (Balastik et al., 2015) which is in agreement with the described specificity of PIN1 for substrates with phosphorylated Ser or Thr preceding Pro (Yaffe et al., 1997). Thus, we decided to test the phospho-specificity of FKBP12-CRMP2A interaction. We performed pull-down experiments using lysates of HEK293T cells expressing CRMP2A in the absence or presence of increased activity of Cdk5 kinase (overexpression of Cdk5 and its activator p25). The results show that CRMP2A phosphorylation differentially regulates binding of PIN1 and FKBP12. While PIN1 strongly prefers phosphorylated CRMP2A (Figure 17A, B; Balastik et al., 2015), FKBP12 binds specifically to non-phosphorylated CRMP2A (p=0.0001; Figure 17A, B).

There are two described Cdk5-phosphorylation sites in CRMP2A – Ser623 (corresponding to Ser522 in CRMP2B) and Ser27 (Balastik et al., 2015). We used de-phospho-mimetic constructs (Ser is replaced by Ala) and performed the pull-down experiments in conditions of high Cdk5 activity. As expected, de-phospho-mimetic mutations abolished the binding of PIN1 to CRMP2A (Figure 17C, D; Balastik et al., 2015). In contrast, the binding of FKBP12 to CRMP2A was non-significantly increased by mutation of the C-terminus (p=0.1271) and significantly promoted by the de-phospho-mimetic mutation of the N-terminus (Ser27; p=0.02; Figure 17C, D). The results strongly support the higher importance of the N-terminus of CRMP2A for the binding to FKBP12 and are consistent with the data presented in (Figure 16B, C) showing the binding of FKBP12 to CRMP2A even in the absence of the C-terminus.

To test whether the binding of the two prolyl isomerases is affected by CRMP2A phosphorylation also in neurons we transfected CRMP2A KO neurons with mCherry-CRMP2A or mCherry-CRMP2AS27A, S623A (de-phospho-mimetic for both Cdk5 phosphorylation sites) and analyzed the colocalization of these proteins with endogenous FKBP12 and PIN1 in the growth cones (Figure 17E). The signal of the two prolyl isomerases

correlated similarly with CRMP2A (correlation coefficient $r_{CRMP2A\text{-}FKBP12} = 0.2998$; $r_{CRMP2A\text{-}PIN1} = 0.2998$; $p_{(between\ the\ correlations)} = 1$) while in the presence of mutated CRMP2A (CRMP2AS27AS623A), the correlation with PIN1 signal was significantly decreased ($r = 0.1763$; $p_{(between\ the\ correlations)} = 0.019$) and correlation with FKBP12 was significantly increased ($r = 0.3959$; $p_{(between\ the\ correlations)} = 0.049$) making the correlations of FKBP12 and PIN1 significantly different ($p_{(between\ the\ correlations)} = 0.0001$; Figure 17F).

These results are consistent with the pull-down experiments and show that FKBP12 binds preferably to non-phosphorylated CRMP2A while PIN1 binds preferably to phosphorylated CRMP2A also in the cellular environment of the active neuronal growth cone.

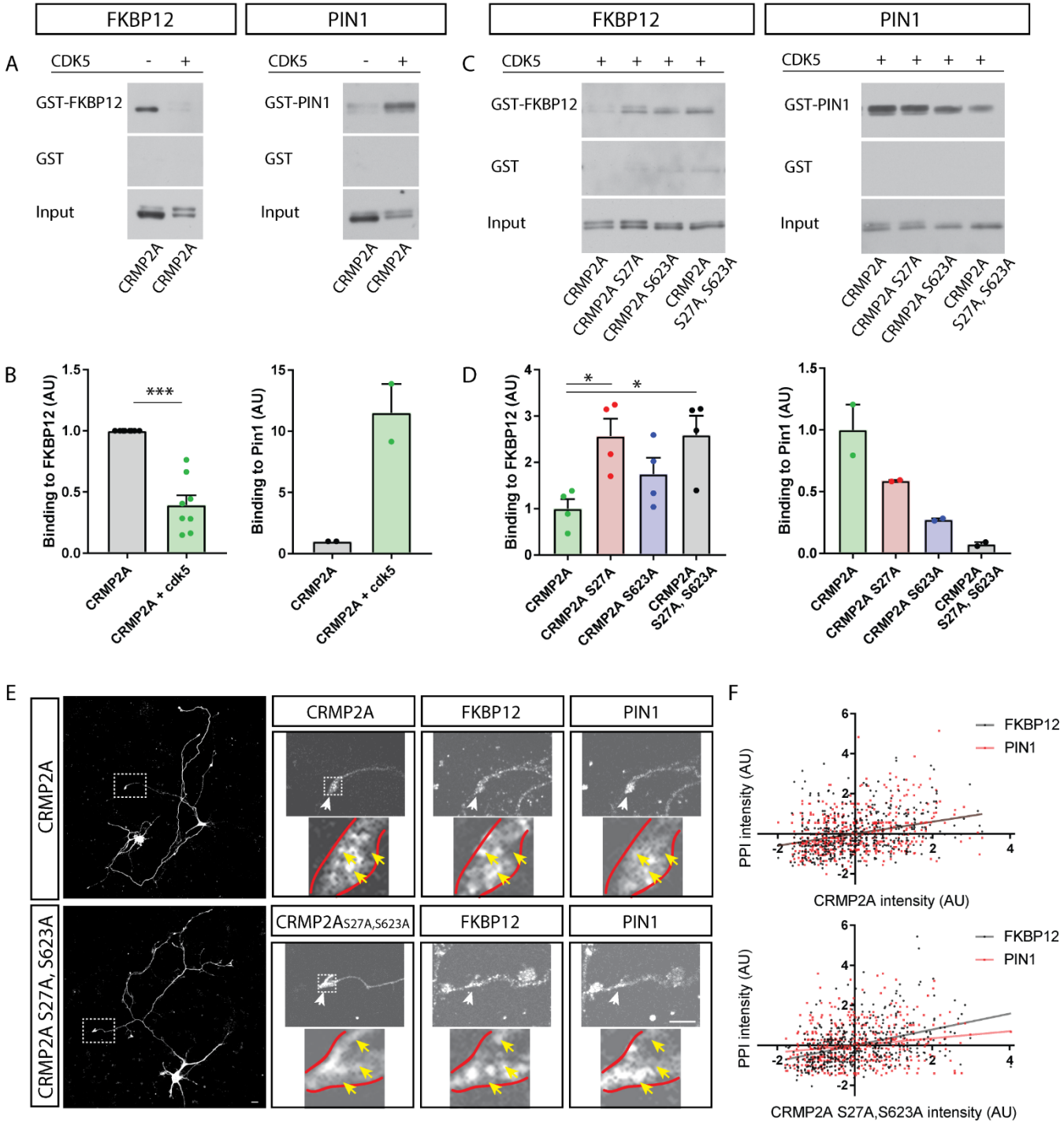

Figure 17: FKPB12 binds non-phosphorylated CRMP2A.

*A) Pull-down of flag-CRMP2A by purified GST-FKBP12 (left panel) or GST-PIN1 (right panel) in the absence (-) or presence (+) of higher Cdk5 activity (overexpression of Cdk5 and its activator p25). GST is used as a negative control. Proteins were visualized using anti-flag antibodies. B) Relative quantification of pull-downs shown in A) normalized to the input (CRMP2A = 1 ± 0; CRMP2A + Cdk5 = 0.39 ± 0.08; mean ± SEM; Welsch's t-test; ***p<0.001; n = 8 experiments; Data for PIN1 are obtained from 2 western blots of one experiment and were not statistically analyzed). C) Pull down of CRMP2A and its de-phospho-mimetic mutants (Ser are replaced by Ala at positions 27, 623, or both)*

*by FKBP12 (left) or PIN1 (right) in the presence of high Cdk5 activity. GST is used as a negative control. Proteins were visualized using anti-flag antibodies. D) Relative quantification of pull-downs shown in C) normalized to the input (CRMP2A = 1 ± 0.21; CRMP2A S27A = 2.57 ± 0.38; CRMP2A S623A = 1.75 ± 0.35; CRMP2A S27A, S623A = 2.59 ± 0.41; mean ± SEM; Welsch's t-test; *p<0.05; n = 4 experiments; Data for PIN1 are obtained from 2 western blots of one experiment and were not statistically analyzed). E) Representative images of analyzed neurons and growth cones used for colocalization of endogenous FKBP12 or PIN1 (stained using antibodies) with CRMP2A (upper panels) or mutated de-phospho-mimetic CRMP2A S27AS623A (lower panels) in CRMP2A KO primary cortical neurons. The dashed rectangle marks the region zoomed in (in the right panels). White arrows show the growth cone which is zoomed in (the lower panels). Yellow arrows show the regions of the colocalization of one or both prolyl isomerases with CRMP2A. Scale bar 10 μm. F) Correlations between the mCherry signal (corresponding to CRMP2A (upper graph) or CRMP2A S27AS623A (lower graph)) and the two prolyl isomerases – PIN1 (red) or FKBP12 (black) presented as scatter plots with linear regression.*

4.2.4 Knockdown of FKBP12 does not significantly affect the amount of CRMP2A protein but it decreases its Ser27 phosphorylation

To understand the effect of FKBP12 on CRMP2A, we decided to study CRMP2A in neurons lacking FKBP12. For this purpose, we prepared several constructs (pGhU6 vector with shRNA sequence) for FKBP12 knockdown (described in methods). We used these vectors for lentiviral transduction of neuronal culture and observed the amount of GFP (reporter used in the pGhU6 vector), FKBP12, and cleaved Caspase-3 (an apoptotic marker) for several days. Two shRNA (TRCN0000416982 and TRCN0000012489) showed increased levels of Casp-3 (Figure 18A). As the other two shRNA (TRCN0000012491 and TRCN0000012492) visibly reduce the amount of FKBP12 without increasing the levels of Caspase-3, we concluded, that the observed harmful effect of some shRNAs is rather a consequence of possible off-target recognition than the effect of FKBP12 knockdown. We decided to use the shRNA TRCN0000012492 for the following experiments.

As we have shown that prolyl isomerase PIN1 stabilizes phosphorylated CRMP2A (Balastik et al., 2015; Figure 8), we first tested how knockdown of PIN1 or FKBP12 affect the amount and phosphorylation of CRMP2A. In neuronal culture, we observed an expected effect of knockdown of PIN1 prolyl isomerase – it decreases the amount of CRMP2A (Figure 18B, D; p=0.0378) and also the ratio between phosphorylated (pS27) and total CRMP2A (Figure 18B, C; p<0.0001). These data confirm the published data (Balastik et al., 2015). Knockdown of FKBP12 showed no significant difference in the CRMP2A amount (Figure 18B, D; p=0.1033) and a slight decrease in the ratio CRMP2A pS27/CRMP2A (Figure 18B, C; p<0.0001). To ensure, that the observed effect is the consequence of the downregulated FKBP12 protein, we

performed a rescue experiment. We prepared a vector expressing FKBP12 with seven silent mutations which should abolish its recognition by the target sequence used in the shFKBP12 construct (described in methods). We then transduced neurons with lentiviral particles carrying the shRNA together with a control vector or vector overexpressing FKBP12 with silent mutations. We observed the same effect of knockdown of FKBP12 – the proportion of Ser27-phosphorylated CRMP2A was decreased (Figure 18E, F; p=0.0167) while the total CRMP2A amount was not significantly changed (Figure 18E, G; p=0.0904). We observed no significant difference between knockdown and rescue group in the amount of CRMP2A (Figure 18E, G; p=0.7097) and in the portion of phosphorylated CRMP2A (Figure 18E, F; p=0.3132) even though there is a trend towards the control levels making the difference between Ctrl and rescue not significant (Figure 18E, F; p=0.0974). The insufficiency of the rescue is probably due to visibly lower level of FKBP12 in the rescue group compared to controls (Figure 18E) which could be due to low efficiency of the expression or blocking only partially its recognition by the silencing target sequence.

Together, the data show that, unlike PIN1, FKBP12 does not affect the amount of CRMP2A, but both prolyl isomerases influence the level of CRMP2A phosphorylation.

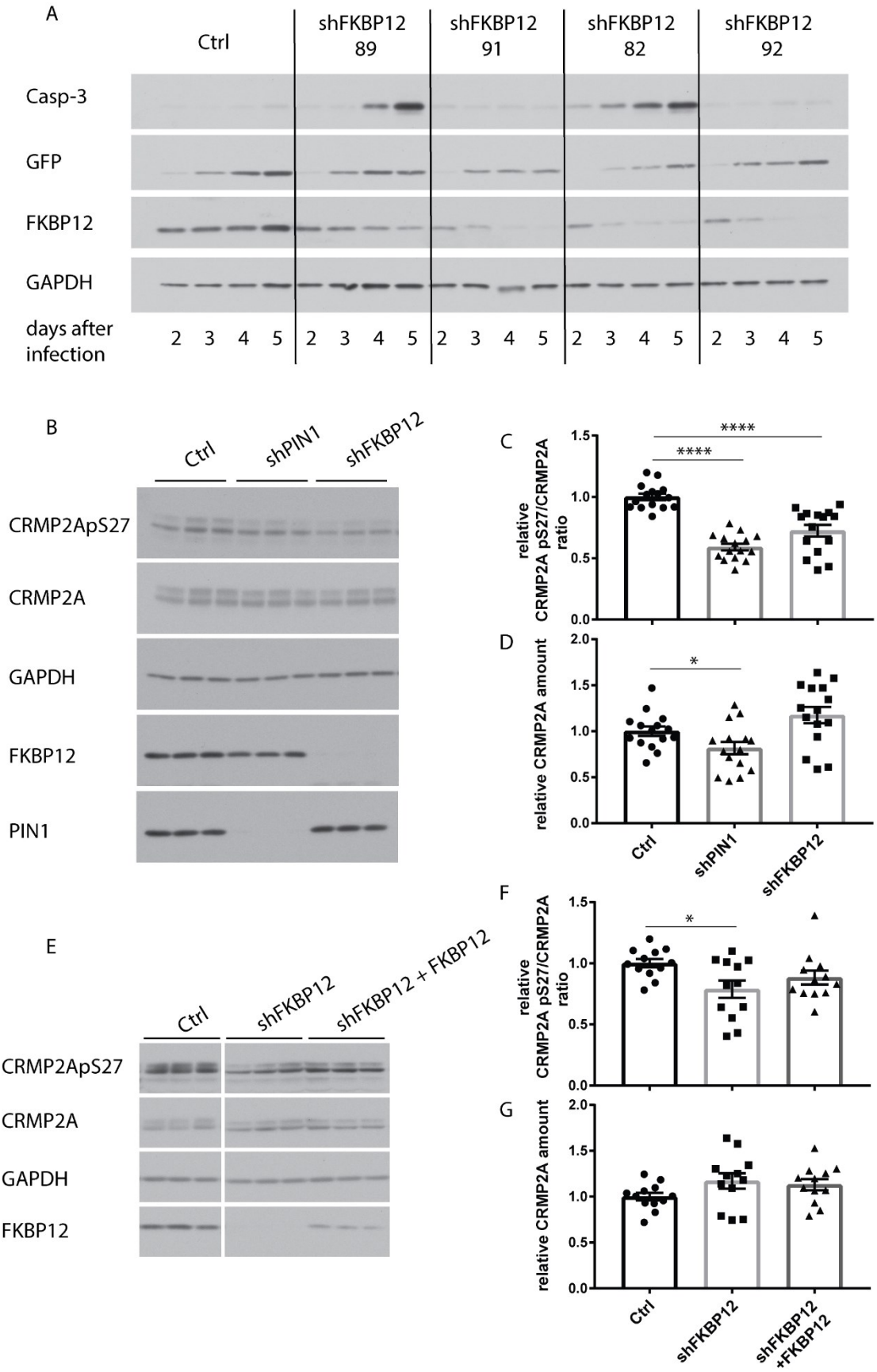
A
Ctrl
shFKBP12 89
shFKBP12 91
shFKBP12 82
shFKBP12 92
Casp-3
GFP
FKBP12
GAPDH
days after infection
2 3 4 5 2 3 4 5 2 3 4 5 2 3 4 5 2 3 4 5
B
Ctrl
shPIN1
shFKBP12
CRMP2ApS27
CRMP2A
GAPDH
FKBP12
PIN1
C
relative CRMP2A pS27/CRMP2A ratio
****
****
D
relative CRMP2A amount
*
Ctrl
shPIN1
shFKBP12
E
Ctrl
shFKBP12
shFKBP12 + FKBP12
CRMP2ApS27
CRMP2A
GAPDH
FKBP12
F
relative CRMP2A pS27/CRMP2A ratio
*
G
relative CRMP2A amount
Ctrl
shFKBP12
shFKBP12 +FKBP12

Figure 18: Knockdown of FKBP12 does not significantly affect the amount of CRMP2A protein but it decreases its Ser27 phosphorylation.

*A) Western blot showing the efficiency of different target sequences used for shRNA knockdown of FKBP12. Antibodies against FKBP12, GFP (reporter protein contained in the pGhU6 vector), cleaved Caspase-3 (a marker of apoptosis) were used, GAPDH was used as a loading control. The neurons were analyzed 2-5 days after transduction. As a control, we used pGhU6 vector with a non-silencing control sequence (Ctrl). We tested four different recognition sequences: TRCN0000012489 (denoted as 89), TRCN0000012491 (denoted as 91), TRCN0000416982 (denoted as 82), and TRCN0000012492 (denoted as 92). B) Representative western blot of primary neurons lysates. Neurons were transduced with the control sequence (non-silencing control, Ctrl), sequence for PIN1 knockdown (shPIN1), or sequence for FKBP12 knockdown (shFKBP12). Antibodies against phosphorylated CRMP2A on Ser27 (CRMP2A pS27), CRMP2A, FKBP12, PIN1 were used. GAPDH was used as a loading control. C-D) Relative quantification of the western blot experiment represented in B). C) Relative CRMP2A pS27/CRMP2A ratio is decreased by knockdown of PIN1 as well as knockdown of FKBP12 (Ctrl = 1 ± 0.03, shPIN1 = 0.59 ± 0.027, shFKBP12 = 0.72 ± 0.05; mean ± SEM, ****p<0.0001, Welch's t-test; n=15 - 5 western blots; 3 samples in each experiment). D) Relative CRMP2A amount is decreased by PIN1 knockdown and not significantly changed by FKBP12 knockdown (Ctrl = 1 ± 0.05, shPIN1 = 0.82 ± 0.07, shFKBP12 = 1.18 ± 0.09; mean ± SEM, *p<0.05, Welch's t-test; n=15 - 5 western blots; 3 samples in each experiment). E) Representative western blot of primary neurons lysates transduced by control vectors (non-silencing control in pGhU6 and empty pWCC vector), knockdown of FKBP12 or knockdown of FKBP12 in combination with overexpressing vector carrying FKBP12 sequence with seven silent mutations in the shRNA-recognition site (rescue; denoted as shFKBP12+FKBP12). The presented picture of the western blot is from one membrane, only the order of the samples has been changed for better readability. F-G) Relative quantification of the western blot experiment represented in E). F) Relative CRMP2A pS27/CRMP2A ratio is significantly decreased by knockdown of FKBP12 but not significantly decreased by the knockdown of FKBP12 in combination with the expressing vector (Ctrl = 1 ± 0.03, shFKBP12 = 0.79 ± 0.07, shFKBP12+FKBP12 = 0.88 ± 0.06; mean ± SEM; *p<0.05, Welch's t-test; n=12 – 4 western blots; 3 samples in each experiment). G) Relative CRMP2A amount is not significantly changed by FKBP12 knockdown and by the knockdown combined with the expressing vector (Ctrl = 1 ± 0.04, shFKBP12 = 1.17 ± 0.08, shFKBP12+FKBP12 = 1.13 ± 0.06; mean ± SEM; Welch's t-test; n=12 – 4 western blots; 3 samples in each experiment).*

4.2.5 Prolyl isomerase FKBP12 inhibits CRMP2A *in vitro*

As we did not observe any distinctive effect of FKBP12 absence on the CRMP2A levels, we decided to test the effect of FKBP12 on CRMP2A activity. CRMP2 is a microtubule-associated protein that was shown to promote microtubule polymerization (Niwa et al., 2017). We decided to test the effect of FKBP12 on microtubule dynamics in the presence of CRMP2A. For this purpose, we used a tubulin turbidity assay. Importantly, it was shown that FKBP12 does not affect microtubule dynamics itself in contrast to other FKBPs such as FKBP52 (Chambraud et al., 2007). We first purified proteins for the *in vitro* assay. We expressed GST-tagged FKBP12 (or GST as a control) in bacteria and purified the protein using glutathione-agarose beads (described in methods; Figure 19A). We expressed GFP-CRMP2A (flag-tagged) in HEK293T cells and purified the protein using anti-DYKDDDDK beads (described in methods; Figure 19B). To be sure that the purification process does not affect the prolyl

isomerase activity of FKBP12, we performed peptidyl-prolyl *cis/trans* isomerase assay showing that our purified FKBP12 has prolyl isomerase activity (Figure 19C).

Using the tubulin turbidity assay, we then tested the effect of the presence of CRMP2A on the tubulin polymerization. The results show that CRMP2A is significantly promoting microtubule growth (Figure 19D, E), which is similar to what was published for CRMP2B (Niwa et al., 2017). When we added FKBP12 together with CRMP2A to tubulin, the polymerization curve was similar to the control conditions (tubulin only, without CRMP2A; Figure 19D, E). To ensure that the effect is because of FKBP12 activity, we performed the assay in the presence of FK506 (tacrolimus, FKBP12 inhibitor). In the presence of FKBP12 and its inhibotor FK506, CRMP2A increases the microtubule growth the similar way as CRMP2A alone (Figure 19D, E).

Together, we show that CRMP2A is promoting microtubule growth and this effect is abolished by the presence of prolyl isomerase FKBP12.

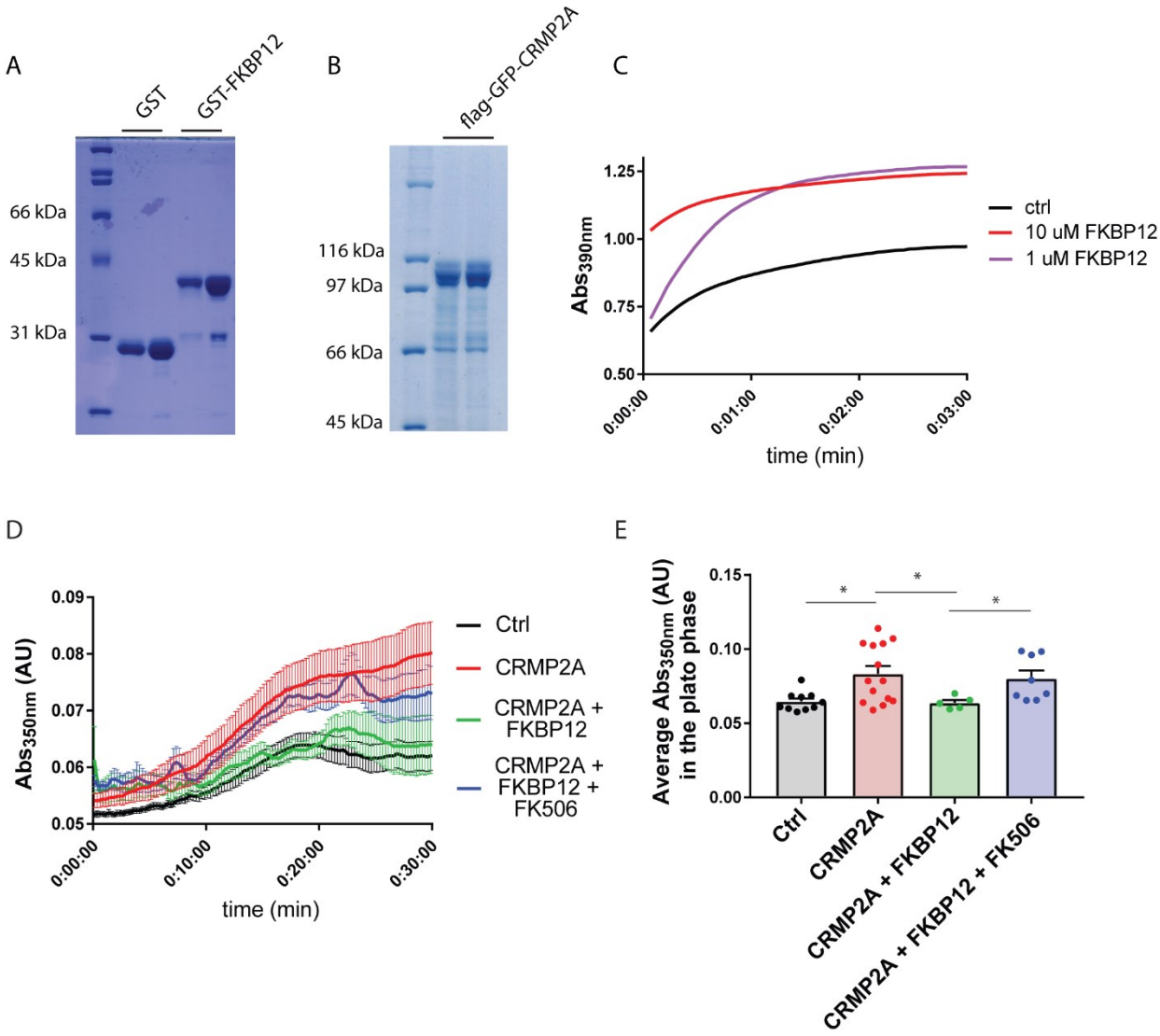

Figure 19: Prolyl isomerase FKBP12 inhibits CRMP2A in vitro.

*A) Coomassie staining of the PAGE-gel showing purified protein GST-FKBP12 and GST (used as a control) used in the in vitro assays. Proteins are loaded in two different concentrations. B) Coomassie staining of the PAGE-gel showing purified flag-tagged-GFP-fused protein CRMP2A used for the in vitro assays. C) Peptidyl-prolyl cis/trans isomerase assay showing the activity of purified FKBP12 prolyl isomerase. Absorbance at 390 nm is reflecting the cis/trans isomerization (described in methods). D) The tubulin turbidity assay showing microtubule growth in the control conditions (in black; denoted as Ctrl; tubulin only), in the presence of CRMP2A (red), in the presence of CRMP2A in combination with FKBP12 (green; CRMP2A+FKBP12), or in the presence of CRMP2A, FKBP12 and its inhibitor FK506 (blue; CRMP2A+FKBP12+FK506). E) Quantification of the absorbance in the plateau phase of the curves shown in D) reflecting the differences in the microtubule growth (Ctrl = 0.065 ± 0.002; CRMP2A = 0.083 ± 0.005; CRMP2A + FKBP12 = 0.064 ± 0.002; CRMP2A + FKBP12 + FK506 = 0.080 ± 0.005; mean + SEM; Mann-Whitney test; *p<0.05; n = 10, 14, 5, 8 experiments).*

I performed the tubulin turbidity assay with the advice of my colleague Djamel Eddine Chafai. Djamel Eddine Chafai prepared the tubulin used in the assay.

4.2.6 Prolyl isomerase FKBP12 affects binding of CRMP2A on growing microtubules and decreases microtubule polymerization velocity

To study the effect of CRMP2A and FKBP12 on microtubule dynamics in more detail, we performed an *in vitro* tubulin polymerization assay. In this assay, prepolymerized and stabilized microtubules are immobilized on the coverslip and after the addition of tubulin, it is possible to analyze the dynamics of growing microtubules in time. We performed this assay in the presence of CRMP2A and observed significantly increased microtubule growth due to: increased microtubule polymerization velocity, decreased depolymerization velocity and increased frequencies of both catastrophe and rescue ($p<0.0001$, $p=0.0001$, $p<0.0001$, $p=0.0199$ respectively, Figure 20A, B). Adding FKBP12 to CRMP2A significantly reduced the microtubule polymerization rate ($p<0.0001$; Figure 20A, B). Microtubule rescue frequency also showed a decreasing trend, although not significant ($p=0.058$; Figure 20A, B). Together, the results are in accordance with the results obtained using tubulin turbidity assay and show that FKBP12 is inhibiting promotion of microtubule growth caused by CRMP2A. The observed effect is mainly the consequence of affected polymerization velocity.

As our CRMP2A was tagged with GFP, we were also able to analyze the binding of CRMP2A to the microtubules. We observed almost no binding to the stabilized microtubules but CRMP2A was clearly binding to the growing ends of microtubules (Figure 20A) which was described before for both CRMP2 isoforms (Yuasa-Kawada et al., 2003). Importantly, the presence of FKBP12 appeared to decrease this binding (Figure 20A). We quantified this observed effect as an average length of GFP-positive ends, and as the persistence of GFP signal on growing microtubule, both showing a significant decrease in the presence of FKBP12 ($p<0.0001$ and $p=0.0005$ respectively; Figure 20C, D).

Together, these results suggest that FKBP12 inhibits CRMP2A activity by inhibiting its binding to microtubules.

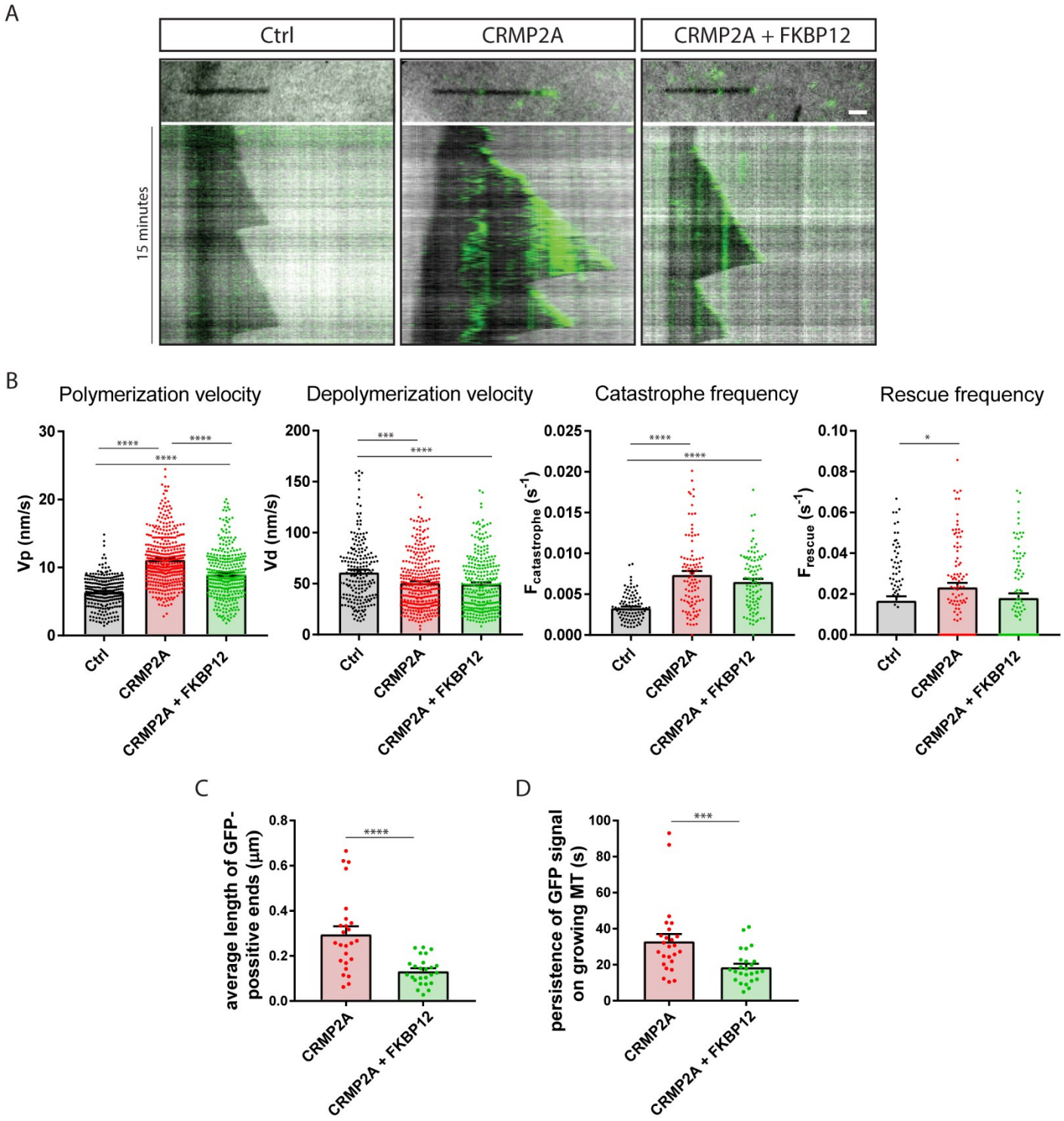

Figure 20: Prolyl isomerase FKBP12 affects binding of CRMP2A on growing microtubules and decreases microtubule polymerization velocity.

A) Represenative pictures of the microtubules and representative kymographs showing microtubule dynamics in in vitro tubulin polymerization assay in control conditions (Ctrl, tubulin only), in the presence of GFP-CRMP2A (CRMP2A), or in the presence of GFP-CRMP2A and FKBP12 (CRMP2A+FKBP12). Microtubules are shown in black, GFP-CRMP2A in green. Scale bar = 1 µm. B) Quantification of the microtubule dynamics parameters: microtubule polymerization velocity (ctrl

*= 6.45 ± 0.14; CRMP2A = 11.17 ± 0.19; CRMP2A + FKBP12 = 9.02 ± 0.19; n = 259, 401, 350 polymerization events in 5 independent experiments), microtubule depolymerization velocity (ctrl = 61.5 ± 2.2; CRMP2A = 51.0 ± 1.4; CRMP2A + FKBP12 = 49.7 ± 1.6; n = 200, 326, 294 depolymerization events in 5 independent experiments), frequency of catastrophes (ctrl = 0.0033 ± 0.0002; CRMP2A = 0.0074 ± 0.0004; CRMP2A + FKBP12 = 0.0066 ± 0.0003; n = 97, 100, 98 microtubules in 5 independent experiments), and frequency of rescues (ctrl = 0.017 ± 0.002; CRMP2A = 0.023 ± 0.002; CRMP2A + FKBP12 = 0.018 ± 0.002; n = 95, 99, 94 microtubules in 5 independent experiments; mean ± SEM; Mann-Whitney test; *p<0.05, ***p<0.001, ****p<0.0001). C) Average length of GFP-positive ends measured as GFP-positive area in the polymerization phase divided by the number of frames in the polymerization phase. (CRMP2A = 0.2966 ± 0.03428 µm, CRMP2A+FKBP12 = 0.1329 ± 0.01207 µm; mean ± SEM.; ****p<0.0001; Mann-Whitney test; n = 25 microtubules in 5 independent experiments). D) Persistence of GFP signal on the growing microtubule (MT) measured as GFP-positive area in the growing phase divided by the length of the growing end. (CRMP2A = 33.07 ± 3.955 s, CRMP2A+FKBP12 = 18.69 ± 1.844 s; mean ± SEM; ***p<0.001; Mann-Whitney test; n = 25 microtubules in 5 independent experiments.*

The in vitro polymerization assay was performed by Jan Sabó at the Institute of Biotechnology, Czech Academy of Sciences. I prepared the proteins used for the experiments (except for tubulin) and analyzed the obtained recordings.

4.2.7 Prolyl isomerase FKBP12 inhibits CRMP2A in IMCD3 cells

We show that FKBP12 inhibits CRMP2A *in vitro*. To see the effect of FKBP12 on CRMP2A-promoted microtubule growth in cells, we used IMCD3 cells suitable to visualize microtubules. We first tested the endogenous expression of CRMP2A and FKBP12 in this cell line. We performed western blot from primary neuron lysates (which have high expression of both CRMP2A and FKBP12) and IMCD3 lysates (Figure 23A). We observed lower expression of FKBP12 in IMCD3 and not detectable expression of both CRMP2B and CRMP2A. With this information, we decided to test both knockdown and overexpression of FKBP12 in control conditions and in the conditions of overexpressed CRMP2A protein. To study the microtubule dynamics in cells, we used vectors expressing GFP-tagged EB3 protein (protein binding to growing microtubule ends). We also tested the effect of de-phosho-mimetic CRMP2A (CRMP2A S27A) as we show that binding of FKBP12 is dependent on the phosphorylation of this site. Using western blot, we first tested the efficiency of overexpressions and knockdowns (Figure 23B, C).

With these groups of cells, we performed the experiment capturing the GFP signal of GFP-EB3 protein and measured the relative microtubule growth speed (Figure 23D, E). The results show that in the control conditions (without CRMP2A protein), neither knockdown nor overexpression of FKBP12 significantly affects microtubule growth (p=0.1775 and p=0.9358 respectively). In agreement with the results obtained *in vitro*, CRMP2A overexpression was able to significantly increase the growth of microtubules (p<0.0001; Figure 23D, E).

Overexpression of CRMP2A in the conditions of elevated levels of FKBP12 increased slightly the microtubule growth in comparison to control ($p=0.016$) but significantly less than CRMP2A overexpression without FKBP12 ($p<0.0001$; Figure 23D, E). The combination of CRMP2A overexpression and knockdown of FKBP12 was not significantly different than CRMP2A overexpression alone ($p=0.430$). Interestingly, and in contrast to CRMP2A, expression of mutated CRMP2A S27A (which cannot be phosphorylated on Ser27) did not increase the microtubule growth ($p=0.2$; Figure 23D, E). As we show in the previous data, the de-phospho-mimetic mutation is bound by FKBP12 more efficiently, so we suggest that the mutated form is more efficiently inhibited by endogenous FKBP12 present in IMCD3 cells. Indeed, the combination of mutated CRMP2A and overexpression of FKBP12 had no effect ($p=0.994$) while, importantly, the combination with FKBP12 knockdown increased the microtubule growth similarly as overexpression of wild-type CRMP2A ($p<0.0001$ in comparison with control and $p=0.822$ in comparison with CRMP2A; Figure 23D, E). Interestingly, even though it was described that tagged CRMP2 is not functional in terms of microtubule orientation determination (Yuasa-Kawada et al., 2003), we see the same effect of CRMP2A on microtubule growth in EB3 assay using not tagged CRMP2A and mCherry-CRMP2A.

Together, the data demonstrate that FKBP12 inhibits the CRMP2A-mediated microtubule polymerization in cells.

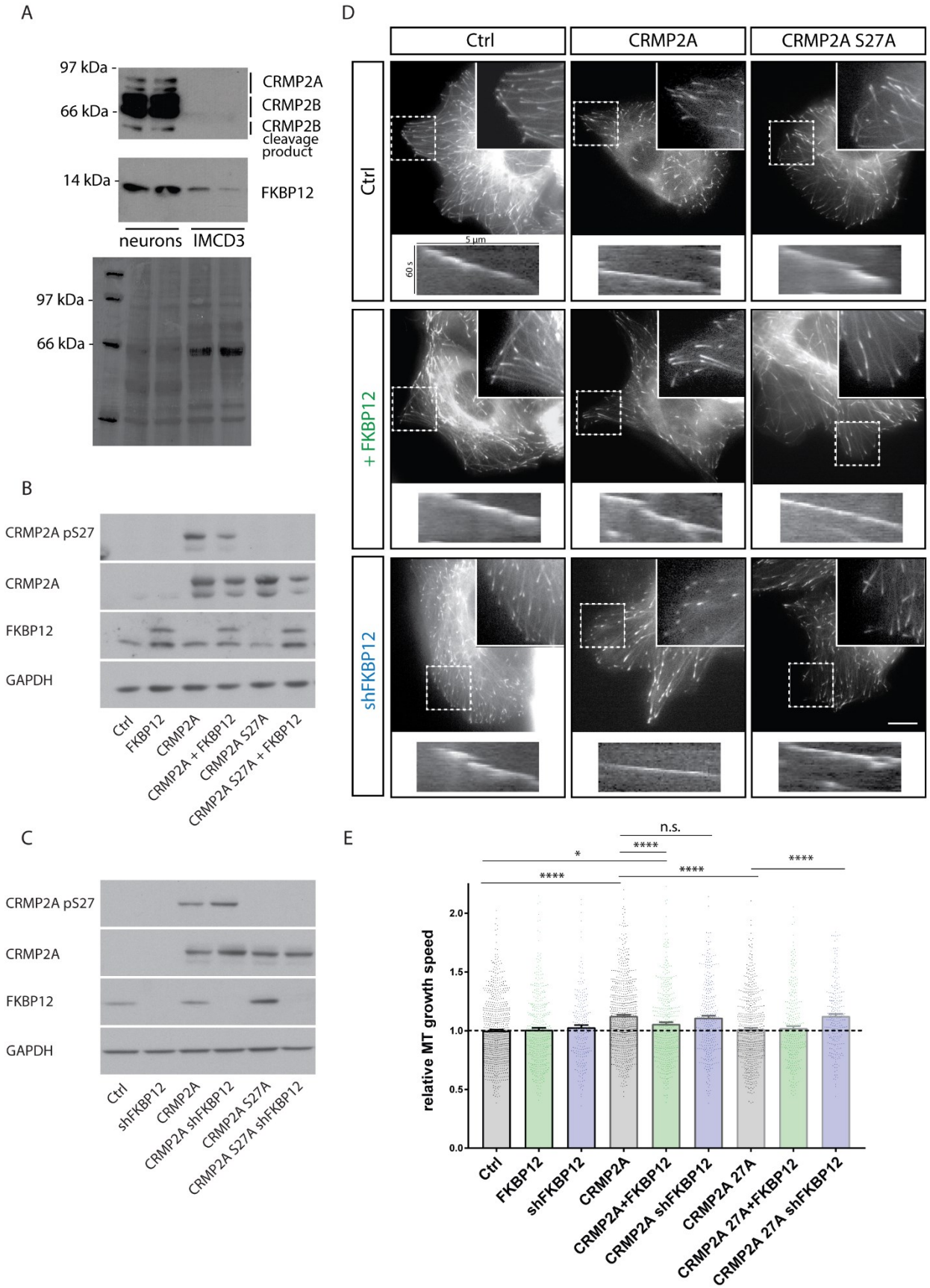
A
97 kDa
66 kDa
CRMP2A
CRMP2B
CRMP2B cleavage product
14 kDa
FKBP12
neurons
IMCD3
97 kDa
66 kDa
B
CRMP2A pS27
CRMP2A
FKBP12
GAPDH
Ctrl
FKBP12
CRMP2A
CRMP2A + FKBP12
CRMP2A S27A
CRMP2A S27A + FKBP12
C
CRMP2A pS27
CRMP2A
FKBP12
GAPDH
Ctrl
shFKBP12
CRMP2A
CRMP2A shFKBP12
CRMP2A S27A
CRMP2A S27A shFKBP12
D
Ctrl
CRMP2A
CRMP2A S27A
Ctrl
+ FKBP12
shFKBP12
5 µm
60 s
E
n.s.
****
*
****
****
****
relative MT growth speed
2.0
1.5
1.0
0.5
0.0
Ctrl
FKBP12
shFKBP12
CRMP2A
CRMP2A+FKBP12
CRMP2A shFKBP12
CRMP2A 27A
CRMP2A 27A+FKBP12
CRMP2A 27A shFKBP12

Figure 21: Prolyl isomerase FKBP12 inhibits CRMP2A in IMCD3 cells.

*A) Western blot showing the comparison of the amount of CRMP2 and FKBP12 in primary neurons and IMCD3 cells. Proteins were visualized using antibody anti-CRMP2 (upper bands correspond to CRMP2A, lower bands correspond to CRMP2B, CRMP2B cleavage product is also visualized), and anti-FKBP12. Coomassie staining of the membrane is shown as a loading control. B,C) Western blot showing IMCD3 cells used for EB3 experiment. Either FKBP12 overexpression (B) or FKBP12 knockdown (C; shFKBP12) was used in combination with CRMP2A or mutated CRMP2A S27A overexpression. Antibodies against phosphorylated CRMP2A on Ser27 (CRMP2A pS27), CRMP2A and FKBP12 were used. GAPDH is used as a loading control. D) Representative images of IMCD3 cells expressing GFP-tagged EB3 protein to visualize the growing ends of microtubules. Combination of either FKBP12 overexpression or FKBP12 knockdown (middle and lower row respectively) were analyzed in combination with CRMP2A or mutated CRMP2A (CRMP2A S27A) overexpression (middle and right column respectively). Dashed rectangles mark the zoomed-in regions shown in the upper right corner. Scale bar 10 µm. A representative kymograph is shown under each picture. E) Quantification of relative microtubule (MT) growth rate (ctrl = 1 ± 0.01; FKBP12 = 1.01 ± 0.02; shFKBP12 = 1.03 ± 0.02; CRMP2A = 1.13 ± 0.01; CRMP2A + FKBP12 = 1.06 ± 0.02; CRMP2A shFKBP12 = 1.11 ± 0.02; CRMP2A S27A = 1.01 ± 0.01; CRMP2A S27A + FKBP12 = 1.02 ± 0.02; CRMP2A S27A shFKBP12 = 1.12 ± 0.02; mean ± SEM; Mann-Whitney test; ns = not significantly different, **p<0.01, ***p<0.001, ****p<0.0001; n = 761, 390, 235, 746, 462, 330, 550, 300, 235 microtubules in at least 7 independent experiments).*

The vectors expressing EB3 were prepared by Carsten Janke's laboratory, Institut Curie in France.

4.2.8 Prolyl isomerase FKBP12 affects microtubule dynamics in neurons and reduces axonal growth

As we have shown that FKBP12 inhibits CRMP2A *in vitro* and in IMCD3 cells artificially expressing CRMP2A, we wanted to see the effect of FKBP12 in neurons, where both CRMP2A and FKBP12 are naturally expressed. For this purpose, we used EB3 assay in DRG (dorsal root ganglia) neurons (Figure 22A). Pseudo-unipolarity of those cells allows us to study the microtubule movement specifically in axons. The results show that even in neurons which have high endogenous level of CRMP2A, CRMP2A overexpression is able to increase microtubule growth ($p<0.0001$; Figure 22A, B). Knockdown of FKBP12 also slightly increased the EB3 movement ($p=0.0281$; Figure 22A, B), which is in agreement with the previous data showing the inhibitory effect of FKBP12 on CRMP2A. Notably, in neurons the effect of FKBP12 knockdown is stronger than in IMCD3 cells, which can be due to different levels of these two proteins in different cell types and/or different phosphorylation states of CRMP2A.

Showing that FKBP12 is affecting microtubule growth also in neurons, we were interested if FKBP12 has some effect also on axonal growth. It was shown that CRMP2 promotes axonal growth (Fukata et al., 2002). Even though it was not shown that CRMP2A overexpression increases axon growth under normal conditions, CRMP2A was shown to have an effect in the

absence of PIN1 prolyl isomerase or in the conditions of increased CRMP2B amount which suggests that CRMP2A supports axonal elongation (Balastik et al., 2015; Yuasa-Kawada et al., 2003). To study the effect of FKBP12 on axonal growth, we plated primary cortical neurons into microfluidic chambers, small compartmentalized silicon devices where axons grow through small channels allowing us to study axonal growth in time. With this approach, we were able to analyze the axonal growth in neurons with increased (+FKBP12) or lowered (shFKBP12) amount of FKBP12 (Figure 22C, D). Average axon growth rate was significantly increased by knockdown of FKBP12 (shFKBP12) ($p=0.04$; Figure 22C, D), while expression of FKBP12 significantly decreased the axon growth rate ($p=0.007$; Figure 22C, D).

These results show that FKBP12 not only regulates microtubule dynamics through the regulation of CRMP2A activity, but it affects axonal growth which makes it a regulator of neural development.

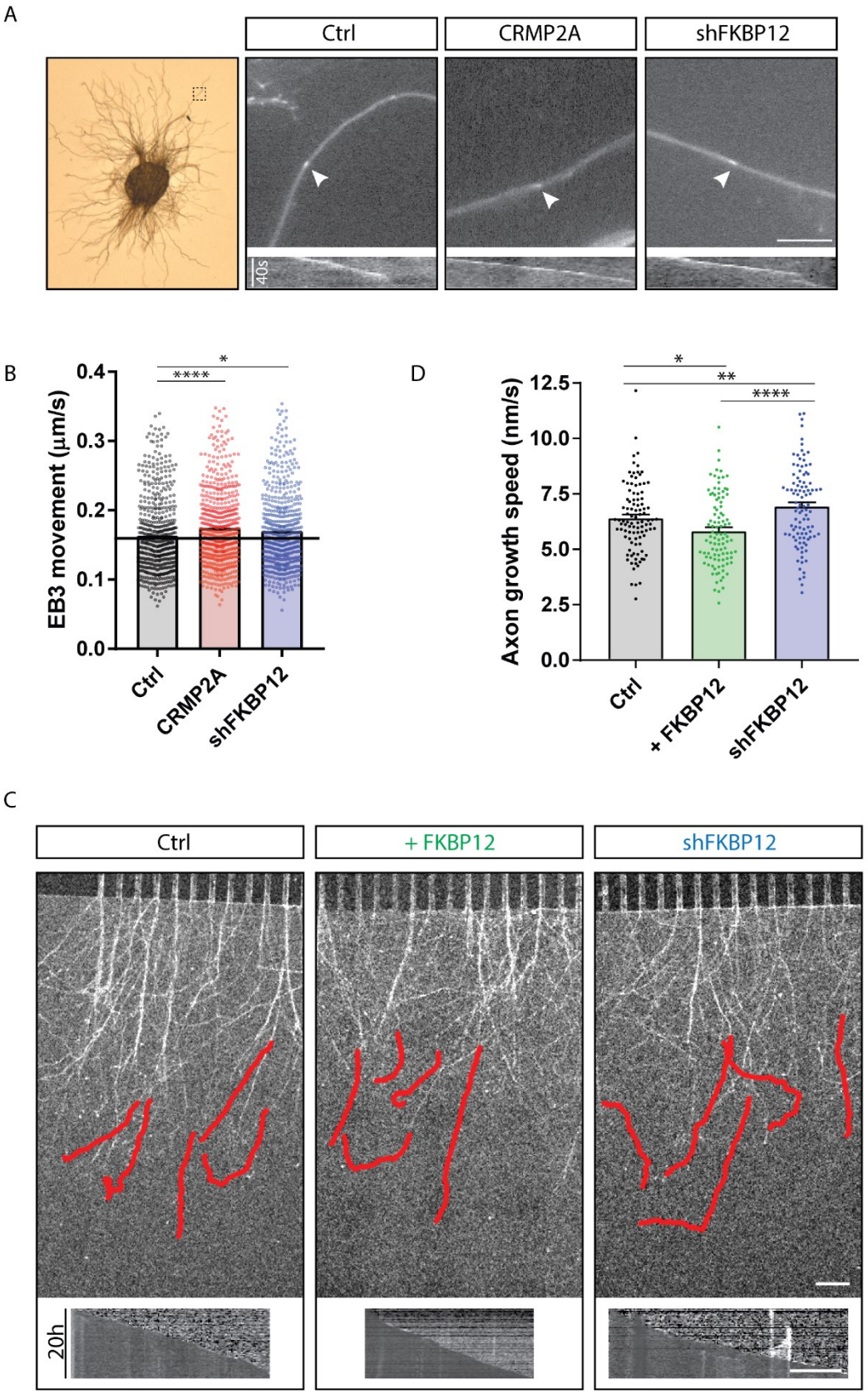
A
Ctrl
CRMP2A
shFKBP12
40s
B
EB3 movement (µm/s)
0.4
0.3
0.2
0.1
0.0
*
****
Ctrl
CRMP2A
shFKBP12
D
Axon growth speed (nm/s)
12.5
10.0
7.5
5.0
2.5
0.0
*
**
****
Ctrl
+ FKBP12
shFKBP12
C
Ctrl
+ FKBP12
shFKBP12
20h

Figure 22: Prolyl isomerase FKBP12 affects microtubule dynamics in neurons and reduces axonal growth.

*A) Representative image of dorsal root ganglia in culture with a dashed rectangle marking analyzed regions of axons. Representative axons are shown in the right panels. We analyzed control cells (Ctrl), cells with CRMP2A overexpression (CRMP2A), and cells with FKBP12 knockdown (shFKBP12). White arrows are marking the GFP-positive ends of growing microtubules (GFP-EB3 signal). Representative kymographs are shown below. Scale bar 5 µm. B) Quantification of EB3 movement in axons of dorsal root ganglia shown in A). Average axonal growth rate was analyzed (ctrl = 0.163 ± 0.002; CRMP2A = 0.175 ± 0.002; shFKBP12 = 0.170 ± 0.002; mean ± SEM µm/s; Mann-Whitney test; *p<0.05, ****p<0.0001; n = 611, 602, 585 microtubules in 4 independent experiments). C) Representative images of neurons in microfluidic chambers with the trajectory of growing axons for 20 hours and representative kymographs corresponding to the trajectories. D) Quantification of average axon growth rate (ctrl = 6.41 ± 0.15, +FKBP12 = 5.83 ± 0.16, shFKBP12 = 6.94 ± 0.18; mean ± SEM nm/s; Mann-Whitney test; *p<0.05, **p<0.01, ****p<0.0001; n=100 axons in 4 independent experiments). Scale bar 100 µm.*

4.2.9 FKBP12 affects neuronal migration

Showing that FKBP12 affects CRMP2A and its function *in vitro*, in a cellular model, and in neurons, we were interested if some effect can be observed also *in vivo* during brain development. As it was shown that CRMP2 is not affecting only axonal growth and guidance but also other processes important in brain development such as neuronal migration, we decided to test the effect of FKBP12 in this process. It was shown that CRMP2 knockdown decreases neuronal migration (Ip et al., 2014; Ip et al., 2012) even though we did not see the same using CRMP2 knockout mice (Ziak et al., 2020). We used in utero electroporation technique to modify the amount of FKBP12 specifically in a population of cells in the developing cortex of murine embryos (Figure 23A). We then fixed and cut the brains (at E18), and analyzed the portion of cells in the upper third of the cortical plate (Figure 23B). The results show that the knockdown of FKBP12 decreased neuronal migration (p=0.0315; Figure 23B, C) which is the same effect as observed before for CRMP2 knockdown (Ip et al., 2014; Ip et al., 2012). This is not in accord with our data as we would expect lower CRMP2A inhibition in the conditions of FKBP12 knockdown and thus increased or at least not changed neuronal migration. However as it was shown that CRMP2A and CRMP2B can have different functions (Yuasa-Kawada et al., 2003), we cannot exclude that CRMP2A can play a different role in the neuronal migration. As we got results similar to the knockdown of CRMP2, we tested if overexpression of CRMP2A can rescue the observed effect. The overexpression of CRMP2A combined with FKBP12 knockdown was not significantly different than FKBP12 knockdown alone (p=0.3975; Figure 23B, C), even though we saw an increasing trend.

Together, the results show that FKBP12 is affecting neuronal development also *in vivo*. Knockdown of FKBP12 decreases neuronal migration. However, the role of FKBP12-CRMP2A interaction in the observed effect is so far not clear and will need to be further characterized. FKBP12 substrates, other than CRMP2A, could mediate or at least contribute to the observed effect.

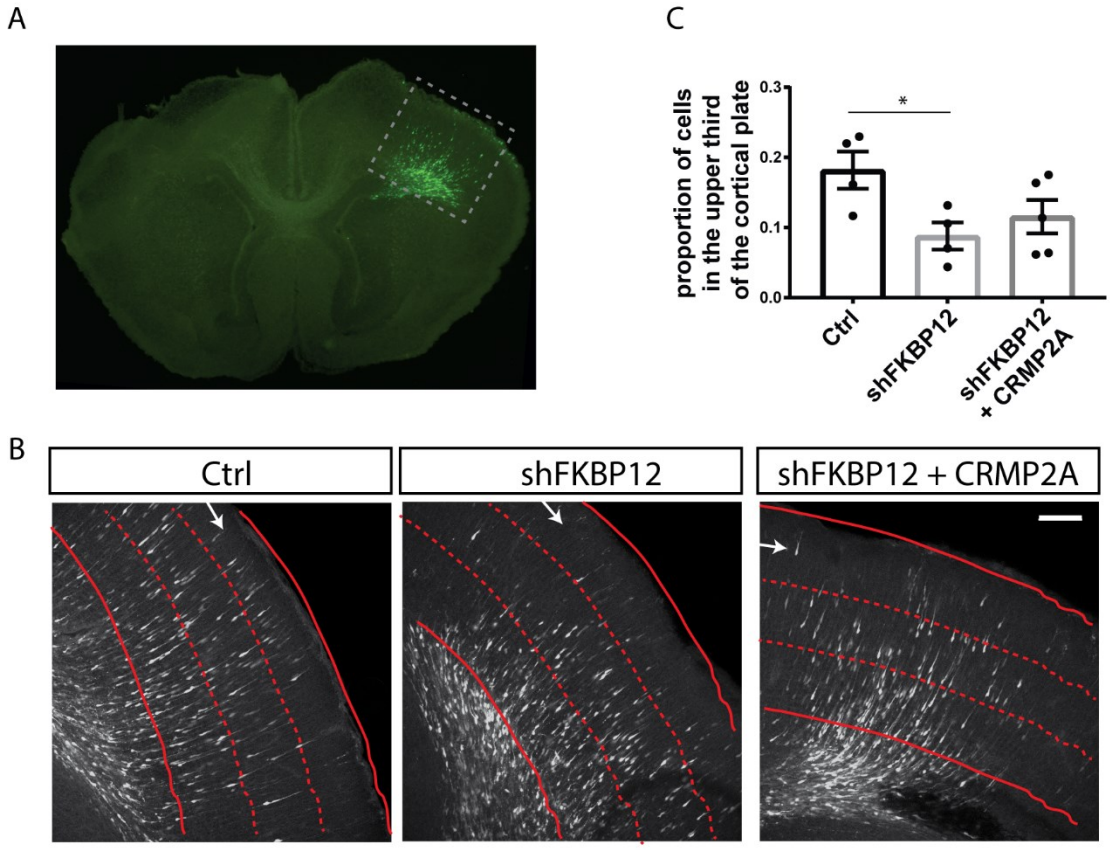

Figure 23: FKBP12 affects neuronal migration.

*A) Representative picture of coronal section of electroporated brain with GFP-positive (electroporated) cells in green. Dashed rectangle marks the analyzed regions shown for each group in B). B) Representative pictures of electroporated brains (E18). Cortical plate (bordered by red lines) was divided into 3 parts (separated by red dashed lines) and the proportion of cells in the upper third (marked by white arrows) was analyzed. C) Quantification of the proportion of cells in the upper third of the cortical plate in electroporated embryos (Ctrl = 0.182 ± 0.026, shFKBP12 = 0.088 ± 0.019, shFKBP12+CRMP2A = 0.116 ± 0.024; mean ± SEM; *p<0.05, Welch's t-test; n=4, 4, 5 embryos respectively from 3 litters). Scale bar: 100 µm.*

4.3 The role of tau phosphorylation in formation of tau envelopes and protection of microtubules

4.3.1 Phosphorylation of tau affects the formation of tau envelopes

As we have shown the dual regulation of CRMP2A protein by two different prolyl isomerases, we were interested if similar regulation is used also for other microtubule-associated proteins. We focused on the tau protein as it is also an axonal microtubule-associated protein and has important implications in the development of Alzheimer's disease. The regulation of tau by phosphorylation and by prolyl isomerase PIN1 has been investigated in multiple publications. While the majority of them has been studying formation of pathological tau aggregates, much less is known about the regulation of tau in its physiological functions. Recently, it was shown that tau can form protective envelopes on microtubules (Siahaan et al., 2019; Tan et al., 2019), but their regulation is so far ill understood. We decided to characterize the effect of tau phosphorylation (specifically by Cdk5 kinase) on tau envelope formation and stability.

Tau can be bound on the microtubule either by diffusive binding (with high turnover) or by cooperative binding (lower turnover, tau making the envelopes; Siahaan et al., 2019). We tested the dynamics of tau binding to microtubules using FRAP in IMCD3 cells either carrying GFP-tagged full-length tau (Ctrl) or truncated tau (tau-ΔN) which was shown to be unable to form tau envelopes. To see the effect of phosphorylation, we co-expressed tau with Cdk5 and its activator p25 (tau-Cdk5; Figure 24A). The GFP signal was photo-bleached under a microscope in the small region of the cells and the recovery of the signal was analyzed on the microtubule in the bleached region (Figure 24A, B). To characterize the dynamics of tau binding to microtubules, we calculated the time constant of the fluorescence recovery (Figure 24C) and the proportion of the immobile fraction (Figure 24D). The FRAP time constant was significantly lower for truncated tau ($p<0.0001$) which is not able of cooperative binding and thus is bound difusively. Interestingly, phosphorylated tau show also lowered time constant ($p=0.0004$) even though slightly higher than truncated tau-ΔN ($p=0.0296$), suggesting that phosphorylated tau is bound less cooperatively than control tau, but more cooperatively than tau-ΔN (Figure 24C). The immobile fraction of control tau was around 20% and was almost completely lost in the tau-ΔN ($p=0.0002$). The immobile fraction of phosphorylated tau was around 8%, which means between the control ($p=0.0117$) and the truncated one ($p=0.1808$; Figure 24C).

Together these data show phosphorylated tau as a state in between cooperative wild-type tau and non-cooperative truncated tau and it supports the data obtained by our colleagues *in vitro* (Siahaan et al., 2024).

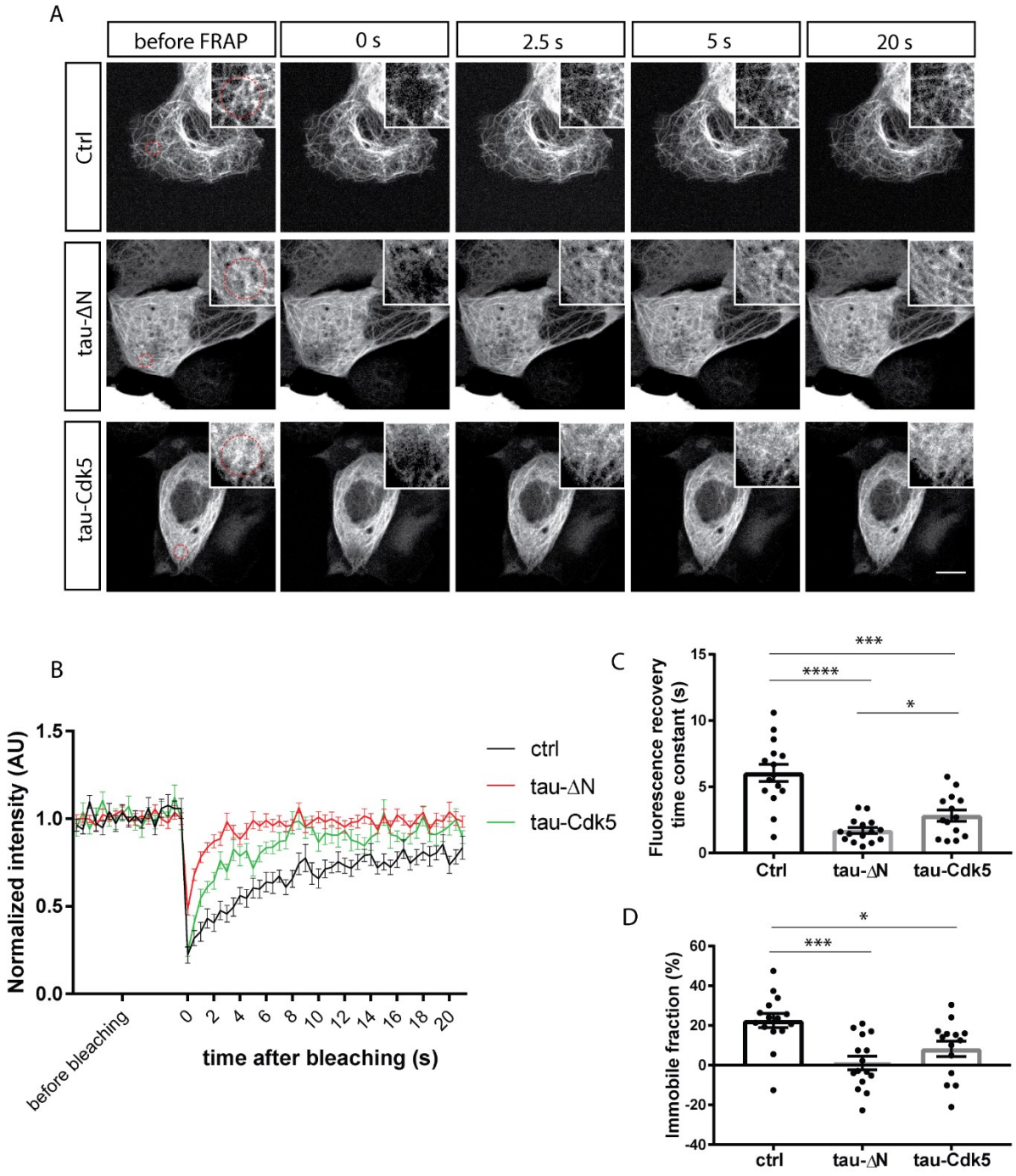

Figure 24: Phosphorylation of tau affects the formation of tau envelopes.

A) Representative pictures of IMCD3 cells before FRAP (left), right after the FRAP (0 s), 2.5, 5 and 20 seconds after the FRAP (2.5 s, 5 s and 20 s respectively). The cells express GFP-tagged tau (Ctrl), truncated tau (tau-ΔN) or tau in combination with Cdk5 and its activator p25 (tau-Cdk5). Bleached area is marked by dashed red circle. Scale bar = 10 µm. B) Relative normalized intensity of GFP signal

*on the microtubule in the bleached region in time. C) Quantification of the fluorescence recovery time constant (Ctrl = 6.05 ± 0.64, tau-ΔN = 1.69 ± 0.23, tau-Cdk5 = 2.83 ± 0.43; mean ± SEM (s); *p<0.05, ***p<0.001, ****p<0.0001; Welch's t-test; n=15, 15, 14 cells in 3 independent experiments). D) Quantification of the percentage of immobile fraction (Ctrl = 22.49 ± 3.55, tau-ΔN = 1.14 ± 3.40, tau-Cdk5 = 8.23 ± 3.88; mean ± SEM (%); *p<0.05, ***p<0.001; Welch's t-test; n=15, 15, 14 cells in 3 independent experiments).*

I prepared the cells for FRAP experiments and analyzed the data. The capturing was done by Valerie Siahaan.

4.3.2 Phosphorylation of tau affects the stability of tau envelopes

Unlike *in vitro*, where the envelopes are readily visible, tau signal in cells usually covers the microtubules homogenously. It was shown before that it is possible to visualize the envelopes in cells using the taxol treatment. Taxol binds to the microtubules and extends the lattice which leads to tau unbinding. During this process the envelopes are observable (Siahaan et al., 2022). We aimed to visualize the envelopes in cells also with a different technique to support the taxol treatment-obtained data. To do this, we tested elevated pH treatment as it was shown before, that tau binding is affected by intracellular pH (Charafeddine et al., 2019). Indeed, although the tau signal in IMCD3 cells transfected with GFP-tau is homogenously covering the microtubules, after elevated pH treatment, tau binding is quickly destabilized forming patches of high tau signal interspersed with gaps of tau signal on the microtubules which are slowly growing and covering again the whole microtubule 9 minutes after the treatment (Figure 25A). During this process, the microtubules stayed intact showing no patches or gaps demonstrating that the mild pH increase primarily affects microtubule-bound tau (Figure 25A).

With this tool, we tested the differences between control wild-type tau, the truncated tau (non-forming envelopes; tau-ΔN), and tau with higher phosphorylation (tau-Cdk5). First, we analyzed the binding of these tau molecules on microtubules before the treatment. In all experimental groups, tau was bound on the microtubule, even though the density on the microtubules was significantly lower for tau-ΔN ($p<0.0001$; Figure 25B). The density of tau-Cdk5 was also significantly lower compared to controls ($p=0.0307$), but significantly higher than tau-ΔN ($p=0.0011$; Figure 25B). To ensure that the observed effect is not the consequence of different transfection efficiencies, we analyzed mean intensity of tau in the cell. Even tough the level of tau was significantly higher in the tau-ΔN, the level of tau was comparable in all groups and it can not explain the differences in tau density on the microtubules (p between control and tau-ΔN = 0.1522; p between control and tau-Cdk5 = 0.1954, p between tau-ΔN and tau-Cdk5 = 0.0161; Figure 25C). The lowered density of tau on the microtubules can be

explained by the lower affinity of tau to microtubules which was published for phosphorylated tau (Cho and Johnson, 2003; Schneider et al., 1999). Alternatively, the lower density of tau on the microtubules can be a consequence of the lower cooperativity described for the truncated tau (Siahaan et al., 2019; Tan et al., 2019).

As expected, after the pH treatment of cells with truncated tau, the tau signal was removed completely and returned in time with no tau patches visible during the process (Figure 25A). The presence of the patches can be quantified as a coefficient of variation along the microtubule, a parameter reflecting the homogeneity/heterogeneity of the signal. While in controls, there is an increase in the coefficient of variation of tau signal along the microtubule after the treatment ($p=0.0102$; $p=0.0096$; while the coefficient of variation of tubulin signal is comparable during the whole process with the means ranging from 7.95 to 9.83; significance not analyzed), no visible changes of coefficient of variation are observed in tau-ΔN (Figure 25D, E). In cells with higher activity of Cdk5 kinase, the signal is usually completely removed after the pH treatment and then recovers exhibiting the high-density patches of tau (Figure 25A) which is observed as an increase of coefficient of variation not right after the pH treatment but 9 minutes after ($p=0.0247$; Figure 25D).

To support that the patches observed in control cells and in cells with phosphorylated tau correspond to tau envelopes, we analyzed the density in patches observed in control and tau-Cdk5 groups and on the microtubule in tau-ΔN group where no visible patches were observed. The results show that the relative density of tau in the patches in both controls and phosphorylated tau stays constant during the recorded period, while the density of tau in tau-ΔN group is gradually increasing (Figure 25F). From this data and from the data obtained *in vitro* (Siahaan et al., 2024), we conclude that phosphorylated tau is, in contrast to truncated tau-ΔN, able to form tau envelopes.

The almost complete removal of tau signal after pH treatment in tau-Cdk5 cells and delayed recovery of the tau signal suggest lower stability of tau envelopes after phosphorylation (Figure 25A, D). To test if the observed recovery delay is only a consequence of larger decline right after the pH treatment or if the regrowth rate itself is also affected, we analyzed the intensity of the tau signal on the microtubules in time and show that the reappearance of tau signal on the microtubule is slower with phosphorylated tau (exponential time constant in controls is 1.3 minutes and in tau-Cdk5 cells 2.5 minutes; Figure 25G).

Together, this data and the data obtained *in vitro* (Siahaan et al., 2024) show that phosphorylated tau can form tau envelopes but these envelopes are less stable and less readily formed than those from unphosphorylated tau.

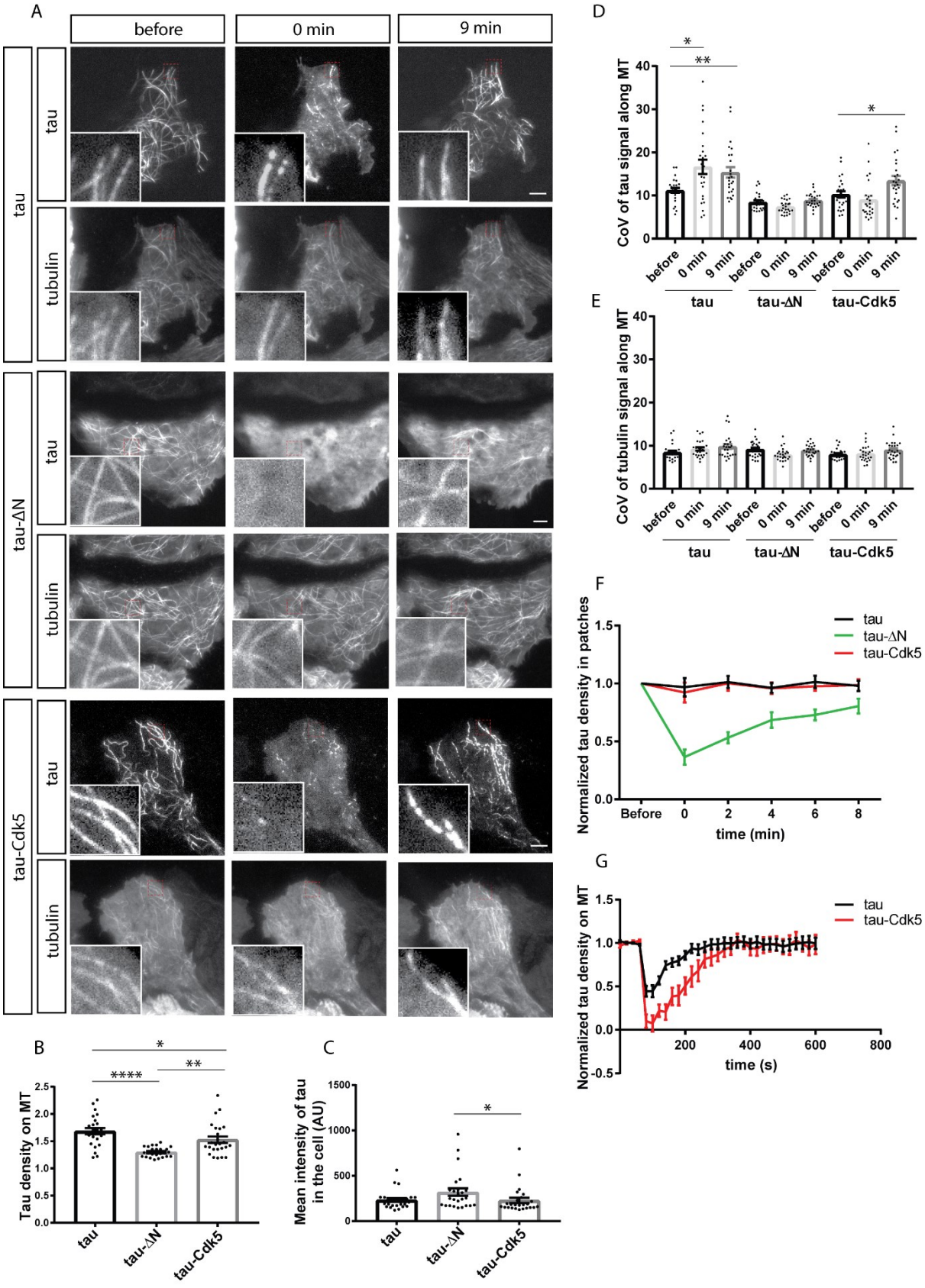

Figure 25: Phosphorylation of tau affects the stability of tau envelopes.

*A) Representative images of IMCD3 cells expressing GFP-tau (denoted as tau), truncated tau (denoted as tau-ΔN) or tau in the conditions of high Cdk5 activity (tau-Cdk5) before the elevated pH treatment (denoted as before, left panels), right after the pH treatment (denoted as 0 min, middle panels), and 9 minutes after the pH treatment (denoted as 9 min, right panels). For each cell, tau and tubulin signal are shown (upper and lower panels respectively). Scale bar = 5 μm. B) Quantification of tau density on the microtubules (MT; tau = 1.69 ± 0.06, tau-ΔN = 1.30 ± 0.02, tau-Cdk5 = 1.53 ± 0.06; mean ± SEM; ****p<0.0001, **p<0.01, *p<0.05; Mann-Whitney test; n=25 cells for each group in 4 independent experiments). C) Quantification of mean intensity of GFP signal in the cells (tau = 232.5 ± 20.2, tau-ΔN = 319.5 ± 41.6, tau-Cdk5 = 227.5 ± 29.5; mean ± SEM; *p<0.05; Mann-Whitney test; n=25 cells for each group in 4 independent experiments). D) Quantification of the coefficient of variation (CoV) of tau signal along the microtubules (MT). **p<0.01, *p<0.05; Mann-Whitney test; n=25 cells for each group in 4 independent experiments. E) Quantification of the coefficient of variation of tubulin signal along the microtubules (MT; not statistically analyzed). F) Normalized tau density in tau patches in control and tau-Cdk5 cells and normalized tau density along the microtubule in tau-ΔN cells where no patches are visible. The densities are analyzed at five time points after the pH-treatment and normalized to the density of tau on the microtubules before the treatment. G) Quantification of tau density on microtubules (MT) through the whole cell (the mean tau intensity subtracted by the mean intensity of the cytoplasm region without microtubules) normalized to the tau density before the pH treatment.*

I prepared the cells and captured them in the Imaging Methods Core Facility at BIOCEV. I analyzed the data and consulted the analyses with Valerie Siahaan and other authors of the paper. The exponential time constants were calculated by Valerie Siahaan.

4.3.3 Phosphorylation of tau decreases the protective function of tau envelopes

It was shown that tau envelopes differently modify access of other microtubule-associated proteins to microtubules regulating their function (Siahaan et al., 2019; Tan et al., 2019). An example of such a protein is microtubule-severing enzyme katanin. It was shown that tau envelopes, but not diffusively bound tau protect microtubules from katanin severing (Siahaan et al., 2019). As we show that phosphorylated tau forms tau envelopes but those envelopes are less stable, we asked if there is also a functional effect of phosphorylation on protectivity of tau envelopes. To answer this question, we tested how tau envelopes in the control conditions and in the conditions of higher Cdk5 activity protect microtubules against katanin digestion in IMCD3 cells (Figure 26A).

As expected, and as shown before, tau expression protected microtubules from katanin severing ($p<0.0001$; Figure 26A, B). Interestingly, tau in conditions of high Cdk5 activity was not able to protect microtubules anymore ($p<0.0001$) and the microtubules were severed similarly as without tau ($p=0.5169$; Figure 26A, B). To show that the observed effect is not because of other cellular targets of Cdk5, we tested the severing in the conditions of high Cdk5 activity without tau. Cdk5 expression itself leads to slightly increased digestion ($p=0.0466$) but this small change can not explain the effect observed with phosphorylated tau (Figure 26A, B).

As the cells were transfected and thus the amount of katanin is different in each cell, we also correlated the relative katanin density with the density of microtubules and observed a negative correlation in all groups. The correlation of cells expressing tau was less strong than in cells with katanin only ($p=0.03$) as well as than cell expressing tau in combination with Cdk5 ($p=0.002$; Figure 26C).

Together, the data show that tau protects microtubules from katanin severing and phosphorylation by Cdk5 abolishes this effect. The data are in accordance with *in vitro* data obtained by our collaborators (Siahaan et al., 2024).

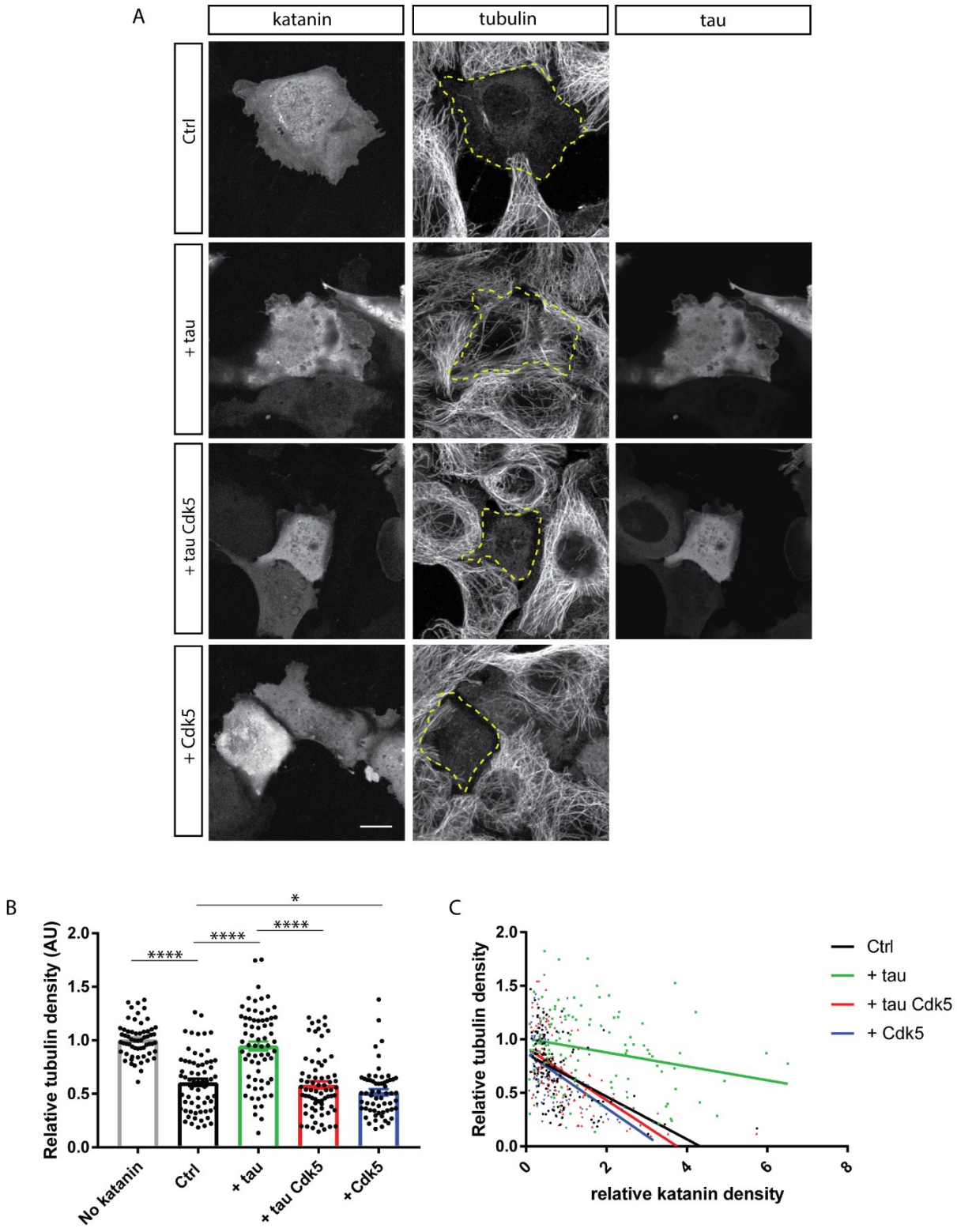

Figure 26: Phosphorylation of tau decreases the protective function of tau envelopes.

A) Representative images of IMCD3 cells transfected with GFP-katanin (left panels) and mCherry-tau (right panels). The cells were fixed and immunostained with anti-tubulin antibodies to visualize microtubules (middle panels). The diffusive signal of tau is a consequence of fixation process as described before (Ebneth et al., 1998). Cells were transfected with katanin (Ctrl), katanin and tau

*(+tau), katanin, tau and Cdk5 with its activator p25 (+ tau Cdk5), or with katanin and Cdk5 with its activator p25 (+ Cdk5). Scale bar = 5 µm. B) Relative tubulin density calculated as intensity of either cells without katanin (No katanin) or transfected cells normalized to surrounding nontransfected cells (No katanin = 1.01 ± 0.02, Ctrl = 0.61 ± 0.03, + tau = 0.95 ± 0.04, + tau Cdk5 = 0.58 ± 0.03, + Cdk5 = 0.51 ± 0.03, Mean ± SEM; *p<0.05, ****p<0.0001 Mann-Whitney test; n=60, 64, 68, 71, 60 cells in 3 independent experiments). C) Correlation between relative tubulin density and relative katanin density. Correlation coefficients are as follows: Ctrl = -0.4855, + tau = -0.2474, + tau Cdk5 = -0.5691, + Cdk5 = -0.5411; n=120, 112, 120, 122 XY pairs.*

I performed the experiments and analyzed the data. Valerie Siahaan analyzed the differences between correlations.

5 Discussion

5.1 CRMP2 isoforms possess different spatiotemporal distribution and distinct roles in the regulation of peripheral nerve growth

Microtubule-associated protein CRMP2 regulates neural development by influencing microtubule polymerization and axon growth and guidance (Fukata et al., 2002; Uchida et al., 2005). CRMP2 exists in two isoforms produced by alternative splicing. While one study claims that, in contrast to humans, pigs or chickens, only one CRMP2 isoform is present in rodents (Moutal et al., 2019), several studies show two CRMP2 isoforms to exist in mouse brain (Balastik et al., 2015; Bretin et al., 2005; Ziak et al., 2020) or in rats (Quinn et al., 2003; Rogemond et al., 2008). Here we show the presence of the two CRMP2 isoforms in the murine brain or in primary neurons using both general CRMP2 antibodies, as well as by using two different antibodies recognizing specifically CRMP2A or CRMP2A phosphorylated on Ser27, antibodies raised specifically against N-terminal exon unique only for CRMP2A. We also use a sequence derived from the murine genome (NCBI Reference Sequence: NP_001365696.1) and use it for the production of functional protein corresponding to CRMP2A. Moreover, our laboratory developed an isoform-specific knockout mice line lacking specifically CRMP2A isoform (Ziak et al., in preparation).

Despite the fact that the two CRMP2 isoforms were described more than twenty years ago (Quinn et al., 2003; Yuasa-Kawada et al., 2003), their distinct roles are not well understood and the majority of experimental studies about CRMP2 are not recognizing between the isoforms or are describing only CRMP2B. The importance of studying the individual isoforms is emphasized mainly by the results showing that the two isoforms are not substituting each other but rather show opposite effects in some aspects and are able to compensate for the effect of each other (Yuasa-Kawada et al., 2003). Recently, it was shown that CRMP2B knockout neurons have unaffected amount of CRMP2A isoform (Feuer et al., 2023), and we show that specific CRMP2A knockout mice have not changed levels of CRMP2B, suggesting that the isoforms are not regulating each other and consenting that they are not substituting each other. Considering this phenomenon, the spatiotemporal distribution of individual isoforms and their ratio could be an important determining factor of the localized function of CRMP2.

The spatial distribution of CRMP2 isoforms in neurons was described several times, showing that while CRMP2B is localized throughout the whole neuron, CRMP2A localization

is more restricted to the somatic and axonal region (Balastik et al., 2015; Bretin et al., 2005; Yuasa-Kawada et al., 2003). We show here that the specific regulation is also temporal, leading to different ratios of the two isoforms during the lifetime. We studied the ratio of the two isoforms from the embryonic until the aging stage showing that the CRMP2A proportion significantly decreases not only after the early development but progressively during the whole life. Several studies show the levels of CRMP2 isoforms in detail during embryonic and early postnatal development and compare it to the levels in the adult brain showing usually that both isoforms are expressed mainly developmentally with CRMP2B remaining until the adult stage while CRMP2A level is diminished faster (Quinn et al., 2003; Rogemond et al., 2008; Yuasa-Kawada et al., 2003). Altogether, the results show that CRMP2A isoform is more developmentally restricted.

We have also studied the portion of CRMP2A phosphorylated on its unique phosphorylation site showing that phosphorylation of CRMP2A is also decreasing with age and the phosphorylated CRMP2A seems to be even more specific only for the stage of brain development. As it was shown that this phosphorylation drives CRMP2A to degradation (Balastik et al., 2015), it is possible that the degradation mechanism could affect the temporal profile of CRMP2A isoform levels. It was shown that proteasome activity decreases during aging while immunoproteasome activity increases (reviewed in Davidson and Pickering, 2023). However, if the phosphorylation of CRMP2A and its degradation drives the distinct profiles of CRMP2 isoform levels would need further research.

It was suggested that CRMP2 binds to tubulin heterodimer in its monomeric form, but is also able to bind to and stabilize microtubules in its tetrameric form (Niwa et al., 2017). We tested the differences between the isoforms in terms of tetramerization and did not find significant difference in an *in vitro* assay. This is in accordance with the data showing that CRMP2B promotes microtubule growth (Niwa et al., 2017; Zheng et al., 2018), and with our results indicating that the longer isoform, CRMP2A, has also a promoting effect on microtubule growth *in vitro* and in cells. Further analysis will need to be done to uncover the molecular basis of the functional differences between the two isoforms.

As one of the main described roles of CRMP2 is mediating Sema3A signaling (Goshima et al., 1995), we studied the growth of peripheral nerves in mice lacking both or only the longer CRMP2 isoform. Our data show an overgrowth of the ophthalmic branch of the trigeminal nerve in total CRMP2 knockout mice resembling the effect of Sema3A-receptor knockout (Kitsukawa et al., 1997), while no significant difference was observed in CRMP2A-specific

knockout mice. These results suggest a specific role of CRMP2B isoform in Sema3A signaling and/or in the regulation of the peripheral axons growth.

The specific role of CRMP2 isoforms in axon growth is so far controversial. CRMP2B has been shown to enhance axon outgrowth in DRG (Niwa et al., 2017) and in hippocampal neurons (Tan et al., 2015). However, another study showed that overexpression of CRMP2B in neurons promotes axon branching, but suppresses axon growth, while the CRMP2A isoform has by itself no effect on axon branching or elongation and it is rather opposing the effect of CRMP2B (Yuasa-Kawada et al., 2003). Yet another study showed no effect of CRMP2 on axonal growth in motoneurons and hippocampal neurons (Duplan et al., 2010). The spinal cord axons from WT and CRMP2 KO mice used in this study grow similarly in the culture (Ziak et al., 2020).

Moreover, it was shown that CRMPs can have different effects in the central and peripheral nervous system and in different types of neurons, e.g. CRMP4 seems to be particularly important in peripheral nervous system and peripheral nerve regeneration (Duplan et al., 2010; Girouard et al., 2020). Furthermore, it was shown that different members of the CRMP family can rescue the absence of another one. Especially, it was shown that CRMP2 and CRMP4 can substitute each other in promoting axon growth (Tan et al., 2015), and CRMP4 level is considerably increased in CRMP2 knockout mice (Ziak et al., 2020). The observed overgrowth of peripheral nerves in CRMP2 knockout mice is thus likely the result of a combined effect of impacted transmission of Sema3A signaling and/or CRMP4 upregulation rather than the direct effect of CRMP2 absence on axon growth.

Still, the observed effect of full-CRMP2 knockout on peripheral nerve growth is lower than the effect of Sema3A-receptor knockout (Kitsukawa et al., 1997) which leads us to speculate that even in this function, the compensatory effect of other members of CRMP family could play a role. However, we show that the addition of Sema3A to spinal cord axons in culture significantly decreases the growth of WT neurons but has no effect on CRMP2 KO ones (Ziak et al., 2020).

In summary, we show that CRMP2 isoforms have a different spatiotemporal distribution and distinct importance in particular developmental processes. However, the understanding of the special functions of the two CRMP2 isoforms would need further research.

5.2 Prolyl isomerases PIN1 and FKBP12 regulate CRMP2A isoform depending on its phosphorylation by Cdk5

CRMP2 function has been shown to be regulated by posttranslational modifications, the best studied of which is phosphorylation. Phosphorylation of CRMP2 is generally considered an inhibitor of CRMP2's microtubule-growth-promoting function (Crews et al., 2011; Uchida et al., 2005; Yoshimura et al., 2005) with the main kinases being Cdk5 and GSK3beta and the major phosphatase PP2A (Zhu et al., 2010).

Moreover, the activity of CRMP2 can be regulated by conformational changes promoted by prolyl isomerases. Prolyl isomerases are considered to be not only proteins involved in protein folding but also in the regulation of protein function (reviewed in Schmidpeter and Schmid, 2015). The most studied prolyl isomerase for its regulatory function which governs the fate of many phosphoproteins is PIN1 (reviewed in Chen and Igumenova, 2023; Liou et al., 2011). Our group has shown that prolyl isomerase PIN1 binds and regulates protein CRMP2 after its phosphorylation by Cdk5 and it counteracts the inhibitory effect of phosphorylation. Surprisingly, it regulates specifically CRMP2A isoform (Balastik et al., 2015).

The binding of PIN1 to CRMP2A is dependent on Cdk5-phosphorylation specifically on two Serines, one of them on the C-terminus and the second (Ser27, specific for CRMP2A isoform) on the N-terminus. PIN1 protects phosphorylated CRMP2A against degradation (Balastik et al., 2015) which was shown also for other PIN1 substrates (reviewed in Liou et al., 2011). PIN1 could also allow protein dephosphorylation as it was described for example for tau protein (Zhou et al., 2000). It was shown that the dephosphorylation of the Cdk5-phosphorylation site on the C-terminus of CRMP2 is rather resistant to dephosphorylation similarly to some phosphorylation sites in tau protein (Cole et al., 2008), so PIN1 could counteract the inhibitory effect of phosphorylation also by allowing CRMP2A dephosphorylation. Nevertheless, PIN1 was not able to accelerate CRMP2 dephosphorylation on the C-terminus (Cole et al., 2008) which was, however, tested only with CRMP2B isoform, which is in our assays not bound by PIN1. Moreover, we have shown that phosphorylation of Ser27 by Cdk5 is the one resulting in proteasomal degradation of CRMP2A as mutation of this site stabilized CRMP2A protein similarly to the presence of PIN1 (Balastik et al., 2015). Our results show that knockdown of PIN1 leads to decreased CRMP2A amount in primary neurons and that the portion of Ser27-phosphorylated CRMP2A is decreased too, which could be the result of high degradation of phosphorylated CRMP2A in PIN1 deficient state.

As we show that CRMP2A and specifically CRMP2A phosphorylated on N-terminus is developmentally restricted and its amount decreases in murine brains during life, we hypothesized that it could be the effect of specific temporal stabilization of CRMP2A by PIN1. We and others (Nakamura et al., 2012b) show that PIN1 amount indeed decreases during life. However, we did not see any striking difference in CRMP2A or CRMP2A pS27 levels in comparison between WT and PIN1 KO mice suggesting another regulatory mechanism keeping the required amount of CRMP2A or a compensatory mechanism, i.e. that another prolyl isomerases could at least partially compensate for PIN1 deficiency. The compensatory mechanism in PIN1 knockout mice was suggested for at least some PIN1 functions (Liou et al., 2002). Nevertheless, no obvious changes in activity or expression of other prolyl isomerases were detected in PIN1 KO mice (Fanghänel et al., 2006).

We now show that another prolyl isomerase, FKBP12, binds to CRMP2A isoform. Interestingly, the binding of FKBP12 is regulated by the same Cdk5-phosphorylation of CRMP2A as the interaction with PIN1, but in the opposite way. Especially Ser27 seems to be critical regulatory site for both FKBP12 and PIN1 suggesting that phosphorylation of this site can switch between regulations with those two prolyl isomerases. FKBP12 shows lower specificity to the amino acid preceding proline in the binding site than PIN1. PIN1 binding is restricted to pSer/pThr-Pro motifs while the binding motif for FKBP12 is usually described as general Xaa-Pro, even though it was described that Leu-Pro is the best target (Jakob et al., 2009) and is used for example in inositol-1,4,5-triphosphate receptor (Cameron et al., 1997). It was shown that motif Ser-Pro is almost 10x less bound by FKBP12 than Leu-Pro but still 50x better than Asp-Pro or Glu-Pro which were shown as the worst substrates (Jakob et al., 2009). Interestingly, FKBP12 binding can be even proline-independent suggesting that the isomerized motif and the binding site do not have to be identical (Ahearn et al., 2011). Recently, it was shown that FKBP12 is able to bind to three different binding sites on tau, from which only the weakest one includes proline (Jiang et al., 2023). Moreover, inhibition of FKBP12 binding by phosphorylation of the substrate was recently shown for tau. The two major FKBP12-binding sites on tau contain tyrosine and the phosphorylation of these sites abolishes the binding of FKBP12 (Jiang et al., 2023). Nevertheless, to our knowledge, a phosphorylation at a specific site affecting the binding of two different prolyl isomerases in the opposite way has not been described yet.

Interestingly, we show not only that phosphorylation of CRMP2A affects the binding of FKBP12, but also that FKBP12 regulates CRMP2A phosphorylation. We show that

knockdown of FKBP12 decreases the Ser27 phosphorylation level in primary neurons without affecting the total amount of CRMP2A. It was shown several times that FKBP12 can affect the phosphorylation of its substrates - for instance FKBP12 affects some signaling pathways by interacting with Ca^{2+}-dependent phosphatase Calcineurin, bringing the phosphatase to the target and allowing its dephosphorylation (Cameron et al., 1997; Shin et al., 2002). FKBP12 binding was also shown to prevent phosphorylation of TGF-beta and EGF receptors (Chen et al., 1997; Lopez-Ilasaca et al., 1998). Our results demonstrate, however, the opposite trend - downregulation of FKBP12 leading to lower phosphorylation. We suggest that FKBP12 could bind to non-phosphorylated CRMP2A and allows its phosphorylation, which could be accomplished by providing the conformational change and subsequent accessibility for conformation-specific protein kinases (reviewed in Wulf et al., 2005). With this mechanism, FKBP12 could regulate the degradation of CRMP2A, as it has been shown before that phosphorylation of Ser27 promotes the degradation of CRMP2A (Balastik et al., 2015). However, we did not observe a significant effect of FKBP12 on the total amount of CRMP2A protein. Also, in our following *in vitro* assays, we can see the effect of FKBP12 on CRMP2A using purified proteins, suggesting that the effect of FKBP12 on CRMP2A function is rather direct, and the effect on CRMP2A phosphorylation present another regulatory pathway.

Together, our data show conformational changes catalyzed by prolyl isomerases as a new level of regulation of CRMP2A activity above its phosphorylation. We show that one protein can be conformationally regulated in its both phosphorylated and nonphosphorylated states suggesting that prolyl isomerases can specifically regulate function and maintain the level of their substrates both spatially and temporally.

5.3 Prolyl isomerase FKBP12 regulates microtubule dynamics and axon growth

We show that in contrast to PIN1, which stabilizes CRMP2A and promotes axonal growth (Balastik et al., 2015), FKBP12 inhibits the activity of CRMP2A, which results in decreased microtubule polymerization *in vitro* and *in vivo* and in reduced axon growth.

It was shown before that two different members of the FKBP family – FKBP52 and FKBP25 – regulate microtubule polymerization directly by binding to tubulin (Dilworth et al., 2018; Chambraud et al., 2007). However, FKBP12 does not bind and regulate tubulin directly (Chambraud et al., 2007). Now we show that FKBP12 regulates microtubule dynamics indirectly by controlling the activity of CRMP2A. Prolyl isomerases regulates micortubules in

neurons also by microtubule-associated protein tau, which is regulated by prolyl isomerases FKBP12, FKBP51, FKBP52, and PIN1 (Chambraud et al., 2010; Ikura and Ito, 2013; Jiang et al., 2023; Jinwal et al., 2010).

Previously, phosphorylation of CRMP2 was suggested as a mechanism inhibiting CRMP2 function (Uchida et al., 2005). Here we show that FKBP12 binds to CRMP2A which is not phosphorylated (specifically on Ser27) and inhibits its function. Moreover, we observed that the mutated form (S27A) of CRMP2A which cannot be phosphorylated on Ser27 is not able to promote the microtubule growth in cells. We suggest that this effect can be the consequence of higher inhibition by prolyl isomerase FKBP12 because of the higher affinity of FKBP12 to this mutated CRMP2A. This is in agreement with the fact that knockdown of FKBP12 in combination with this mutated CRMP2A mimicked the WT CRMP2A and overexpression of FKBP12 in combination with WT CRMP2A mimicked the mutated one.

It was shown that CRMP2B is able to increase microtubule growth in DRG (Xia et al., 2013). We now show that CRMP2A isoform is also increasing microtubule growth in DRG. In our assay we observed slightly higher velocity values even in control conditions compared to published data (Eira et al., 2021; Xia et al., 2013). This discrepancy could be a consequence of different stage of isolated DRG, different cultivation conditions or by the use of different EB3-expression constructs, as it was shown that expression of EB3 increases by itself the growth velocity (Roth et al., 2018). Interestingly, FKBP12 silencing is also increasing microtubule growth in DRG, even though the differences are small. This may be due to measurements in axon shafts in our assays, as it was shown that the effects on microtubule growth differ depending on the analyzed area of axon (Eira et al., 2021). However, the increase in microtubule growth observed with CRMP2A expression as well as silencing of FKBP12 is in agreement with our other results and with the inhibitory effect of FKBP12 on CRMP2A.

Even though FKBP12 is studied mainly in connection to immunoregulation and cardiac research, there are many studies describing its importance in neurons and in the brain. We now show that FKBP12 overexpression decreases while FKBP12 knockdown increases axon growth and suggest that the effect is through binding of FKBP12 to CRMP2A. This is in agreement with the results showing that inhibitor of FKBP12 (FK506) promotes neurite outgrowth (Lyons et al., 1994), and this inhibitor, as well as other FKBP12-inhibitor without immunosuppressive function, accelerates nerve regeneration (Gold et al., 1995; Gold et al., 1997; Khan et al., 2002). However, the mechanism of this phenomenon is not well understood and similar effect was described also for FK506 derivatives that do not bind FKBP12 (Gold et

al., 2005). Since CRMP2 (Suzuki et al., 2003) and microtubule stabilization itself (Hellal et al., 2011) were also shown to increase neurite outgrowth and nerve regeneration, we suggest that FKBP12 could regulate axon growth through its regulation of CRMP2A function.

It was shown that removing FKBP12 specifically in the brain leads to enhanced late-phase LTP (L-LTP) and perseveration in several assays of memory (Hoeffer et al., 2008), while brain-specific CRMP2 knockout mice show reduced LTP and impaired learning and memory (Zhang et al., 2016; Ziak et al., 2020). Together, these results are in agreement with FKBP12-mediated inhibition of CRMP2A. Also, both those proteins were connected to behavioral phenotypes that have been observed in several cognitive disorders, including autism spectrum disorder (ASD), obsessive-compulsive disorder (OCD), and schizophrenia (Hoeffer et al., 2008; Zhang et al., 2016; Ziak et al., 2020).

We also show the effect of FKBP12 downregulation on neuronal migration during embryonic development. The role of CRMP2 in neuronal migration is so far not clear, as in our total CRMP2 knockouts, we did not observe any significant effect of CRMP2 absence on neuronal migration (Ziak et al., 2020), while CRMP2 silencing was shown to perturb neuronal migration (Ip et al., 2012). However, neither of these outcomes is in agreement with our results showing decreased neuronal migration in FKBP12 knockdown cortices and the observed inhibitory effect of FKBP12 on CRMP2A. As we show that FKBP12 regulates specifically CRMP2A isoform and that the two CRMP2 isoforms could have different effects, we could still speculate about a specific role of the isoforms in neuronal migration. However, our FKBP12 knockdown phenotype was neither compensated nor amplified by the expression of CRMP2A protein. Thus, we suggest that the observed effect of FKBP12 on neuronal migration is mediated by another FKBP12 substrate than CRMP2A.

We show that specifically CRMP2A isoform is bound and regulated by prolyl isomerase FKBP12. CRMP2A isoform is much less expressed but its relative amount is higher in axonal growth cones (Balastik et al., 2015). From our data, it seems that the CRMP2A isoform is much more tightly conformationally regulated than the more abundant isoform CRMP2B which further demonstrates their different roles in the cell. We show that FKBP12 inhibits CRMP2A, which leads to decreased microtubule dynamics and axon growth. The inhibitory effect of FKBP12 would deserve further research as we are not showing the mechanism of CRMP2A inhibition. It was recently suggested that FKBP12 could alter the conformation of proteins by two different mechanisms either by the *cis*/*trans* isomerization or by chaperone activity and that these two activities could have opposing effects as it was shown for tau protein (Jiang et

al., 2023) or alpha-synuclein and another prolyl isomerase Cyclophilin A (Favretto et al., 2020). This phenomenon was shown particularly in the regulation of protein aggregation which could be interesting considering that CRMP2 and also FKBP12 were found in neurofibrillary tangles, aggregates found in Alzheimer's disease brain (reviewed in Quach et al., 2020; Sugata et al., 2009) and interestingly, FKBP12 can prevent tau from aggregation (Ikura and Ito, 2013).

Together, we show that FKBP12 is a novel regulator of microtubule dynamics and neural development through its binding to CRMP2A and inhibiting its function. However, the role of FKBP12 in brain development is probably more complex as FKBP12 has other substrates which could play a role in these processes, e.g. tau.

5.4 Cdk5 phosphorylation affects tau envelope formation, stability, and functionality

Phosphorylation of microtubule-associated proteins has a widespread effect on microtubule function and stability. Recently, it was shown that microtubule-associated protein tau can bind to microtubules cooperatively making protective tau envelopes and we tested the effect of Cdk5 phosphorylation on the formation and functionality of tau envelopes. It was shown before, that tau in envelopes has lower turnover (Tan et al., 2019). Thus, we tested first the differences in the turnover between control tau (making envelopes), delta-tau (not making envelopes), and phosphorylated tau in cells. In control cells, we observed a recovery time constant of around 6 seconds and in delta-tau around 1.7 seconds (approximately 3.5x difference between control and delta tau) which is much faster than what was described *in vitro* by FRAP (22.2 s in envelopes and 10.4 s outside the envelopes; Tan et al., 2019) or by another method (20 s in envelopes and 3 s outside the envelopes; Siahaan et al., 2019). However, the recovery time observed in our experiment is comparable with the recovery observed in different cell models (half-time recovery of 3 s in Vero cells and 3.8 s in neurons (Konzack et al., 2007) or 5.8 s in human 356 fibroblasts (Samsonov et al., 2003)). The observed differences between cell types could be caused by the different natural levels of phosphorylation in the different cell lines or by a slightly different experimental approach. It was also shown that the recovery time as well as the portion of immobile fraction differs in neurons even between different stages of development as well as between the cellular compartments (Iwata et al., 2019). Importantly, the recovery time of our Cdk5-phosphorylated tau lies in between cooperative control tau and

non-cooperative delta-tau suggesting that phosphorylated tau binds cooperatively but the cooperativity is lower than in control tau.

Another parameter used to describe the behavior of tau envelopes is their assembly/disassembly, which can be reached in cells using taxol (Siahaan et al., 2022). It was shown before that pH affects the binding of tau to microtubules showing that elevated pH increases the diffusion coefficient of tau and decreases the duration of the interactions (Hinrichs et al., 2012). It was also shown that higher pH decreases the binding of tau to microtubules in cells (Charafeddine et al., 2019). So, we decided to use increased pH as a model for challenging tau binding which could show us the envelopes. With this method, we show that phosphorylated tau more readily dissociates from microtubules than control tau, but importantly, during the recovery, it still shows a patches-like pattern even though the regrowth is slower than in control cells. Together, the data is in agreement with *in vitro* results showing that a higher concentration of phosphorylated tau is needed to see comparable envelope coverage as with control tau. Also, the disassembly of tau envelopes is much faster in the presence of active Cdk5 (Siahaan et al., 2024).

Finally, as it was shown that tau envelopes can affect differently the binding of microtubule-associated proteins thereby regulating their function (Siahaan et al., 2019; Tan et al., 2019), our collaborators tested the effect of Cdk5 phosphorylation on kinesin and katanin accessibility to microtubules *in vitro* (Siahaan et al., 2024) showing that kinesin is not able to walk through the envelopes and that this effect is not affected by tau phosphorylation. On the other hand, they show the difference between phosphorylated and non-phosphorylated tau in the case of katanin accessibility showing that katanin is not able to digest inside the tau envelopes in control conditions, but it is in the case of phosphorylated tau. Together, the data indicate that tau phosphorylation does not make tau envelopes dysfunctional, but rather forms a regulatory mechanism precluding kinesin transport, but allowing katanin severing. As katanin severing was affected *in vitro*, we tested the functionality of tau envelopes in microtubule protection against katanin digestion in cells. We show, similarly to others (Qiang et al., 2006), that tau protects microtubules from katanin severing. Interestingly, phosphorylated tau was not able to protect the microtubules. This effect was suggested before, hypothesizing that hyperphosphorylated tau is detaching from microtubules leaving them unprotected and this presumption was suggested as a possible mechanism for axonal branching (Qiang et al., 2006; Sudo and Baas, 2011).

Even though it is generally accepted that phosphorylation detaches tau from microtubules,

it depends on the phosphorylation level. It was shown that some phosphorylation is, on the contrary, needed for binding of tau to microtubules. Some phosphorylations are found exclusively in the microtubule-bound fraction (Cho and Johnson, 2003), and it was shown that neither under-phosphorylated nor highly phosphorylated tau isoforms are associated with microtubules, suggesting that phosphorylation can affect the binding positively as well as negatively (Deancos et al., 1993).

There are over 80 possible phosphorylation sites in the human longest tau isoform (Kimura et al., 2018) with more than 30 of them described as phosphorylated in paired-helical filaments in AD brains (reviewed in Gong et al., 2006). It was shown that tau from AD brains does not bind to tubulin (Alonso et al., 1994) and some specific phosphorylation sites that affect tau's affinity to microtubules were described, mainly Ser262 and Thr231 (Biernat et al., 1993; Drewes et al., 1995; Cho and Johnson, 2004; Sengupta et al., 1998; Schneider et al., 1999). On the other hand, it was also shown that phospho-epitopes specific to AD affect tubulin assembly but not binding to microtubules (Amniai et al., 2009). In our experiments, we are using the high activity of Cdk5 as a model of higher phosphorylation. Several phosphorylation sites were described to be phosphorylated by Cdk5 with the 4 major phosphorylation sites (shown in the majority of the studies) being Ser202, Thr205, Ser235, and Ser404 (Kimura et al., 2016; Kimura et al., 2014). These phosphorylations are found in both control and AD brains (Martin et al., 2013) and are also increased in bacterial tau treated with Cdk5/p35 used in our *in vitro* assays (Siahaan et al., 2024). Phosphorylation of sites Ser202/Thr205/Ser235 was shown not to affect binding to taxol-stabilized microtubules and it was demonstrated that Cdk5 epitopes can cause functional defects of tau even though the binding of tau to microtubules is not affected (Amniai et al., 2009; Barbier et al., 2019). On the other hand, it was also shown that Ser235 inhibits binding to microtubules by 10% (Sengupta et al., 1998).

In our experiments using cell cultures, other phosphorylations can play a role as it was shown that phosphorylation by one kinase can promote or inhibit phosphorylation of specific sites by other kinases creating a large variety of phosphorylated tau species. Such an example is GSK3beta kinase which can phosphorylate tau after priming by Cdk5 kinase (Liu et al., 2006). Also, we used p25 as an activator of Cdk5 kinase in our experiment in cells and while some studies show that Cdk5/p25 phosphorylates tau similarly to Cdk5/p35 (Kimura et al., 2016), other results show that Cdk5/p25 transfection leads to a different phosphorylation and decreased tau binding to microtubules (Patrick et al., 1999). Interestingly, it was suggested that p25 is not only a pathological product of p35 cleavage but plays also a physiological role in

neurons showing that transient p25 activation regulates synaptic plasticity learning, memory, and synaptogenesis (Angelo et al., 2006; Fischer et al., 2005; Seo et al., 2014).

In our experiments in cells, we see a lower density of tau on the microtubules which could be the effect of lower affinity of tau to tubulin or lower tau-tau cooperative binding. *In vitro*, the envelopes from phosphorylated tau are less dense than envelopes from control tau (in the concentration of tau making the similar coverage of microtubules by envelopes; Siahaan et al., 2024). In general, it is difficult to separate tau affinity to tubulin from tau cooperative interaction as they are both intrinsically intertwined. Thus, lower binding of tau to microtubules can contribute to the observed effects in cells but together with the data shown *in vitro*, where is possible to visualize the envelopes and see immediately the difference between the regions where tau is bound non-cooperatively and the regions covered by tau envelopes (Siahaan et al., 2024), we suggest that effects observed in cells is the effect of tau ability to form protective tau envelopes.

Tau is phosphorylated by numerous kinases in healthy neurons, but deregulation of Cdk5 seems critical in the neuropathological process leading to neurodegeneration (Cruz and Tsai, 2004). The precise understanding of the function of phosphorylation is still not fully understood. We are now showing that Cdk5 phosphorylation could affect the protectiveness of tau envelopes which could be one part of the mechanism in physiological as well as pathological regulation of tau.

As Cdk5 phosphorylation affects tau envelopes, it would be interesting to test if there is an additional effect of PIN1 prolyl isomerase. Until now, it was shown that PIN1 binds to tau and is able to restore the function of phosphorylated tau through affecting dephosphorylation of tau by phosphatases (Kutter et al., 2016; Lu et al., 1999; Zhou et al., 2000). The interaction between FKBP12 and tau and the role of FKBP12 in the pathology of tau aggregation was also described (Ikura and Ito, 2013; Jiang et al., 2023; Zhuang et al., 2024). However, the effect of prolyl isomerases on tau envelopes was not yet shown and will be a subject of further studies.

6 Summary

Microtubule-associated proteins are important regulators of many cellular processes. Their importance is emphasized in neurons, cells with long protrusions for whose formation and function the cytoskeleton is essential. We focused here on collapsin response mediator proteins and tau protein. Both of these microtubule-associated proteins can regulate the stability of microtubules, both are the target of many posttranslational modifications, mainly phosphorylation and both are related to Alzheimer's disease. Even though both of these proteins have been analyzed in detail, their precise regulation and cooperation to build and maintain complex neuronal network in physiological conditions as well as their deregulation accompanying neurodegeneration is not fully understood. The main common player in the regulation of tau and CRMP2 is phosphorylation provided by many different protein kinases, from which Cdk5 kinase is one of the most studied. We show that Cdk5 phosphorylation specifically controls yet another level of regulation of CRMP2, conformational changes catalyzed by prolyl isomerases. Interestingly, this special regulation concerns only one isoform of CRMP2 protein, suggesting distinct regulation and distinct roles of individual CRMP2 isoforms in neural development. Moreover, a specific Cdk5-dependent phosphorylation site determines the accessibility for two different prolyl isomerases suggesting the importance of this regulatory mechanism. We also show an effect of Cdk5 phosphorylation on protective tau envelopes. As it was shown that tau could be bound by several prolyl isomerases, it would be interesting to continue studying the effect of prolyl isomerases on tau envelopes and their protective function. As prolyl isomerases PIN1 and FKBP12 as well as Cdk5 and both mentioned microtubule-associated proteins are connected to neurodegenerative disorders such as Alzheimer’s disease, the observed regulatory mechanism and its changes could be a part of the pathogenesis of this disorder.

Together, we show regulatory mechanisms controlling microtubule stability in neuronal cells specifically driven by kinase Cdk5 and prolyl isomerases applicable in neural development as well as in neurodegeneration.

7 References

Ackmann, M., H. Wiech, and E. Mandelkow. 2000. Nonsaturable binding indicates clustering of tau on the microtubule surface in a paired helical filament-like conformation. *J Biol Chem*. 275:30335-30343.

Ahearn, I.M., F.D. Tsai, H. Court, M. Zhou, B.C. Jennings, M. Ahmed, N. Fehrenbacher, M.E. Linder, and M.R. Philips. 2011. FKBP12 binds to acylated H-ras and promotes depalmitoylation. *Mol Cell*. 41:173-185.

Ahlijanian, M.K., N.X. Barrezueta, R.D. Williams, A. Jakowski, K.P. Kowsz, S. McCarthy, T. Coskran, A. Carlo, P.A. Seymour, J.E. Burkhardt, R.B. Nelson, and J.D. McNeish. 2000. Hyperphosphorylated tau and neurofilament and cytoskeletal disruptions in mice overexpressing human p25, an activator of cdk5. *Proc Natl Acad Sci U S A*. 97:2910-2915.

Al-Bassam, J., R.S. Ozer, D. Safer, S. Halpain, and R.A. Milligan. 2002. MAP2 and tau bind longitudinally along the outer ridges of microtubule protofilaments. *Journal of Cell Biology*. 157:1187-1196.

Alonso, A.D., T. Zaidi, I. Grundkeiqbal, and K. Iqbal. 1994. Role of Abnormally Phosphorylated Tan in the Breakdown of Microtubules in Alzheimer-Disease. *P Natl Acad Sci USA*. 91:5562-5566.

Alquezar, C., S. Arya, and A.W. Kao. 2020. Tau Post-translational Modifications: Dynamic Transformers of Tau Function, Degradation, and Aggregation. *Frontiers in neurology*. 11:595532.

Ambadipudi, S., J. Biernat, D. Riedel, E. Mandelkow, and M. Zweckstetter. 2017. Liquid-liquid phase separation of the microtubule-binding repeats of the Alzheimer-related protein Tau. *Nature communications*. 8:275.

Amniai, L., P. Barbier, A. Sillen, J.M. Wieruszeski, V. Peyrot, G. Lippens, and I. Landrieu. 2009. Alzheimer disease specific phosphoepitopes of Tau interfere with assembly of tubulin but not binding to microtubules. *Faseb Journal*. 23:1146-1152.

Angelo, M., F. Plattner, and K.P. Giese. 2006. Cyclin-dependent kinase 5 in synaptic plasticity, learning and memory. *Journal of Neurochemistry*. 99:353-370.

Arimura, N., A. Hattori, T. Kimura, S. Nakamuta, Y. Funahashi, S. Hirotsune, K. Furuta, T. Urano, Y.Y. Toyoshima, and K. Kaibuchi. 2009. CRMP-2 directly binds to cytoplasmic dynein and interferes with its activity. *Journal of Neurochemistry*. 111:380-390.

Arimura, N., C. Ménager, Y. Kawano, T. Yoshimura, S. Kawabata, A. Hattori, Y. Fukata, M. Amano, Y. Goshima, M. Inagaki, N. Morone, J. Usukura, and K. Kaibuchi. 2005. Phosphorylation by Rho kinase regulates CRMP-2 activity in growth cones. *Mol Cell Biol*. 25:9973-9984.

Avramut, M., and C.L. Achim. 2002. Immunophilins and their ligands: insights into survival and growth of human neurons. *Physiol Behav*. 77:463-468.

Balastik, M., X.Z. Zhou, M. Alberich-Jorda, R. Weissova, J. Ziak, M.F. Pazyra-Murphy, K.E. Cosker, O. Machonova, I. Kozmikova, C.H. Chen, L. Pastorino, J.M. Asara, A. Cole, C. Sutherland, R.A. Segal, and K.P. Lu. 2015. Prolyl Isomerase Pin1 Regulates Axon

Guidance by Stabilizing CRMP2A Selectively in Distal Axons. *Cell reports*. 13:812-828.

Barbier, P., O. Zejneli, M. Martinho, A. Lasorsa, V. Belle, C. Smet-Nocca, P.O. Tsvetkov, F. Devred, and I. Landrieu. 2019. Role of Tau as a Microtubule-Associated Protein: Structural and Functional Aspects. *Front Aging Neurosci*. 11.

Becker, E.B., and A. Bonni. 2006. Pin1 mediates neural-specific activation of the mitochondrial apoptotic machinery. *Neuron*. 49:655-662.

Bhandare, V.V., B.V. Kumbhar, and A. Kunwar. 2019. Differential binding affinity of tau repeat region R2 with neuronal-specific β-tubulin isotypes. *Sci Rep-Uk*. 9.

Bierer, B.E., P.S. Mattila, R.F. Standaert, L.A. Herzenberg, S.J. Burakoff, G. Crabtree, and S.L. Schreiber. 1990. Two distinct signal transmission pathways in T lymphocytes are inhibited by complexes formed between an immunophilin and either FK506 or rapamycin. *Proc Natl Acad Sci U S A*. 87:9231-9235.

Biernat, J., N. Gustke, G. Drewes, E.M. Mandelkow, and E. Mandelkow. 1993. Phosphorylation of Ser(262) Strongly Reduces Binding of Tau-Protein to Microtubules - Distinction between Phf-Like Immunoreactivity and Microtubule-Binding. *Neuron*. 11:153-163.

Biernat, J., and E.M. Mandelkow. 1999. The development of cell processes induced by tau protein requires phosphorylation of serine 262 and 356 in the repeat domain and is inhibited by phosphorylation in the proline-rich domains. *Molecular biology of the cell*. 10:727-740.

Blasco, H., N. Bernard-Marissal, P. Vourc'h, Y.O. Guettard, C. Sunyach, O. Augereau, J. Khederchah, K. Mouzat, C. Antar, P.H. Gordon, C. Veyrat-Durebex, G. Besson, P.M. Andersen, F. Salachas, V. Meininger, W. Camu, B. Pettmann, C.R. Andres, P. Corcia, and F.A.S. Grp. 2013. A Rare Motor Neuron Deleterious Missense Mutation in the DPYSL3 (CRMP4) Gene is Associated with ALS. *Hum Mutat*. 34:953-960.

Bodakuntla, S., A.S. Jijumon, C. Villablanca, C. Gonzalez-Billault, and C. Janke. 2019. Microtubule-Associated Proteins: Structuring the Cytoskeleton. *Trends in cell biology*. 29:804-819.

Boyko, S., X. Qi, T.H. Chen, K. Surewicz, and W.K. Surewicz. 2019. Liquid-liquid phase separation of tau protein: The crucial role of electrostatic interactions. *J Biol Chem*. 294:11054-11059.

Bretin, S., S. Reibel, E. Charrier, M. Maus-Moatti, N. Auvergnon, A. Thevenoux, J. Glowinski, V. Rogemond, J. Premont, J. Honnorat, and C. Gauchy. 2005. Differential expression of CRMP1, CRMP2A, CRMP2B, and CRMP5 in axons or dendrites of distinct neurons in the mouse brain. *The Journal of comparative neurology*. 486:1-17.

Bretin, S., V. Rogemond, P. Marin, M. Maus, Y. Torrens, J. Honnorat, J. Glowinski, J. Prémont, and C. Gauchy. 2006. Calpain product of WT-CRMP2 reduces the amount of surface NR2B NMDA receptor subunit. *J Neurochem*. 98:1252-1265.

Breuzard, G., P. Hubert, R. Nouar, T. De Bessa, F. Devred, P. Barbier, J.N. Sturgis, and V. Peyrot. 2013. Molecular mechanisms of Tau binding to microtubules and its role in microtubule dynamics in live cells. *Journal of cell science*. 126:2810-2819.

Brillantes, A.B., K. Ondrias, A. Scott, E. Kobrinsky, E. Ondriasová, M.C. Moschella, T. Jayaraman, M. Landers, B.E. Ehrlich, and A.R. Marks. 1994. Stabilization of calcium

release channel (ryanodine receptor) function by FK506-binding protein. *Cell*. 77:513-523.

Brion, J.P., C. Smith, A.M. Couck, J.M. Gallo, and B.H. Anderton. 1993. Developmental changes in tau phosphorylation: fetal tau is transiently phosphorylated in a manner similar to paired helical filament-tau characteristic of Alzheimer's disease. *J Neurochem*. 61:2071-2080.

Brown, M., T. Jacobs, B. Eickholt, G. Ferrari, M. Teo, C. Monfries, R.Z. Qi, T. Leung, L. Lim, and C. Hall. 2004. α2-chimaerin, cyclin-dependent kinase 5/p35, and its target collapsin response mediator protein-2 are essential components in semaphorin 3A-induced growth-cone collapse. *J Neurosci*. 24:8994-9004.

Brunden, K.R., J.Q. Trojanowski, and V.M. Lee. 2008. Evidence that non-fibrillar tau causes pathology linked to neurodegeneration and behavioral impairments. *J Alzheimers Dis*. 14:393-399.

Butner, K.A., and M.W. Kirschner. 1991. Tau protein binds to microtubules through a flexible array of distributed weak sites. *The Journal of cell biology*. 115:717-730.

Butterfield, D.A., H.F. Poon, D. St Clair, J.N. Keller, W.M. Pierce, J.B. Klein, and W.R. Markesbery. 2006. Redox proteomics identification of oxidatively modified hippocampal proteins in mild cognitive impairment: insights into the development of Alzheimer's disease. *Neurobiology of disease*. 22:223-232.

Byk, T., T. Dobransky, C. Cifuentes-Diaz, and A. Sobel. 1996. Identification and molecular characterization of Unc-33-like phosphoprotein (Ulip), a putative mammalian homolog of the axonal guidance-associated unc-33 gene product. *J Neurosci*. 16:688-701.

Cameron, A.M., F.C. Nucifora, Jr., E.T. Fung, D.J. Livingston, R.A. Aldape, C.A. Ross, and S.H. Snyder. 1997. FKBP12 binds the inositol 1,4,5-trisphosphate receptor at leucine-proline (1400-1401) and anchors calcineurin to this FK506-like domain. *J Biol Chem*. 272:27582-27588.

Carrell, R.W., and D.A. Lomas. 1997. Conformational disease. *Lancet (London, England)*. 350:134-138.

Castle, B.T., K.M. McKibben, E. Rhoades, and D.J. Odde. 2020. Tau Avoids the GTP Cap at Growing Microtubule Plus-Ends. *iScience*. 23:101782.

Cole, A.R., F. Causeret, G. Yadirgi, C.J. Hastie, H. Mclauchlan, E.J. McManus, F. Hernández, B.J. Eickholt, M. Nikolic, and C. Sutherland. 2006. Distinct priming kinases contribute to differential regulation of collapsin response mediator proteins by glycogen synthase kinase-3. *J Biol Chem*. 281:16591-16598.

Cole, A.R., W. Noble, L. van Aalten, F. Plattner, R. Meimaridou, D. Hogan, M. Taylor, J. LaFrancois, F. Gunn-Moore, A. Verkhratsky, S. Oddo, F. LaFerla, K.P. Giese, K.T. Dineley, K. Duff, J.C. Richardson, S.D. Yan, D.P. Hanger, S.M. Allan, and C. Sutherland. 2007. Collapsin response mediator protein-2 hyperphosphorylation is an early event in Alzheimer's disease progression. *J Neurochem*. 103:1132-1144.

Cole, A.R., M.P. Soutar, M. Rembutsu, L. van Aalten, C.J. Hastie, H. McLauchlan, M. Peggie, M. Balastik, K.P. Lu, and C. Sutherland. 2008. Relative resistance of Cdk5-phosphorylated CRMP2 to dephosphorylation. *J Biol Chem*. 283:18227-18237.

Crews, L., R. Ruf, C. Patrick, W. Dumaop, M. Trejo-Morales, C.L. Achim, E. Rockenstein, and E. Masliah. 2011. Phosphorylation of collapsin response mediator protein-2

disrupts neuronal maturation in a model of adult neurogenesis: Implications for neurodegenerative disorders. *Mol Neurodegener*. 6.

Cruz, J.C., and L.H. Tsai. 2004. Cdk5 deregulation in the pathogenesis of Alzheimer's disease. *Trends Mol Med*. 10:452-458.

Cruz, J.C., H.C. Tseng, J.A. Goldman, H. Shih, and L.H. Tsai. 2003. Aberrant Cdk5 activation by p25 triggers pathological events leading to neurodegeneration and neurofibrillary tangles. *Neuron*. 40:471-483.

Davidson, K., and A.M. Pickering. 2023. The proteasome: A key modulator of nervous system function, brain aging, and neurodegenerative disease. *Frontiers in cell and developmental biology*. 11:1124907.

Dawson, H.N., A. Ferreira, M.V. Eyster, N. Ghoshal, L.I. Binder, and M.P. Vitek. 2001. Inhibition of neuronal maturation in primary hippocampal neurons from tau deficient mice. *Journal of cell science*. 114:1179-1187.

Deancos, J.G., I. Correas, and J. Avila. 1993. Differences in Microtubule Binding and Self-Association Abilities of Bovine Brain Tau-Isoforms. *J Biol Chem*. 268:7976-7982.

Deleersnijder, A., A.S. Van Rompuy, L. Desender, H. Pottel, L. Buée, Z. Debyser, V. Baekelandt, and M. Gerard. 2011. Comparative analysis of different peptidyl-prolyl isomerases reveals FK506-binding protein 12 as the most potent enhancer of alpha-synuclein aggregation. *J Biol Chem*. 286:26687-26701.

Deo, R.C., E.F. Schmidt, A. Elhabazi, H. Togashi, S.K. Burley, and S.M. Strittmatter. 2004. Structural bases for CRMP function in plexin-dependent semaphorin3A signaling. *Embo J*. 23:9-22.

Despres, C., C. Byrne, H. Qi, F.X. Cantrelle, I. Huvent, B. Chambraud, E.E. Baulieu, Y. Jacquot, I. Landrieu, G. Lippens, and C. Smet-Nocca. 2017. Identification of the Tau phosphorylation pattern that drives its aggregation. *Proc Natl Acad Sci U S A*. 114:9080-9085.

Di Primio, C., V. Quercioli, G. Siano, M. Rovere, B. Kovacech, M. Novak, and A. Cattaneo. 2017. The Distance between N and C Termini of Tau and of FTDP-17 Mutants Is Modulated by Microtubule Interactions in Living Cells. *Front Mol Neurosci*. 10:210.

Dilworth, D., G. Gudavicius, X. Xu, A.K.J. Boyce, C. O'Sullivan, J.J. Serpa, M. Bilenky, E.V. Petrochenko, C.H. Borchers, M. Hirst, L.A. Swayne, P. Howard, and C.J. Nelson. 2018. The prolyl isomerase FKBP25 regulates microtubule polymerization impacting cell cycle progression and genomic stability. *Nucleic acids research*. 46:2459-2478.

Dixit, R., J.L. Ross, Y.E. Goldman, and E.L. Holzbaur. 2008. Differential regulation of dynein and kinesin motor proteins by tau. *Science*. 319:1086-1089.

Drewes, G., B. Trinczek, S. Illenberger, J. Biernat, G. Schmittulms, H.E. Meyer, E.M. Mandelkow, and E. Mandelkow. 1995. Microtubule-Associated Protein Microtubule Affinity-Regulating Kinase (P110(Mark)) - a Novel Protein-Kinase That Regulates Tau-Microtubule Interactions and Dynamic Instability by Phosphorylation at the Alzheimer-Specific Site Serine-262. *J Biol Chem*. 270:7679-7688.

Drubin, D.G., and M.W. Kirschner. 1986. Tau-Protein Function in Living Cells. *Journal of Cell Biology*. 103:2739-2746.

Dugger, B.N., C.M. Whiteside, C.L. Maarouf, D.G. Walker, T.G. Beach, L.I. Sue, A. Garcia, T. Dunckley, B. Meechoovet, E.M. Reiman, and A.E. Roher. 2016. The Presence of

Select Tau Species in Human Peripheral Tissues and Their Relation to Alzheimer's Disease. *J Alzheimers Dis*. 54:1249.

Duplan, L., N. Bernard, W. Casseron, K. Dudley, E. Thouvenot, J. Honnorat, V. Rogemond, B. De Bovis, P. Aebischer, P. Marin, C. Raoul, C.E. Henderson, and B. Pettmann. 2010. Collapsin Response Mediator Protein 4a (CRMP4a) Is Upregulated in Motoneurons of Mutant SOD1 Mice and Can Trigger Motoneuron Axonal Degeneration and Cell Death. *J Neurosci*. 30:785-796.

Ebneth, A., R. Godemann, K. Stamer, S. Illenberger, B. Trinczek, E.M. Mandelkow, and E. Mandelkow. 1998. Overexpression of tau protein inhibits kinesin-dependent trafficking of vesicles, mitochondria, and endoplasmic reticulum: Implications for Alzheimer's disease. *Journal of Cell Biology*. 143:777-794.

Eira, J., J. Magalhães, N. Macedo, M.E. Pero, T. Misgeld, M.M. Sousa, F. Bartolini, and M.A. Liz. 2021. Transthyretin Promotes Axon Growth via Regulation of Microtubule Dynamics and Tubulin Acetylation. *Frontiers in cell and developmental biology*. 9:747699.

Engmann, O., T. Hortobágyi, A.J. Thompson, J. Guadagno, C. Troakes, S. Soriano, S. Al-Sarraj, Y. Kim, and K.P. Giese. 2011. Cyclin-dependent kinase 5 activator p25 is generated during memory formation and is reduced at an early stage in Alzheimer's disease. *Biological psychiatry*. 70:159-168.

Esmaeliazad, B., J.H. Mccarty, and S.C. Feinstein. 1994. Sense and Antisense Transfection Analysis of Tau-Function - Tau-Influences Net Microtubule Assembly, Neurite Outgrowth and Neuritic Stability. *Journal of cell science*. 107:869-879.

Fagiani, F., S. Govoni, M. Racchi, and C. Lanni. 2021. The Peptidyl-prolyl Isomerase Pin1 in Neuronal Signaling: from Neurodevelopment to Neurodegeneration. *Molecular neurobiology*. 58:1062-1073.

Fanale, D., G. Bronte, F. Passiglia, V. Calò, M. Castiglia, F. Di Piazza, N. Barraco, A. Cangemi, M.T. Catarella, L. Insalaco, A. Listì, R. Maragliano, D. Massihnia, A. Perez, F. Toia, G. Cicero, and V. Bazan. 2015. Stabilizing versus destabilizing the microtubules: a double-edge sword for an effective cancer treatment option? *Analytical cellular pathology (Amsterdam)*. 2015:690916.

Fanghänel, J., H. Akiyama, C. Uchida, and T. Uchida. 2006. Comparative analysis of enzyme activities and mRNA levels of peptidyl prolyl/isomerases in various organs of wild type and mice. *FEBS letters*. 580:3237-3245.

Favretto, F., D. Flores, J.D. Baker, T. Strohäker, L.B. Andreas, L.J. Blair, S. Becker, and M. Zweckstetter. 2020. Catalysis of proline isomerization and molecular chaperone activity in a tug-of-war. *Nature communications*. 11:6046.

Feuer, K.L., X. Peng, C.K. Yovo, and D. Avramopoulos. 2023. DPYSL2/CRMP2 isoform B knockout in human iPSC-derived glutamatergic neurons confirms its role in mTOR signaling and neurodevelopmental disorders. *Molecular psychiatry*. 28:4353-4362.

Fischer, A., F. Sananbenesi, P.T. Pang, B. Lu, and L.H. Tsai. 2005. Opposing roles of transient and prolonged expression of p25 in synaptic plasticity and hippocampus-dependent memory. *Neuron*. 48:825-838.

Fischer, G., H. Bang, and C. Mech. 1984. [Determination of enzymatic catalysis for the cis-trans-isomerization of peptide binding in proline-containing peptides]. *Biomed Biochim Acta*. 43:1101-1111.

Flaherty, D.B., J.P. Soria, H.G. Tomasiewicz, and J.G. Wood. 2000. Phosphorylation of human tau protein by microtubule-associated kinases: GSK3beta and cdk5 are key participants. *Journal of neuroscience research*. 62:463-472.

Fletcher, D.A., and R.D. Mullins. 2010. Cell mechanics and the cytoskeleton. *Nature*. 463:485-492.

Frappier, T.F., I.S. Georgieff, K. Brown, and M.L. Shelanski. 1994. Tau-Regulation of Microtubule-Microtubule Spacing and Bundling. *Journal of Neurochemistry*. 63:2288-2294.

Fujimori, F., K. Takahashi, C. Uchida, and T. Uchida. 1999. Mice lacking Pin1 develop normally, but are defective in entering cell cycle from G(0) arrest. *Biochemical and biophysical research communications*. 265:658-663.

Fukata, Y., T.J. Itoh, T. Kimura, C. Menager, T. Nishimura, T. Shiromizu, H. Watanabe, N. Inagaki, A. Iwamatsu, H. Hotani, and K. Kaibuchi. 2002. CRMP-2 binds to tubulin heterodimers to promote microtubule assembly. *Nat Cell Biol*. 4:583-591.

Gasic, I. 2022. Regulation of Tubulin Gene Expression: From Isotype Identity to Functional Specialization. *Frontiers in cell and developmental biology*. 10:898076.

Gerard, M., Z. Debyser, L. Desender, P.J. Kahle, J. Baert, V. Baekelandt, and Y. Engelborghs. 2006. The aggregation of alpha-synuclein is stimulated by FK506 binding proteins as shown by fluorescence correlation spectroscopy. *FASEB journal : official publication of the Federation of American Societies for Experimental Biology*. 20:524-526.

Giese, K.P. 2009. GSK-3: a key player in neurodegeneration and memory. *IUBMB life*. 61:516-521.

Giese, K.P. 2014. Generation of the Cdk5 activator p25 is a memory mechanism that is affected in early Alzheimer's disease. *Front Mol Neurosci*. 7:36.

Girouard, M.P., T. Simas, L. Hua, B. Morquette, M.R. Khazaei, N. Unsain, A.D. Johnstone, I. Rambaldi, R.L. Sanz, M.E. Di Raddo, K.K. Gamage, Y. Yong, D.E. Willis, V.M.K. Verge, P.A. Barker, C. Deppmann, and A.E. Fournier. 2020. Collapsin Response Mediator Protein 4 (CRMP4) Facilitates Wallerian Degeneration and Axon Regeneration following Sciatic Nerve Injury. *eNeuro*. 7.

Goedert, M. 2005. Tau gene mutations and their effects. *Movement disorders : official journal of the Movement Disorder Society*. 20 Suppl 12:S45-52.

Goedert, M., and R. Jakes. 1990. Expression of Separate Isoforms of Human Tau-Protein - Correlation with the Tau-Pattern in Brain and Effects on Tubulin Polymerization. *Embo J*. 9:4225-4230.

Goedert, M., R. Jakes, R.A. Crowther, J. Six, U. Lübke, M. Vandermeeren, P. Cras, J.Q. Trojanowski, and V.M. Lee. 1993. The abnormal phosphorylation of tau protein at Ser-202 in Alzheimer disease recapitulates phosphorylation during development. *Proc Natl Acad Sci U S A*. 90:5066-5070.

Gold, B.G., D.M. Armistead, and M.S. Wang. 2005. Non-FK506-binding protein-12 neuroimmunophilin ligands increase neurite elongation and accelerate nerve regeneration. *Journal of neuroscience research*. 80:56-65.

Gold, B.G., K. Katoh, and T. Storm-Dickerson. 1995. The immunosuppressant FK506 increases the rate of axonal regeneration in rat sciatic nerve. *J Neurosci*. 15:7509-7516.

Gold, B.G., M. Zeleny-Pooley, M.S. Wang, P. Chaturvedi, and D.M. Armistead. 1997. A nonimmunosuppressant FKBP-12 ligand increases nerve regeneration. *Exp Neurol*. 147:269-278.

Gong, C.X., F. Liu, I. Grundke-Iqbal, and K. Iqbal. 2006. Dysregulation of protein phosphorylation/dephosphorylation in Alzheimer's disease: A therapeutic target. *J Biomed Biotechnol*.

Goode, B.L., M. Chau, P.E. Denis, and S.C. Feinstein. 2000. Structural and functional differences between 3-repeat and 4-repeat tau isoforms - Implications for normal tau function and the onset of neurodegenerative disease. *J Biol Chem*. 275:38182-38189.

Goodson, H.V., and E.M. Jonasson. 2018. Microtubules and Microtubule-Associated Proteins. *Cold Spring Harbor perspectives in biology*. 10.

Goshima, Y., F. Nakamura, P. Strittmatter, and S.M. Strittmatter. 1995. Collapsin-Induced Growth Cone Collapse Mediated by an Intracellular Protein Related to Unc-33. *Nature*. 376:509-514.

Grant, N.J., P.J. Coates, Y.L. Woods, S.E. Bray, N.A. Morrice, C.J. Hastie, D.J. Lamont, F.A. Carey, and C. Sutherland. 2015. Phosphorylation of a splice variant of collapsin response mediator protein 2 in the nucleus of tumour cells links cyclin dependent kinase-5 to oncogenesis. *BMC cancer*. 15:885.

Gu, Y., F. Oyama, and Y. Ihara. 1996. Tau is widely expressed in rat tissues. *J Neurochem*. 67:1235-1244.

Gurung, D., J.A. Danielson, A. Tasnim, J.T. Zhang, Y. Zou, and J.Y. Liu. 2023. Proline Isomerization: From the Chemistry and Biology to Therapeutic Opportunities. *Biology*. 12.

Haddad-Tvólli, R., N.E. Szabó, X.L. Zhou, and G. Alvarez-Bolado. 2013. Genetic Manipulation of the Mouse Developing Hypothalamus through Electroporation. *Jove-J Vis Exp*.

Hagestedt, T., B. Lichtenberg, H. Wille, E.M. Mandelkow, and E. Mandelkow. 1989. Tau-Protein Becomes Long and Stiff Upon Phosphorylation - Correlation between Paracrystalline Structure and Degree of Phosphorylation. *Journal of Cell Biology*. 109:1643-1651.

Hallows, J.L., K. Chen, R.A. DePinho, and I. Vincent. 2003. Decreased cyclin-dependent kinase 5 (cdk5) activity is accompanied by redistribution of cdk5 and cytoskeletal proteins and increased cytoskeletal protein phosphorylation in p35 null mice. *J Neurosci*. 23:10633-10644.

Hamdane, M., P. Dourlen, A. Bretteville, A.V. Sambo, S. Ferreira, K. Ando, O. Kerdraon, S. Bégard, L. Geay, G. Lippens, N. Sergeant, A. Delacourte, C.A. Maurage, M.C. Galas, and L. Buée. 2006. Pin1 allows for differential Tau dephosphorylation in neuronal cells. *Molecular and cellular neurosciences*. 32:155-160.

Hanger, D.P., and W. Noble. 2011. Functional implications of glycogen synthase kinase-3-mediated tau phosphorylation. *International journal of Alzheimer's disease*. 2011:352805.

Hani, J., G. Stumpf, and H. Domdey. 1995. PTF1 encodes an essential protein in Saccharomyces cerevisiae, which shows strong homology with a new putative family of PPIases. *FEBS letters*. 365:198-202.

Harding, M.W., A. Galat, D.E. Uehling, and S.L. Schreiber. 1989. A receptor for the immunosuppressant FK506 is a cis-trans peptidyl-prolyl isomerase. *Nature*. 341:758-760.

Hashiguchi, M., T. Saito, S. Hisanaga, and T. Hashiguchi. 2002. Truncation of CDK5 activator p35 induces intensive phosphorylation of Ser202/Thr205 of human tau. *J Biol Chem*. 277:44525-44530.

Hausch, F. 2015. FKBPs and their role in neuronal signaling. *Biochimica et biophysica acta*. 1850:2035-2040.

Hefti, M.M., S. Kim, A.J. Bell, R.K. Betters, K.L. Fiock, M.A. Iida, M.E. Smalley, K. Farrell, M.E. Fowkes, and J.F. Crary. 2019. Tau Phosphorylation and Aggregation in the Developing Human Brain. *Journal of neuropathology and experimental neurology*. 78:930-938.

Hellal, F., A. Hurtado, J. Ruschel, K.C. Flynn, C.J. Laskowski, M. Umlauf, L.C. Kapitein, D. Strikis, V. Lemmon, J. Bixby, C.C. Hoogenraad, and F. Bradke. 2011. Microtubule stabilization reduces scarring and causes axon regeneration after spinal cord injury. *Science*. 331:928-931.

Hensley, K., and P. Kursula. 2016. Collapsin Response Mediator Protein-2 (CRMP2) is a Plausible Etiological Factor and Potential Therapeutic Target in Alzheimer's Disease: Comparison and Contrast with Microtubule-Associated Protein Tau. *J Alzheimers Dis*. 53:1-14.

Hensley, K., K. Venkova, A. Christov, W. Gunning, and J. Park. 2011. Collapsin response mediator protein-2: an emerging pathologic feature and therapeutic target for neurodisease indications. *Molecular neurobiology*. 43:180-191.

Hernández-Vega, A., M. Braun, L. Scharrel, M. Jahnel, S. Wegmann, B.T. Hyman, S. Alberti, S. Diez, and A.A. Hyman. 2017. Local Nucleation of Microtubule Bundles through Tubulin Concentration into a Condensed Tau Phase. *Cell reports*. 20:2304-2312.

Hinrichs, M.H., A. Jalal, B. Brenner, E. Mandelkow, S. Kumar, and T. Scholz. 2012. Tau Protein Diffuses along the Microtubule Lattice. *J Biol Chem*. 287:38559-38568.

Hoeffer, C.A., W. Tang, H. Wong, A. Santillan, R.J. Patterson, L.A. Martinez, M.V. Tejada-Simon, R. Paylor, S.L. Hamilton, and E. Klann. 2008. Removal of FKBP12 enhances mTOR-Raptor interactions, LTP, memory, and perseverative/repetitive behavior. *Neuron*. 60:832-845.

Hohmann, T., and F. Dehghani. 2019. The Cytoskeleton-A Complex Interacting Meshwork. *Cells*. 8.

Hou, S.T. 2020. The regulatory and enzymatic functions of CRMPs in neuritogenesis, synaptic plasticity, and gene transcription. *Neurochemistry international*. 139:104795.

Hutton, M., C.L. Lendon, P. Rizzu, M. Baker, S. Froelich, H. Houlden, S. Pickering-Brown, S. Chakraverty, A. Isaacs, A. Grover, J. Hackett, J. Adamson, S. Lincoln, D. Dickson, P. Davies, R.C. Petersen, M. Stevens, E. de Graaff, E. Wauters, J. van Baren, M. Hillebrand, M. Joosse, J.M. Kwon, P. Nowotny, L.K. Che, J. Norton, J.C. Morris, L.A. Reed, J. Trojanowski, H. Basun, L. Lannfelt, M. Neystat, S. Fahn, F. Dark, T. Tannenberg, P.R. Dodd, N. Hayward, J.B.J. Kwok, P.R. Schofield, A. Andreadis, J. Snowden, D. Craufurd, D. Neary, F. Owen, B.A. Oostra, J. Hardy, A. Goate, J. van Swieten, D. Mann, T. Lynch, and P. Heutink. 1998. Association of missense and 5′-splice-site mutations in with the inherited dementia FTDP-17. *Nature*. 393:702-705.

Chambraud, B., H. Belabes, V. Fontaine-Lenoir, A. Fellous, and E.E. Baulieu. 2007. The immunophilin FKBP52 specifically binds to tubulin and prevents microtubule formation. *FASEB journal : official publication of the Federation of American Societies for Experimental Biology*. 21:2787-2797.

Chambraud, B., E. Sardin, J. Giustiniani, O. Dounane, M. Schumacher, M. Goedert, and E.E. Baulieu. 2010. A role for FKBP52 in Tau protein function. *Proc Natl Acad Sci U S A*. 107:2658-2663.

Charafeddine, R.A., W.A. Cortopassi, P. Lak, R. Tan, R.J. McKenney, M.P. Jacobson, D.L. Barber, and T. Wittmann. 2019. Tau repeat regions contain conserved histidine residues that modulate microtubule-binding in response to changes in pH. *J Biol Chem*. 294:8779-8790.

Charrier, E., S. Reibel, V. Rogemond, M. Aguera, N. Thomasset, and J. Honnorat. 2003. Collapsin response mediator proteins (CRMPs): involvement in nervous system development and adult neurodegenerative disorders. *Molecular neurobiology*. 28:51-64.

Chen, C.H., W. Li, R. Sultana, M.H. You, A. Kondo, K. Shahpasand, B.M. Kim, M.L. Luo, M. Nechama, Y.M. Lin, Y. Yao, T.H. Lee, X.Z. Zhou, A.M. Swomley, D.A. Butterfield, Y. Zhang, and K.P. Lu. 2015. Pin1 cysteine-113 oxidation inhibits its catalytic activity and cellular function in Alzheimer's disease. *Neurobiology of disease*. 76:13-23.

Chen, J., Y. Kanai, N.J. Cowan, and N. Hirokawa. 1992. Projection Domains of Map2 and Tau Determine Spacings between Microtubules in Dendrites and Axons. *Nature*. 360:674-676.

Chen, X.R., and T.I. Igumenova. 2023. Regulation of eukaryotic protein kinases by Pin1, a peptidyl-prolyl isomerase. *Advances in biological regulation*. 87:100938.

Chen, Y., Y.R. Wu, H.Y. Yang, X.Z. Li, M.M. Jie, C.J. Hu, Y.Y. Wu, S.M. Yang, and Y.B. Yang. 2018. Prolyl isomerase Pin1: a promoter of cancer and a target for therapy. *Cell death & disease*. 9:883.

Chen, Y.G., F. Liu, and J. Massague. 1997. Mechanism of TGFbeta receptor inhibition by FKBP12. *Embo J*. 16:3866-3876.

Cho, J.H., and G.V.W. Johnson. 2003. Glycogen synthase kinase 3β phosphorylates tau at both primed and unprimed sites -: Differential impact on microtubule binding. *J Biol Chem*. 278:187-193.

Cho, J.H., and G.V.W. Johnson. 2004. Primed phosphorylation of tau at Thr231 by glycogen synthase kinase 3β (GSK3β) plays a critical role in regulating tau's ability to bind and stabilize microtubules. *Journal of Neurochemistry*. 88:349-358.

Ikura, T., and N. Ito. 2013. Peptidyl-prolyl isomerase activity of FK506 binding protein 12 prevents tau peptide from aggregating. *Protein Eng Des Sel*. 26:539-546.

Inagaki, N., K. Chihara, N. Arimura, C. Ménager, Y. Kawano, N. Matsuo, T. Nishimura, M. Amano, and K. Kaibuchi. 2001. CRMP-2 induces axons in cultured hippocampal neurons. *Nature neuroscience*. 4:781-782.

Ionescu, A., E.E. Zahavi, T. Gradus, K. Ben-Yaakov, and E. Perlson. 2016. Compartmental microfluidic system for studying muscle-neuron communication and neuromuscular junction maintenance. *Eur J Cell Biol*. 95:69-88.

Ip, J.P.K., A.K.Y. Fu, and N.Y. Ip. 2014. CRMP2: Functional Roles in Neural Development and Therapeutic Potential in Neurological Diseases. *Neuroscientist*. 20:589-598.

Ip, J.P.K., L. Shi, Y. Chen, Y. Itoh, W.Y. Fu, A. Betz, W.H. Yung, Y. Gotoh, A.K.Y. Fu, and N.Y. Ip. 2012. α2-chimaerin controls neuronal migration and functioning of the cerebral cortex through CRMP-2. *Nature neuroscience*. 15:39-U55.

Ishiguro, K., M. Takamatsu, K. Tomizawa, A. Omori, M. Takahashi, M. Arioka, T. Uchida, and K. Imahori. 1992. Tau protein kinase I converts normal tau protein into A68-like component of paired helical filaments. *J Biol Chem*. 267:10897-10901.

Iwata, M., S. Watanabe, A. Yamane, T. Miyasaka, and H. Misonou. 2019. Regulatory mechanisms for the axonal localization of tau protein in neurons. *Molecular biology of the cell*. 30:2441-2457.

Jakob, R.P., G. Zoldák, T. Aumüller, and F.X. Schmid. 2009. Chaperone domains convert prolyl isomerases into generic catalysts of protein folding. *Proc Natl Acad Sci U S A*. 106:20282-20287.

Janke, C., and M.M. Magiera. 2020. The tubulin code and its role in controlling microtubule properties and functions. *Nature reviews. Molecular cell biology*. 21:307-326.

Jeong, J.Y., H.S. Yim, J.Y. Ryu, H.S. Lee, J.H. Lee, D.S. Seen, and S.G. Kang. 2012. One-step sequence- and ligation-independent cloning as a rapid and versatile cloning method for functional genomics studies. *Appl Environ Microbiol*. 78:5440-5443.

Jiang, L.L., P. Chakraborty, L.S. Zhang, M. Wong, S.E. Hill, C.J. Webber, J. Libera, L.J. Blair, B. Wolozin, and M. Zweckstetter. 2023. Chaperoning of specific tau structure by immunophilin FKBP12 regulates the neuronal resilience to extracellular stress. *Science Advances*. 9.

Jinwal, U.K., J. Koren, 3rd, S.I. Borysov, A.B. Schmid, J.F. Abisambra, L.J. Blair, A.G. Johnson, J.R. Jones, C.L. Shults, J.C. O'Leary, 3rd, Y. Jin, J. Buchner, M.B. Cox, and C.A. Dickey. 2010. The Hsp90 cochaperone, FKBP51, increases Tau stability and polymerizes microtubules. *J Neurosci*. 30:591-599.

Kamata, T., M. Subleski, Y. Hara, N. Yuhki, H. Kung, N.G. Copeland, N.A. Jenkins, T. Yoshimura, W. Modi, and T.D. Copeland. 1998. Isolation and characterization of a bovine neural specific protein (CRMP-2) cDNA homologous to unc-33, a C. elegans gene implicated in axonal outgrowth and guidance. *Brain Res Mol Brain Res*. 54:219-236.

Kanai, Y., R. Takemura, T. Oshima, H. Mori, Y. Ihara, M. Yanagisawa, T. Masaki, and N. Hirokawa. 1989. Expression of Multiple Tau Isoforms and Microtubule Bundle Formation in Fibroblasts Transfected with a Single Tau Cdna. *Journal of Cell Biology*. 109:1173-1184.

Kar, S., J. Fan, M.J. Smith, M. Goedert, and L.A. Amos. 2003. Repeat motifs of tau bind to the insides of microtubules in the absence of taxol. *Embo J*. 22:70-77.

Karlsson, M., C. Zhang, L.R. Méar, W. Zhong, A. Digre, B. Katona, E. Sjöstedt, L. Butler, J. Odeberg, P. Dusart, F. Edfors, P. Oksvold, K. von Feilitzen, M. Zwahlen, M. Arif, O. Altay, X.Y. Li, M. Ozcan, A. Mardonoglu, L. Fagerberg, J. Mulder, Y.L. Luo, F. Ponten, M. Uhlén, and C. Lindskog. 2021. A single-cell type transcriptomics map of human tissues. *Science Advances*. 7.

Kawano, Y., T. Yoshimura, D. Tsuboi, S. Kawabata, T. Kaneko-Kawano, H. Shirataki, T. Takenawa, and K. Kaibuchi. 2005. CRMP-2 is involved in kinesin-1-dependent transport of the Sra-1/WAVE1 complex and axon formation. *Mol Cell Biol*. 25:9920-9935.

Kellogg, E.H., N.M.A. Hejab, S. Poepsel, K.H. Downing, F. DiMaio, and E. Nogales. 2018. Near-atomic model of microtubule-tau interactions. *Science*. 360:1242-1245.

Kempf, M., A. Clement, A. Faissner, G. Lee, and R. Brandt. 1996. Tau binds to the distal axon early in development of polarity in a microtubule- and microfilament-dependent manner. *J Neurosci*. 16:5583-5592.

Kenessey, A., and S.H. Yen. 1993. The extent of phosphorylation of fetal tau is comparable to that of PHF-tau from Alzheimer paired helical filaments. *Brain research*. 629:40-46.

Khan, Z., G. Ferrari, M. Kasper, D.A. Tonge, J.P. Steiner, G.S. Hamilton, and P.R. Gordon-Weeks. 2002. The non-immunosuppressive immunophilin ligand GPI-1046 potently stimulates regenerating axon growth from adult mouse dorsal root ganglia cultured in Matrigel. *Neuroscience*. 114:601-609.

Khanna, R., S.M. Wilson, J.M. Brittain, J. Weimer, R. Sultana, A. Butterfield, and K. Hensley. 2012. Opening Pandora's jar: a primer on the putative roles of CRMP2 in a panoply of neurodegenerative, sensory and motor neuron, and central disorders. *Future neurology*. 7:749-771.

Kimura, T., T. Hosokawa, M. Taoka, K. Tsutsumi, K. Ando, K. Ishiguro, M. Hosokawa, M. Hasegawa, and S. Hisanaga. 2016. Quantitative and combinatory determination of phosphorylation of tau and its FTDP-17 mutants. *Sci Rep-Uk*. 6.

Kimura, T., K. Ishiguro, and S. Hisanaga. 2014. Physiological and pathological phosphorylation of tau by Cdk5. *Front Mol Neurosci*. 7:65.

Kimura, T., G. Sharma, K. Ishiguro, and S. Hisanaga. 2018. Phospho-Tau Bar Code: Analysis of Phosphoisotypes of Tau and Its Application to Tauopathy. *Front Neurosci-Switz*. 12.

Kimura, T., K. Tsutsumi, M. Taoka, T. Saito, M. Masuda-Suzukake, K. Ishiguro, F. Plattner, T. Uchida, T. Isobe, M. Hasegawa, and S.I. Hisanaga. 2013. Isomerase Pin1 stimulates dephosphorylation of tau protein at cyclin-dependent kinase (Cdk5)-dependent Alzheimer phosphorylation sites. *J Biol Chem*. 288:7968-7977.

Kimura, T., H. Watanabe, A. Iwamatsu, and K. Kaibuchi. 2005. Tubulin and CRMP-2 complex is transported via Kinesin-1. *J Neurochem*. 93:1371-1382.

Kitsukawa, T., M. Shimizu, M. Sanbo, T. Hirata, M. Taniguchi, Y. Bekku, T. Yagi, and H. Fujisawa. 1997. Neuropilin-semaphorin III/D-mediated chemorepulsive signals play a crucial role in peripheral nerve projection in mice. *Neuron*. 19:995-1005.

Konzack, S., E. Thies, A. Marx, E.M. Mandelkow, and E. Mandelkow. 2007. Swimming against the tide: Mobility of the microtubule-associated protein tau in neurons. *J Neurosci*. 27:9916-9927.

Kutter, S., T. Eichner, A.M. Deaconescu, and D. Kern. 2016. Regulation of Microtubule Assembly by Tau and not by Pin1. *Journal of molecular biology*. 428:1742-1759.

Lasagna-Reeves, C.A., D.L. Castillo-Carranza, U. Sengupta, J. Sarmiento, J. Troncoso, G.R. Jackson, and R. Kayed. 2012. Identification of oligomers at early stages of tau aggregation in Alzheimer's disease. *FASEB journal : official publication of the Federation of American Societies for Experimental Biology*. 26:1946-1959.

Lenhard, W., Lenhard, A. . 2014. Hypothesis Tests for Comparing Correlations. *Psychometrica*.

Li, T., C. Hawkes, H.Y. Qureshi, S. Kar, and H.K. Paudel. 2006. Cyclin-dependent protein kinase 5 primes microtubule-associated protein tau site-specifically for glycogen synthase kinase 3beta. *Biochemistry*. 45:3134-3145.

Lin, P.C., P.M. Chan, C. Hall, and E. Manser. 2011. Collapsin response mediator proteins (CRMPs) are a new class of microtubule-associated protein (MAP) that selectively interacts with assembled microtubules via a taxol-sensitive binding interaction. *J Biol Chem*. 286:41466-41478.

Liou, Y.C., A. Ryo, H.K. Huang, P.J. Lu, R. Bronson, F. Fujimori, T. Uchida, T. Hunter, and K.P. Lu. 2002. Loss of Pin1 function in the mouse causes phenotypes resembling cyclin D1-null phenotypes. *P Natl Acad Sci USA*. 99:1335-1340.

Liou, Y.C., A. Sun, A. Ryo, X.Z. Zhou, Z.X. Yu, H.K. Huang, T. Uchida, R. Bronson, G. Bing, X. Li, T. Hunter, and K.P. Lu. 2003. Role of the prolyl isomerase Pin1 in protecting against age-dependent neurodegeneration. *Nature*. 424:556-561.

Liou, Y.C., X.Z. Zhou, and K.P. Lu. 2011. Prolyl isomerase Pin1 as a molecular switch to determine the fate of phosphoproteins. *Trends in biochemical sciences*. 36:501-514.

Liu, F., I. Grundke-Iqbal, K. Iqbal, and C.X. Gong. 2005. Contributions of protein phosphatases PP1, PP2A, PP2B and PP5 to the regulation of tau phosphorylation. *The European journal of neuroscience*. 22:1942-1950.

Liu, F., B. Li, E.J. Tung, I. Grundke-Iqbal, K. Iqbal, and C.X. Gong. 2007. Site-specific effects of tau phosphorylation on its microtubule assembly activity and self-aggregation. *The European journal of neuroscience*. 26:3429-3436.

Liu, F., Z.H. Liang, J.H. Shi, D.M. Yin, E. El-Akkad, I. Grundke-Iqbal, K. Iqbal, and C.X. Gong. 2006. PKA modulates GSK-3β- and cdk5-catalyzed phosphorylation of tau in site- and kinase-specific manners. *FEBS letters*. 580:6269-6274.

Liu, F.L., T.Y. Liu, and F.L. Kung. 2014. FKBP12 regulates the localization and processing of amyloid precursor protein in human cell lines. *Journal of biosciences*. 39:85-95.

Liu, H.T., and J.H. Naismith. 2008. An efficient one-step site-directed deletion, insertion, single and multiple-site plasmid mutagenesis protocol. *Bmc Biotechnol*. 8.

Liu, J., M.W. Albers, T.J. Wandless, S. Luan, D.G. Alberg, P.J. Belshaw, P. Cohen, C. MacKintosh, C.B. Klee, and S.L. Schreiber. 1992. Inhibition of T cell signaling by immunophilin-ligand complexes correlates with loss of calcineurin phosphatase activity. *Biochemistry*. 31:3896-3901.

Liu, S.L., C. Wang, T. Jiang, L. Tan, A. Xing, and J.T. Yu. 2016. The Role of Cdk5 in Alzheimer's Disease. *Molecular neurobiology*. 53:4328-4342.

Liz, M.A., F.M. Mar, T.E. Santos, H.I. Pimentel, A.M. Marques, M.M. Morgado, S. Vieira, V.F. Sousa, H. Pemble, T. Wittmann, C. Sutherland, J.R. Woodgett, and M.M. Sousa. 2014. Neuronal deletion of GSK3β increases microtubule speed in the growth cone and enhances axon regeneration via CRMP-2 and independently of MAP1B and CLASP2. *BMC biology*. 12:47.

Lopez-Ilasaca, M., C. Schiene, G. Küllertz, T. Tradler, G. Fischer, and R. Wetzker. 1998. Effects of FK506-binding protein 12 and FK506 on autophosphorylation of epidermal growth factor receptor. *J Biol Chem*. 273:9430-9434.

Lu, K.P. 2004. Pinning down cell signaling, cancer and Alzheimer's disease. *Trends in biochemical sciences*. 29:200-209.

Lu, K.P., S.D. Hanes, and T. Hunter. 1996. A human peptidyl-prolyl isomerase essential for regulation of mitosis. *Nature*. 380:544-547.

Lu, K.P., and X.Z. Zhou. 2007. The prolyl isomerase PIN1: a pivotal new twist in phosphorylation signalling and disease. *Nature reviews. Molecular cell biology*. 8:904-916.

Lu, P.J., G. Wulf, X.Z. Zhou, P. Davies, and K.P. Lu. 1999. The prolyl isomerase Pin1 restores the function of Alzheimer-associated phosphorylated tau protein. *Nature*. 399:784-788.

Lyons, W.E., E.B. George, T.M. Dawson, J.P. Steiner, and S.H. Snyder. 1994. Immunosuppressant FK506 promotes neurite outgrowth in cultures of PC12 cells and sensory ganglia. *Proc Natl Acad Sci U S A*. 91:3191-3195.

Ma, S.L., L. Pastorino, X.Z. Zhou, and K.P. Lu. 2012. Prolyl isomerase Pin1 promotes amyloid precursor protein (APP) turnover by inhibiting glycogen synthase kinase-3β (GSK3β) activity: novel mechanism for Pin1 to protect against Alzheimer disease. *J Biol Chem*. 287:6969-6973.

Maimon, R., L. Ankol, T. Gradus Pery, T. Altman, A. Ionescu, R. Weissova, M. Ostrovsky, E. Tank, G. Alexandra, N. Shelestovich, Y. Opatowsky, A. Dori, S. Barmada, M. Balastik, and E. Perlson. 2021. A CRMP4-dependent retrograde axon-to-soma death signal in amyotrophic lateral sclerosis. *Embo J*. 40:e107586.

Maimon, R., A. Ionescu, A. Bonnie, S. Sweetat, S. Wald-Altman, S. Inbar, T. Gradus, D. Trotti, M. Weil, O. Behar, and E. Perlson. 2018. miR126-5p Downregulation Facilitates Axon Degeneration and NMJ Disruption via a Non-Cell-Autonomous Mechanism in ALS. *J Neurosci*. 38:5478-5494.

Makrides, V., M.R. Massie, S.C. Feinstein, and J. Lew. 2004. Evidence for two distinct binding sites for tau on microtubules. *Proc Natl Acad Sci U S A*. 101:6746-6751.

Makrides, V., T.E. Shen, R. Bhatia, B.L. Smith, J. Thimm, R. Lal, and S.C. Feinstein. 2003. Microtubule-dependent oligomerization of tau. Implications for physiological tau function and tauopathies. *J Biol Chem*. 278:33298-33304.

Mandelkow, E.M., J. Biernat, G. Drewes, N. Gustke, B. Trinczek, and E. Mandelkow. 1995. Tau Domains, Phosphorylation, and Interactions with Microtubules. *Neurobiol Aging*. 16:355-362.

Martin, L., X. Latypova, C.M. Wilson, A. Magnaudeix, M.L. Perrin, C. Yardin, and F. Terro. 2013. Tau protein kinases: Involvement in Alzheimer's disease. *Ageing Res Rev*. 12:289-309.

McVicker, D.P., G.J. Hoeprich, A.R. Thompson, and C.L. Berger. 2014. Tau interconverts between diffusive and stable populations on the microtubule surface in an isoform and lattice specific manner. *Cytoskeleton (Hoboken, N.J.)*. 71:184-194.

Mokhtar, S.H., M.J. Kim, K.A. Magee, P.M. Aui, S. Thomas, M.M. Bakhuraysah, A.A. Alrehaili, J.Y. Lee, D.L. Steer, R. Kenny, C. McLean, M.F. Azari, A. Birpanagos, E. Lipiec, P. Heraud, B. Wood, and S. Petratos. 2018. Amyloid-beta-dependent phosphorylation of collapsin response mediator protein-2 dissociates kinesin in Alzheimer's disease. *Neural regeneration research*. 13:1066-1080.

Morgan-Fisher, M., J.R. Couchman, and A. Yoneda. 2013. Phosphorylation and mRNA splicing of collapsin response mediator protein-2 determine inhibition of rho-associated protein kinase (ROCK) II function in carcinoma cell migration and invasion. *J Biol Chem*. 288:31229-31240.

Moutal, A., and R. Khanna. 2018. Unconventional Signaling by Extracellular CRMP2: Possible Role as an Atypical Neurotransmitter? *Neuroscience*. 376:224-226.

Moutal, A., K.A. White, A. Chefdeville, R.N. Laufmann, P.F. Vitiello, D. Feinstein, J.M. Weimer, and R. Khanna. 2019. Dysregulation of CRMP2 Post-Translational Modifications Drive Its Pathological Functions. *Molecular neurobiology*. 56:6736-6755.

Mueller, R.L., B. Combs, M.M. Alhadidy, S.T. Brady, G.A. Morfini, and N.M. Kanaan. 2021. Tau: A Signaling Hub Protein. *Front Mol Neurosci*. 14.

Mukrasch, M.D., S. Bibow, J. Korukottu, S. Jeganathan, J. Biernat, C. Griesinger, E. Mandelkow, and M. Zweckstetter. 2009. Structural polymorphism of 441-residue tau at single residue resolution. *PLoS biology*. 7:e34.

Muñoz-Lasso, D.C., C. Romá-Mateo, F.V. Pallardó, and P. Gonzalez-Cabo. 2020. Much More Than a Scaffold: Cytoskeletal Proteins in Neurological Disorders. *Cells*. 9.

Nakamura, F., T. Ohshima, and Y. Goshima. 2020. Collapsin Response Mediator Proteins: Their Biological Functions and Pathophysiology in Neuronal Development and Regeneration. *Front Cell Neurosci*. 14:188.

Nakamura, H., N. Yamashita, A. Kimura, Y. Kimura, H. Hirano, H. Makihara, Y. Kawamoto, A. Jitsuki-Takahashi, K. Yonezaki, K. Takase, T. Miyazaki, F. Nakamura, F. Tanaka, and Y. Goshima. 2016. Comprehensive behavioral study and proteomic analyses of CRMP2-deficient mice. *Genes to Cells*. 21:1059-1079.

Nakamura, K., A. Greenwood, L. Binder, E.H. Bigio, S. Denial, L. Nicholson, X.Z. Zhou, and K.P. Lu. 2012a. Proline isomer-specific antibodies reveal the early pathogenic tau conformation in Alzheimer's disease. *Cell*. 149:232-244.

Nakamura, K., I. Kosugi, D.Y. Lee, A. Hafner, D.A. Sinclair, A. Ryo, and K.P. Lu. 2012b. Prolyl Isomerase Pin1 Regulates Neuronal Differentiation via β-Catenin. *Mol Cell Biol*. 32:2966-2978.

Nishimura, T., Y. Fukata, K. Kato, T. Yamaguchi, Y. Matsuura, H. Kamiguchi, and K. Kaibuchi. 2003. CRMP-2 regulates polarized Numb-mediated endocytosis for axon growth. *Nat Cell Biol*. 5:819-826.

Niwa, S., F. Nakamura, Y. Tomabechi, M. Aoki, H. Shigematsu, T. Matsumoto, A. Yamagata, S. Fukai, N. Hirokawa, Y. Goshima, M. Shirouzu, and R. Nitta. 2017. Structural basis for CRMP2-induced axonal microtubule formation. *Sci Rep*. 7:10681.

Noble, W., V. Olm, K. Takata, E. Casey, O. Mary, J. Meyerson, K. Gaynor, J. LaFrancois, L. Wang, T. Kondo, P. Davies, M. Burns, Veeranna, R. Nixon, D. Dickson, Y. Matsuoka, M. Ahlijanian, L.F. Lau, and K. Duff. 2003. Cdk5 is a key factor in tau aggregation and tangle formation in vivo. *Neuron*. 38:555-565.

Panda, D., J.C. Samuel, M. Massie, S.C. Feinstein, and L. Wilson. 2003. Differential regulation of microtubule dynamics by three- and four-repeat tau: Implications for the onset of neurodegenerative disease. *P Natl Acad Sci USA*. 100:9548-9553.

Pao, P.C., and L.H. Tsai. 2021. Three decades of Cdk5. *Journal of biomedical science*. 28:79.

Pastorino, L., A. Sun, P.J. Lu, X.Z. Zhou, M. Balastik, G. Finn, G. Wulf, J. Lim, S.H. Li, X. Li, W. Xia, L.K. Nicholson, and K.P. Lu. 2006. The prolyl isomerase Pin1 regulates amyloid precursor protein processing and amyloid-beta production. *Nature*. 440:528-534.

Patrick, G.N., L. Zukerberg, M. Nikolic, S. de la Monte, P. Dikkes, and L.H. Tsai. 1999. Conversion of p35 to p25 deregulates Cdk5 activity and promotes neurodegeneration. *Nature*. 402:615-622.

Peterson, D.W., D.M. Ando, D.A. Taketa, H. Zhou, F.W. Dahlquist, and J. Lew. 2010. No difference in kinetics of tau or histone phosphorylation by CDK5/p25 versus CDK5/p35 in vitro. *Proc Natl Acad Sci U S A*. 107:2884-2889.

Piedrahita, D., I. Hernández, A. López-Tobón, D. Fedorov, B. Obara, B.S. Manjunath, R.L. Boudreau, B. Davidson, F. Laferla, J.C. Gallego-Gómez, K.S. Kosik, and G.P. Cardona-Gómez. 2010. Silencing of CDK5 reduces neurofibrillary tangles in transgenic alzheimer's mice. *J Neurosci*. 30:13966-13976.

Plattner, F., M. Angelo, and K.P. Giese. 2006. The roles of cyclin-dependent kinase 5 and glycogen synthase kinase 3 in tau hyperphosphorylation. *J Biol Chem*. 281:25457-25465.

Qiang, L., X.H. Sun, T.O. Austin, H. Muralidharan, D.C. Jean, M. Liu, W.Q. Yu, and P.W. Baas. 2018. Tau Does Not Stabilize Axonal Microtubules but Rather Enables Them to Have Long Labile Domains. *Curr Biol*. 28:2181-+.

Qiang, L., W.Q. Yu, A. Andreadis, M.H. Luo, and P.W. Baas. 2006. Tau protects microtubules in the axon from severing by katanin. *J Neurosci*. 26:3120-3129.

Quach, T.T., A. Moutal, R. Khanna, N.P. Deems, A.M. Duchemin, and R.M. Barrientos. 2020. Collapsin Response Mediator Proteins: Novel Targets for Alzheimer's Disease. *J Alzheimers Dis*. 77:949-960.

Quinn, C.C., E. Chen, T.G. Kinjo, G. Kelly, A.W. Bell, R.C. Elliott, P.S. McPherson, and S. Hockfield. 2003. TUC-4b, a novel TUC family variant, regulates neurite outgrowth and associates with vesicles in the growth cone. *J Neurosci*. 23:2815-2823.

Radomska, H.S., M. Alberich-Jordà, B. Will, D. Gonzalez, R. Delwel, and D.G. Tenen. 2012. Targeting CDK1 promotes FLT3-activated acute myeloid leukemia differentiation through C/EBPα. *Journal of Clinical Investigation*. 122:2955-2966.

Ranganathan, R., K.P. Lu, T. Hunter, and J.P. Noel. 1997. Structural and functional analysis of the mitotic rotamase Pin1 suggests substrate recognition is phosphorylation dependent. *Cell*. 89:875-886.

Ricard, D., B. Stankoff, D. Bagnard, M. Aguera, V. Rogemond, J.C. Antoine, N. Spassky, B. Zalc, C. Lubetzki, M.F. Belin, and J. Honnorat. 2000. Differential expression of collapsin response mediator proteins (CRMP/ULIP) in subsets of oligodendrocytes in the postnatal rodent brain. *Molecular and Cellular Neuroscience*. 16:324-337.

Rogemond, V., C. Auger, P. Giraudon, M. Becchi, N. Auvergnon, M.F. Belin, J. Honnorat, and M. Moradi-Améli. 2008. Processing and nuclear localization of CRMP2 during brain development induce neurite outgrowth inhibition. *J Biol Chem*. 283:14751-14761.

Roll-Mecak, A. 2020. The Tubulin Code in Microtubule Dynamics and Information Encoding. *Developmental cell*. 54:7-20.

Rossi, A., Z. Kontarakis, C. Gerri, H. Nolte, S. Hölper, M. Krüger, and D.Y.R. Stainier. 2015. Genetic compensation induced by deleterious mutations but not gene knockdowns. *Nature*. 524:230-+.

Roth, D., B.P. Fitton, N.P. Chmel, N. Wasiluk, and A. Straube. 2018. Spatial positioning of EB family proteins at microtubule tips involves distinct nucleotide-dependent binding properties. *Journal of cell science*. 132.

Ryo, A., T. Togo, T. Nakai, A. Hirai, M. Nishi, A. Yamaguchi, K. Suzuki, Y. Hirayasu, H. Kobayashi, K. Perrem, Y.C. Liou, and I. Aoki. 2006. Prolyl-isomerase Pin1 accumulates in lewy bodies of parkinson disease and facilitates formation of alpha-synuclein inclusions. *J Biol Chem*. 281:4117-4125.

Sabatini, D.M., H. Erdjument-Bromage, M. Lui, P. Tempst, and S.H. Snyder. 1994. RAFT1: a mammalian protein that binds to FKBP12 in a rapamycin-dependent fashion and is homologous to yeast TORs. *Cell*. 78:35-43.

Samsonov, A.V., J.Z. Yu, M.M. Rasenick, and S.V. Popov. 2003. Rapid interaction of tau with microtubules in vivo: the effects of phosphatase inhibitors, ATP-reducing and taxol. *Biophysical journal*. 84:112a-113a.

Sengupta, A., J. Kabat, M. Novak, Q.L. Wu, I. Grundke-Iqbal, and K. Iqbal. 1998. Phosphorylation of tau at both Thr 231 and Ser 262 is required for maximal inhibition of its binding to microtubules. *Arch Biochem Biophys*. 357:299-309.

Seo, J., P. Giusti-Rodríguez, Y. Zhou, A. Rudenko, S. Cho, K.T. Ota, C. Park, H. Patzke, R. Madabhushi, L. Pan, A.E. Mungenast, J.S. Guan, I. Delalle, and L.H. Tsai. 2014. Activity-Dependent p25 Generation Regulates Synaptic Plasticity and Aβ-Induced Cognitive Impairment. *Cell*. 157:486-498.

Sferra, A., F. Nicita, and E. Bertini. 2020. Microtubule Dysfunction: A Common Feature of Neurodegenerative Diseases. *Int J Mol Sci*. 21.

Shelton, S.B., and G.V. Johnson. 2004. Cyclin-dependent kinase-5 in neurodegeneration. *J Neurochem*. 88:1313-1326.

Shin, D.W., Z. Pan, A. Bandyopadhyay, M.B. Bhat, D.H. Kim, and J. Ma. 2002. Ca(2+)-dependent interaction between FKBP12 and calcineurin regulates activity of the Ca(2+) release channel in skeletal muscle. *Biophysical journal*. 83:2539-2549.

Shou, W., B. Aghdasi, D.L. Armstrong, Q. Guo, S. Bao, M.J. Charng, L.M. Mathews, M.D. Schneider, S.L. Hamilton, and M.M. Matzuk. 1998. Cardiac defects and altered ryanodine receptor function in mice lacking FKBP12. *Nature*. 391:489-492.

Schiene, C., U. Reimer, M. Schutkowski, and G. Fischer. 1998. Mapping the stereospecificity of peptidyl prolyl cis/trans isomerases. *FEBS letters*. 432:202-206.

Schmidpeter, P.A., and F.X. Schmid. 2015. Prolyl isomerization and its catalysis in protein folding and protein function. *Journal of molecular biology*. 427:1609-1631.

Schmidt, E.F., and S.M. Strittmatter. 2007. The CRMP family of proteins and their role in Sema3A signaling. *Advances in experimental medicine and biology*. 600:1-11.

Schneider, A., J. Biernat, M. von Bergen, E. Mandelkow, and E.M. Mandelkow. 1999. Phosphorylation that detaches tau protein from microtubules (Ser262, Ser214) also protects it against aggregation into Alzheimer paired helical filaments. *Biochemistry*. 38:3549-3558.

Schutkowski, M., A. Bernhardt, X.Z. Zhou, M. Shen, U. Reimer, J.U. Rahfeld, K.P. Lu, and G. Fischer. 1998. Role of phosphorylation in determining the backbone dynamics of the serine/threonine-proline motif and Pin1 substrate recognition. *Biochemistry*. 37:5566-5575.

Schweers, O., E. Schonbrunnhanebeck, A. Marx, and E. Mandelkow. 1994. Structural Studies of Tau-Protein and Alzheimer Paired Helical Filaments Show No Evidence for Beta-Structure. *J Biol Chem*. 269:24290-24297.

Siahaan, V., J. Krattenmacher, A.A. Hyman, S. Diez, A. Hernández-Vega, Z. Lansky, and M. Braun. 2019. Kinetically distinct phases of tau on microtubules regulate kinesin motors and severing enzymes. *Nat Cell Biol*. 21:1086-+.

Siahaan, V., R. Tan, T. Humhalova, L. Libusova, S.E. Lacey, T. Tan, M. Dacy, K.M. Ori-McKenney, R.J. McKenney, M. Braun, and Z. Lansky. 2022. Microtubule lattice spacing governs cohesive envelope formation of tau family proteins. *Nat Chem Biol*. 18:1224-+.

Siahaan, V., R. Weissova, E. Lanska, A. Karhanova, V. Dostal, V. Henriot, C. Janke, L. Libusova, M. Braun, M. Balastik, and Z. Lansky. 2024. Tau phosphorylation impedes functionality of protective tau envelopes. *bioRxiv*:2024.2003.2025.586522.

Siekierka, J.J., S.H. Hung, M. Poe, C.S. Lin, and N.H. Sigal. 1989. A cytosolic binding protein for the immunosuppressant FK506 has peptidyl-prolyl isomerase activity but is distinct from cyclophilin. *Nature*. 341:755-757.

Sosa, L.J., J.S. Malter, J. Hu, F. Bustos Plonka, M. Oksdath, A.F. Nieto Guil, S. Quiroga, and K.H. Pfenninger. 2016. Protein interacting with NIMA (never in mitosis A)-1 regulates axonal growth cone adhesion and spreading through myristoylated alanine-rich C kinase substrate isomerization. *J Neurochem*. 137:744-755.

Spillantini, M.G., J.R. Murrell, M. Goedert, M.R. Farlow, A. Klug, and B. Ghetti. 1998. Mutation in the tau gene in familial multiple system tauopathy with presenile dementia. *P Natl Acad Sci USA*. 95:7737-7741.

Steiner, J.P., T.M. Dawson, M. Fotuhi, C.E. Glatt, A.M. Snowman, N. Cohen, and S.H. Snyder. 1992. High brain densities of the immunophilin FKBP colocalized with calcineurin. *Nature*. 358:584-587.

Stenmark, P., D. Ogg, S. Flodin, A. Flores, T. Kotenyova, T. Nyman, P. Nordlund, and P. Kursula. 2007. The structure of human collapsin response mediator protein 2, a regulator of axonal growth. *Journal of Neurochemistry*. 101:906-917.

Stewart, D.E., A. Sarkar, and J.E. Wampler. 1990. Occurrence and role of cis peptide bonds in protein structures. *Journal of molecular biology*. 214:253-260.

Stratton, H., L. Boinon, A. Moutal, and R. Khanna. 2020. Coordinating Synaptic Signaling with CRMP2. *The international journal of biochemistry & cell biology*. 124:105759.

Sudo, H., and P.W. Baas. 2011. Strategies for diminishing katanin-based loss of microtubules in tauopathic neurodegenerative diseases. *Hum Mol Genet*. 20:763-778.

Sugata, H., K. Matsuo, T. Nakagawa, M. Takahashi, H. Mukai, Y. Ono, K. Maeda, H. Akiyama, and T. Kawamata. 2009. A peptidyl-prolyl isomerase, FKBP12, accumulates in Alzheimer neurofibrillary tangles. *Neuroscience letters*. 459:96-99.

Sultana, R., D. Boyd-Kimball, H.F. Poon, J. Cai, W.M. Pierce, J.B. Klein, W.R. Markesbery, X.Z. Zhou, K.P. Lu, and D.A. Butterfield. 2006. Oxidative modification and down-

regulation of Pin1 in Alzheimer's disease hippocampus: A redox proteomics analysis. *Neurobiol Aging*. 27:918-925.

Suzuki, Y., S. Nakagomi, K. Namikawa, S. Kiryu-Seo, N. Inagaki, K. Kaibuchi, H. Aizawa, K. Kikuchi, and H. Kiyama. 2003. Collapsin response mediator protein-2 accelerates axon regeneration of nerve-injured motor neurons of rat. *J Neurochem*. 86:1042-1050.

Takashima, A., M. Murayama, K. Yasutake, H. Takahashi, M. Yokoyama, and K. Ishiguro. 2001. Involvement of cyclin dependent kinase5 activator p25 on tau phosphorylation in mouse brain. *Neuroscience letters*. 306:37-40.

Tan, F., C.J. Thiele, and Z. Li. 2014. Collapsin response mediator proteins: Potential diagnostic and prognostic biomarkers in cancers (Review). *Oncology letters*. 7:1333-1340.

Tan, M.H., C.H. Cha, Y.H. Ye, J.F. Zhang, S.M. Li, F.M. Wu, S.T. Gong, and G.Q. Guo. 2015. CRMP4 and CRMP2 Interact to Coordinate Cytoskeleton Dynamics, Regulating Growth Cone Development and Axon Elongation. *Neural plasticity*. 2015.

Tan, R., A.J. Lam, T. Tan, J. Han, D.W. Nowakowski, M. Vershinin, S. Simó, K.M. Ori-McKenney, and R.J. McKenney. 2019. Microtubules gate tau condensation to spatially regulate microtubule functions. *Nat Cell Biol*. 21:1078-+.

Tandon, A., H. Yu, L. Wang, E. Rogaeva, C. Sato, M.A. Chishti, T. Kawarai, H. Hasegawa, F. Chen, P. Davies, P.E. Fraser, D. Westaway, and P.H. St George-Hyslop. 2003. Brain levels of CDK5 activator p25 are not increased in Alzheimer's or other neurodegenerative diseases with neurofibrillary tangles. *J Neurochem*. 86:572-581.

Taniguchi, M., S. Yuasa, H. Fujisawa, I. Naruse, S. Saga, M. Mishina, and T. Yagi. 1997. Disruption of Semaphorin III/D gene causes severe abnormality in peripheral nerve projection. *Neuron*. 19:519-530.

Taylor, R.J., J. Carrington, L.R. Gerlach, K.L. Taylor, K.E. Richters, and E.W. Dent. 2020. Double UP: A Dual Color, Internally Controlled Platform for Knockdown or Overexpression. *Front Mol Neurosci*. 13.

Theillet, F.X., L. Kalmar, P. Tompa, K.H. Han, P. Selenko, A.K. Dunker, G.W. Daughdrill, and V.N. Uversky. 2013. The alphabet of intrinsic disorder: I. Act like a Pro: On the abundance and roles of proline residues in intrinsically disordered proteins. *Intrinsically disordered proteins*. 1:e24360.

Thibault, O., J.C. Gant, and P.W. Landfield. 2007. Expansion of the calcium hypothesis of brain aging and Alzheimer's disease: minding the store. *Aging cell*. 6:307-317.

Tong, M.M., and Y. Jiang. 2016. FK506-Binding Proteins and Their Diverse Functions. *Curr Mol Pharmacol*. 9:48-65.

Uchida, Y., T. Ohshima, Y. Sasaki, H. Suzuki, S. Yanai, N. Yamashita, F. Nakamura, K. Takei, Y. Ihara, K. Mikoshiba, P. Kolattukudy, J. Honnorat, and Y. Goshima. 2005. Semaphorin3A signalling is mediated via sequential Cdk5 and GSK3beta phosphorylation of CRMP2: implication of common phosphorylating mechanism underlying axon guidance and Alzheimer's disease. *Genes to cells : devoted to molecular & cellular mechanisms*. 10:165-179.

Valdez, G., J.C. Tapia, J.W. Lichtman, M.A. Fox, and J.R. Sanes. 2012. Shared Resistance to Aging and ALS in Neuromuscular Junctions of Specific Muscles. *Plos One*. 7.

Venkova, K., A. Christov, Z. Kamaluddin, P. Kobalka, S. Siddiqui, and K. Hensley. 2014. Semaphorin 3A Signaling Through Neuropilin-1 Is an Early Trigger for Distal

Axonopathy in the SOD1 Mouse Model of Amyotrophic Lateral Sclerosis. *Journal of neuropathology and experimental neurology*. 73:702-713.

Vershinin, M., B.C. Carter, D.S. Razafsky, S.J. King, and S.P. Gross. 2007. Multiple-motor based transport and its regulation by Tau. *Proc Natl Acad Sci U S A*. 104:87-92.

Wang, L.H., and S.M. Strittmatter. 1996. A family of rat CRMP genes is differentially expressed in the nervous system. *J Neurosci*. 16:6197-6207.

Wang, L.H., and S.M. Strittmatter. 1997. Brain CRMP forms heterotetramers similar to liver dihydropyrimidinase. *Journal of Neurochemistry*. 69:2261-2269.

Wang, Q., R.L. Woltjer, P.J. Cimino, C. Pan, K.S. Montine, J. Zhang, and T.J. Montine. 2005. Proteomic analysis of neurofibrillary tangles in Alzheimer disease identifies GAPDH as a detergent-insoluble paired helical filament tau binding protein. *FASEB journal : official publication of the Federation of American Societies for Experimental Biology*. 19:869-871.

Wang, T., P.K. Donahoe, and A.S. Zervos. 1994. Specific interaction of type I receptors of the TGF-beta family with the immunophilin FKBP-12. *Science*. 265:674-676.

Wegmann, S., J. Biernat, and E. Mandelkow. 2021. A current view on Tau protein phosphorylation in Alzheimer's disease. *Current opinion in neurobiology*. 69:131-138.

Wegmann, S., B. Eftekharzadeh, K. Tepper, K.M. Zoltowska, R.E. Bennett, S. Dujardin, P.R. Laskowski, D. MacKenzie, T. Kamath, C. Commins, C. Vanderburg, A.D. Roe, Z. Fan, A.M. Molliex, A. Hernandez-Vega, D. Muller, A.A. Hyman, E. Mandelkow, J.P. Taylor, and B.T. Hyman. 2018. Tau protein liquid-liquid phase separation can initiate tau aggregation. *Embo J*. 37.

Weingarten, M.D., A.H. Lockwood, S.Y. Hwo, and M.W. Kirschner. 1975. Protein Factor Essential for Microtubule Assembly. *P Natl Acad Sci USA*. 72:1858-1862.

Weiwad, M., G. Küllertz, M. Schutkowski, and G. Fischer. 2000. Evidence that the substrate backbone conformation is critical to phosphorylation by p42 MAP kinase. *FEBS letters*. 478:39-42.

Wen, Y., E. Planel, M. Herman, H.Y. Figueroa, L. Wang, L. Liu, L.F. Lau, W.H. Yu, and K.E. Duff. 2008. Interplay between cyclin-dependent kinase 5 and glycogen synthase kinase 3 beta mediated by neuregulin signaling leads to differential effects on tau phosphorylation and amyloid precursor protein processing. *J Neurosci*. 28:2624-2632.

Wu, D., and G. Piszczek. 2021. Standard protocol for mass photometry experiments. *Eur Biophys J Biophy*. 50:403-409.

Wu, X.L., J. Piña-Crespo, Y.W. Zhang, X.C. Chen, and H.X. Xu. 2017. Tau-mediated Neurodegeneration and Potential Implications in Diagnosis and Treatment of Alzheimer's Disease. *Chinese medical journal*. 130:2978-2990.

Wulf, G., G. Finn, F. Suizu, and K.P. Lu. 2005. Phosphorylation-specific prolyl isomerization: is there an underlying theme? *Nat Cell Biol*. 7:435-441.

Xia, C., M. Nguyen, A.K. Garrison, Z. Zhao, Z. Wang, C. Sutherland, and L. Ma. 2013. CNP/cGMP signaling regulates axon branching and growth by modulating microtubule polymerization. *Developmental neurobiology*. 73:673-687.

Yaffe, M.B., M. Schutkowski, M.H. Shen, X.Z. Zhou, P.T. Stukenberg, J.U. Rahfeld, J. Xu, J. Kuang, M.W. Kirschner, G. Fischer, L.C. Cantley, and K.P. Lu. 1997. Sequence-

specific and phosphorylation-dependent proline isomerization: A potential mitotic regulatory mechanism. *Science*. 278:1957-1960.

Yamaguchi, H., K. Ishiguro, T. Uchida, A. Takashima, C.A. Lemere, and K. Imahori. 1996. Preferential labeling of Alzheimer neurofibrillary tangles with antisera for tau protein kinase (TPK) I/glycogen synthase kinase-3 beta and cyclin-dependent kinase 5, a component of TPK II. *Acta neuropathologica*. 92:232-241.

Ye, H., Y. Han, P. Li, Z. Su, and Y. Huang. 2022. The Role of Post-Translational Modifications on the Structure and Function of Tau Protein. *Journal of molecular neuroscience : MN*. 72:1557-1571.

Yoshida, H., A. Watanabe, and Y. Ihara. 1998. Collapsin response mediator protein-2 is associated with neurofibrillary tangles in Alzheimer's disease. *J Biol Chem*. 273:9761-9768.

Yoshimura, T., Y. Kawano, N. Arimura, S. Kawabata, A. Kikuchi, and K. Kaibuchi. 2005. GSK-3beta regulates phosphorylation of CRMP-2 and neuronal polarity. *Cell*. 120:137-149.

Yu, W., and B. Lu. 2012. Synapses and dendritic spines as pathogenic targets in Alzheimer's disease. *Neural plasticity*. 2012:247150.

Yuasa-Kawada, J., R. Suzuki, F. Kano, T. Ohkawara, M. Murata, and M. Noda. 2003. Axonal morphogenesis controlled by antagonistic roles of two CRMP subtypes in microtubule organization. *The European journal of neuroscience*. 17:2329-2343.

Zhang, H., Y. Cao, L. Ma, Y. Wei, and H. Li. 2021. Possible Mechanisms of Tau Spread and Toxicity in Alzheimer's Disease. *Frontiers in cell and developmental biology*. 9:707268.

Zhang, J.N., U. Michel, C. Lenz, C.C. Friedel, S. Köster, Z. d'Hedouville, L. Tönges, H. Urlaub, M. Bähr, P. Lingor, and J.C. Koch. 2016. Calpain-mediated cleavage of collapsin response mediator protein-2 drives acute axonal degeneration. *Sci Rep*. 6:37050.

Zheng, M., C.L. Leung, and R.K.H. Liem. 1998. Region-specific expression of cyclin-dependent kinase 5 (cdk5) and its activators, p35 and p39, in the developing and adult rat central nervous system. *J Neurobiol*. 35:141-159.

Zheng, Y.Y., R. Sethi, L.S. Mangala, C. Taylor, J. Goldsmith, M. Wang, K. Masuda, M. Karaminejadranjbar, D. Mannion, F. Miranda, S. Herrero-Gonzalez, K. Hellner, F. Chen, A. Alsaadi, A. Albukhari, D.C. Fotso, C. Yau, D.H. Jiang, S. Pradeep, C. Rodriguez-Aguayo, G. Lopez-Berestein, S. Knapp, N.S. Gray, L. Campo, K.A. Myers, S. Dhar, D. Ferguson, R.C. Bast, A.K. Sood, F. von Delft, and A.A. Ahmed. 2018. Tuning microtubule dynamics to enhance cancer therapy by modulating FER-mediated CRMP2 phosphorylation. *Nature communications*. 9.

Zhou, X.Z., O. Kops, A. Werner, P.J. Lu, M.H. Shen, G. Stoller, G. Küllertz, M. Stark, G. Fischer, and K.P. Lu. 2000. Pin1-dependent prolyl isomerization regulates dephosphorylation of Cdc25C and tau proteins. *Mol Cell*. 6:873-883.

Zhu, L.Q., H.Y. Zheng, C.X. Peng, D. Liu, H.L. Li, Q. Wang, and J.Z. Wang. 2010. Protein Phosphatase 2A Facilitates Axonogenesis by Dephosphorylating CRMP2. *J Neurosci*. 30:3839-3848.

Zhuang, S.N., P. Chakraborty, and M. Zweckstetter. 2024. Regulation of tau by peptidyl-prolyl isomerases. *Curr Opin Struc Biol*. 84.

Ziak, J., R. Weissova, K. Jerabkova, M. Janikova, R. Maimon, T. Petrasek, B. Pukajova, M. Kleisnerova, M. Wang, M.S. Brill, P. Kasparek, X. Zhou, G. Alvarez-Bolado, R. Sedlacek, T. Misgeld, A. Stuchlik, E. Perlson, and M. Balastik. 2020. CRMP2 mediates Sema3F-dependent axon pruning and dendritic spine remodeling. *EMBO Rep*. 21:e48512.

Zwetsloot, A.J., G. Tut, and A. Straube. 2018. Measuring microtubule dynamics. *Essays Biochem*. 62:725-735.

8 Supplement

8.1 Publications and manuscripts related to the thesis

CRMP2 mediates Sema3F-dependent axon pruning and dendritic spine remodeling

In this publication, knockout mice line lacking CRMP2 gene (CRMP2 KO) was generated and the role of CRMP2 in both Sema3A and Sema3F signaling pathways was analyzed. We demonstrated that CRMP2 mediates stereotyped axon pruning in hippocampus and visual cortex and dendritic spine remodeling, which are consistent with implication of Sema3F signaling and with models of autism spectrum disorder (ASD). CRMP2 has also a moderate effect on Sema3A-dependent axon guidance *in vivo*, and its deficiency leads to a mild defect in axon guidance in peripheral nerves and corpus callosum. Indeed, the data demonstrated that CRMP2 mediates Sema3F signaling in primary neurons culture and that CRMP2 KO mice display ASD-related social behavior changes. Together, the data implicate that CRMP2 mediates Sema3F signaling and plays an important role in ASD pathogenesis.

I participated on the generation of the CRMP2 knockout mouse line, established the protocol for its genotyping, maintained the colony, and contributed to analysis of its phenotype. I established the method of the whole-mount immunolabeling of the embryos and contributed to acquiring and analysis of the peripheral neuron growth using this method.

Ziak J, Weissova R, Jeřábková K, Janikova M, Maimon R, Petrasek T, Pukajova B, Kleisnerova M, Wang M, Brill MS, Kasparek P, Zhou X, Alvarez-Bolado G, Sedlacek R, Misgeld T, Stuchlik A, Perlson E, Balastik M. **CRMP2 mediates Sema3F-dependent axon pruning and dendritic spine remodeling.** EMBO Rep. 2020 Mar 4;21(3):e48512. doi: 10.15252/embr.201948512. Epub 2020 Jan 9. PMID: 31919978; PMCID: PMC7054682. IF8.8

The publication is available online at:
https://www.embopress.org/doi/10.15252/embr.201948512

A CRMP4-dependent retrograde axon-to-soma death signal in amyotrophic lateral sclerosis

In this publication, we show that CRMP4 protein is mislocalized in Amyotrophic lateral sclerosis because of its increased interaction with the retrograde motor protein dynein. Blocking of the interaction between CRMP4 and dynein reduces loss of motor neurons in mouse model of Amyotrophic lateral sclerosis. Together, the data show CRMP4 transport as a death signal that underlies loss of motor neurons in Amyotrophic lateral sclerosis.

I contributed to this publication by designing and cloning of the vectors used in its experimental part. I prepared the vector expressing CRMP4, the mutated and truncated forms, tested their expression in cell lines and contributed to the writing of the manuscript.

Maimon R, Ankol L, Gradus Pery T, Altman T, Ionescu A, Weissova R, Ostrovsky M, Tank E, Alexandra G, Shelestovich N, Opatowsky Y, Dori A, Barmada S, Balastik M, Perlson E. **A CRMP4-dependent retrograde axon-to-soma death signal in amyotrophic lateral sclerosis.** EMBO J. 2021 Sep 1;40(17):e107586. doi: 10.15252/embj.2020107586. Epub 2021 Jun 30. PMID: 34190355; PMCID: PMC8408612. IF 14

The publication is available online at:
https://www.embopress.org/doi/full/10.15252/embj.2020107586

Tau phosphorylation impedes functionality of protective tau envelopes

In this study, the effect of phosphorylation on tau envelopes and their microtubule-protective function was studied. We have shown that phosphorylated tau creates tau envelopes less efficiently and it can even destabilize established envelopes. We show that when tau is phosphorylated by Cdk5 kinase, it can create tau envelopes but they are less stable and more prone to disassembly which then lead to decreased protection of enveloped microtubules against the digestion with severing enzyme katanin. Together the results show that tau phosphorylation can regulate the stability of microtubules in cells.

I contributed to this study by developing the methods of elevated pH treatment and katanin overexpression in cells. I provided cell lysates (transfected HEK293T cells) for *in vitro* experiments. I prepared construct expressing the truncated form of tau and I planned and performed all the experiments done in IMCD3 cells - which means experiments showing the stability of tau envelopes in cells and experiments of katanin overexpression in cells. I acquired and analyzed all the data from the experiments done with IMCD3 cells. I prepared the cells for FRAP experiments and I analyzed the FRAP data, but the data were captured by Valerie Siahaan. I participated on writing of the manuscript and revision.

Siahaan V, Weissova R, Lanska E, Karhanova A, Dostal V, Henriot V, Janke C, Libusova L, Braun M, Balastik M, Lansky Z. **Tau phosphorylation impedes functionality of protective tau envelopes.** bioRxiv:2024.2003.2025.586522

The publication is available in the supplement of the thesis, and online: https://www.biorxiv.org/content/10.1101/2024.03.25.586522v1.full, and its revision in Nature Chemical Biology is currently pending.

Prolyl isomerase FKBP12 reduces microtubule dynamics and axon growth by inhibiting CRMP2A

In this manuscript, we show that prolyl isomerase FKBP12 binds to CRMP2A isoform preferably in its non-phosphorylated state. We show that CRMP2A increases the polymerization velocity of microtubules in vitro and this function is inhibited by the presence of prolyl isomerase FKBP12. We show that CRMP2A promotes microtubule growth also in cells and FKBP12 has again the inhibitory affect. Finally, we show that prolyl isomerase FKBP12 regulates axon growth. Together, out data show that prolyl isomerase FKBP12 binds to CRMP2A protein and regulates microtubule dynamics and axon growth.

I planned and performed all experiments except of *in vitro* tubulin polymerization assay. I analyzed all the data and made the figures. I wrote the manuscript. The vectors used for EB3 experiments were provided by collaborators from Institute Curie. Graphic processing of the scheme was done by Peter Buran.

Weissova R, Sabo J, Chafai DE, Ziak J, Buran P, Bodakuntla S, Janke C, Braun M, Lansky Z and Balastik M. **Prolyl isomerase FKBP12 reduces microtubule dynamics and axon growth by inhibiting CRMP2A.**

The manuscript is available in the supplement of the thesis.

Tau phosphorylation impedes functionality of protective tau envelopes

Valerie Siahaan*[1,2], Romana Weissova*[2,3], Eva Lanska[1,2], Adela Karhanova[1], Vojtech Dostal[2], Veronique Henriot[4,5], Carsten Janke[4,5], Lenka Libusova[2], Marcus Braun[#1], Martin Balastik[#3], Zdenek Lansky[#1]

1. Institute of Biotechnology, Czech Academy of Sciences, BIOCEV, Prague-West, Czech Republic
2. Department of Cell Biology, Faculty of Science, Charles University, Prague, Czech Republic
3. Institute of Physiology, Czech Academy of Sciences, Prague, Czech Republic
4. Institut Curie, Université PSL, CNRS UMR3348, Orsay, France
5. Université Paris-Saclay, CNRS UMR3348, Orsay, France

*,#Contributed equally
Correspondence: marcus.braun@ibt.cas.cz, martin.balastik@fgu.cas.cz, zdenek.lansky@ibt.cas.cz

Abstract

Tau, an axonal microtubule-associated protein, is a critical regulator of microtubule function and stability. Tau interaction with microtubules is regulated by tau phosphorylation. Tau hyperphosphorylation is implicated in microtubule destabilization related to neurodegenerative disorders. How tau phosphorylation leads to microtubule destabilization is however unknown. Recently, it was shown that tau molecules on microtubules cooperatively assemble into cohesive layers termed envelopes. Tau envelopes protect microtubules against degradation by microtubule-severing enzymes, suggesting a functional link between envelopes and microtubule stability. Here we show that tau phosphorylation has deleterious effects on the microtubule-protective function of tau envelopes. Using reconstitution and live-cell experiments, we found that tau phosphorylation destabilizes tau envelopes and decreases their integrity, leading to reduced microtubule protection against microtubule-severing enzymes. Our data suggest that a perturbation of microtubule homeostasis linked to tau hyperphosphorylation in neurodegeneration, could be explained by the disassembly and impaired functionality of the tau envelopes.

Introduction

Microtubules are rigid filaments, which are essential for neuronal function and homeostasis e.g. by providing tracks for intracellular cargo transport. Microtubules are dynamic polymers, frequently switching between phases of assembly and disassembly[1]. The lifetime of a microtubule is regulated by a multitude of microtubule-associated proteins, which either affect microtubule assembly and disassembly[2,3], or can sever microtubules into fragments[4]. Deregulation of various microtubule-associated proteins, e.g. tau, has been shown to trigger changes in microtubule dynamics, induce loss of microtubule mass from axons and dendrites, and is associated with multiple neurodegenerative disorders[2,5].

Tau is an intrinsically disordered microtubule-associated protein, which in healthy neurons localizes predominantly to axonal microtubules. Tau regulates the functioning of other microtubule-associated proteins and protects microtubules against microtubule-severing enzymes, such as katanin[6]. During neurodegeneration, tau is found aggregated in neurofibrillary tangles, which is one of the hallmarks of neurodegenerative disorders collectively termed tauopathies, such as Alzheimer's disease[7,8]. It was proposed that tau aggregation causes a depletion of functional tau[9,10], thereby leaving the axonal microtubules unprotected against microtubule-severing enzymes, such as katanin, which could lead to pathological microtubule destabilization. Moreover, aggregated tau has an increased phosphorylation state as compared to physiological tau, and has been shown to have reduced interaction with microtubules[11,12]. These findings suggest a relation between hyperphosphorylation of tau and microtubule instability related to neurodegeneration, nevertheless, the underlying molecular mechanism remains unclear.

It has recently been shown that tau molecules associate with microtubules in two distinct modes – either (i) diffusing individually along the microtubule lattice, rapidly binding and unbinding, or (ii) binding cooperatively, with much longer interaction times, constituting cohesive envelopes, previously referred to as 'condensates' or 'islands'[13–15]. These envelopes enclose the microtubules and act as selectively permeable barriers for other microtubule-associated proteins[13,14]. Tau envelopes can differentially modulate the action of microtubule-related molecular motors, e.g. decreasing the kinesin-1 walking distance[14,16], while permitting dynein-mediated transport[13]. While microtubules covered by individually diffusing tau

molecules are prone to disintegration by microtubule severing enzymes, such as katanin[14], tau envelopes efficiently protect the microtubule surface from the action of microtubule severing enzymes[13,14]. These observations suggest that the protective function of tau is mediated by the cohesion of tau envelopes. We thus hypothesized that pathological effects of tau phosphorylation can be explained by the impact of tau phosphorylation on the formation and function of protective tau envelopes.

Here, we demonstrate that the formation and maintenance of tau envelopes is indeed critically regulated by phosphorylation. We found that phosphorylation of tau decreases the propensity of tau to form envelopes and that envelopes formed by phosphorylated tau have altered functionality with decreased protection against microtubule severing enzymes. Our findings suggest that the cohesive binding mode of tau may provide a causal connection between tau phosphorylation and impaired tau functionality: the reduction of tau envelopes and their impaired functionality, caused by tau phosphorylation, results in decreased shielding of microtubules from severing enzymes, and consequently in a decrease of microtubule stability.

Results

Tau phosphorylation induces envelope disassembly

To investigate whether phosphorylation of tau affects the formation of tau envelopes, we expressed GFP-labelled human 2N4R tau (full length tau protein, 441 amino acids), in insect cells and used Alkaline phosphatase to dephosphorylate the tau in vitro (Methods). This approach yielded two tau samples: phosphorylated tau (native, insect cell expressed tau, denoted as ‘phospho-tau’), and dephosphorylated tau (phosphatase treated, insect cell expressed tau, denoted as ‘dephospho-tau’) (Fig. 1a). To confirm the efficiency of the phosphatase-treatment, we determined the degree of phosphorylation of these samples at all potential phosphorylation sites using mass spectrometry (Methods, Fig. 1b, for individual sites see Supplementary Fig. 1a,b). We then added the phospho-tau or dephospho-tau samples at 1.5 nM to surface-immobilized taxol-stabilized microtubules and visualized the interaction using TIRF microscopy. While dephospho-tau readily formed micrometer-sized envelopes at this concentration, by contrast, phospho-tau was present on microtubules only

diffusively and did not form envelopes (Fig. 1c, Supplementary Movie 1,2). Repeating this experiment at two higher concentrations of tau, we found that tau envelopes were formed by both tau samples (Supplementary Fig. 1c), nevertheless, at all concentrations tested, dephospho-tau covered a higher percentage of the microtubules compared to phospho-tau (Fig. 1d), demonstrating higher propensity of dephosphorylated tau to form envelopes. To confirm our findings, we repeated these experiments with tau expressed in bacterial cells which possesses a low phosphorylation state (denoted by Bact-tau) and used a kinase to increase its phosphorylation state (Supplementary Fig. 1d, Methods). Multitude of kinases have been shown to phosphorylate tau, including proline-directed kinases (e.g. Cdk5, GSK-3β or MAP kinases). Cdk5-mediated phosphorylation of tau has been shown in healthy conditions to control multiple processes in neural development (e.g. axonal growth and guidance), while hyperactivation of Cdk5 (e.g. in Alzheimer's disease) has been shown to result in heightened tau phosphorylation, promoting tau mislocalization, aggregation and formation of neurofibrillary tangles[9,17,18]. Therefore, we phosphorylated the Bact-tau sample using Cdk5 kinase with its activator p35 (denoted by Bact-Cdk5-tau, Supplementary Fig. 1d, Methods) yielding a sample with higher phosphorylation degree as confirmed by mass spectrometry (Supplementary Fig. 1e, for individual sites see Supplementary Fig. 1f,g). We then added these samples separately to surface-immobilized taxol-stabilized microtubules and studied the envelope coverage after 3 minutes of incubation. In accordance with our previous results, we found that the Bact-tau formed envelopes at much lower concentrations compared to Bact-Cdk5-tau (Supplementary Fig. 1h). We next asked if tau phosphorylation can destabilize preexisting tau envelopes formed by dephosphorylated tau. To test this, we formed envelopes using 15 nM Bact-tau and after 10 minutes we added active Cdk5 kinase to the channel while keeping tau in solution. After the addition of active kinase we observed that the tau envelopes started to disassemble from their boundaries (Fig. 1e, Supplementary movie 3, Methods) with occasional fission events within the boundaries of the envelope during disassembly (0.01 ± 0.08 fissions $mm^{-1}s^{-1}$). In a control experiment, we added deactivated Cdk5 (Methods) to the envelopes while keeping tau in solution, in which case no disassembly was observed and, on the contrary, a significant increase of the envelope coverage was detected (Fig. 1e,f, Supplementary movie 4). Combined, these experiments show that phosphorylation of tau decreases the propensity of tau to form envelopes and destabilizes preexisting envelopes.

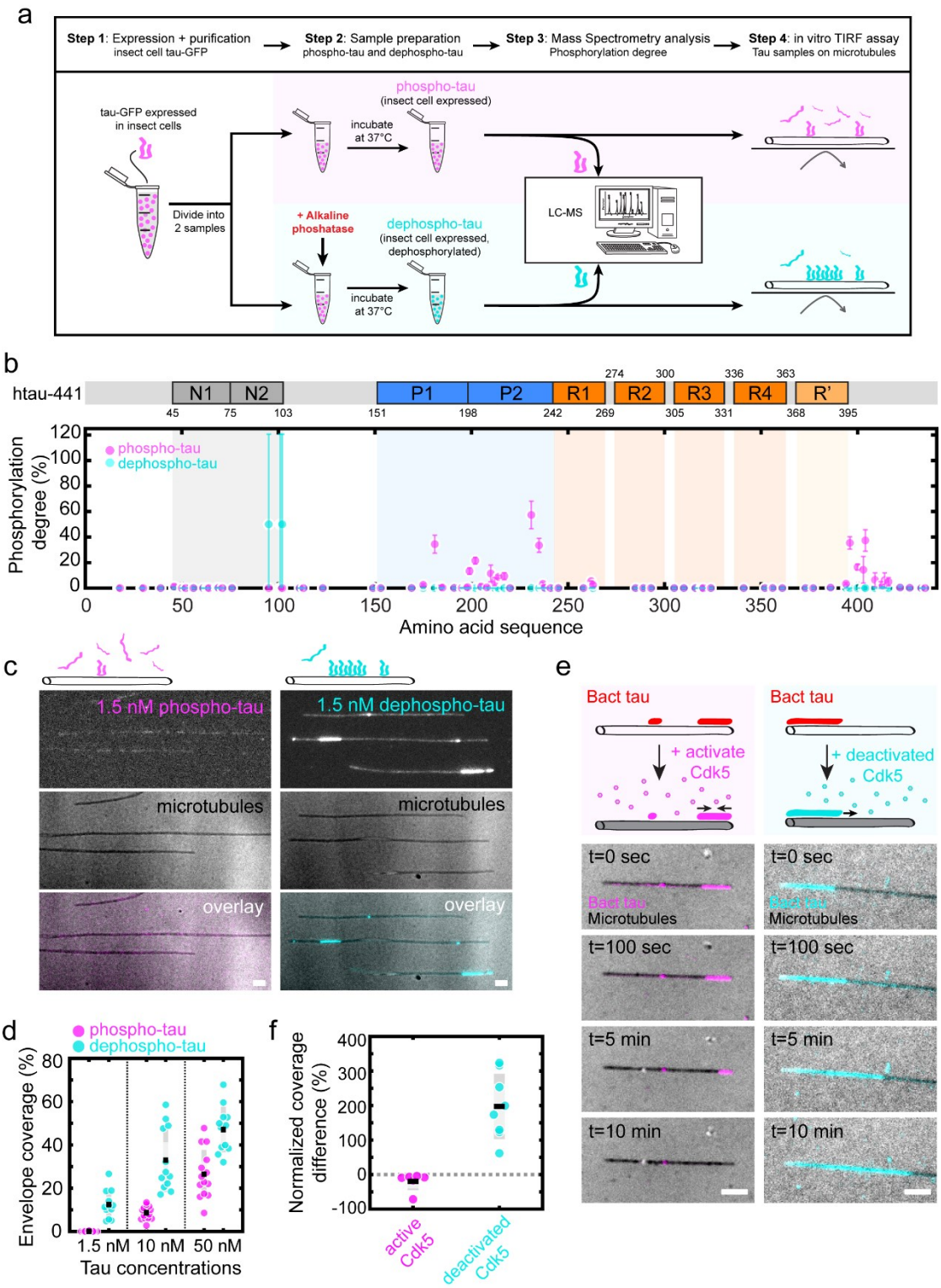

Fig. 1. Tau phosphorylation induces envelope disassembly. a. Schematics of the sample preparation. **b**. Mass-spectrometry-determined degree of phosphorylation of phospho-tau (insect cell expressed tau, magenta) and dephospho-tau (phosphatase-treated insect cell expressed tau, cyan). Phosphorylation degree is presented as the mean ± s.d. (Methods) and displayed at the location of the phosphorylation site along the amino acid sequence of tau (schematic of the sequence is shown above the plot). The domains on the tau sequence are

color-coded: N-terminal domains (N1, N2, grey), proline-rich domains (P1, P2, blue), microtubule-binding repeats (R1-R4, orange), and the domain pseudo-repeat (R', light orange). **c**. Multichannel fluorescence micrographs of 1.5 nM phospho-tau (magenta, left), and 1.5 nM dephospho-tau (cyan, right) on taxol-stabilized microtubules (black, middle panels) after 3 min incubation. Scale bars: 2 µm. **d**. Percentage of taxol-stabilized microtubules covered with tau envelopes after 3 min of tau incubation on surface-immobilized microtubules. Envelope coverage for phospho-tau (magenta) at 1.5 nM was 0.1 ± 0.1%, at 10 nM was 8.6 ± 3.1%, and at 50 nM was 26.5 ± 11.2% (mean ± s.d., n=14, 14, 14 fields of view in 11 independent experiments). Envelope coverage for dephospho-tau (cyan) at 1.5 nM was 12.5 ± 6.4%, at 10 nM was 32.9 ± 14.7%, and at 50 nM was 47.1 ± 10.5%, n=12, 12, 12 independent experiments). **e**. Multichannel fluorescence micrographs of 15 nM Bact-tau (red in schematics) after treatment with active Cdk5 (left, Bact-tau in magenta) or with deactivated Cdk5 (right, Bact-tau in cyan). Microtubules (black) imaged using IRM. Scale bars: 2µm. **f.** Normalized difference between the coverage before and after treatment with active Cdk5 or deactivated Cdk5. Normalized coverage difference for active Cdk5: -19.4 ± 25.9% (mean ± s.d., n=6 independent experiments); deactivated Cdk5: 197.6 ± 94.3% (n=8 independent experiments). Two-sided t-test: $p=1.52*10^{-4}$.

Phosphorylation reduces envelope integrity

We next asked why tau phosphorylation leads to a decrease in envelope formation. We hypothesized that phosphorylated tau might not be able to participate in the formation of tau envelopes. Our phosphorylated tau samples are heterogeneous, meaning that they consist of tau molecules with different patterns and degrees of phosphorylation, which could be differently competent in forming envelopes. To test which tau molecules, out of a given sample, can participate in envelope formation, we added phospho-tau at high concentration (1 µM) to microtubules in solution, ensuring that microtubules were fully covered by tau envelopes. By spinning down the microtubules, we then separated the sample into (i) tau, which participated in envelope formation (tau in envelopes – characterized by limited translocation along the microtubule lattice and with very low turnover[13,14] - found in the pellet along with the microtubules) and (ii) tau, which did not participate in envelope formation (tau in solution – unbound tau or tau characterized by rapid diffusion along the microtubule lattice and high turnover[13,14] - found in the supernatant) (Fig. 2a, Methods). When we then analyzed the phosphorylation degree of these two samples by mass spectrometry, we did not find any striking differences in the phosphorylation patterns between the two samples (Fig. 2b, for individual sites see Supplementary Fig. 2a,b), demonstrating that phosphorylated tau is competent in envelope formation. We did,

nevertheless, find that the phosphorylation degree of tau in the supernatant (not participating in envelope formation) was slightly elevated compared to tau in the envelopes. While we observed almost no phosphorylation in the N-terminal region as well as the microtubule-binding repeats for both tau samples, we found on average about a 5% increase in phosphorylation degree within the proline-rich region and C-terminal regions in tau found in solution. This data demonstrates that although phosphorylation of tau decreases its propensity to form envelopes, phosphorylated tau can (particularly at higher concentration) be incorporated into the tau envelopes.

Knowing that phosphorylated tau participates in envelope formation, we hypothesized that the lowered propensity to form envelopes is caused by a combination of (i) a reduced interaction of phosphorylated tau with the microtubule lattice, as observed previously[11,12,19–21], and (ii) reduced cohesiveness of the envelope, presumably due to reduced tau-tau interaction between phosphorylated tau molecules. To demonstrate (i) the reduction of the affinity of phosphorylated tau molecules on microtubules, we investigated the density of tau on the surface of microtubules. We performed the tau-microtubule interaction experiment at two different conditions; on GMPCPP-microtubules (which prevent the envelope formation) and on native GDP-microtubules (where tau binds preferentially in the envelope form[15]) (Methods, Supplementary Fig. 2c,d,e). Consistent with previous findings[11,12,19–21], at most conditions, except for the saturating conditions on GDP-lattices, we found that phospho-tau is present on the microtubule lattice at lower densities compared to dephospho-tau (Supplementary Fig. 2c,d,e), confirming that phosphorylation reduces tau-microtubule interaction. To test if, furthermore, phosphorylation of tau, (ii) influences the cohesiveness of the envelopes, we mixed 8 nM mCherry-labeled phospho-tau with 8 nM GFP-labeled dephosho-tau, added this mixture to surface immobilized microtubules and observed the formation of envelopes. In line with the results of our pelleting assay, we observed that these envelopes exhibited both GFP and mCherry fluorescence (Fig. 2c), demonstrating that phosphorylated tau molecules are competent to participate in envelope formation. We then analyzed the ratio of phospho-tau to dephospho-tau outside of the envelope region and compared it to the ratio within the envelopes. This analysis revealed a significant relative decrease of phospho-tau within the tau envelopes compared to the regions outside the envelopes (Fig. 2d), showing that, additional to lower affinity to the microtubule lattice,

phosphorylated tau less readily participates in envelope formation. Next, we prepared tau envelopes of either phospho- or dephospho-tau and studied the density of tau molecules within the enveloped regions. We found that for any given envelope coverage, the density of tau within the envelope region is lower in envelopes prepared from phospho-tau compared to envelopes prepared from dephospho-tau (Fig. 2e). This data suggests that envelopes formed by phosphorylated tau consist of a less dense and potentially more gap-prone structure. To test this hypothesis, we prepared tau envelopes on surface-immobilized microtubules using 10 nM Bact-tau, that has a low phosphorylation degree, and removed tau from solution to observe the disassembly of the envelopes. The removal of tau from solution was either performed in presence of (i) active Cdk5 kinase, (ii) deactivated Cdk5 kinase, or (iii) in the absence of a kinase (control) (Methods). In presence of active Cdk5, we observed that the disassembly of the envelopes was significantly faster compared to the conditions with deactivated Cdk5 or the control (Fig. 2f,g(note the different experimental timeframes), Supplementary Movie 5,6). These findings indicate that the Cdk5 kinase actively phosphorylated the tau in the envelopes, causing envelope destabilization. Interestingly, we observed a striking increase in the number of fission events within the envelopes in the presence of active Cdk5, compared to the deactivated Cdk5 or control envelopes (Fig. 2g,h). Combined, these data suggest that tau phosphorylation compromises the integrity and cohesiveness of the tau envelopes.

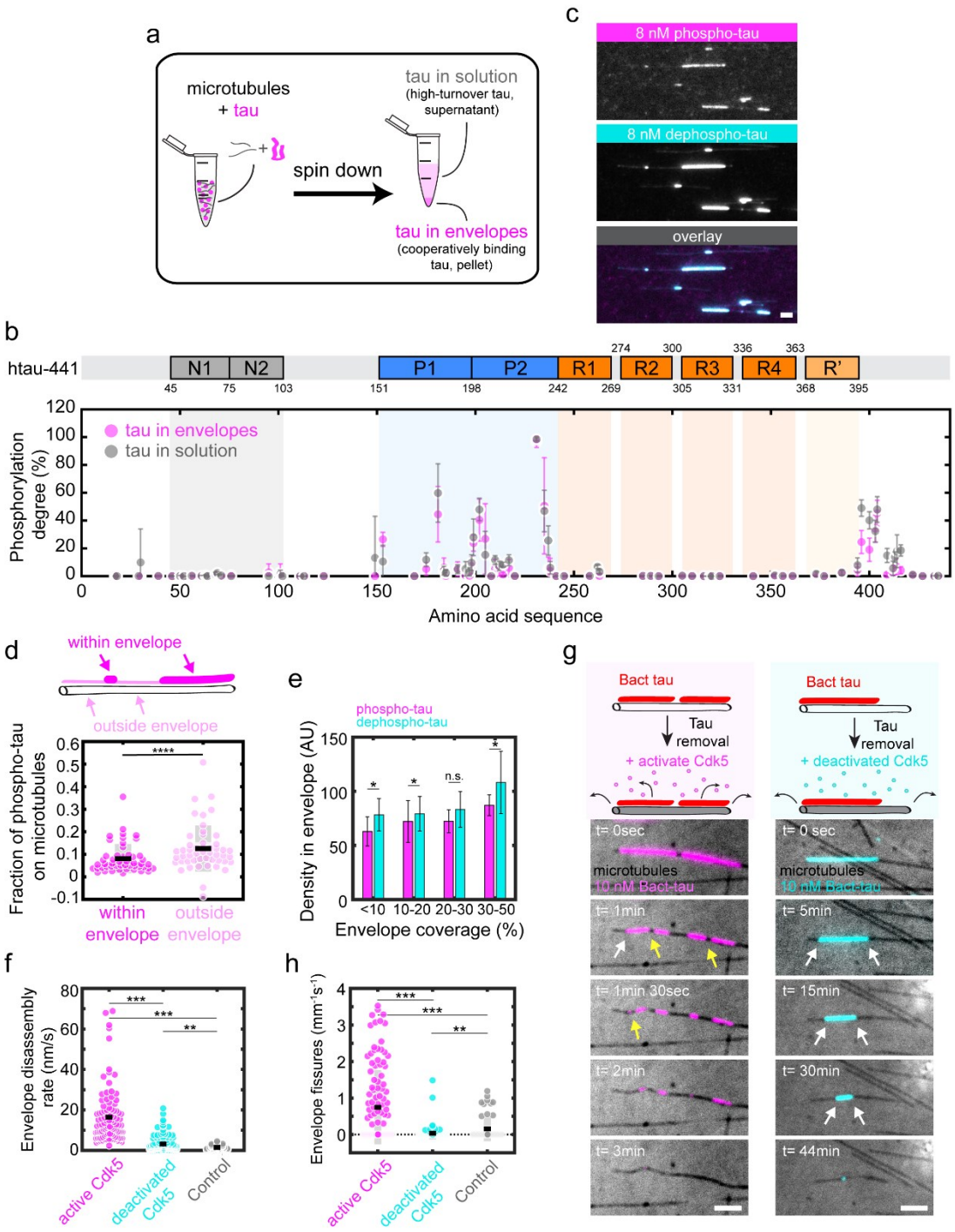

Fig. 2. Phosphorylation reduces envelope integrity. a. Schematics of the sample preparation (Methods). **b**. Mass-spectrometry-determined degree of phosphorylation of cooperatively bound tau found in the pellet (slow-turnover tau in envelopes, magenta) and unbound tau found in the supernatant (high-turnover tau in solution, grey). The phosphorylation degree was presented as the mean ± s.d. for each sample (Methods) and displayed at the location of the phosphorylation site along the amino acid sequence of tau (schematic of the sequence is shown above the plot). The domains on the tau sequence are color-coded: N-terminal domains (N1, N2, grey), proline-rich domains (P1, P2, blue), microtubule-binding repeats (R1-

R4, orange), and the domain pseudo-repeat (R', light orange). **c**. Multichannel fluorescence micrographs of 8 nM phospho-tau (magenta, top panel) and 8 nM dephospho-tau (cyan, middle panel) incubated simultaneously (overlay, bottom panel) and imaged after 3 min incubation. Scale bar: 2 µm. **d.** Fraction of the density of phospho-tau compared to the total density of all tau within tau envelope region (magenta), or outside of tau envelope region (light pink). Location of the envelope and non-envelope region are schematically drawn in the cartoon above the plot. Fraction of phospho-tau within the envelope was 0.08 ± 0.06 (mean ± s.d., n=50 envelopes in 10 independent experiments), and outside the envelope 0.12 ± 0.10 (n=50 regions in 10 independent experiments). Two-sided t-test, $p=6.63*10^{-4}$. **e.** Density of tau within the envelope region for phospho-tau (magenta) and dephosho-tau (cyan) envelopes. Tau density in phospho-tau envelopes: 63.0 ± 13.5 (0 – 10% coverage), 72.1 ± 19.4 (10-20%), 72.4 ± 10.7 (20-30%), and 87.2 ± 95.6 (30-50%) (mean ± s.d., n=18, 16, 18, 12 envelopes in 5, 3, 4, 1 independent experiments); in dephospho-tau envelopes: 78.3 ± 15.0 5 (0 – 10% coverage), 79.3 ± 16.0 (10-20%), 83.3 ± 16.5 (20-30%), 108.2 ± 28.8 (30-50%) (n=7, 17, 30, 37 envelopes in 2, 2, 4, 5 independent experiments. Two-sided t-test between tau samples (left to right): p=0.0207, p=0.2569, p=0.0165, p=0.0169. **f.** Envelope disassembly rate after addition of active Cdk5 (magenta), deactivated Cdk5 (cyan), or in absence of Cdk5 (control, grey). Envelope disassembly rate for active Cdk5: 16.4 ± 13.7 nm/s (mean ± s.d., n=99 envelopes in 7 independent experiments); for deactivated Cdk5 3.2 ± 3.8 nm/s (n=123 envelopes in 8 independent experiments); for control 1.5 ± 1.1 nm/s (n=38 envelopes in 4 independent experiments). Two-sided t-test (left to right): $p=2.30*10^{-20}$, $p=5.92*10^{-10}$, p=0.0075. **g.** Fluorescence micrographs of removal of 10 nM Bact-tau in presence of active Cdk5 (left panels, Bact-tau in magenta) or deactivated Cdk5 (right panels, Bact-tau in cyan). Microtubules (black) are visualized using IRM. Envelope disassembly from the boundaries is indicated by the white arrows while fission events within the boundaries of the envelopes are indicated by yellow arrows (only observable in the active Cdk5 example). Note the different timepoints and intervals for the two samples. Scale bars: 2 µm. **h.** Number of fission events within the boundaries of Bact-tau envelopes during disassembly in presence of Cdk5 (magenta), deactivated Cdk5 (cyan), or in absence of kinase (control, grey). Number of envelope fissures in presence of active Cdk5: 0.75 ± 1.02 $mm^{-1}s^{-1}$ (mean ± s.d., n=117 envelopes in 7 independent experiments); deactivated Cdk5: 0.03 ± 0.17 $mm^{-1}s^{-1}$ (n=119 envelopes in 8 independent experiments); in absence of kinase (control): 0.16 ± 0.34 $mm^{-1}s^{-1}$ (n=52 envelopes in 4 independent experiments). Two-sided t-test (left to right): $p=8.85*10^{-13}$, $p=7.39*10^{-5}$, p=0.001364.

Tau phosphorylation affects envelope formation in cells

We next investigated how envelope formation is regulated by tau phosphorylation in a cellular environment. Initially, we performed TIRF assays with cell lysates (Supplementary Fig. 3a, Methods). To generate tau lysates, we either overexpressed GFP-tau in HEK cells (denoted as HEK lysate), or we overexpressed GFP-tau together with proline-directed kinase Cdk5 and its activator p25 (Cdk5/p25) in HEK cells (denoted as Cdk5 lysate). We then lysed the cells,

added the lysates to surface-immobilized microtubules, and followed the tau-microtubule interaction using TIRF microscopy (Supplementary Fig. 3a,b). While we observed tau envelopes forming in the HEK lysate, there were no envelopes forming in the Cdk5 lysate (Supplementary Fig. 3b,c). These observations are in line with our in vitro experiments showing that phosphorylation of tau decreases the propensity of tau to form envelopes. Next, we overexpressed GFP-tau and mScarlet-tubulin in U-2 OS cells and followed the tau signal correlated to the microtubule signal throughout the cell cycle, which is tightly regulated by activation of specific proline-directed cyclin-dependent kinases known to phosphorylate tau[22]. When following the tau signal throughout the cell cycle, we observed high tau signal on microtubules in interphase cells, where the overall activity of kinases is low, and a significant reduction of the tau signal on microtubules in mitotic cells (Supplementary Fig. 3d,e,f), where multiple mitotic kinases are active[23]. This observation is in agreement with our in vitro findings and published data of decreased affinity of phosphorylated tau for microtubules[11,12].

To discern details of the tau-microtubule interaction in living cells and its regulation by phosphorylation, we overexpressed GFP-tau together with Cdk5/p25 in IMCD-3 cells, denoted as tau-Cdk5. In a control experiment, we overexpressed GFP-tau in IMCD-3 cells in the absence of Cdk5/p25, denoted as tau. Additionally, we overexpressed N-terminally truncated GFP-tau that is not able to form tau envelopes[13,14], denoted as tau-ΔN (Methods). At elevated (micromolar) tau concentrations, tau envelopes are not readily discernable by a local increase in tau density[15]. We thus did not expect to observe regions of high and low tau density in cells, since tau is present at micromolar concentrations in cells[24,25]. Indeed, in both tau and tau-ΔN overexpressing cells, as well as in the tau-Cdk5 cells, tau covered microtubules uniformly along their entire lengths (Supplementary Fig. 3g). In tau-ΔN and tau-Cdk5 cells, tau signal on the microtubule was however weaker (Supplementary Fig. 3h), although the expression levels were comparable (Supplementary Fig. 3i), suggesting that in tau-ΔN and tau-Cdk5 cells, tau has a lower affinity for the microtubule surface or is bound at lower density because of reduced cohesiveness between the tau molecules.

To assess the turnover of tau on microtubules in our differently transfected cells, we used fluorescence recovery after photobleaching (FRAP). We photobleached a circular region of the cell that contained microtubules covered by tau, and studied the recovery of the tau signal

on the microtubules over time (Fig. 3a, Supplementary Fig. 3j, Supplementary Movie 7-9). We found that the recovery of the fluorescent tau signal was slowest and the immobile fraction highest in our control cells expressing full length tau (Fig. 3b,c, Supplementary Fig. 3j), while in cells expressing tau-ΔN, which does not form envelopes, the recovery was fastest and there was no detectable immobile fraction. Since cooperatively bound tau shows lower turnover[14], this data suggests that full length tau is bound to the microtubules in the form of a tau envelope. Interestingly, the recovery time and immobile fraction of the tau signal in tau-Cdk5 cells fell inbetween that of the control cells and the tau-ΔN cells, further supporting our in vitro data and indicating that phosphorylated tau is able to form envelopes, however, their turnover is faster and the envelopes are therefore less stable.

Tau binding is sensitive to pH of the environment in vitro as well as in cells[26,27]. It was shown that changing the pH of the media of cells manifests in the change of the intracellular pH, which can rapidly affect binding of tau to microtubules in cells[26]. As the presence of envelope-incorporated tau can be detected during the assembly or disassembly of the envelopes[14,15], we used pH change to directly test the presence of tau envelopes in cells by exchanging the media during imaging for a solution with slightly higher pH (from pH 7.4 to pH 8.4, Methods). In these conditions, any tau molecules that are non-cooperatively bound to the microtubule, due to their much higher turnover compared with tau in the envelopes, would be readily released from microtubules, while cooperatively bound tau forming envelopes would be more resilient to disassembly. Indeed, in our positive control cells expressing full length GFP-tau (denoted as tau), we observed gaps forming in the tau signal (manifested as increased coefficient of variation of the tau signal along the microtubule, Supplementary Fig. 3g,k) while the microtubules remained unaffected (coefficient of variation of the tubulin signal is not affected, Supplementary Fig. 3g,k). These gaps in the tau signal left clearly separated tau patches on the microtubules, strongly suggesting the presence of cooperatively binding tau molecules forming envelopes, constituting the observed patches (Fig 3d, t=0 min), and confirming our previous observations, where taxol treatment led to dissociation of tau from microtubules in cells in a patch-like pattern[15]. The advantage of the elevated pH treatment compared to the taxol treatment is that the tau unbinding is faster and reversible, which allowed us to analyze the re-binding of tau to microtubules. Presumably due to a recovery of the intracellular pH after the treatment, the gaps started to close and the tau patches regrew

(Fig 3d, t = 5 and 9 min), which is analogous to the growth of envelopes in vitro, when excess tau is available[14,15]. During the whole process, the density of the GFP-tau signal (GFP intensity per unit length) in the patches remained constant (Fig. 3f), further suggesting that these patches represent tau envelopes (which grow and shrink only at the boundaries). Within 9 minutes after the elevated-pH treatment, the microtubules regained full tau coverage (Fig. 3d, Supplementary Fig. 3g (whole cell images),k,l, Supplementary Movie 10). When we performed the elevated-pH treatment on tau-ΔN (incompetent of envelope formation), we did not detect any tau patches on the microtubules after the elevated-pH treatment (Fig 3e, t=0 min). Instead, we observed that the tau signal was removed uniformly and fully along the entire lengths of the microtubules (Fig. 3e, Supplementary Fig. 3g (whole cell images),k,l, Supplementary Movie 11), which suggests that tau molecules were bound to the microtubules individually, non-cooperatively. Subsequently, when following the recovery after elevated-pH treatment, we observed that the tau-ΔN signal returned, again uniformly, along the microtubule lattice. Unlike full-length tau molecules, which exhibited regrowth of the patches while remaining a constant density within the patches, the density of tau-ΔN signal on the microtubule uniformly increased during recovery (Fig. 3e,f, Supplementary Fig. 3g (whole cell images),k,l, Supplementary Movie 11). This further suggests that ΔN-tau, in these cells, does not form envelopes, and instead binds to microtubules non-cooperatively (i.e. with high turnover and high diffusivity). Strikingly, when following the recovery after elevated-pH treatment in the tau-Cdk5 cells, we observed that the reappearance and recovery of the signal occurred in a patch-like manner, closely resembling the reappearance of the tau signal in our positive control cells (Fig 3g, Supplementary Fig. 3g (whole cell images),k,l, Supplementary movie 12). Moreover, the density of the tau signal on microtubules within the patches remained constant throughout the treatment in the tau-Cdk5 cells (Fig. 3f), indicating that tau was bound cooperatively to the microtubules. Interestingly, the reappearance of the tau signal on microtubules was slower in tau-Cdk5 cells than in the control cells indicating that tau phosphorylation leads to slower envelope recovery (Fig. 3h). Combined, these data suggest that in control and tau-Cdk5 cells, the patches and the high-density tau areas covering microtubules consisted of cooperatively bound tau molecules forming cohesive tau envelopes, while N-terminally truncated tau in tau-ΔN cells bound non-cooperatively only. The fact that after the elevated-pH treatment, tau signal disappeared almost completely and reappeared slower in the tau-Cdk5 cells compared to

cells overexpressing control tau is in agreement with our in vitro data showing that tau phosphorylation does not prevent tau envelope formation but makes tau less prone to form envelopes and makes the resulting envelopes less stable. Combined, our data suggests that tau phosphorylation decreases the cohesiveness of tau envelopes, thereby negatively affecting the stability of the tau envelopes in living cells.

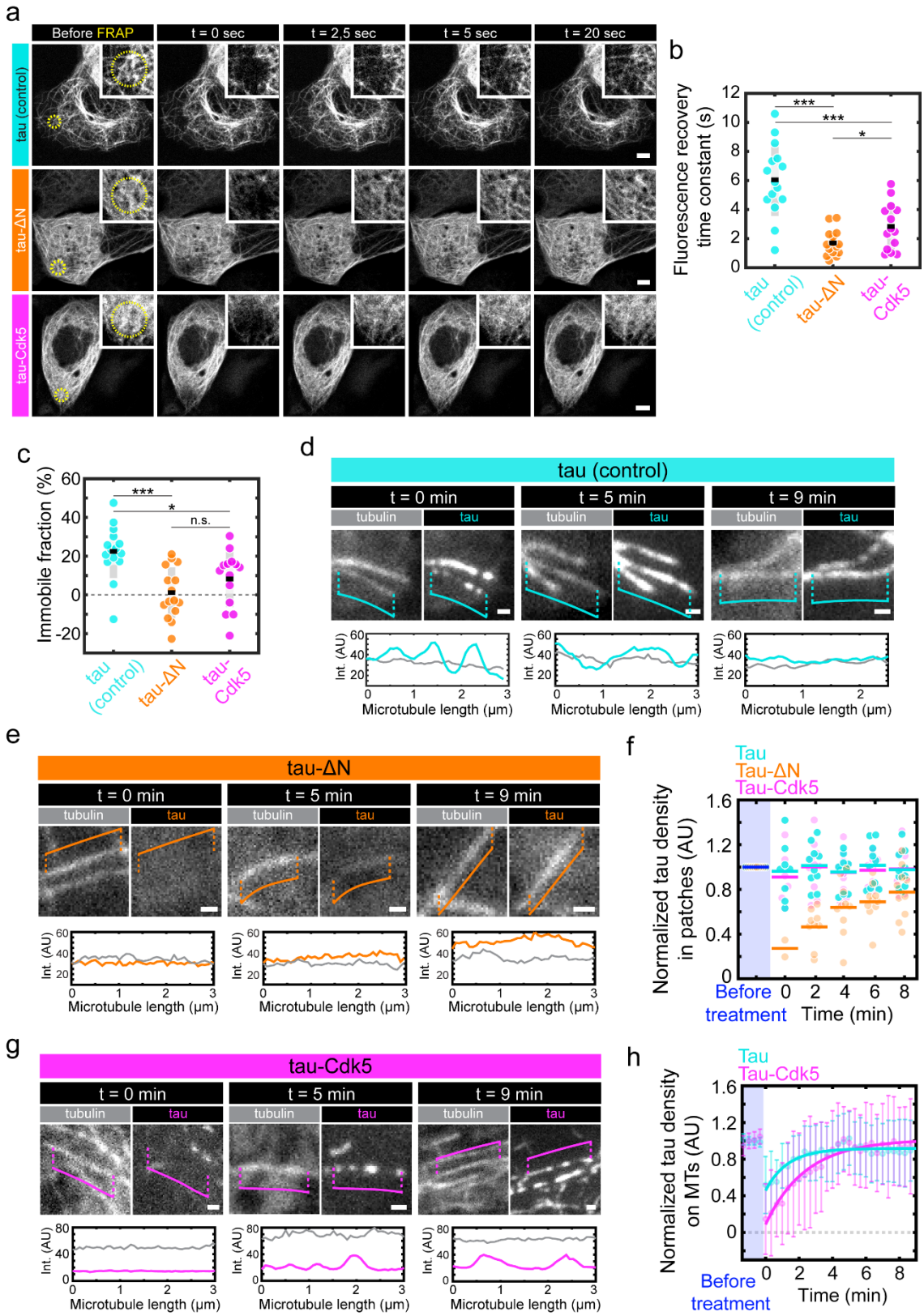

Fig. 3. Tau phosphorylation affects envelope formation in cells. a. Fluorescence micrographs of FRAP experiment on IMCD-3 cells expressing GFP-tau (control, cyan), GFP-tau-ΔN (tau-ΔN, orange), or GFP-tau with Cdk5/p25 (tau-Cdk5, magenta) at different timepoints before and after FRAP. The FRAP-region is drawn as a yellow-dotted circle in the left panels (before FRAP), a zoom-in containing the FRAP-region is shown in the top right corner of each micrograph.

Scale bars: 5µm. **b.** Time constant of the fluorescence recovery of the tau signal in the different groups. Time constant in control cells was 6.05 ± 2.50 sec (mean ± s.d., n=15 cells in 15 independent experiments); in tau-ΔN cells was 1.69 ± 0.89 sec (mean ± s.d., n=15 cells in 15 independent experiments); in tau-Cdk5 cells was 2.83 ± 1.61 sec (mean ± s.d., n=14 cells in 14 independent experiments). Two-sided t-test p-values (from left to right): $p=6.76*10^{-7}$, p=0.00034, p=0.0242. **c.** Immobile fraction measured from fluorescence recovery curve. Immobile fraction in control cells was 22.49 ± 13.77 % (mean ± s.d., n=15 cells in 15 independent experiments); in tau-ΔN cells 1.14 ± 13.15 % (mean ± s.d., n=15 cells in 15 independent experiments); in tau-Cdk5 cells 8.23 ± 14.52 % (mean ± s.d., n=14 cells in 14 independent experiments). Two-sided t-test p-values (left to right): p=0.000167, p=0.0114, p=0.179. . Fluorescence micrographs of IMCD-3 cells expressing mScarlet-tubulin and GFP-tau in control cells (tau, cyan) at t=0 min (left), t=5 min (middle), and t=9 min (right) after elevated-pH treatment. Corresponding linescans are shown below the micrographs. Different microtubules were selected at different timepoints due to dynamic behavior of the microtubules. Scale bars: 1µm. **e.** Fluorescence micrographs of mScarlet-tubulin and GFP-tau signal in tau-ΔN cells (orange) at t=0 min (left), t=5 min (middle), and t=9 min (right) after elevated-pH treatment. Corresponding linescans are shown below the micrographs. Different microtubules were selected at different timepoints due to dynamic behavior of the microtubules. Scale bars: 1µm. **f.** Normalized tau density in patches in GFP-tau control cells (tau, cyan) and GFP-tau-Cdk5/p25 cells (tau-Cdk5, magenta). Normalized tau density along the microtubule lattice (no patches are visible) in GFP-tau-ΔN cells (tau-ΔN, orange). Tau densities were measured at 5 timepoints after elevated-pH treatment and normalized to the tau density along the microtubules before the treatment (dark blue). **g.** Fluorescence micrographs of mScarlet-tubulin and GFP-tau signal in tau-Cdk5 (magenta) at t=0 min (left), t=5 min (middle), and t=9 min (right) after elevated-pH treatment. Corresponding linescans are shown below the micrographs. Different microtubules were selected at different timepoints due to dynamic behavior of the microtubules. Scale bars: 1µm. **h.** Time-trace of tau density on the MTs in the whole cell after elevated-pH treatment normalized to the tau density on the MT before the treatment in GFP-tau cells (tau, cyan) and GFP-tau-Cdk5/p25 cells (tau-Cdk5, magenta). Exponential time constant was 1.3 min for tau cells and 2.5 min for tau-Cdk5 cells (Methods).

Tau phosphorylation affects envelope functionality in vitro and in living cells

Finding that tau envelopes could be formed by tau in both its phosphorylated and non-phosphorylated states, albeit at different efficiencies, and that phosphorylation leads to compromised envelope integrity, we asked if tau phosphorylation additionally affects the functionality of the envelope. Tau envelopes regulate the accessibility of the microtubule surface for other microtubule-associated proteins, such as molecular motors or microtubule severing enzymes, thereby regulating their function[13,14]. To test if envelopes formed by phospho-tau and dephospho-tau differentially regulate typical molecular motors, like kinesin-1, and typical severing enzymes, like katanin, we employed in vitro reconstitution: in separate

measurement chambers, we formed envelopes of similar sizes either with dephospho-tau (5 nM) or phospho-tau (30 nM). Keeping the tau concentrations in solution, we then added kinesin-1 to the measurement chamber and studied the effect of the tau envelopes on kinesin-1. In accordance with previous findings[14], we found that molecules of kinesin-1 could walk on microtubules outside of the envelope regions and were mostly excluded from the envelopes (Supplementary Fig. 4a, Supplementary Movie 13,14). Quantifying the landing rate of kinesin-1 inside the envelope regions, we found no significant difference between the functioning of dephospho-tau and phospho-tau envelopes (Supplementary Fig. 4b). We then repeated the experiment with microtubule severing enzyme katanin. In line with previously published data[14,28], we observed that the regions of microtubules, which were covered only by diffusible tau and not by tau envelopes, were quickly disintegrated by katanin (Fig. 4a), confirming that the cooperatively-bound tau and not the diffusibly-bound tau, can protect microtubules against katanin severing. The envelope-coated regions of the microtubule were protected and prevailed for longer periods. While the density of tau envelopes remained constant (Supplementary Fig. 4c), the envelopes were slowly disassembled by katanin from their boundaries, with occasional severing events within the enveloped region (Fig. 4a, Supplementary Movie 15). The disassembly rate of enveloped regions from their boundaries did not show any significant difference between phospho-tau and dephospho-tau envelopes (Fig. 4b). However, we observed significantly increased rates of katanin severing events within the envelope regions formed by phosphorylated tau compared to non-phosphorylated tau (Fig. 4c), which may be explained by the reduced density of tau within envelopes formed by phospho-tau and reduced tau envelope integrity, as shown above. Combined, these experiments show that envelopes constituted by either phosphorylated or non-phosphorylated tau similarly inhibit kinesin-1 movement, while differentially protect against katanin-mediated severing. Tau phosphorylation thus, in addition to reducing the propensity of tau molecules to bind cooperatively, furthermore reduces the protective functionality of the formed tau envelopes.

We next asked if tau phosphorylation affects the functionality of envelopes in living cells. To test this, we prepared IMCD-3 cells overexpressing katanin-GFP (denoted as ‘katanin only’), or IMCD-3 cells overexpressing katanin-GFP in combination with mCherry-tau (denoted as ‘+ tau’), or mCherry-tau and Cdk5/p25 (denoted as ‘+ tau-Cdk5’). As a control we prepared

IMCD-3 cells overexpressing katanin-GFP in combination with Cdk5/p25 without overexpression of mCherry-tau (denoted as '+ Cdk5'). Cells were fixed 12 hours after transfection and stained for tubulin to visualize the presence of microtubules (Methods). In cells expressing katanin in absence of tau (Fig. 4d, transfected cells, yellow marker), a clear reduction in tubulin signal was observed in comparison with cells not expressing katanin (Fig. 4d,e, non-transfected cells, white marker). Consistent with previously published data[6,14], in cells expressing katanin in combination with tau, no reduction in tubulin signal was measured, indicating that tau protected microtubules against the severing activity of katanin, which is in agreement with our in vitro data. Strikingly, phosphorylation of tau by overexpression of Cdk5/p25, impeded this protective ability, resulting in a reduction in tubulin signal to similar level as in cells expressing katanin only or in cells expressing katanin in combination with Cdk5/p25 (Fig. 4d,e). Comparing the relative density of tubulin with the relative density of katanin 12 hours after transfection, we found that tubulin density inversely correlated with katanin density in all cell groups (Fig. 4f). This correlation was weaker in presence of tau, and stronger in presence of tau-Cdk5, further supporting the notion that phosphorylation of tau decreases its protective functionality (Fig. 4f). Combined, these experiments show that phosphorylation of tau impedes its protective functionality both in vitro and in living cells.

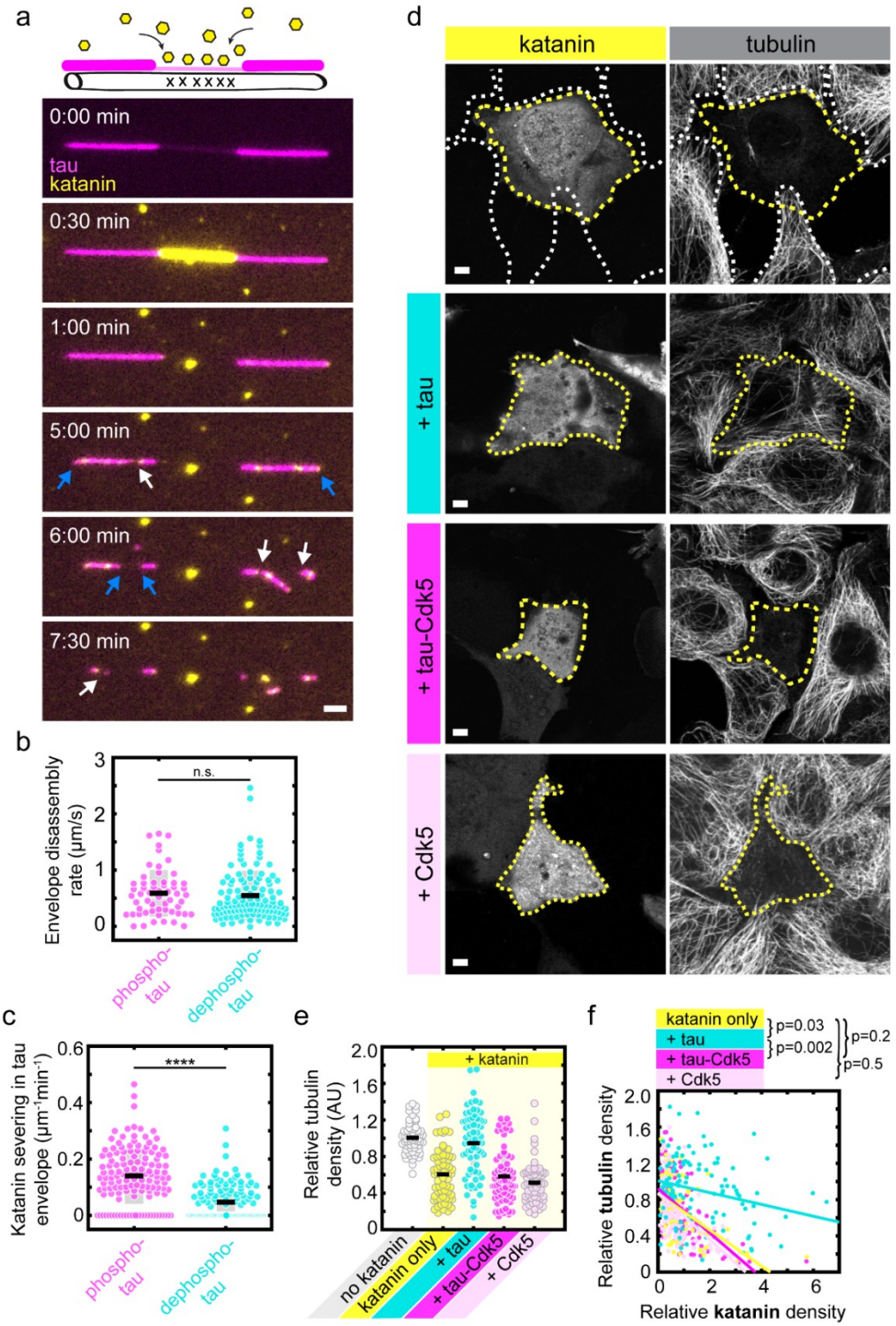

Fig 4. Tau phosphorylation affects envelope functionality in vitro and in living cells. a. Schematics and multichannel fluorescence micrographs showing rapid katanin-GFP-mediated severing of a microtubule region not covered by a tau envelope (panel 2, tau in magenta, katanin in yellow) and subsequently the much slower disassembly of the microtubule regions protected by a tau envelope (panels 3-6). Katanin severing leading to disassembly of envelope-covered portions of the microtubule from their boundaries is indicated by blue arrows, while occasional katanin severing within a tau envelope (severing event) is indicated by white arrows. Scale bar: 2 µm. **b**. Envelope disassembly rate from the boundaries due to

katanin severing of phospho-tau envelopes (magenta) was 0.59 ± 0.41 µm/s; dephospho-tau envelopes (cyan) was 0.50 ± 0.50 µm/s (mean ± s.d., n=57, 112 envelopes in 4,3 experiments). Two-sided t-test, p=0.2638. **c**. Katanin severing events within tau envelope boundaries in phospho-tau envelopes (magenta) was 0.14 ± 0.10 $\mu m^{-1}min^{-1}$; dephospho-tau envelopes (cyan) was 0.05 ± 0.06 $\mu m^{-1}min^{-1}$ (mean ± s.d., n=127,132 envelopes in 4,4 experiments). Two-sided t-test, $p=1.85*10^{-17}$. **d.** Fluorescence micrographs of IMCD-3 cells expressing katanin-GFP (left panels) and stained to visualize tubulin (right panels). Cells were fixed and stained 12 hours after transfection. Additionally, cells are expressing tau (+ tau, cyan), tau and Cdk5/p25 (+ tau-Cdk5, magenta), or Cdk5/p25 in the absence of tau (+ Cdk5, light pink). Cells expressing katanin are marked with a yellow dotted line and cells not expressing katanin (non-transfected cells) are marked with white dotted lines. Scale bars: 5µm. **e.** Relative tubulin density 12 hours after transfection. Relative tubulin density in 'no katanin' cells was 1.01 ± 0.16 (white), in 'katanin-only' cells was 0.61 ± 0.27 (yellow), in '+ tau' cells was 0.95 ± 0.35 (cyan), in '+ tau-Cdk5' cells was 0.58 ± 0.28 (magenta), in '+ Cdk5' cells was 0.51 ± 0.23 (light pink) (mean ± s.d., n=60, 64, 68, 71, 60 cells in 3 independent experiments). **f.** Correlation of the relative tubulin density (y-axis) compared to the relative katanin density (x-axis). Correlation coefficients of 'katanin only' is -0.49 (yellow), of '+ tau' is -0.25 (cyan), of '+ tau-Cdk5' is -0.57 (magenta), and of '+ Cdk5' is -0.54 (light pink). Correlation coefficient comparisons are indicated above the graph.

Discussion

Tau has been shown to modulate many neurodevelopmental processes through its interaction with microtubules, while its deregulation is associated with pathogenesis of numerous neurodegenerative disorders. It is known that phosphorylation regulates tau, but the detailed mechanism of how it affects tau function is still ill-understood. Here we show that phosphorylation of tau controls the formation of the protective tau envelopes. Tau envelopes are cohesive patches of cooperatively binding tau molecules characterized by limited lateral translocation and low turnover of the constituting tau molecules, which enclose the microtubule lattice and are selectively permeable for some proteins, while protecting the microtubules from others, for example the severing enzyme katanin[14]. This mode of tau binding to microtubules is contrasted by non-cooperative interactions of tau molecules binding individually, observed in vitro at low tau concentration[13,14] and upon disturbance of the cellular homeostasis, for example by pH-shock (Fig.4d-g). This non-cooperative mode of tau binding is characterized by rapid diffusion and high turnover of the individual tau molecules, which, in absence of cohesion, does not shield against the binding of other proteins, and thus leaves the microtubule lattice vulnerable to severing enzymes like

katanin[14]. Here, we showed that phosphorylation of tau impedes the envelope formation and integrity and reduces their protective functionality.

Previous results showed that tau phosphorylation reduces tau association with microtubules [19–21,29]. In accordance with these findings, we observed, outside of the tau envelopes, reduced binding of phosphorylated tau to microtubules, compared to non-phoshorylated tau. We suggest that increased binding of non-phosphorylated tau to the microtubule lattice and consequent higher tau densities on the microtubule lead to an increase in frequency of tau-tau encounters on the microtubule lattice, leading to a higher probability of nucleation of a tau envelope and increased envelope growth. Additionally, our finding that the relevant phosphorylation sites are located in the proline-rich regions and the C-terminus of tau (Fig. 2b), but not in the microtubule binding repeats (a) demonstrates that phosphorylation of tau domains other than the binding repeats play a significant role in the interaction of tau with the microtubule lattice, and (b) suggests that tau-tau interaction might play a significant role in the envelope formation. This notion is consistent with the observation that tau molecules, under certain conditions, can phase-separate[30] and that phosphorylation regulates condensate formation[31]. For both reasons (a) and (b), the concentration required to achieve comparable microtubule envelope coverage, is much higher for phosphorylated tau as compared to non-phosphorylated tau. At any given tau concentration, phosphorylated tau generated envelopes which cover, and thus protect, a smaller fraction of the microtubule surface, leaving it completely uncovered at low nanomolar concentrations. The reduced protection resulting from tau phosphorylation could be due to higher turnover of phosphorylated tau, which might result in transient defects in the envelope. Thus, in cells, tau phosphorylation, at any given tau concentration, will dramatically reduce microtubule envelope coverage and thereby protection. And, importantly, due to the reduced protection, microtubule instability can be observed even before tau envelope disassembly occurs.

As non-phosphorylated tau more readily participates in envelope formation, our data suggests that the different affinities are not the only reason for the observed effect of the phosphorylation on tau envelope behavior. Our data suggest that, additionally, the increased envelope coverage observed for non-phosphorylated tau may be due to stronger tau-tau interactions on the microtubule surface, creating a more cohesive and impenetrable

structure. Tau phosphorylation weakens these interactions and creates a structure that is easier to penetrate by microtubule severing enzymes such as katanin. This notion is corroborated by the finding that phosphorylated tau forms envelopes that have lower tau density compared to dephosphorylated tau envelopes (suggesting weaker tau-tau interactions) and that katanin severs microtubules even within the boundaries of envelopes consisting of phosphorylated tau. This hypothesis is especially plausible when considering the position of phosphorylation in our phospho-tau samples: While little phosphorylation was detected within the binding repeats (R1-R4 and R'), which directly interact with the microtubule, most phosphorylation was detected in the projection domains of tau (in particular P1, P2, and the C-terminus), which are the regions thought of as establishing tau-tau interaction[13,14].

Increased tau phosphorylation has been detected in multiple neurodegenerative disorders and has been associated with formation of phosphorylated tau aggregates[32,33]. The specific effect of tau phosphorylation in the pathogenesis of different diseases is still being analyzed. Using in vitro and in vivo models we demonstrate that increased phosphorylation interferes with formation of protective tau envelopes. Moreover, we show that the presence of phosphorylated tau leads to disassembly of already formed tau envelopes. This can critically amplify the deleterious effect of phospho-tau on neurons as release of tau from envelopes may locally increase its concentration and promote formation of phosphorylated tau aggregates with additional toxic effect on neuronal transport and function.

Tau is phosphorylated by numerous kinases in healthy neurons, but deregulation of Cdk5 seems critical in the neuropathological process leading to neurodegeneration. We now demonstrate that upregulation of Cdk5 has a deleterious effect on microtubule protective functions of tau envelope formation and maintenance, and that microtubules covered by tau envelopes formed by phosphorylated tau are more prone to disintegration, e.g. by microtubule severing enzymes, such as katanin. Thus, by linking Cdk5 upregulation with tau phosphorylation and tau envelope disintegration, our work provides a mechanism of microtubule regulation in cells and in pathogenesis of neurodegenerative disorders, such as Alzheimer's disease. Neurodegeneration and microtubule destabilization is often linked to

tau hyper-phosphorylation. Our results suggest that microtubule destabilization could be the result of the impaired protective functionality of tau envelopes upon phosphorylation of tau.

References

1. Mitchison, T. & Kirschner, M. Dynamic instability of microtubule growth. *Nature* **312**, 237–42 (1984).
2. Drechsel, D. N., Hyman, A. A., Cobb, M. H. & Kirschner, M. W. Modulation of the dynamic instability of tubulin assembly by the microtubule-associated protein tau. *Mol. Biol. Cell* **3**, 1141–1154 (1992).
3. Kowalski, R. J. & Williams, R. C. Microtubule-associated protein 2 alters the dynamic properties of microtubule assembly and disassembly. *J. Biol. Chem.* **268**, 9847–55 (1993).
4. McNally, F. J. & Vale, R. D. Identification of katanin, an ATPase that severs and disassembles stable microtubules. *Cell* **75**, 419–29 (1993).
5. Qiang, L. *et al.* Tau does not stabilize axonal microtubules but rather enables them to have long labile domains. *Curr. Biol.* **28**, 2181–2189 (2018).
6. Qiang, L., Yu, W., Andreadis, A., Luo, M. & Baas, P. W. Tau protects microtubules in the axon from severing by katanin. *J. Neurosci.* **26**, 3120–3129 (2006).
7. Berger, Z. *et al.* Accumulation of pathological tau species and memory loss in a conditional model of tauopathy. *J. Neurosci.* **27**, 3650–62 (2007).
8. Lasagna-Reeves, C. A. *et al.* Identification of oligomers at early stages of tau aggregation in Alzheimer's disease. *FASEB J.* **26**, 1946–59 (2012).
9. Guo, T., Noble, W. & Hanger, D. P. Roles of tau protein in health and disease. *Acta Neuropathol.* **133**, 665–704 (2017).
10. Lee, G. & Leugers, C. J. Tau and tauopathies. *Prog. Mol. Biol. Transl. Sci.* **107**, 263–93 (2012).
11. Schneider, A., Biernat, J., von Bergen, M., Mandelkow, E.-M. & Mandelkow, E. M. Phosphorylation that detaches tau protein from microtubules (Ser262, Ser214) also protects it against aggregation into Alzheimer paired helical filaments. *Biochemistry* **38**, 3549–58 (1999).
12. Cho, J.-H. & Johnson, G. V. W. Glycogen synthase kinase 3beta phosphorylates tau at both primed and unprimed sites. Differential impact on microtubule binding. *J. Biol.*

Chem. **278**, 187–93 (2003).

13. Tan, R. *et al.* Microtubules gate tau condensation to spatially regulate microtubule functions. *Nat. Cell Biol.* **21**, 1078–1085 (2019).
14. Siahaan, V. *et al.* Kinetically distinct phases of tau on microtubules regulate kinesin motors and severing enzymes. *Nat. Cell Biol.* **21**, 1086–1092 (2019).
15. Siahaan, V. *et al.* Microtubule lattice spacing governs cohesive envelope formation of tau family proteins. *Nat. Chem. Biol.* **18**, 1224–1235 (2022).
16. Henrichs, V. *et al.* Mitochondria-adaptor TRAK1 promotes kinesin-1 driven transport in crowded environments. *Nat. Commun. 2020 111* **11**, 1–13 (2020).
17. Cruz, J. C., Tseng, H.-C., Goldman, J. A., Shih, H. & Tsai, L.-H. Aberrant Cdk5 activation by p25 triggers pathological events leading to neurodegeneration and neurofibrillary tangles. *Neuron* **40**, 471–83 (2003).
18. Kimura, T., Ishiguro, K. & Hisanaga, S. Physiological and pathological phosphorylation of tau by Cdk5. *Front. Mol. Neurosci.* **7**, 65 (2014).
19. Cho, J.-H. & Johnson, G. V. W. Primed phosphorylation of tau at Thr231 by glycogen synthase kinase 3beta (GSK3beta) plays a critical role in regulating tau's ability to bind and stabilize microtubules. *J. Neurochem.* **88**, 349–58 (2004).
20. Biernat, J., Gustke, N., Drewes, G., Mandelkow, E. M. & Mandelkow, E. Phosphorylation of Ser262 strongly reduces binding of tau to microtubules: distinction between PHF-like immunoreactivity and microtubule binding. *Neuron* **11**, 153–63 (1993).
21. Lindwall, G. & Cole, R. D. Phosphorylation affects the ability of tau protein to promote microtubule assembly. *J. Biol. Chem.* **259**, 5301–5305 (1984).
22. Preuss, U., Döring, F., Illenberger, S. & Mandelkow, E. M. Cell cycle-dependent phosphorylation and microtubule binding of tau protein stably transfected into Chinese hamster ovary cells. *Mol. Biol. Cell* **6**, 1397–1410 (1995).
23. Nigg, E. A. Mitotic kinases as regulators of cell division and its checkpoints. *Nat. Rev. Mol. Cell Biol.* **2**, 21–32 (2001).
24. Gamblin, T. C., Berry, R. W. & Binder, L. I. Modeling tau polymerization in vitro: a review and synthesis. *Biochemistry* **42**, 15009–15017 (2003).
25. Reynolds, M. R., Berry, R. W. & Binder, L. I. Site-specific nitration differentially influences tau assembly in vitro. *Biochemistry* **44**, 13997–14009 (2005).

26. Charafeddine, R. A. *et al.* Tau repeat regions contain conserved histidine residues that modulate microtubule-binding in response to changes in pH. *J. Biol. Chem.* **294**, 8779–8790 (2019).
27. Hinrichs, M. H. *et al.* Tau Protein Diffuses along the Microtubule Lattice. *J. Biol. Chem.* **287**, 38559–38568 (2012).
28. Sudo, H. & Baas, P. W. Strategies for diminishing katanin-based loss of microtubules in tauopathic neurodegenerative diseases. *Hum. Mol. Genet.* **20**, 763–78 (2011).
29. Drewes, G. *et al.* Microtubule-associated protein/microtubule affinity-regulating kinase (p110mark). A novel protein kinase that regulates tau-microtubule interactions and dynamic instability by phosphorylation at the Alzheimer-specific site serine 262. *J. Biol. Chem.* **270**, 7679–88 (1995).
30. Hernández-Vega, A. *et al.* Local nucleation of microtubule bundles through tubulin concentration into a condensed tau phase. *Cell Rep.* **20**, 2304–2312 (2017).
31. Söding, J., Zwicker, D., Sohrabi-Jahromi, S., Boehning, M. & Kirschbaum, J. Mechanisms for Active Regulation of Biomolecular Condensates. *Trends Cell Biol.* **30**, 4–14 (2020).
32. Grundke-Iqbal, I. *et al.* Microtubule-associated protein tau. A component of Alzheimer paired helical filaments. *J. Biol. Chem.* **261**, 6084–9 (1986).
33. Stoothoff, W. H. & Johnson, G. V. W. Tau phosphorylation: physiological and pathological consequences. *Biochim. Biophys. Acta* **1739**, 280–97 (2005).
34. Jiang, K. *et al.* Microtubule minus-end regulation at spindle poles by an ASPM-katanin complex. *Nat. Cell Biol.* **19**, 480–492 (2017).
35. Henrichs, V. *et al.* Mitochondria-adaptor TRAK1 promotes kinesin-1 driven transport in crowded environments. *Nat. Commun.* **11**, 3123 (2020).
36. Castoldi, M. & Popov, A. V. Purification of brain tubulin through two cycles of polymerization-depolymerization in a high-molarity buffer. *Protein Expr. Purif.* **32**, 83–8 (2003).
37. Schindelin, J. *et al.* Fiji: an open-source platform for biological-image analysis. *Nat. Methods* **9**, 676–682 (2012).
38. Liu, H. & Naismith, J. H. An efficient one-step site-directed deletion, insertion, single and multiple-site plasmid mutagenesis protocol. *BMC Biotechnol.* **8**, 91 (2008).
39. Chu, D. T. W. & Klymkowsky, M. W. The appearance of acetylated alpha-tubulin

during early development and cellular differentiation in Xenopus. *Dev. Biol.* **136**, 104–17 (1989).

Methods

Protein constructs and purification

Insect cell expressed tau

For in vitro experiments, GFP- or mCherry-labelled tau (h441-tau; NM_005910.6:151-1476) was expressed in insect cell and purified using the baculovirus expression system (DefBac DNA). Sf9 cells were infected with 8 ml of P2 baculovirus stock (1:100 ratio of P2 virus to cell culture), incubated at 27°C with moderate shaking, and harvested 72 hours post infection. Cells were harvested by centrifugation at 300 x g for 10 min and resuspended in PBS before snap-freezing the cells, or prior to purification in lysis buffer (25 mM HEPES pH 7.4, 150 mM KCl, 20 mM imidazole, with 1 mM DTT, benzonase (1.25 µL of 25 U/µl, 70664, Novagen) and 1x Protease inhibitor cocktail (34044100, Roche Diagnostics GmBH). Cells were lysed by spinning at 70000 x g for 1 hour at 4°C and collecting the supernatant. The lysate was incubated with NiNTA agarose resin (XF340049, Thermo Scientific) HiTrap for 2 hours at 4°C by slowly rotating. After incubation, beads were washed with 3x20 ml wash buffer (25 mM HEPES, 150 mM KCl (or 700 mM KCl in wash step 2), 1mM DTT, 20 mM imidazole). 6xhis tag was removed by incubating the beads with PreScission protease (homemade 3C HRV protease, 1:100, 1µg enzyme/100 µg of protein, overnight at 4°C while rotating). The next day the cleaved protein was collected and concentrated by spinning the sample at 3500 RPM at 4°C using -50kDa centrifugal filter tube (Amicon Ultra-15, Merck). The protein was purified by size-exclusion chromatography using a Superdex 200 10/300 GL column (GE28-9909-44, Sigma) with an NGC Chromatography system (Bio-Rad), equipped with ChromLab software (Bio-Rad) in 25 mM HEPES pH 7.4, 150 mM KCl, 1 mM DTT, 0.1 mM ATP, 1 mM EDTA. Collected peak fractions were concentrated to 10-40 µM using -50kDa centrifugal filter tube (Amicon Ultra-15, Merck). Protein concentration was measured with a NanoDrop ND-1000 spectrophotometer (Thermo Scientific) at 280 nm absorbance. Proteins were flash-frozen in liquid nitrogen and stored at -80°C. All steps in the purification were performed at 4°C.

Bacterial cell expressed tau

Fluorescently tagged tau used for in vitro experiments (h441-tau was subcloned into the expression vector based on pET11Kan-N-HIS6-3C-mNeonGreen or pET11Kan-N-HIS6-3C-mRuby3) was expressed in E. coli BL21(DE3)-RIPL strain. The cells were grown at 30°C until OD_{600} of 0.5-0.6, the protein expression was then induced by 0.1 mM IPTG, and the cells were grown overnight at 16°C. Bacterial cells (3-4 g) were lysed in 45 ml of lysis buffer (50 mM Tris pH 8.0, 300 mM NaCl, 2 mM bME, 20 mM Imidazole, 0.5 µL Benzonase, and 1x Protease inhibitor cocktail), sonicated (5 min; On/Off: 2/4 s) and centrifuged (40000 x g; 30 min; 4 °C). The soluble fraction was then subjected to Strep-Tactin XT purification (washing buffer: 50 mM Tris pH 8.0, 300 mM NaCl, 2 mM bME), and eluted using BXT buffer (100 mM Tris pH 8.0, 150 mM NaCl, 1 mM EDTA, 50 mM Biotin). The purified protein was concentrated using VivaSpin-10kDa-HY and subjected to Size exclusion chromatography (see Insect cell expressed tau; buffer: 50 mM Tris pH 8.0, 300 mM NaCl, 1 mM DTT). Protein concentration was measured with a NanoDrop (see Insect cell expressed tau) at 280 nm absorbance. Proteins were flash-frozen in liquid nitrogen and stored at -80°C. All purification steps were performed at 4°C.

Katanin + Kinesin expression and purification

Katanin-GFP[34] (p60 & p80-GFP)and kinesin-1-GFP[35] were expressed and purified as previously described.

TIRF microscopy

Total internal reflection fluorescent (TIRF) microscopy experiments were performed on an inverted microscope (Nikon-Ti E, Nikon TI2 E) with H-TIRF module or iLas2 equipped with 60x or 100x NA 1.49 oil immersion objectives (Apo TIRF or SR Apo TIRF, respectively, Nikon) and CMOS Hamamatsu Orca Flash 4.0 LT, sCMOS Hamamatsu ORCA 4.0 V2, or PRIME BSI (Hamamatsu Photonics, Teledyne Photometrics) cameras. Microtubules were visualized using interference reflection microscopy (IRM) and fluorescent proteins by switching between microscope filter cubes for EGFP, mCherry, and Cy5 channels or by using a quad band set (405/488/561/640). The microscopes were controlled with Nikon NIS Elements software (v5.02, v5.20 or v5.42). All experiments were performed at room temperature by several experimentalists over the course of multiple months. No data was excluded from the study.

Experimental chamber preparation

For TIRF experiments, chambers were assembled by melting thin strips of parafilm in between two glass coverslips silanized with 0.05% dichlorodimethylsilane (DDS, #440272, Sigma). The chambers were incubated with 20 µg/mL anti-biotin antibodies (in PBS, #B3640, Sigma) for 5 min or 20 µg/mL anti-β-tubulin antibodies (in PBS, #T7816, Sigma) for 5 min, followed by 1% Pluronic (F127 in PBS, #P2443, Sigma) for at least 30 min. (Biotin-labeled) Microtubules (Methods) were diluted into BRB80T (BRB80: 80mM PIPES pH 6.9, 1mM EGTA, 1mM MgCl2, supplemented with 10 µM paclitaxel (#17191, Sigma)), then incubated in the chamber and allowed to adhere to the antibodies for 30 sec. Unbound microtubules were washed away with BRB80T and chambers were pre-incubated with TIRF assay buffer AB (50 mM HEPES pH 7.4, 1 mM EGTA, 2 mM $MgCl_2$, 75 mM KCl, 10 mM dithiothreitol, 0.02 mg/ml casein, 10 µM taxol, 1 mM Mg-ATP, 20 mM D-glucose, 0.22 mg/ml glucose oxidase and 20 µg/ml catalase) prior to experiments. Unless stated otherwise, all experiments were conducted in TIRF assay buffer (AB). All experiments were quantified by pooling data from multiple chambers performed on at least two different days. Chambers were never re-used for additional experiments.

Microtubule Assembly

Porcine brains were obtained from a local abattoir and used within ~4 h of death. Porcine brain tubulin was isolated using the high-molarity PIPES procedure[36]. Biotin-labeled tubulin was purchased from Cytoskeleton Inc. (#T333P) and diluted 1:50 with unlabeled porcine brain tubulin to obtain biotin-labeled tubulin mix for surface-immobilization assays using biotin antibodies.

Taxol-stabilized microtubules (GTP polymerized, then taxol-stabilized; stored and imaged in presence of taxol) were polymerized from 4 mg/ml tubulin for 30 min at 37°C in BRB80

supplemented with 4 mM $MgCl_2$, 5% DMSO, and 1mM GTP (#NU-1012, Jena Bioscience). The polymerized microtubules were diluted in BRB80T and centrifuged for 30 min at 18000 x g in a Microfuge 18 Centrifuge (Beckman Coulter). After centrifugation the pellet was resuspended and kept in BRB80T at room temperature.

GMPCPP-microtubules (GMPCPP polymerized, then taxol-stabilized; stored and imaged in presence of taxol) were polymerized from 4 mg/ml tubulin for 2 h at 37°C in BRB80 supplemented with 1mM $MgCl_2$ and 1mM GMPCPP (#NU-405, Jena Bioscience). The polymerized microtubules were centrifuged for 30 min at 18000 x g in a Microfuge 18 Centrifuge (Beckman Coulter). After centrifugation the pellet was resuspended and kept in BRB80T at room temperature.

GDP-microtubules (GTP polymerized, then glycerol-stabilized; stored and imaged in presence of 40% glycerol) were polymerized as described for taxol-stabilized microtubules. After polymerization, the microtubules were gently diluted in BRB80-Gly40 buffer (80 nM PIPES, 2 mM $MgCl_2$ and 1 mM EGTA, pH 6.8, 40% glycerol) and centrifuged as described above. After centrifugation the supernatant was discarded, and the pellet was resuspended gently in 50 µl of BRB80-Gly40. Microtubules were then kept at room temperate at least 1 hour (maximum overnight) before usage.

Tau sample preparation

To study the effect of phosphorylation of tau on envelope formation 4 samples were produced with various degrees of phosphorylation, as described below:

Phospho-tau. Tau expressed in insect cells, treated with buffer in absence of Alkaline Phosphatase. 2µM (0,2 mg/ml) insect cell expressed tau was incubated in 1x Fast Phosphatase Buffer (stock 10x) for 15 min at 37°C.

Dephospho-tau. Tau expressed in insect cells, treated with Alkaline Phosphatase (FastAP Phosphatase, #EF0651, Themofisher). 2µM (0,2 mg/ml) insect cell expressed tau was incubated with 2,5 g/mol Alkaline Phosphatase (stock 10 g/mol) and 1x Fast Phosphatase Buffer (stock 10x) for 15 min at 37°C.

Bact-tau. Tau expressed in bacterial cells, treated with buffer in absence of Cdk5/p35 kinase. 2µM (0,2 mg/ml) Bact-tau was incubated in Reaction Buffer A (K03-09, stock 5x) supplemented with 50µM DTT, 50µM ATP for 15 min at 37°C.

Bact-Cdk5-tau. Tau expressed in bacterial cells, treated with Cdk5/p35 kinase (#V3271, Promega). 2µM (0,2 mg/ml) Bact-tau was incubated in Reaction Buffer A (K03-09, stock 5x) supplemented with 50µM DTT, 50µM ATP and 0.02 µg/µl Cdk5/p35 kinase (stock 0.1 µg/µl) for 15 min at 37°C.

TIRF assays

In all TIRF experiments, chambers were prepared as described above and microtubules were observed using interference reflection microscopy (IRM). Movies were captured with

appropriate frame interval and analysis was done after a certain incubation time as stated in the caption or methods.

Tau on microtubules. Tau samples were diluted in AB to the final concentration stated in the main text. After microtubule incubation, the diluted tau sample was added to the measurement chamber with at least four-fold amount of the chamber volume.

Cdk5 treatment in channel. Tau-mNeonGreen was diluted in AB buffer (supplemented with 0.5 mg/ml casein) to final concentration 15 nM and incubated on surface-immobilized microtubules for 10 min. After incubation, either i) active cdk5/p35 (activity: 0.1 μg/μl, diluted 10x) or ii) deactivated cdk5/p35 (deactivated by incubating at 95 °C for 10 min, diluted 10x), were added to the chamber, while tau concentration remained unchanged. Tau envelopes were observed for 15 min.

Kinesin-1 assay. Phospho-tau-mCherry or dephospho-tau-mCherry were diluted to concentrations at which envelopes of similar microtubule coverage assembled (30 nM and 5 nM, respectively). After microtubule incubation, tau was added to the measurement chamber and incubated for 3 minutes after which 25 nM kinesin-1-GFP was added in the presence of tau. Microtubules and the location of the tau envelopes were determined by taking a snapshot after which kinesin-1 was imaged for 30 sec using single molecule approach (no delay, 20 ms exposure time).

Katanin assay. Dephospho-tau-mCherry or phospho-tau-mCherry was diluted in AB and incubated on surface-immobilized microtubules for 5 min. Concentrations of dephospho- and phospho-tau were chosen such as to achieve similar microtubule coverage (0.8 nM for dephospho-tau and 3.5 nM for phospho-tau). After incubation, 100 nM katanin-GFP was added to the measurement chamber in presence of the established tau concentration. Chambers were imaged for 30 min with 5 sec interval.

Tau on GDP-microtubules. Tau-mCherry (insect cell expressed) was dephosphorylated using phosphatase as stated above. Dephosphorylated or phosphorylated (untreated) tau diluted in BRB80-Gly40-AB was added to surface immobilized GDP-microtubules (glycerol-stabilized) at concentrations: 0.2 nM, 1 nM, 2 nM, 4 nM, 10 nM, 50 nM or 100 nM, and incubated for 5 minutes. For the lower concentrations (0.2-4nM), tau was sequentially added to the same experimental chamber. For concentrations 10 nM and above, a new channel was used for every concentration. All experiments with Glycerol-stabilized microtubules were performed in BRB80-Gly40 buffer to ensure that microtubules remained stable. For in vitro TIRF assays, BRB80-Gly40 buffer was supplemented with 10 mM dithiothreitol, 20 mM d-Glucose, 1 mM ATP, 0.02 mg/ml Casein, 0.22 mg/ml Glucose Oxidase and 0.02 mg/ml Catalase (henceforth called BRB80-Gly40-AB).

Cdk5 treatment with tau envelope disassambly. Tau-mNeonGreen (bacterial expressed) was diluted in AB to a final concentration between 10-20 nM and incubated on surface-immobilized microtubules for 5 min. After incubation, tau was removed from the channel by the addition of 20 μl AB that contained either i) active Cdk5/p35 (activity: 0.1 μg/μl, diluted 10x), ii) deactivated Cdk5/p35 (deactivated by incubating at 95 °C for 10 min, diluted 10x) or iii) in absence of any kinase (i.e only AB, control). The disassembly of tau envelopes was

observed for: 5 min (for active Cdk5); 10-45 min (for deactivated Cdk5); and 10 min (for control).

TIRF Image analysis

Microscopy data were analyzed using ImageJ 2.3.0/1.53t (FIJI)[37] and custom written Matlab (R2020b) codes. In images with substantial drift, the 'StackregJ' plugin was used to correct the drift (kindly provided by Jay Unruh at Stowers Institute for medical research in Kansas City, MO).

Kymographs. Kymographs were generated by drawing a line along the microtubule lattice and using the ImageJ kymographBuilder plugin.

Envelope coverage. Microtubule lengths were measured by using the IRM signal, tau envelope lengths were measured by using the fluorescent signal after 3 min of incubation. The envelope coverage represents the sum of all tau envelopes lengths divided by the sum of all microtubule lengths within one field of view.

Coverage difference after Cdk5 treatment. Tau envelope coverage difference was calculated by subtracting coverage by tau envelopes before the addition of active/deactivated cdk5/p35 and after 15 min after adding active/deactivated cdk/p35. Coverage was measured as described above.

Tau envelope growth rate. Length of the dephospho-tau envelopes was measured prior to (t=0 min) the 45 min incubation with either phospho- or dephospho-tau and then at the end of the experiment (t=45 min). The difference between the two lengths was calculated and subsequently divided by time to get the growing/shrinking rate (µm/min) of each tau envelope.

Tau density estimation. Tau density on the microtubules was measured in ImageJ by drawing a rectangle around the microtubule and measuring the mean. For background-subtraction the rectangle was then moved to an area directly adjacent to the microtubule where no microtubule is present and the mean was measured again and subtracted from the mean on the microtubule.

Affinities (Tau density plotted against tau concentration). GMPCPP-lattice microtubules were immobilized on the coverslips surface and increasing concentrations of phosphorylated or dephosphorylated tau were added to the measurement chamber. The tau density was then measured on the microtubule lattice and plotted against the tau concentration in nM as a measure of the affinity of tau to the microtubule.

Fraction of phospho-tau in- or outside envelope region. Chambers were prepared as described above. 8.5 nM dephospho-tau-mCherry was mixed with 8.5 nM phospho-tau-mCherry (diluted in AB). The tau mixture was incubated on surface-immobilized microtubules for 5 min. The fraction of phospho-tau within the envelope was calculated as the density of phospho- tau in the enveloped region, divided by the total density of phospho- and

dephospho-tau within the same region. The fraction of phospho-tau outside the envelope region was calculated as the density of phospho- tau in the non-enveloped region, divided by the total density of phospho- and dephospho-tau within the same region.

Envelope disassembly rate due to Cdk5 treatment. The envelope length was measured at the start of the video (before tau removal), and after 5-45 min (see above). Envelope lengths were determined by eye and measured using ImageJ. The disassembly rate was calculated as the difference in the envelope lengths at the beginning and at the end of the video, divided by the time between the two measurements. If an envelope disappeared fully before the end of the video, the beginning length was divided by the time it took for the envelope to completely disassemble.

Gaps in disassembling envelopes. Gaps appearing during the disassembly of the tau envelopes were counted manually. The number of gaps on each envelope were then divided by the envelope length at the start of the movie and by the length (in sec) of the movie.

Tau density on GDP-microtubules. The maximum intensity projection from the last 5 frames of the video was made to eliminate the impact of slight fluorescent intensity fluctuations on the intensity measurements. The mean intensity of tau signal on microtubules was measured from these maximum intensity projections, subtracted by the mean intensity of the background and divided by 5 (number of frames). Mean intensities were measured for all tested concentrations.

Kinesin landing rate. Kinesin-1 landings were counted manually from kymographs of the kinesin channel. Kinesin-1 landings were counted when landings visually appeared to be kinesin-1 molecules (based on fluorescence intensity and size).

Katanin-mediated microtubule disassembly rate. Katanin-mediated microtubule disassembly rate was measured as the change of envelope length over time. Tau envelopes were measured at their longest length and at the end of the captured movie (t=30 min). If a tau envelope disassembled completely before t=30 min, the disappearance of the fluorescence signal marked the end of the measurement. Envelope length was measured by manually drawing a line along the envelope in ImageJ and calculating the length in nm. Subsequently, the lengths were divided by time in sec and normalized to the length of the envelope prior to disassembly (at t=0 min).

Katanin severing in envelope. Katanin severing events were counted manually from fluorescence videos. Severing events were counted when a clear gap appeared in the tau-mCherry signal and disassembly of the microtubule was observed from the newly acquired boundaries.

Normalized tau density in envelopes after katanin addition. Tau density was measured at 5 timepoints after addition of katanin. First frame after katanin addition marks t=0 min. Tau density was measured within the envelope region, and normalized to the tau density within the same envelope at t=0 min.

Live-cell experiments

Plasmids

Human tau sequence (h441-tau) N-terminally tagged with eGFP in pCDNA.4 vector was used as control tau. Tau sequence with deleted N terminus (tau 242-441) was created from control tau using one-step site-directed deletion[38]; primers Fwd: CGGCCGCACGCCTGCAGACAGCCCCCGTGCCCAT, Rev: GCAGGCGTGCGGCCGCGGCTCCGAATTCTTTGTATAGT). Human tubulin sequence (TUBA1B) fused with mScarlet was used for lentiviral and retroviral particles production. To increase the phosphorylation level, co-transfection was used with vectors pCDNA3 overexpressing Cdk5 and p25. For katanin overexpression, co-transfection of pLL vectors expressing katanin subunit p60 and GFP-tagged katanin subunit p80 was used.

Tau lysate preparation

HEK293T cells were co-transfected either with GFP-tau and empty pCDNA3 vector (1:1) or with GFP-tau and vectors pCDNA3 overexpressing Cdk5 and p25 (1:0.85:0.15) using linear Polyethylenimine (PEI; Polysciences, Inc.). Cells were harvested 48 hours after transfection by centrifugation and flash-frozen. Cell pellets were resuspended in 0.5 pellet volumes of lysis buffer (BRB80 supplemented with 1x phosphatase inhibitors (#4906845001, Sigma), 1x protease inhibitors (#04693159001, Sigma) and 0.05% Triton X-100 (# X100, Sigma)). The mixture was sonicated with three short pulses using the sonotrode MS1 (Hielscher Ultrasonics), setting “cycle” 1, “amplitude” 100% (30 kHz) on ice. The solution was transferred to 270 µl Beckman ultracentrifuge tubes and ultra-centrifuged in the Beckman 42.2 Ti rotor at 30000 x g, 4°C for 30 min in the Beckman Coulter Optima XPN-90 ultracentrifuge. The supernatant was directly used for experiments or flash-frozen in liquid nitrogen and stored at -80 °C. Lysate concentrations were measured at 488nm absorbance using NanoDrop ND-1000 spectrophotometer (Thermo Scientific).

Tau lysate imaging

Chambers were prepared as described before. Tau lysates were diluted 10x in AB buffer and added to surface-immobilized microtubules where tau envelope formation was captured for 3 min with 5 sec interval.

Elevated-pH treatment and live-cell imaging

IMCD-3 cells were transduced by lentiviral particles produced by co-transfection of HEK293T cells with lentiviral vector carrying the sequence for mScarlet-tubulin together with gag/pol and vsv-g vector (1:0.9:0.1). Medium containing lentiviral particles was collected 48 hours after transfection, filtered (0.45 µm pores), and used for transduction of IMCD-3 cells.

IMCD-3 cells expressing mScarlet tubulin were then transfected in OptiMEM media (Thermo Scientific) using Lipofectamine 2000 (Thermo Scientific) according to the manufacturer’s protocol. Cells were transfected in 8-well chambered coverslips (Ibidi), 0.5 µg DNA/well was used. Co-transfection of GFP-tau, Cdk5, and p25 was done in the ratio 1:0.85:0.15. The cells

were grown in DMEM/F12 supplemented by FBS and Penicillin/Streptomycin (Thermo Scientific). The imaging was done 24 hours after transfection.

Cells were imaged every 20 sec for 10 min. After 1 min of imaging, the media (DMEM/F12 supplemented by FBS and Penicillin/Streptomycin) was changed for the regular media with pH adjusted to 8.4 with NaOH. Imaging was performed using TIRF microscope (Apo TIRF 60x Oil DIC N2; 488+561 exposure: 300 ms) using OKO-lab chamber (37°C, 5% CO_2).

FRAP experiments

For FRAP experiments, the cells were prepared the same way as described in section 'Elevated-pH treatment and live-cell imaging'. A spinning-disk confocal microscope (Nikon CSU-W1) equiped with FRAP/photoactivation module was used to image and FRAP cells. Cells were imaged using CF Plan Apo VC 60XC WI objective (water immersion) and 488nm laser and FITC filter. Imaging was done on a single cell using 3 different settings: (1) the cell was imaged for 17 frames (100 ms exposure time, 500ms interval) before FRAP; (2) FRAP was performed on a circular region of 0.5 µm diameter; (3) the cell was imaged for 22 seconds directly after FRAP to visualize the recovery. The imaging was done at 37°C and 5% CO_2.

Cell cycle experiments

For the monitoring of tau during cell cycle, U-2 OS human cell line (ATCC HTB-96) was transfected with the GFP-tau vector using the X-tremeGENE HP reagent (Sigma Aldrich) and then selected with 200 µg/mL zeocin. GFP-positive cells were sorted by fluorescent-activated cell sorting (BD FACS Aria Fusion). Cells were then transduced with retroviral particles containing the mScarlet-tubulin. Briefly, Platinum A cells were transfected with pMXs-Puro-mScarletI-Tubulinα, particles were collected after 48 hours and applied to cells, which were selected with 2.5 µg/mL puromycin. The resulting GFP-tau/mScarlet-tubulin cell line was grown on glass-bottom dishes in Fluorobrite medium with 10% FBS and glutamine and observed on a confocal Zeiss LSM 880 microscope at 37°C and 5% CO_2.

Katanin experiment in cells – preparation

IMCD-3 cells were co-transfected with vectors for overexpression of mCherry-tau or mCherry, katanin subunit p60, katanin subunit p80-GFP, and Cdk5 and p25 or empty pCDNA3 vector (in the ratio: 1: 0.375: 0.375: 0.375: 0.375). 12 hours after transfection the cells were fixed using 4% PFA/PBS for 15 min followed by methanol at -20 °C for 2 min. Fixed cells were kept in PBS at 4 °C.

Katanin experiment in cells – immunostaining

Cells were blocked for 1 hour in 0.1% BSA/PBS and then stained with anti-β-tubulin antibody overnight (1:400; DSHB Hybridoma Product E7 deposited to the DSHB by Klymkowsky, M.[39]). After washing, cells were incubated with anti-mouse secondary antibody conjugated with Alexa-647 (Thermo Scientific). Cells were captured using a confocal microscope Leica Stellaris 8 (HC PL APO CS2 63x/1.40 OIL, WLL laser).

Live-cell image analysis

Tau lysate analysis. Microtubule lengths were measured by using the IRM signal, tau envelope lengths were measured by using the fluorescent tau signal after 3 min of incubation. The envelope coverage represents the sum of all tau envelopes lengths divided by the sum of all microtubule lengths within one field of view.

Coefficient of variation (CoV). To determine the CoV in the elevated-pH treatment experiments, a circle was drawn inside the cell, covering (most of) the area of the cell (in case of large cells, two circular areas were averaged). For monitoring GFP-tau during the cell cycle, whole cells were manually selected. The CoV was determined using ImageJ from the standard deviation of the tau fluorescent signal within the ROI, divided by the mean. In elevated-pH treatment experiment, coV was analyzed before, at t = 0 min and t = 9 min after elevated-pH treatment.

Microtubule CoV. The microtubule CoV was determined as the regular CoV, however, the ROI in this case was a line drawn on a single microtubule inside the cell. For every cell, 3 random microtubules were measured and the CoV was averaged.

Pearson's R. Cells in interphase or in mitosis were manually selected based on the presence or absence of a mitotic spindle, and Pearson's correlation coefficient between the GFP-tau and the mScarlet-tubulin channels was calculated with the Coloc 2 plug-in in ImageJ.

Tau density on microtubules. To show that the affinity of tau to the microtubule is different in different cell groups, the mean intensity of tau on the microtubule was measured before elevated-pH treatment and divided by the mean intensity of the same-size region in the cytoplasm next to the measured microtubule at the same timepoint. 25 cells were analyzed (average of 5 microtubules was used for each cell).

Mean intensity of tau in the cell. To show that the transfection of tau was comparable between the groups, the mean intensity of the GFP signal was measured in random circular regions of the cytoplasm before elevated-pH treatment.

Normalized tau density in patches. To show that the density of tau in patches is stable over time for the tau and tau-Cdk5 group, while the density of tau-ΔN is increasing, the intensity of tau in the patches at 5 different timepoints after elevated-pH treatment was analyzed. For tau-ΔN the intensity over the entire length of the microtubule was analyzed. The mean intensity in a tau positive region on the microtubule (tau patch or full microtubule) was measured and subtracted by the mean intensity of the same-size region next to the microtubule. All timepoints were normalized to the intensity of tau before the elevated-pH treatment. 10 cells were analyzed and at each timepoint the average tau density on 5 microtubules was used.

Normalized tau density in the cell. To quantify the recovery of tau signal, the mean density of tau signal on the microtubules was analyzed during the time course. The mean tau intensity in the cell (ROI comprising most of the cell) was measured at all time points and subtracted

by the intensity of the GFP signal in the cytoplasm next to the microtubules). The intensity in each time point was then normalized to the intensity before elevated-pH treatment. Both curves (control tau cells and tau-Cdk5 cells) were fitted using Matlab fitting tool using exponential recovery curve: f(x)= a-b*exp(-c*x) with exponential time constant 1/c [min].

FRAP analysis – recovery time constant. To analyze the recovery of the GFP signal on the microtubule after photobleaching, the intensity of the GFP signal in a small ROI on the microtubule in the bleached region of the cell was analyzed using ImageJ. The same-size region on the microtubule in the same cell but outside the bleached area was used as a reference (ref) and the same-size region outside the cell was used as a background (bg). 14-15 cells were analyzed. The curves were double-normalized according to the equation: $F_{frap\text{-}normalized}(t) = (F_{ref\text{-}pre}/[F_{ref}(t) - F_{bg}(t)])([F_{frap}(t) - F_{bg}(t)]/F_{frap\text{-}pre})$, where $F_{ref\text{-}pre} = \Sigma_{(t=0;t=17)} ([F_{ref}(t) - F_{bg}(t)]/f_{prebleach})$; $F_{frap\text{-}pre} = \Sigma_{(t=0;t=17)} ([F_{frap}(t) - F_{bg}(t)]/f_{prebleach})$; $f_{prebleach} = 17$; $F_{ref}(t)$ is the reference fluorescence intensity on the microtubule in the same cell but not in the bleached region; $F_{frap}(t)$ is the fluorescence intensity on the microtubule in the bleached ROI; $F_{bg}(t)$ is the fluorescence intensity in a background ROI outside the cells; $F_{ref\text{-}pre}$ is the mean fluorescence intensity of the reference ROI before the bleaching after background subtraction; $F_{frap\text{-}pre}$ is the mean fluorescence intensity of the bleached ROI before the bleaching after background subtraction. The normalized data was fitted using the Matlab fitting tool using the equation: $y = a*exp(-b*x)+c$; where b = rate constant and c = asymptote.

FRAP analysis – immobile fraction. To calculate the percentage of immobile fraction, we used the equation: Immob = $[1-(c-F_0)/(1-F_0)]*100$; where c is the asymptote (of the fitted curve), and F_0 is the normalized intensity immediately after the bleaching.

Katanin experiment – relative tubulin and katanin density. The mean density of stained tubulin signal in the transfected cell relative to the mean density of surrounding cells non-transfected with katanin was analyzed using ImageJ (average tubulin intensity of 3 circular ROIs in the cytoplasm of the transfected cell divided by the average tubulin intensity in 3 circular ROIs in 3 randomly selected cells in close vicinity to the analyzed cell). The relative tubulin density was either correlated to the relative density of the katanin signal (correlation plot with the linear regression) or plotted according to the experimental groups in a scatter plot (for this purpose only cells with relative intensity of katanin between 0.5-3 were plotted).

Mass Spectrometry

Samples were analyzed using a liquid chromatography system Agilent 1200 (Agilent Technologies) connected to the timsToF Pro PASEF mass spectrometer equipped with Captive spray (Bruker Daltonics). Mass spectrometer was operated in a positive data-dependent mode. Five microliters of peptide mixture were injected by autosampler on the C18 trap column (UHPLC Fully Porous Polar C18 2.1mm ID, Phenomenex). After 5 min of trapping at a flow rate of 20 µL/min, peptides were eluted from the trap column and separated on a C18 column (Luna Omega 3 µm Polar C18 100 Å, 150 x 0.3 mm, Phenomenex) by a linear 35 min water−acetonitrile gradient from 5% (v/v) to 35% (v/v) acetonitrile at a flow rate of 4 µL/min. The trap and analytical columns were both heated to 50°C. Parameters from the standard proteomics PASEF method were used to set timsTOF Pro. The target intensity per individual PASEF precursor was set to 6000, and the intensity threshold was set to 1500. The scan range

was set between 0.6 and 1.6 V s/ cm^2 with a ramp time of 100 ms. The number of PASEF MS/MS scans was 10. Precursor ions in the m/z range between 100 and 1700 with charge states ≥2+ and ≤6+ were selected for fragmentation. The active exclusion was enabled for 0.4 min. The raw data were processed by PeaksStudio 10.0 software (Bioinformatics Solutions, Canada). The search parameters were set as follows: enzyme – trypsin (specific), carbamidomethylation as a fixed modification, oxidation of methionine, phosphorylation (STY) and acetylation of protein N-terminus as variable modifications.

Mass spectrometry sample preparation

Tau samples. Tau with different levels of phosphorylation (phospho-tau, dephospho-tau, Bact-tau, Bact-tau-Cdk5) was prepared as stated above.

Spin down samples. 1µM phospho-tau (insect cell expressed) was diluted in Mass Spec buffer (50mM HEPES, 75mM KCl, 10 µM taxol, 10 mM dithiothreitol, 1 mM Mg-ATP) and added to taxol-stabilized microtubules to reach a final volume of 100 µl. Microtubules and tau were incubated for 10 min at room temp and centrifuged for 30 min at 18000 x g in a Microfuge 18 Centrifuge (Beckman Coulter). After centrifugation the supernatant was separated from the pellet and used as the sample indicated by the 'tau in solution'. The pellet was resuspended in a four-fold lower volume of Mass Spec buffer and centrifuged again to ensure a more homogeneous sample. After the second centrifugation, the supernatant was discarded and the pellet was resuspended in BRB80 and used as the sample indicated by the 'tau in envelopes'.

Mass Spectrometry analysis

Phosphorylation degree. For each phosphorylation site, all peptides were studied that include the specific site, phosphorylated or not. Each peptide is found with a relative intensity, that gives an indication of the density at which that peptide is detected in the sample. Each peptide can be found with the specific phosphorylation site phosphorylated or not. The sum of the relative intensities of the peptide in phosphorylated state was divided by the sum of the relative intensities of the peptide in non-phosphorylated state to obtain the phosphorylation degree of the phosphorylation site. Each tau sample was prepared as triplicates and each individual sample was analyzed separately, resulting in 3 individual phosphorylation degree values for each phosphorylation site. The graphs in the paper display the mean ± s.d. for each sample at each phosphorylation site, either plotted along the amino acid sequence of tau, or as individual phosphorylation sites.

Total relative intensity. For each phosphorylation site, all relative intensities at which the peptides covering the specific phosphorylation were summed up to get the total relative intensity.

Statistics and reproducibility

For representative plots and figures, whenever not specifically stated in the caption, all data was collected from at least three independent trials. All repeated independent experiments showed similar results and no data was excluded from the manuscript. Unless stated

otherwise, all data were analyzed manually using ImageJ (FIJI) or Matlab (R2020b). Graphs were created using Matlab R2020b and statistical analyses were performed using the same software. Major points on graphs represent data means and the error bars represent variation or associated estimates of uncertainty.

Data availability

Source data files for all figures and supplementary figures, are available with this manuscript.

Acknowledgements

We thank the members of the Lansky-Braun lab and Balastik lab for their feedback and helpful discussion and T. Šmídová and K. Konečná for their technical support. This work was supported by Czech Science Foundation grant 19–27477X to Z.L. and L.L., 21-24571S to R.W. and 23-07703S to M.Br., the project National Institute for Neurological Research (Programme EXCELES, ID LX22NPO5107) - Funded by the European Union - Next Generation EU, the Charles University Grant Agency (GAUK no. 373821 to V.S.), the project 'Grant Schemes at CU' (reg. no. CZ.02.2.69/0.0/0.0/19_073/0016935) to V.S. and V.D and by Czech Health Research Council grant no. NV18-04-00085 to M.Ba. We acknowledge the Imaging Methods Core Facility at BIOCEV, institution supported by the MEYS CR (LM2023050 Czech-BioImaging) for their support & assistance in this work, the CF Protein Production of CIISB, Instruct-CZ Centre, supported by MEYS CR (LM2023042) for protein production, CF Structural mass spectometry of CIISB, Instruct-CZ Centre, supported by MEYS CR (LM2018127) and European Regional Development Fund-Project „UP CIISB" (No. CZ.02.1.01/0.0/0.0/18_046/0015974) for mass spectometry sample analysis, the microscope facility of FGU, supported by MEYS CR (Large RI Project LM2018129 Czech-BioImaging) and ERDF (project No. CZ.02.1.01/0.0/0.0/18_046/0016045) and Vinicna Microscopy Core Facility co-financed by the Czech-BioImaging large RI project LM2023050 for their support and assistance in microscopy. Computational resources were supplied by the project "e-Infrastruktura CZ" (e-INFRA LM2018140) provided within the program Projects of Large Research, Development and Innovations Infrastructures.

Author contributions

The manuscript was conceptualized by M.Br., M.Ba., Z.L.; methods were developed by V.S., R.W., E. L., A.K., V.D.; TIRF in vitro experiments were performed by V.S., E. L., A.K.; tau lysate preparation and experiments were performed by R.W., E.L.; live-cell experiments were performed by R.W., V.D.; FRAP experiments were performed and optimized by V.S., R.W.; data were analyzed by V.S., R.W., E.L., A.K., V.D.; resources were provided by V.H., C.J.; the manuscript was written by V.S., M.Br., Z.L., with reviewing and editing by R.W., M.Ba.; visualization was done by V.S.; the project was supervised by L.L., M.Br., M.Ba., Z.L.; funding was acquired by V.S., R.W., V.D., L.L., M.Br., M.Ba., and Z.L.

Competing interests

The authors declare no competing interests.

Supplemental information

Supplementary movie captions

Movie 1 related to Fig. 1c: **1.5nM phospho-tau on taxol-stabilized microtubules.**

A time-lapse movie of 1.5 nM phospho-tau-GFP (magenta) added to surface-immobilized taxol-stabilized microtubules and imaged for 5 minutes.

Movie 2 related to Fig. 1c: **1.5nM dephospho-tau on taxol-stabilized microtubules.**

A time-lapse movie of 1.5 nM dephospho-tau-GFP (cyan) added to surface-immobilized taxol-stabilized microtubules and imaged for 5 minutes.

Movie 3 related to Fig. 1e: **10nM Bact-tau in presence of active Cdk5.**

A time-lapse movie of 10 nM Bact-tau-GFP (magenta) on surface-immobilized taxol-stabilized microtubules (black). Active Cdk5/p35 was added to the measurement chamber at t=0 min.

Movie 4 related to Fig. 1e: **10nM Bact-tau in presence of deactivated Cdk5.**

A time-lapse movie of 10 nM Bact-tau-GFP (cyan) on surface-immobilized taxol-stabilized microtubules (black). Deactivated Cdk5/p35 (control) was added to the measurement chamber at t=0 min.

Movie 5 related to Fig. 2g: **10nM Bact-tau removal in presence of active Cdk5.**

A time-lapse movie of 10 nM Bact-tau-GFP (magenta) on surface-immobilized taxol-stabilized microtubules (black). Bact-tau was removed from solution in presence of active Cdk5/p35.

Movie 6 related to Fig. 2g: **10nM Bact-tau removal in presence of deactivated Cdk5.**

A time-lapse movie of 10 nM Bact-tau-GFP (cyan) on surface-immobilized taxol-stabilized microtubules (black). Bact-tau was removed from solution in presence of deactivated Cdk5/p35.

Movie 7 related to Fig. 3a: **FRAP of tau-GFP (control) cell.**

A time-lapse movie showing an IMCD-3 cell overexpressing GFP-tau (control, cyan) on which FRAP is performed at t=0 min. GFP-tau signal was monitored for 10 seconds before FRAP and 20 seconds after FRAP.

Movie 8 related to Fig. 3a: **FRAP of tau-GFP-deltaN cell.**

A time-lapse movie showing an IMCD-3 cell overexpressing GFP-tau-ΔN (tau-ΔN) on which FRAP is performed at t=0 min. GFP-tau signal was monitored for 10 seconds before FRAP and 20 seconds after FRAP.

Movie 9 related to Fig. 3a: **FRAP of tau-GFP-Cdk5 cell.**

A time-lapse movie showing an IMCD-3 cell overexpressing GFP-tau-Cdk5/p25 (tau-Cdk5) on which FRAP is performed at t=0 min. GFP-tau signal was monitored for 10 seconds before FRAP and 20 seconds after FRAP.

Movie 10 related to Supplementary Fig. 3g (left): **pH treatment on tau (control) cell.**

A time-lapse movie showing an IMCD-3 cell overexpressing GFP-tau (control) on which elevated-pH treatment is performed at t=0 min. GFP-tau signal (left) and mScarlet-tubulin signal (right) were monitored for 10 minutes; 1 min before treatment and 9 minutes after treatment.

Movie 11 related to Supplementary Fig. 3g (middle): **pH treatment on tau-ΔN cell.**

A time-lapse movie showing an IMCD-3 cell overexpressing GFP-tau-ΔN (tau-ΔN) on which elevated-pH treatment is performed at t=0 min. GFP-tau signal (left) and mScarlet-tubulin signal (right) were monitored for 10 minutes; 1 min before treatment and 9 minutes after treatment.

Movie 12 related to Supplementary Fig. 3g (right): **pH treatment on tau-Cdk5 cell.**

A time-lapse movie showing an IMCD-3 cell overexpressing GFP-tau-Cdk5/p25 (tau-Cdk5) on which elevated-pH treatment is performed at t=0 min. GFP-tau signal (left) and mScarlet-tubulin signal (right) were monitored for 10 minutes; 1 min before treatment and 9 minutes after treatment.

Movie 13 related to Supplementary Fig. 4a (left): **Kinesin-1 molecules walking on microtubules in presence of phospho-tau envelopes.**

A time-lapse movie showing kinesin-1-GFP molecules (white) walking on taxol-stabilized microtubules partly covered by phospho-tau envelopes (magenta).

Movie 14 related to Supplementary Fig. 4a (right): **Kinesin-1 molecules walking on microtubules in presence of dephospho-tau envelopes.**

A time-lapse movie showing kinesin-1-GFP molecules (white) walking on taxol-stabilized microtubules partly covered by dephospho-tau envelopes (cyan).

Movie 15 related to Fig. 4a: **Katanin severing microtubules covered with phospho-tau envelopes.**

A time-lapse movie showing katanin-GFP (yellow) severing taxol-stabilized microtubules partly covered by phospho-tau envelopes (magenta).

Supplementary figures

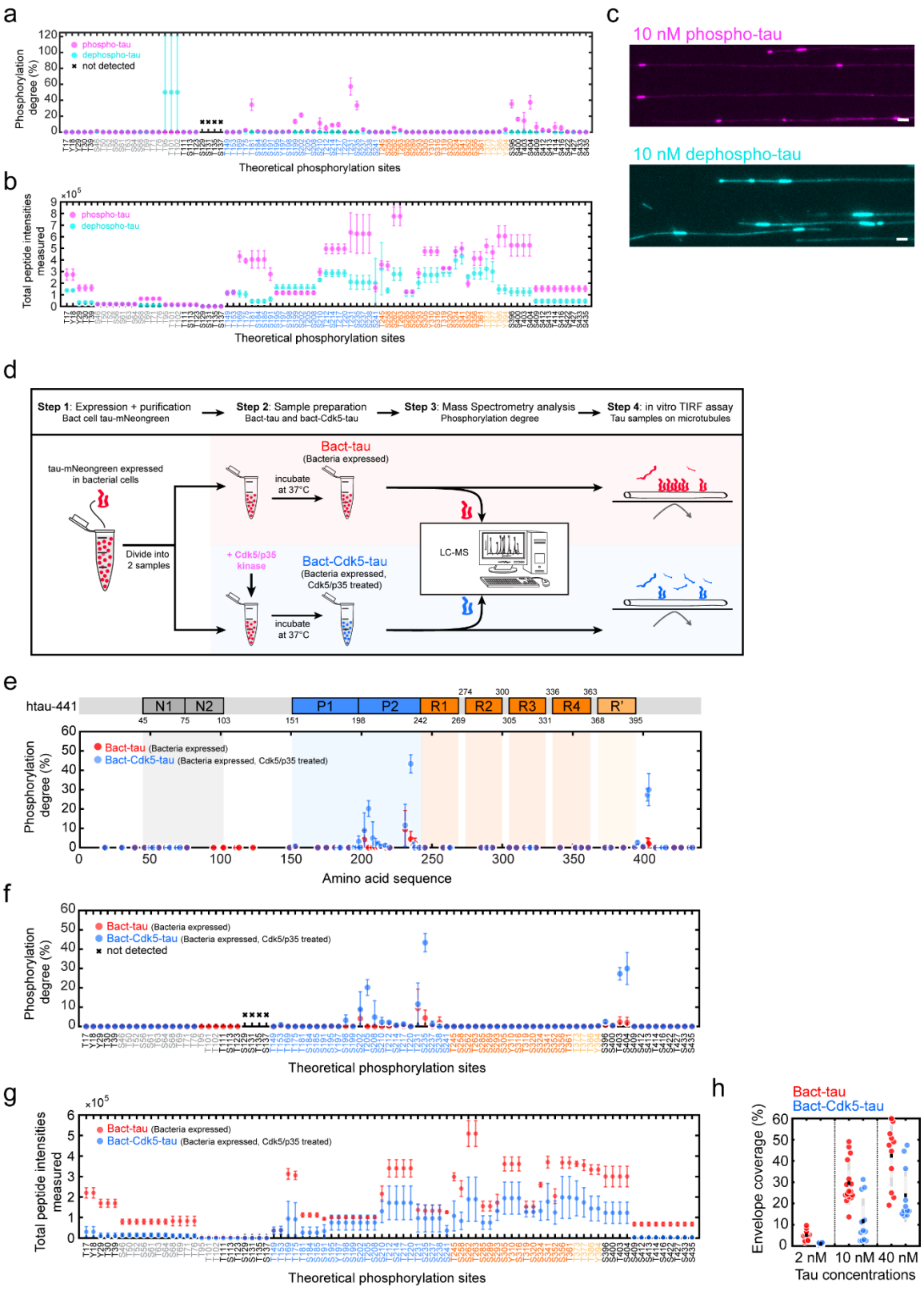

Supplementary Fig. 1: a. Mass-spectrometry-determined degree of phosphorylation of phospho-tau (magenta) and dephospho-tau (cyan). Phosphorylation degrees are presented as mean ± s.d. for each tau sample. If no peptides were detected that covered a specific

phosphorylation site, these phosphorylation sites are marked with a black cross. The color-coded legend corresponds to the domains along the tau sequence highlighted in Fig. 1b. **b**. Total relative intensities measured for all peptides covering the specific phosphorylation site, corresponding to data in a and Fig. 1b. Relative intensities are presented as mean ± s.d. for each tau sample. The color-coded legend corresponds to the domains along the tau sequence as shown in Fig. 1b. **c**. Fluorescence micrographs of 10 nM phospho-tau (left, phospho-tau in magenta) or 10 nM dephospho-tau (right, dephospho-tau in cyan) on surface-immobilized microtubules after 3 min of incubation. Scale bars: 2 µm. **d**. Schematics of sample preparation of bacterial expressed tau-mNeongreen (red), and Cdk5/p35-treated bacterial expressed tau-mNeongreen (blue). **e**. Mass-spectrometry-determined degree of phosphorylation of Bact-tau (red) and Bact-Cdk5-tau (blue). Phosphorylation degree is presented as mean ± s.d. and displayed at the location of the phosphorylation site along the amino acid sequence (schematic of the sequence is shown above the plot). The domains on the tau sequence are color-coded: N-terminal domains (N1, N2, grey), proline-rich domains (P1, P2, blue), microtubule-binding repeats (R1-R4, orange), and the domain pseudo-repeat (R‘, light orange). **f**. Mass-spectrometry-determined degree of phosphorylation of Bact-tau or Bact-Cdk5-tau for individual phosphorylation sites. Phosphorylation degree is presented as mean ± s.d. If no peptides were detected that covered a specific phosphorylation site, these phosphorylation sites are marked with a black cross. The color-coded legend corresponds to the domains along the tau sequence in Fig. 1e. **g**. Total relative intensities measured for all peptides covering the specific phosphorylation site, corresponding to data in e and f. Relative intensities are presented as mean ± s.d. The color-coded legend corresponds to the domains along the tau sequence as shown in Fig. 1e. **h**. Percentage of taxol-stabilized microtubules covered with a tau envelopes after 3 min incubation. Envelope coverage for Bact-tau was 5.1 ± 2.5% at 2 nM, 29.6 ± 10.1% at 10 nM, and 42.4 ± 14.4% at 40 nM (mean ± s.d., each data point represents a single field of view, n=12, 16, 11 independent experiments). Envelope coverage for Bact-Cdk5-tau was 0.9 ± 0.5% at 2nM, 11.7 ± 10.7% at 10nM, and 23.8 ± 12.6% at 40nM (mean ± s.d., each data point represents a single field of view, n=12, 12, 11 independent experiments).

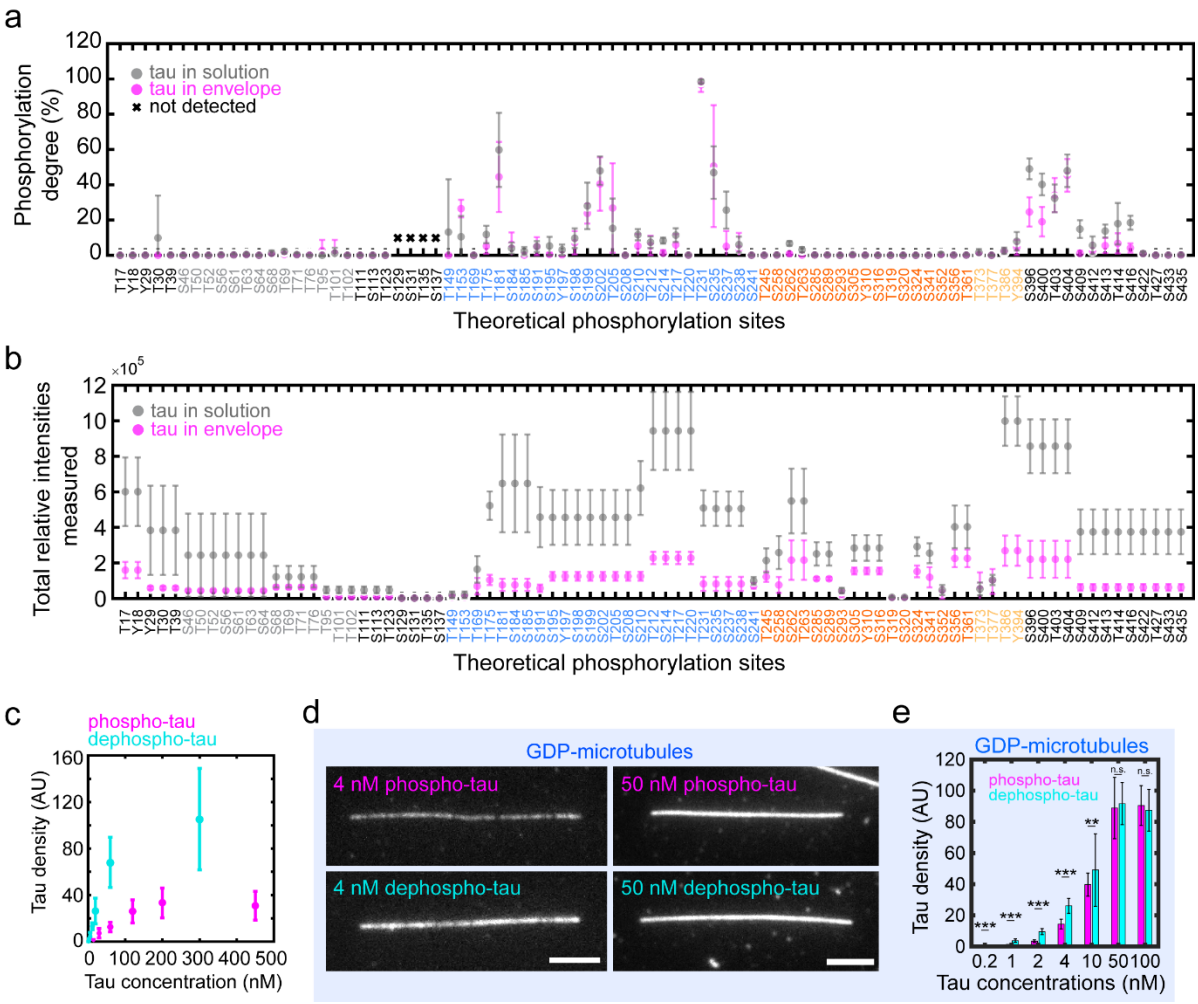

Supplementary Fig. 2: a. Mass-spectrometry-determined phosphorylation degree of spin down sample, where unbound tau was found in the supernatant (tau in solution, grey), and cooperatively bound tau found in the pellet (tau in envelope, magenta). Phosphorylation degrees are displayed as mean ± s.d. If no peptides were detected that covered a specific phosphorylation site, these phosphorylation sites are marked with a black cross. The color-coded legend corresponds to the domains along the tau sequence as shown in Fig. 2b. **b.** Total relative intensities of all peptides that covered the specific phosphorylation site, corresponding to data in a and Fig. 2b. Intensities are displayed as mean ± s.d. for unbound tau from the supernatant (tau in solution, grey), and cooperatively bound tau from the pellet (tau in envelope, magenta). The color-coded legend corresponds to the domains along the tau sequence as shown in Fig. 2b. **c**. Density of phospho-tau (magenta) or dephosho-tau (cyan) measured on GMPCPP microtubules as a function of the concentration of phospho-tau or dephosho-tau in solution (phospho-tau: n=12 fields of view in 4 independent experiments; dephospho-tau: n=9 fields of view in 3 independent experiments). **d.** Fluorescence micrographs of phospho-tau (magenta) or dephospho-tau (cyan) on glycerol-stabilized GDP-microtubules after 1 min of incubation. Scale bars: 2 µm. **e.** Concentration (nM) of phospho-tau (magenta) and dephospho-tau (cyan) plotted against the tau density (AU) on GDP-microtubules. For 0.2 nM: 0.07 ± 0.21 (phospho-tau) and 0.37 ± 0.20 (dephospho-tau) (mean ± s.d., n=36 microtubules in N=2 independent experiments, two-sided t-test: $p=1.31*10^{-8}$); 1

nM: 0.91 ± 0.36 (phospho-tau) and 3.75 ± 1.09 (dephospho-tau) (mean ± s.d., n=36 microtubules in N=2 independent experiments, two-sided t-test: $p=7.81*10^{-26}$); 2 nM: 3.43 ± 0.89 (phospho-tau) and 9.51 ± 1.92 (dephospho-tau) (mean ± s.d., n=36 microtubules in N=2 independent experiments, two-sided t-test: $p=2.53*10^{-33}$); 4 nM: 14.35 ± 3.10 (phospho-tau) and 26.12 ± 4.79 (dephospho-tau) (mean ± s.d., n=36 microtubules in N=2 independent experiments, two-sided t-test: $p=3.29*10^{-28}$); 10 nM: 39.71 ± 7.38 (phospho-tau) and 49.12 ± 23.25 (dephospho-tau) (mean ± s.d., n=51 and 57 microtubules respectively in N=3 independent experiments, two-sided t-test: p=0.0048); 50 nM: 88.88 ± 19.70 (phospho-tau) and 91.69 ± 13.45 (dephospho-tau) (mean ± s.d., n=45 and 44 microtubules respectively in N=3 independent experiments, two-sided t-test: p=0.3939); 100 nM: 90.43 ± 12.77 (phospho-tau) and 87.40 ± 13.38 (dephospho-tau) (mean ± s.d., n=20 and 30 microtubules respectively in N=1 independent experiment, two-sided t-test: p=0.4397).

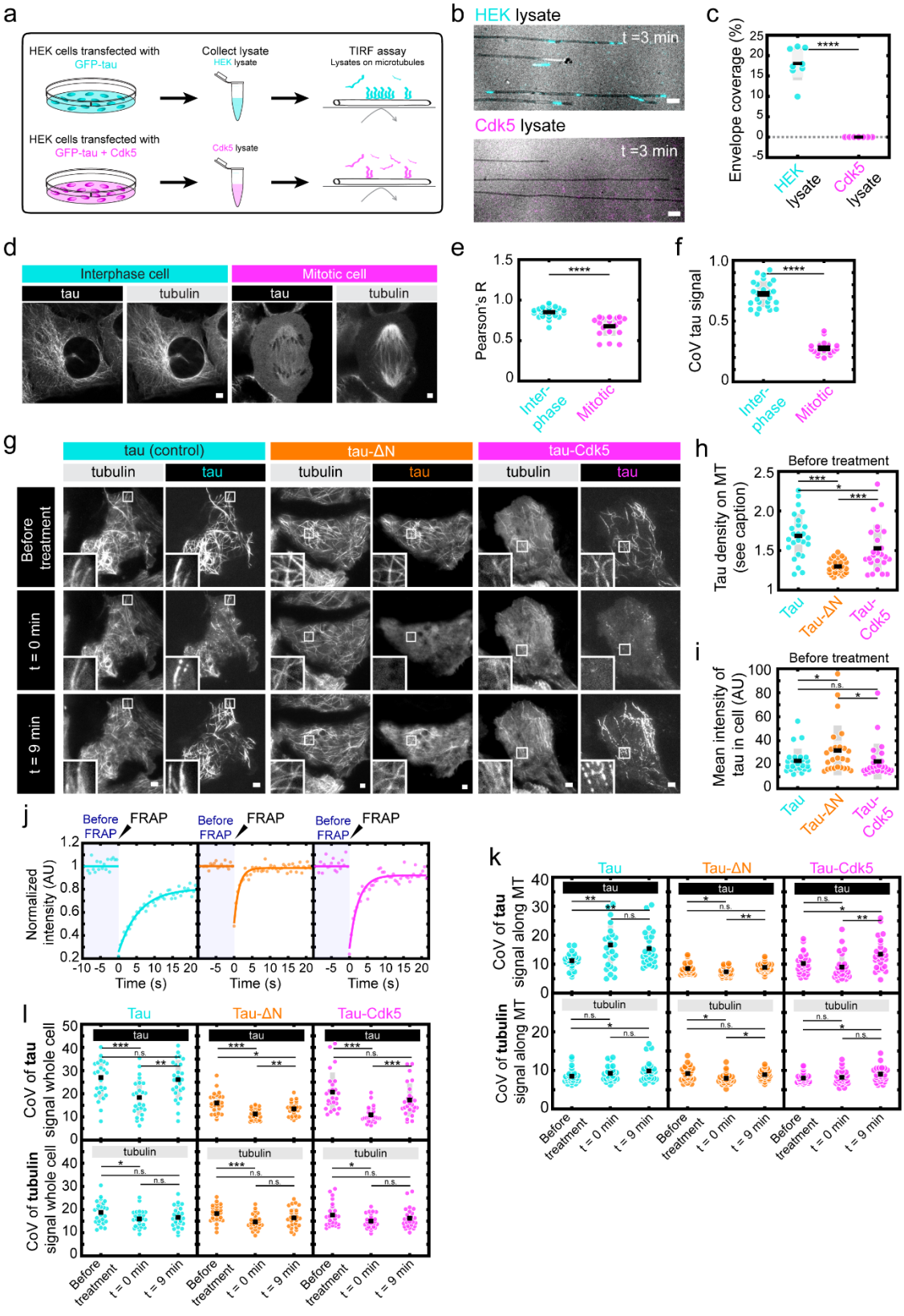

Supplementary Fig. 3: a. Schematics of preparation of lysates from HEK cells transfected with GFP-tau (HEK lysate, top, cyan) and of lysate prepared from HEK cells transfected with GFP-tau and Cdk5/p25 (Cdk5 lysate, bottom, magenta). **b**. Multichannel fluorescence micrographs of HEK lysate (top, cyan) and Cdk5 lysate (bottom, magenta) added to surface immobilized

taxol-stabilized microtubules (black) after 3 min of incubation. Scale bars: 2 µm. **c**. Percentage of taxol-stabilized microtubules covered by a tau envelope (envelope coverage) after addition of HEK lysate was 18.2 ± 3.4% (mean ± s.d., n = 8 fields of view in 8 independent experiments), and after addition of Cdk5 lysate was 0.0 ± 0.0% (mean ± s.d., n = 8 fields of view in 4 independent experiments). Two-sided t-test, $p=4.3821*10^{-10}$. **d**. Fluorescence micrographs of GFP-tau (left) and mScarlet-tubulin (right) in U-2 OS cells at different phases of the cell cycle. Cells in interphase (left panels, cyan) show higher binding of tau to microtubules compared to cells in mitosis (right panels, magenta). **e**. Pearson's R correlation coefficient between the GFP-tau and mScarlet-tubulin signal differs significantly between interphase and mitotic cells. Pearson's R in interphase cells was 0.85 ± 0.06 and in mitotic cells 0.68 ± 0.12 (mean ± s.d., interphase, n=25 cells in 3 independent experiments; mitosis, n=20 cells in 3 independent experiments). Two-sided t-test, $p=1.4224*10^{-7}$. **f**. Coefficient of variation (CoV) of the tau signal measured over the whole cell reflecting the difference between tau signal on microtubules and in cytoplasm. CoV of tau signal in interphase cells was 0.72 ± 0.11 and in mitotic cells 0.28 ± 0.06 (mean ± s.d., interphase n=25 cells in 3 independent experiments, mitosis n=19 cells in 3 independent experiments). Two-sided t-test, p=5.2528e-20. **g.** Fluorescence micrographs of cells before elevated-pH treatment (left), at t=0 min after elevated-pH treatment (middle) and t=9 min after elevated-pH treatment (right). 3 types of cells were subjected to elevated-pH treatment; control GFP-tau cells (tau, cyan), GFP-tau-ΔN cells (tau-ΔN, orange), and GFP-tau-Cdk5 cells (tau-Cdk5, magenta). Top panels represent the GFP-tau channel, bottom panels the mScarlet-tubulin channel. Scale bars: 10µm. **h.** Density of tau on microtubules before elevated-pH treatment, compared to density of tau in the cytoplasm, to give a measure of the binding affinity of tau in the different cells. Tau density on microtubules compared to cytoplasm in tau cells was 1.68 ± 0.28, in tau-ΔN cells was 1.30 ± 0.09, in tau-Cdk5 cells was 1.53 ± 0.30 (mean ± s.d., n=25 cells for each group in 4 independent experiments). Two-sided t-test p-values (left-to-right): $3.26*10^{-8}$, 0.0594, $5.89*10^{-4}$. **i.** Mean intensity of tau over the whole cell, as an indication of the expression level. Mean intensity over the wholle cell in tau cells was 23.2 ± 10.1, in tau-ΔN cells was 31.9 ± 20.8, and in tau-Cdk5 cells was 22.8 ± 14.7 (mean ± s.d., n=25 cells for each group in 4 independent experiments). Two-sided t-test p-values (left-to-right): 0.0658, 0.8901, 0.0774. **j**. Fluorescence recovery curves after FRAP for control GFP-tau cells (left, cyan); GFP-tau-ΔN cells (middle, orange); GFP-tau-Cdk5 cells (right, magenta). Normalized tau intensity within the FRAP area is plotted over time. The shaded blue area marks the period before FRAP, the black arrow indicates the timepoint at which FRAP occurred. **k.** Coefficient of variation of GFP-tau signal (top) or mScarlet-tubulin signal (bottom) measured along the microtubule lattice in GFP-tau (cyan), GFP-tau-ΔN (orange), and GFP-tau-Cdk5 cells (magenta). Coefficient of variation was measured at 3 timepoints: before elevated-pH treatment (left), at t=0 min after elevated-pH treatment (middle), and at t=9 min after elevated-pH treatment (right). **l.** Coefficient of variation of GFP-tau signal (top) or mScarlet-tubulin signal (bottom) measured over the whole cell in GFP-tau (cyan), GFP-tau-ΔN (orange), and GFP-tau-Cdk5 cells (magenta). Coefficient of variation was measured at three timepoints: before elevated-pH treatment (left), at t=0 min after elevated-pH treatment (middle), and t=9 min after elevated-pH treatment (right).

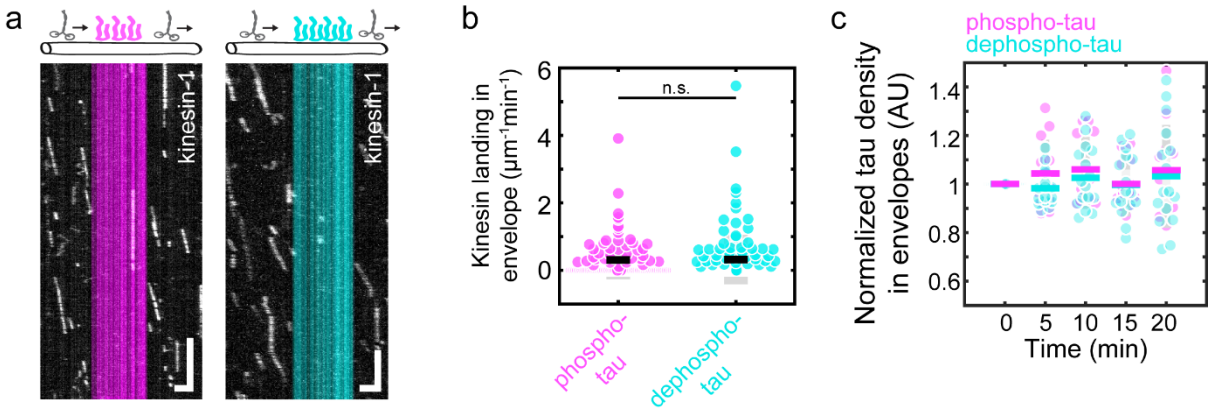

Supplementary Fig. 4: a. Fluorescence kymographs showing kinesin-1-GFP molecules (white) moving processively outside tau envelope region, independent of the phosphorylation degree of tau molecules forming the envelope (phospho-tau, left, magenta; dephospho-tau, right, cyan). Kinesin-1 landing but no processive movement was observed within the envelope boundaries. Scale bars: 2 µm, 1 s. **b**. Kinesin-1 landing rate within phospho-tau envelopes was 0.31 ± 0.58 $\mu m^{-1}min^{-1}$ and within dephospho-tau envelopes was 0.32 ± 0.73 $\mu m^{-1}min^{-1}$ (mean ± s.d., phospho-tau: n=100 envelopes in 5 experiments; dephospho-tau: n=125 envelopes in 5 experiments). Two-sided t-test, p=0.8894. **c**. Normalized tau density in envelopes after katanin addition for dephospho-tau was 0.98 ± 0.07, 1.02 ± 0.13, 1.00 ± 0.13, 1.03 ± 0.21 for 5, 10, 15, 20 minutes, respectively (mean ± s.d., n=16 envelopes in 2 individual experiments). Normalized tau density for phospho-tau was 1.04 ± 0.14, 1.06 ± 0.13, 1.00 ± 0.10, 1.06 ± 0.18 for 5, 10, 15, 20 minutes, respectively (mean ± s.d., n=13 envelopes in 4 individual experiments).

Prolyl isomerase FKBP12 reduces microtubule dynamics and axon growth by inhibiting CRMP2A

Romana Weissova[1,2], Jan Sabo[3], Djamel Eddine Chafai[1], Jakub Ziak[1], Peter Buran[1,2], Satish Bodakuntla[4], Carsten Janke[4], Marcus Braun[3], Zdenek Lansky[3], Martin Balastik[1,*]

1 Institute of Physiology of the Czech Academy of Sciences, Czech Republic
2 Faculty of Science, Charles University in Prague, Czech Republic
3 Institute of Biotechnology, Czech Academy of Sciences, BIOCEV, Czech Republic
4 Institut Curie, PSL Research University, France

*Corresponding author: martin.balastik@fgu.cas.cz

Abstract

Prolyl isomerases are enzymes catalyzing conformational changes of peptide bonds between proline and another amino acid in proteins and as such, they are important in many processes in cells. We have shown that a significant substrate of phospho-specific prolyl isomerase Pin1 is Collapsin response mediator protein 2A (CRMP2A), a microtubule-associated protein highly expressed in neurons, particularly in axon growth cones. The activity of CRMP2A is regulated by phosphorylation and in phosphorylated form, prolyl isomerase Pin1 can bind and stabilize the protein. It is not known if CRMP2A can be conformationally regulated in its unphosphorylated state. Here, we show that prolyl isomerase FKBP12 is able to bind to CRMP2A specifically in its unphosphorylated state and regulate its function. Using in vitro assays, we show that CRMP2A is promoting microtubule growth and that this effect is abolished by the presence of FKBP12. To test the effect of FKBP12 on CRMP2A-mediated microtubule polymerization also in cells, we introduced the GFP-EB3 assay to track growing microtubule ends in the IMCD3 cells and observed the same effect as in vitro. Moreover, as CRMP2A is important mainly in neurons and in growth cones, we tested the effect of FKBP12 on axonal growth. Overexpression of FKBP12 decreased the axon growth while knockdown had the opposite effect, which agrees with the results obtained in microtubule dynamics assays. In conclusion, our data demonstrate that FKBP12 binds to CRMP2A and regulates microtubule dynamics and neural development.

Keywords

Prolyl isomerases, FKBP12, CRMP2A, microtubule dynamics

Abbreviations

CRMP2A = Collapsin response mediator protein 2A; FKBP12 = FK506 binding protein-12; Pin1 = peptidyl-prolyl *cis/trans* isomerase, NIMA-interacting 1; PPI = Peptidyl-prolyl *cis/trans* isomerase; Cdk5 = Cyclin-dependent kinase 5; GST = Glutathione S-transferase

Introduction

Conformational changes provide a rapid mechanism to change protein properties (such as activity or stability) and represent, together with covalent posttranslational modifications, an essential level of protein regulation. While the majority of the peptide bonds are largely in *trans* conformation with regard to the position of their side chains, peptide bonds immediately preceding prolyl residues are prone to conformational changes between *trans* and *cis* conformation with a possible direct effect on the function of the protein. Conformational changes of those peptide bonds are facilitated by peptidyl-prolyl *cis/trans* isomerases (PPIs), ubiquitous proteins expressed in both eukaryotes and prokaryotes (Schmid, 2001). Prolyl isomerases are regulators of many cellular processes such as transcription or the cell cycle (Aghdasi et al., 2001; Hanes, 2015; Lin et al., 2015; Shaw, 2007) and the deregulation of many prolyl isomerases has been linked to several human diseases such as cancer, and cardiovascular or neurodegenerative disorders (Blair et al., 2015; Gerard et al., 2011; Perrucci et al., 2015; Theuerkorn et al., 2011).

There are 3 structurally diverse families of prolyl isomerases – cyclophilins, FK506-binding proteins (FKBPs), and parvulins (Schmid, 2001). Among them, Pin1 of the parvulin family is the only known phospho-specific prolyl isomerase specifically recognizing substrates after their phosphorylation at serine or threonine immediately preceding proline (Yaffe et al., 1997). We have shown that Pin1 plays a critical role in neural development by changing the conformation and stability of one isoform of Collapsin response mediator protein 2 - CRMP2 (Balastik et al., 2015). CRMP2 is a microtubule-associated protein that is highly expressed in neurons mainly during development. CRMP2 has been shown to bind microtubules, promote their polymerization, and mediate growth cone collapse upon Semaphorin 3A signaling (Fukata et al., 2002; Uchida et al., 2005). We have shown that CRMP2 is downstream of Semaphorin 3F signaling and that its deficiency results in synapse pruning defects and histological and behavioral changes associated with autism spectrum disorder (Ziak et al., 2020). As such, CRMP2 is an important regulator of neural development.

The activity of CRMP2 is regulated at multiple levels, e.g. phosphorylation by kinases such as Cdk5, GSK3β, and Rho kinase has been shown to control its affinity to tubulin (Nakamura et al., 2020). Moreover, CRMP2 exists in two isoforms produced by alternative splicing. CRMP2B is a shorter isoform, particularly abundant in the adult brain, and has been analyzed in most previous studies. CRMP2A is a longer isoform extended at the N-terminus by an alternative exon. Although CRMP2A is generally less expressed, it is abundant in axonal growth cones (Balastik et al., 2015; Bretin et al., 2005). The functional differences between those two isoforms are still elusive. We have shown that the CRMP2A isoform plays a unique role in distal axons, where its function is regulated by Cdk5 phosphorylation and subsequent isomerization by prolyl isomerase Pin1 (Balastik et al., 2015). While Pin1-mediated isomerization demonstrates regulation of phosphorylated CRMP2A, whether (and what) prolyl isomerase controls conformation of the unphosphorylated CRMP2A and what effect on microtubules and axons it has, is not known.

Here, we demonstrate that prolyl isomerase FKBP12 (FK506 binding protein-12; FKBP1A) specifically binds to and inhibits unphosphorylated CRMP2A. FKBP12 was first described for its role in immunoregulation as a major binder of immunosuppressant FK506 (Siekierka et al., 1989). Later, it was shown that FKBP12 is highly expressed in the brain (Steiner et al., 1992) and has been linked to neurodegeneration, synaptic plasticity, or neuronal regeneration (Caminati and Procacci, 2020; Gold et al., 1997; Hoeffer et al., 2008; Lyons et al., 1995). We show that FKBP12 interacts with CRMP2A and that phosphorylation of CRMP2A abolishes the binding. Moreover, we demonstrate that FKBP12 regulates CRMP2A activity. While CRMP2A promotes microtubule polymerization *in vitro* and *in vivo*,

FKBP12 significantly inhibits this effect. In contrast, the de-phosphomimetic mutant of CRMP2A (that binds to FKBP12 more efficiently) does not promote microtubule polymerization, unless FKBP12 is silenced in the cell. Furthermore, we demonstrate that FKBP12 regulates axon growth in cultured neurons.

Together, our data shows that FKBP12 is a novel regulator of microtubule dynamics and neural development. Moreover, since Pin1 has been shown to positively regulate axon growth *in vitro* and *in vivo*, we now demonstrate how growing neurons utilize various prolyl isomerases to differentially control microtubule dynamics and axon growth. Our data thus show for the first time that prolyl isomerases not merely control protein conformation in distal axons but specifically regulate axon growth.

Results

Prolyl isomerase FKBP12 binds to CRMP2A

Phosphorylated CRMP2 (isoform A) is specifically bound and regulated by prolyl isomerase Pin1 (Balastik et al., 2015). In order to understand the conformational regulation of unphosphorylated CRMP2, we first tested whether prolyl isomerase FKBP12, which shares multiple substrates with Pin1 (Blair et al., 2015), binds to CRMP2A. Using anti-CRMP2A antibodies, we were able to co-immunoprecipitate FKBP12 together with CRMP2A from WT (wild-type), but not CRMP2-KO (CRMP2 knock-out) mouse brain lysates (Figure 1A).

To further support the interaction and analyze it in more detail, we performed pull-down assays using purified GST-tagged FKBP12, and lysates of HEK293T cells expressing CRMP2 protein or its modified forms tagged with FLAG-tag (Figure 1B, C). First, to verify the specificity of the binding, we performed a pull-down in the presence or absence of FKBP12 inhibitor – FK506 (tacrolimus). The inhibitor decreased the binding distinctly, suggesting that the interaction between FKBP12 and CRMP2A is specific and competing with the inhibitor for a hydrophobic binding site pocket (Figure 1B).

Next, since CRMP2 exists in two isoforms (CRMP2A and CRMP2B; Figure 1E), and we have previously shown, that only the CRMP2A isoform is isomerized by Pin1 (Balastik et al., 2015), we tested if the binding of FKBP12 is also isoform-specific. Using pull-down assays with lysates of CRMP2A- or CRMP2B- expressing HEK293T cells, we show that FKBP12 was preferably pulling down CRMP2A but not CRMP2B isoform ($p = 0.01$, Figures 1C-D).

CRMP2 activity is regulated by phosphorylation of several phosphorylation sites on its C-terminus, of which phosphorylation of S522 (S623 for CRMP2A isoform) is considered a priming site for further phosphorylation of the C terminus (Yoshimura et al., 2005). To test whether the C-terminus of CRMP2 regulates FKBP12 binding, we performed a pull-down assay with CRMP2A and CRMP2B lacking their C-terminal domains (Figure 1E). Deletion of the C-terminus increased, non-significantly, CRMP2A binding to FKBP12 ($p = 0.16$, Figures 1C-D), while it did not affect the binding of CRMP2B. Together our data indicate that FKBP12 binds to the unique N-terminus of CRMP2A (which is not present in CRMP2B) and that the C-terminal domain negatively regulates the interaction.

Both CRMP2 and FKBP12 are abundant in neurons (Kamata et al., 1998; Steiner et al., 1992). We have shown before, that CRMP2A is localized particularly in axons and growth cones (Balastik et al., 2015). To analyze whether FKBP12 and CRMP2A co-localize in neurons, we performed CRMP2A and FKBP12 double-immunostaining in primary neuron cultures. We detected a partial co-localization of FKBP12

and CRMP2A in distal axons and growth cones (Figure 1F) suggesting: 1. that the two proteins, indeed, can interact in neurons, but 2. that their interaction is likely controlled by other specific mechanisms.

CRMP2A phosphorylation inhibits FKBP12 binding

We have previously shown that the binding of Pin1 to CRMP2A is dependent on the phosphorylation of CRMP2A by Cdk5 (Balastik et al., 2015). To test whether FKBP12 also preferentially binds phosphorylated CRMP2A, we co-transfected HEK293T cells with CRMP2A together with Cdk5 kinase and its activator p25 and performed Pin1 or FKBP12 pull-down assays. While Cdk5 upregulation increased the binding of CRMP2A to Pin1, as shown previously ((Balastik et al., 2015); Figure 2A-B), it, surprisingly, virtually inhibited its binding to FKBP12 (Figure 2A-B; $p < 0.0001$).

There are two known Cdk5 phosphorylation sites in the CRMP2A molecule, Ser27 (S27), and Ser623 (S623), out of which S27 is present only in the CRMP2A isoform (Figure 2C). To analyze which of the phosphorylation sites is critical for abolishing the binding to FKBP12, we performed pull-down assays using various dephospho-mimetic (Ala) mutations of the two Cdk5 sites of CRMP2A (confirmation of the mutated sites in Supplementary figure A). As demonstrated before (Balastik et al., 2015), dephospho-mimetic CRMP2A mutations S27A, as well as S623A, reduced Pin1 binding in a control experiment (Figure 2D-E). In contrast, the S27A mutation was sufficient to rescue the binding to FKBP12 in the presence of Cdk5 (Figure 2D-E; $p = 0.02$). S623A mutation showed the same trend (but not significant; $p = 0.1271$). The combination of both mutations (S27A and S623A) increased the binding compared to CRMP2A ($p = 0.02$) but not beyond the S27A levels (Figure 2D-E; $p = 0.97$) indicating that the N-terminus of CRMP2A, and its dephosphorylation, is critical for the interaction with FKBP12. The results are in accord with the data we obtained by pull-down assays using C-terminally truncated CRMP2A (Figure 1C-E) showing that removing the C-terminus of CRMP2A did not reduce FKBP12 binding.

In order to test whether CRMP2A phosphorylation controls its interaction with FKBP12 also in neurons, we analyzed the co-localization of CRMP2A (or of its dephospho-mimetic mutant) with FKBP12 or Pin1 within the growth cones (Figure 1F). We first transfected CRMP2A-deficient cortical neurons with vectors expressing mCherry-CRMP2A or its dephospho-mimetic mutant form (mCherry-CRMP2A S27A, S623A). Next, we correlated mCherry levels with endogenous (immuno-stained) FKBP12 or Pin1 (Figure 2F). The data showed that non-mutated CRMP2A co-localizes with both Pin1 and FKBP12 and that the correlation coefficients between CRMP2A - FKBP12 and CRMP2A - Pin1 in the growth cones are not significantly different (correlation coefficient $r_{CRMP2A\text{-}FKBP12} = 0.2998$; $r_{CRMP2A\text{-}Pin1} = 0.2998$; $p_{(between\ the\ correlations)} = 1$). Importantly, di-dephospho-mimetic mutation (mCherry-CRMP2A S27A, S623A) significantly increased co-localization of CRMP2A with FKBP12 ($r = 0.3959$; $p_{(between\ the\ correlations)} = 0.049$), but significantly decreased co-localization with Pin1 ($r = 0.1763$; $p_{(between\ the\ correlations)} = 0.019$). The co-localization of CRMP2A S27A, S623A with FKBP12 and Pin1 is thus significantly different ($p_{(between\ the\ correlations)} = 0.0001$). These data are in agreement with the results obtained by pull-down assays (Figure 2A-E) together demonstrating that dephosphorylation of CRMP2A (on its Cdk5 phosphorylation sites) prevents its interaction with Pin1 while promotes its binding to FKBP12 - both *in vitro* and in the neuronal growth cones.

FKBP12 inhibits microtubule polymerization by isomerizing CRMP2A

Considering CRMP2A is a microtubule-associated protein regulating microtubule dynamics (Fukata et al., 2002), we next tested whether FKBP12 also regulates microtubule dynamics through its interaction with CRMP2A. First, we performed an *in vitro* tubulin turbidity assay. As expected, the application of CRMP2A promoted tubulin polymerization over the control tubulin sample (Figure 3A-B). Importantly,

the addition of FKBP12 abolished the effect of CRMP2A on tubulin polymerization (Figure 3A-B) indicating that FKBP12 negatively regulates CRMP2A. Next, we tested whether the isomerase activity of FKBP12 is critical for the inhibition of CRMP2A. Indeed, the addition of an inhibitor of FKBP12 isomerase activity (FK506) rescued the effect of CRMP2A on tubulin polymerization indicating that CRMP2A is inhibited by conformational change catalyzed by FKBP12 (Figure 3A-B). Together, the results show that CRMP2A increases the growth of microtubules *in vitro* and FKBP12 inhibits this effect.

The application of FKBP12 resulted in differences in both the slope of the curves in the exponential phase of tubulin polymerization as well as their plateau phase (Figure 3A). This suggests that FKBP12 could affect tubulin polymerization rate, microtubule rescue frequencies, or both. To distinguish the two possible mechanisms, we performed *in vitro* tubulin polymerization assays using TIRF microscopy (Figure 3C). In accordance with the results of the turbidity assay, GFP-CRMP2A bound to growing microtubules and increased microtubule polymerization rate, decreased depolymerization rate, and increased the frequency of both catastrophes and rescues ($p < 0.0001$, $p = 0.0001$, $p < 0.0001$, $p = 0.0199$ respectively; Figure 3D-E). Adding FKBP12 significantly reduced the microtubule polymerization rate ($p < 0.0001$; Figure 3D-E). Microtubule rescue frequency also showed a decreasing trend, although not significant ($p = 0.058$; Figure 3D-E). Thus, FKBP12 negatively regulates microtubule dynamics by reducing particularly the tubulin polymerization rate. Interestingly, while GFP-CRMP2A forms large comets at the microtubule plus ends in control conditions (Figure 3D), in the presence of FKBP12, CRMP2A appears to bind only to the very tip of growing microtubules (Figure 3D). This may indicate that FKBP12 reduces the affinity of CRMP2A to tubulin. To explore this observation, we measured the average length of GFP-positive growing ends and the persistence of GFP signal on the microtubule. Both of these parameters show a decrease in the presence of FKBP12 ($p<0.0001$ and $p=0.0005$ respectively; Figure 3F-G). Together, these results show that FKBP12 inhibits CRMP2A function by lowering the binding of CRMP2A to microtubules.

FKBP12 negatively regulates microtubule growth in cells

To test whether FKBP12 negatively regulates microtubule dynamics not only *in vitro* but also in cells, we visualized microtubule dynamics in IMCD3 cells using GFP-tagged microtubule plus end-tracking protein EB3 (Figure 4A). GFP-EB3 was expressed in the IMCD3 cells together with CRMP2A and FKBP12, or FKBP12 was silenced by shRNA (Supplementary figure E-F). We then analyzed the average velocity of growing microtubules. In agreement with the *in vitro* data (Figure 3), the expression of CRMP2A significantly increased the velocity of microtubule growing ends ($p < 0.0001$; Figure 4B-C). Co-expression of FKBP12 reverted the CRMP2A-increased velocity significantly ($p < 0.0001$) almost to the control level ($p = 0.016$; Figure 4B-C), while FKBP12 knockdown had no significant effect ($p = 0.430$). These results are again in agreement with the results of the *in vitro* microtubule polymerization assays (Figure 3). Importantly, unlike CRMP2A, expression of dephospho-mimetic mutant CRMP2A-S27A (which binds stronger to FKBP12 even upon Cdk5 activation) (Figure 2D), did not increase microtubule growth velocity ($p = 0.2$), possibly due to increased binding and inhibition by FKBP12 (Figure 4B-C). Indeed, simultaneous knockdown of FKBP12 significantly increased microtubule growth rate upon CRMP2A-S27A expression ($p < 0.0001$) – i.e. to a similar level as CRMP2A ($p = 0.822$). Co-expression of CRMP2A-S27A with FKBP12 had no significant effect on microtubule growth ($p = 0.994$) (Figure 4B-C) indicating that the endogenous level of FKBP12 was high enough to inhibit CRMP2A-S27A. Together, the data demonstrate that FKBP12 expression inhibits the CRMP2A-mediated microtubule polymerization also in cells.

The level of FKBP12 in neurons modulates axon growth

CRMP2 and its isoform CRMP2A have been shown to promote axon growth and regulate axon guidance in the developing neurons (Balastik et al., 2015; Fukata et al., 2002; Ziak et al., 2020). Similarly, inhibition of microtubule growth has been demonstrated to negatively affect axon growth (Tanaka et al., 1995). Our data demonstrate that FKBP12 reduces microtubule polymerization by inhibiting CRMP2A activity. Thus, we tested whether changes of FKBP12 could affect the growth of cultured neurons. In order to specifically analyze axonal growth, we cultured primary cortical neurons in microfluidic chambers (Figure 5A) and quantified the average axonal growth rate. Knockdown of FKBP12 (shFKBP12) significantly increased axonal growth ($p = 0.04$; Figure 5B-D). In contrast, expression of FKBP12 significantly decreased the axon growth rate ($p = 0.007$; Figure 5B-D). These results are in agreement with the effect of FKBP12 on microtubules, which we measured in the IMCD3 cells as well as in vitro using microtubule polymerization assays, and support the view of FKBP12 as a negative regulator of axon microtubule polymerization and axon growth.

Discussion

During brain development, microtubule-associated protein CRMP2 either promotes microtubule polymerization and axon growth or mediates Semaphorin 3A-induced growth cone collapse and axon retraction (Uchida et al., 2005). The dual function of CRMP2 is tightly controlled by several mechanisms. Previously, phosphorylation has been shown to regulate CRMP2 through a competing activity of protein kinases and phosphatases. While upregulation of various kinases (e.g. Cdk5 or GSK3β) has been shown to increase phosphorylation of CRMP2, inhibit its activity and axon growth (Crews et al., 2011; Uchida et al., 2005; Yoshimura et al., 2005) upregulation of phosphatases (e.g. PP2A) has been shown to promote axon growth by dephosphorylating CRMP2 (Zhu et al., 2010). In addition, conformational changes are considered to control CRMP2 activity, but little evidence has been provided so far. We have previously demonstrated that conformational changes of (specifically) Cdk5-phosphorylated CRMP2A isoform catalyzed by prolyl isomerase Pin1 counteracts the inhibitory effect of CRMP2A phosphorylation (Balastik et al., 2015). This allows Pin1-containing axons to withstand low concentrations of repulsive guidance cue Semaphorin 3A in the environment (which activates Cdk5) and enables these axons to grow further into the Semaphorin 3A gradients than Pin1-deficient axons. Whether the unphosphorylated CRMP2 is conformationally regulated has not been shown by now. Here, we provide evidence that unphosphorylated CRMP2 - specifically the CRMP2A isoform - is conformationally regulated by another prolyl isomerase - FKBP12. In contrast to Pin1, which stabilizes CRMP2A and promotes axonal growth, FKBP12 inhibits the activity of CRMP2A, which results in lower microtubule polymerization activity *in vitro* and *in vivo* and reduces axon growth. Our data demonstrate that conformational changes catalyzed by various prolyl isomerases not only keep native/active conformation of their substrates but rather represent a novel regulatory system that controls proteins and can either increase or decrease their activity. As such, conformational changes catalyzed by prolyl isomerases may represent a new level of regulation of protein activity above protein phosphorylation.

CRMP2A as a specific target for conformational regulation by prolyl isomerases

CRMP2 exists in two isoforms produced by alternative splicing but the shorter, more abundant CRMP2B isoform is far more analyzed. CRMP2B has been previously shown to promote microtubule growth (Fukata et al., 2002). We now demonstrate that, similar to CRMP2B, CRMP2A has also a

promoting effect on microtubule growth *in vitro* and *in vivo*. CRMP2A has an N-terminal domain which is not present in CRMP2B and it contains a unique Cdk5-phosphorylation site (S27) (Balastik et al., 2015). Phosphorylation of this site and another C-terminal Cdk5 phosphorylation site (S623 on CRMP2A, corresponding to S522 on CRMP2B) is required for binding to prolyl isomerase Pin1 (Balastik et al., 2015). Here we show that particularly S27 is important for binding to prolyl isomerase FKBP12 and that its phosphorylation serves as a switch from isomerization by FKBP12 to Pin1. The critical role of the N-terminal S27 for the conformational regulation of CRMP2 also explains why only the longer CRMP2A isoform is regulated by this mechanism - S27 is not present in CRMP2B.

Previously, phosphorylation of CRMP2 has been shown to inhibit its function (Uchida et al., 2005). Interestingly, our data indicate that even dephosphorylated CRMP2 - specifically isoform A - may be readily inactivated by FKBP12 isomerization. Indeed, dephospho-mimetic CRMP2A mutant (CRMP2A-S27A) was not able to promote the microtubule growth in cells (Figure 4B, C) - likely due to its higher affinity to FKBP12 (Figure 2D, E) and subsequent rapid conformational inhibition. Supporting this, upon FKBP12 knockdown, CRMP2A-S27A was able to promote microtubule growth (Figure 4B, C), and overexpression of FKBP12 inhibited microtubule growth promotion induced even by WT CRMP2A (Figure 4B, C).

CRMP2A isoform is less abundant in the adult brain, but its relative amount is higher in active growth cones during development (Balastik et al., 2015) when precise regulation of microtubule growth and guidance is critical. Thus, a combination of various levels of phosphorylation, alternative splicing, and isomerization of CRMP2A could help to diversify responses of different growing axons to extracellular stimuli, which is necessary for the formation of specific connectivity pattern.

FKBP12 as a microtubule regulator in development and disease

FKBP protein family contains in humans at least 15 members (Tong and Jiang, 2016) targeting several cytoskeleton-related substrates such as microtubule-associated protein tau isomerized by FKBP12, FKBP51, FKBP52 (Chambraud et al., 2010; Ikura and Ito, 2013; Jiang et al., 2023; Jinwal et al., 2010). Importantly, two FKBP family members – FKBP52 and FKBP25 – have been previously shown to regulate microtubule polymerization directly by binding to tubulin (Dilworth et al., 2018; Chambraud et al., 2007). FKBP12 was considered not to regulate microtubule polymerization since (as one of the smallest FKBP family members) it has no tubulin binding domain and no direct effect on tubulin polymerization (Chambraud et al., 2007). In contrast, we demonstrate here, that FKBP12 also controls microtubule polymerization, but its effect is indirect by isomerization of CRMP2A protein.

FKBP12 has been studied mainly in connection to immunoregulation and cardiac research, but its role in neurons and brain function has been also analyzed. It was shown that expression of FKBP12 is enhanced during neural regeneration (Lyons et al., 1995; Mason et al., 2003) and at the same time, it was shown, that FKBP12 inhibitor (FK506) as well as another inhibitor without immunosupressing function accelerates nerve regeneration (Gold et al., 1995; Gold et al., 1997; Khan et al., 2002). Moreover, FK506 has been shown to promote neurite outgrowth (Lyons et al., 1994), which is all in agreement with our in vitro and in vivo data. The mechanism by which FK506 inhibitor supports neurite growth and nerve regeneration has not been well understood, but our data indicate that activation of CRMP2A could play an important role. Indeed, CRMP2 was shown to promote growth of axons, its mRNA level increases upon hypoglossal nerve injury and it promotes its regeneration (Suzuki et al., 2003). Similarly, moderate stabilization of microtubules with microtubule-stabilizing drugs has been demonstrated to enhance axon regeneration and growth (Hellal et al., 2011; Ruschel et al., 2015; Sengottuvel et al., 2011).

In mouse models, brain-specific knockout of FKBP12 has been shown to result in enhanced late-phase long-term potentiation (L-LTP) and perseveration in several memory assays (Hoeffer et al., 2008). In contrast, brain-specific CRMP2 deletion leads to reduced LTP and impaired learning and memory (Zhang et al., 2016; Ziak et al., 2020), which is again in accord with the inhibitory role of FKBP12 on CRMP2. Deregulation of both FKBP12 as well as CRMP2 was also linked to behavioral changes associated with neurodevelopmental disorders, including autism spectrum disorder (ASD), obsessive-compulsive disorder (OCD), and schizophrenia (Hoeffer et al., 2008; Zhang et al., 2016; Ziak et al., 2020).

Prolyl isomerases are becoming the center of attention not only because of their roles in physiological conditions as signaling regulators, but they were also connected to many diseases mainly so-called conformational diseases such as Alzheimer's disease. Moreover, it was shown that both CRMP2 and FKBP12 accumulate in neurofibrillary tangles (Sugata et al., 2009; Yoshida et al., 1998). Another microtubule-associated protein and marker of neurofibrillary tangles - tau - is bound by prolyl isomerases FKBP12 and Pin1 and it was shown that both are regulators of tau aggregation into neurofibrillary tangles (Ikura and Ito, 2013; Kimura et al., 2013).

Taking together the data obtained in this study and the data obtained before (Balastik et al., 2015), we propose the regulatory mechanism of CRMP2A isoform by two different prolyl isomerases (Figure 6). Interestingly, the binding of both prolyl isomerases is regulated by the same two Cdk5-dependent phosphorylation sites. Even though in the case of Pin1, the two phosphorylation sites seem to contribute equally, while for FKBP12 the N-terminal phosphorylation site (S27) could play a more significant role. One possible explanation of this phenomenon could be the presence of two domains capable of substrate binding in the Pin1 molecule (WW and PPI domain) and only one domain in FKBP12 (PPI domain only). Nevertheless, phosphorylated CRMP2A interacts with prolyl isomerase Pin1 which protects it from degradation and possibly allows its dephosphorylation as it was shown for other Pin1 substrates e.g. tau (Zhou et al., 2000). By this mechanism, Pin1 can return CRMP2A to its functional unphosphorylated state. The function of unphosphorylated CRMP2A can be regulated by another prolyl isomerase FKBP12 which inhibits CRMP2A function in promoting microtubule growth (Figure 6).

In conclusion, we now show for the first time the binding of two different prolyl isomerases on one substrate and affecting it in the opposite direction suggesting fine tuning of the regulation of this protein's function. We show that one protein can be conformationally regulated in its phosphorylated and also in its unphosphorylated state and that those two prolyl isomerases can have buffering functions keeping the level of functional protein spatially and temporally needed.

Methods

Plasmids

Plasmids for expression of mouse CRMP2A and CRMP2B with N-terminal FLAG-tag in pCDNA3, as well as mutated forms of CRMP2A (S27A, S623A, and S27A+S623A), were published before (Balastik et al., 2015). Sequences of truncated forms of CRMP2A (1-604) and CRMP2B (1-503) were prepared using PCR from full-length CRMP2A or CRMP2B and cloned into pCDNA3 with N-terminal FLAG-tag. For the purification of GST-tagged proteins from bacteria, pGEX-KG-GST and pGEX-KG-GST-Pin1 were used (Balastik et al., 2015). FKBP12 sequence was prepared by PCR from mouse brain cDNA library and inserted into pGEX-KG-GST to produce fused protein GST-FKBP12.

To get phosphorylated CRMP2A, we co-transfected FLAG-tagged CRMP2A plasmid together with pCDNA3-Cdk5 and pCDNA3-p25 (Balastik et al., 2015; Patrick et al., 1999) in the ratio 1: 0.6: 0.13. Fusion mCherry-CRMP2A used for visualization of CRMP2A in cells was prepared by insertion of mCherry in front of CRMP2A sequence in pCDNA3.1 vector. Mutated mCherry-CRMP2A (S27A) was prepared by site-directed mutagenesis as described previously (Balastik et al., 2015).

For purification of CRMP2A for *in vitro* experiments, we inserted a sequence of FLAG-tag in front of the sequence for GFP-CRMP2A fusion protein, which was prepared by insertion of GFP in front of CRMP2A sequence in pCDNA3.1 vector.

Microtubule +tip tracking was done using a lentiviral pTRIP vector containing GFP-EB3 and CRMP2A under the CAG promoter and separated by P2A site and shRNA (either control shRNA for luciferase or shRNA for FKBP12) under the H1 promoter. For FKBP12 overexpression, the CRMP2A sequence in pTRIP was exchanged by the FKBP12 sequence using the SLIC cloning method (Jeong et al., 2012). For overexpression of FKBP12 in microfluidic chambers, we used a pTRIP vector derived from the one with GFP-EB3 and FKBP12 by removing the EB3 sequence.

FKBP12 knockdown was made by lentiviral transduction using vector pGhU6 (Radomska et al., 2012) or pGhU6 with marker GFP fluorescent protein exchanged for mCherry. The target sequence for shRNA design was selected using the TRC library database (TRCN0000012492 – TGATTCCTCTCGGGACAGAAA; nonspecific control (NSC) - ATCTCGCTTGGGCGAGAGTAAG).

All insertions were confirmed by DNA sequencing. Plasmids were amplified using RbCl competent E. Coli TOP10.

Animals

All experimental procedures were performed in compliance with European directive 2010/63/EU and were approved by the Czech Central Commission for Animal Welfare. Mice (C57BL6/N background) were housed and handled according to the institutional committee guidelines with free access to food and water. For immunoprecipitation, WT or CRMP2-KO murine brains were used (Ziak et al., 2020). For primary neurons culture, WT or CRMP2A-KO mice were used (Ziak et al., in preparation).

Antibodies

We used Anti-FLAG (Millipore, F7425; 1:5000), Anti-FKBP12 (Abcam, ab2918; 1:10000), Anti-CRMP2 (FUJIFILM Wako chemicals, 9F; 1:5000), Anti-CRMP2A ((Balastik et al., 2015); 1:10000), Anti-CRMP2A pS27 (antibody produced in rabbit using the peptide CNLGSG(Sp)PKPRQK and affinity purified using the same peptide, antibodies against unphosphorylated peptide were removed by affinity purification with the unphosphorylated peptide; 1:20000), and Anti-GAPDH (Merck, G9545; 1:20000) for western blot analysis. For immunocytochemistry, we used Anti-CRMP2A ((Balastik et al., 2015), affinity purified; 1:50), Anti-FKBP12 (Abcam, ab2918, ab58072; 1:600), Anti-Pin1 (R&D systems, MAB2294; 1:250), and fluorescently labeled secondary antibodies anti-Rabbit A488, anti-Mouse A647, anti-Rabbit A594, and anti-Mouse A488 (A-11029, A21236, A-11037, A-11029, ThermoFisher Scientific; 1:500). Immunoprecipitation was done using affinity purified Anti-CRMP2A (Balastik et al., 2015).

Immunoprecipitation

Immunoprecipitation was performed as described (Balastik et al., 2015). Briefly, one half of the murine brain (WT or CRMP2-KO, 1-3 months old) was homogenized in lysis buffer (50 mM HEPES pH 7.4, 150 mM NaCl, 10% glycerol, 1% Triton X-100, 1.5 mM $MgCl_2$, 1 mM EGTA, 100 mM NaF, 1 mM Na_3VO_4, 1 mM DTT, cOmplete™ EDTA-free Protease Inhibitor Cocktail (Merck)) using ultraturrax. The lysate was

sonicated (30 s, 30%), centrifuged (20 minutes, 20000 x g, 4°C), and incubated with Protein A Sepharose CL-4B (Merck) for 1 hour, 4°C (pre-clearing). The sepharose beads were spun down and the lysate was incubated with 25 µl of Protein A Sepharose CL-4B (preincubated ON with antibodies (Anti-CRMP2A antibody affinity purified (Balastik et al., 2015)). After washing (4x), the beads were boiled in 2x Sample Buffer and the supernatant was loaded into 15% and 7.5% gel for western blot analysis. Proteins were visualized using antibodies anti-FKBP12 and anti-CRMP2.

Bacterial protein production and purification

Protein production using the pGEX-KG vector and E. Coli BL21 was done as described previously (Harper and Speicher, 2011). Glutathione-agarose beads (Millipore, G4510) were used for protein purification as described previously (Balastik et al., 2015). Briefly, bacterial pellet was resuspended in lysis buffer (50 mM TrisCl pH 8.0, 500 mM NaCl, 1 mM EDTA, 1 mM EGTA, 5% glycerol, 1 mM DTT, 1% Triton X-100, cOmplete™ EDTA-free Protease Inhibitor Cocktail (Merck)) and incubated with lysozyme (final concentration 0.2 mg/ml; Merck, L6876). The lysate was sonicated (5 x 1 minute) and centrifuged (28000 x g, 60 minutes). The supernatant was incubated with glutathione-agarose beads for 3 hours, washed, and eluted using 30 mM glutathione (Merck, G4251). Eluted protein was dialyzed (dialysis buffer: 25 mM Tris pH 7.4, 150 mM NaCl, 5% glycerol, 1 mM DTT, 50 µg/ml PMSF; SnakeSkin dialysis tubing, 10K MWCO, ThermoFisher Scientific), aliquoted and flash-frozen. Purified protein was analyzed by acrylamide gel electrophoresis (Supplementary figure C), and the concentration of the protein was determined using Bradford assay and/or measured by NanoDrop One (ThermoFisher Scientific).

Peptidyl-prolyl *cis-trans* isomerase assay

PPI activity was assayed in a chymotrypsin-coupled assay as described previously (Fischer et al., 1984). The activity was measured as the change in absorption at 390 nm (every 3 s for 5 minutes) due to digestion of the *trans* isoform of the peptide Suc-AAPF-pNA (Santa Cruz; 3 mM, dissolved in 20 mg/ml LiCl in trifluoroethanol) by chymotrypsin (Merck; 60 mg/ml in 1 mM HCl) in 96well plates with glass bottom (Invitrogen, M33089) in final volume 200 µl (buffer: 50 mM HEPES, 100 mM NaCl, pH8) using BioTek Cytation3.

Transfection and lentiviral particles production

HEK293T cells were transfected using linear polyethylenimine (PEI; Polysciences, Inc.; 23966) and cells were collected 48 hours after transfection unless stated otherwise.

Lentiviral particles were produced by co-transfection of HEK293T cells with lentiviral vectors carrying the sequence coding protein of interest or shRNA (pTRIP or pGhU6 respectively) together with Gag/Pol and VSV-G vector (1: 0.9: 0.1, (Balastik et al., 2015)). Medium containing lentiviral particles was collected 48 hours after transfection, filtered (0.45 µm pores), and used for transduction or stored at -80°C.

Pull-down

Pull-down was performed as described previously (Balastik et al., 2015). Briefly, HEK293T cells were transfected with a pCDNA3 vector expressing proteins of interest with FLAG-tag. Two days after the transfection, cells were harvested and homogenized in lysis buffer (50 mM HEPES pH 7.4, 150 mM NaCl, 10% glycerol, 0.5% Triton X-100, 1.5 mM $MgCl_2$, 1 mM EGTA, 1 mM NaF, 1 mM Na_3VO_4, 1 mM DTT, cOmplete™ EDTA-free Protease Inhibitor Cocktail (Merck)).

Dialyzed protein fused to GST (1 µM) was incubated with the glutathione-agarose for 3 hours, washed 2x, and then incubated with 200 µl of the lysate for 4 h, 4°C, rotating. Beads were washed 5x, boiled in the 2x Sample buffer and the supernatant was subjected to western blot analysis. The bands were visualized using anti-FLAG antibodies.

In the case of inhibitor treatment, FK506 was preincubated with the protein bound on the beads for 1 hour (20 µM; InvivoGen, tlrl-fk5) before incubation with the lysate.

Purification of proteins produced in HEK293T cells

FLAG-tagged proteins were purified from transfected HEK293T cells. Harvested cells were resuspended in lysis buffer and sonicated (Lysis buffer: BRB40 + 0.1% Tween, 5% glycerol, 1 mM DTT, 10 µg/ml Cytochalasin D, Benzonase (5U; Merck, 70664), cOmplete™ EDTA-free Protease Inhibitor Cocktail (Merck) + 10 mM ATP). After centrifugation, the supernatant was incubated with anti-FLAG agarose beads ON, 4°C, rotating (Anti-DYKDDDDK Tag (L5) Affinity Gel Antibody; BioLegend). After washing, the protein was eluted using 3x DYKDDDDK Peptide (ThermoFisher Scientific, A36805), dialyzed against BRB80, 1 mM DTT, and flash-frozen. Purified protein was subjected to SDS-PAGE electrophoresis and stained using coomassie brilliant blue staining (Supplementary figure B).

***In vitro* tubulin polymerization assay**

Porcine brain tubulin was prepared as previously described (Castoldi and Popov, 2003; Gell et al., 2011). GMPCPP, GTP, and ATP were obtained from Jena Bioscience. Anti-Biotin Antibody, PIPES, pluronic F127, D-glucose, DTT, casein, glucose oxidase, and catalase were purchased from Merck.

Microtubule GMPCPP seeds - 5 µl of biotin-labeled tubulin at 4 mg/ml (Cytoskeleton, Inc., unlabeled to biotin-labeled tubulin ratio - 150:1) was diluted in the 95 µl of the GMPCPP polymerization mixture (84 µl BRB80 (80 mM PIPES, 1 mM EGTA, 1 mM $MgCl_2$, pH 6.8) with 10 µl of 10 mM GMPCPP and additional 1 µl of 100 mM $MgCl_2$) and then pre-incubated for 5 min on ice as described previously (Gell et al., 2010). Microtubules were polymerized at 37°C for 1 h, centrifuged at 18000 x g with a tabletop centrifuge for 30 min at room temperature, and the pellet was subsequently resuspended in 150 µl BRB80. Microtubule seeds were stored at room temperature and used within one week.

In vitro assay - Flow chambers were assembled from 2 sizes of DDS-silanized coverslips (22x22 and 18x18 mm) and multiple parallel strips of parafilm between the coverslips to form separated chambers after a heat cycle on an electric heater. Flow chambers were then incubated for 5 min with 20 µg/ml anti-biotin antibody and subsequently blocked by 1% Pluronic F127 in PBS for 1 hour. Residual F127 was removed from the chambers by BRB80, and microtubules were attached to the surface by incubation of GMPCPP microtubule seeds in the chambers for 2 minutes. Unbound microtubules were removed by BRB80 that was subsequently exchanged by experimental buffer (BRB80 containing 10 mM DTT, 20 mM D-glucose, 0.1% Tween-20, 0.5 mg/ml casein, 1 mM Mg-ATP, 1 mM GTP, 0.22 mg/ml glucose oxidase and 20 µg/ml catalase). Microtubule growth was initiated by the addition of a mixture of proteins (10 µM FKBP12, 4 µM GFP-CRMP2A) in the presence of 12-16 µM tubulin (tubulin concentration was tested before each session to get similar tubulin dynamics).

Imaging - For fluorescence imaging, the total internal reflection (TIRF) mode of an inverted widefield microscope Nikon Eclipse Ti-E equipped with 100x HP Apo TIRF objective, H-TIRF module, LU-NV Laser Unit (all, Nikon, Tokyo, Japan), and sCMOS camera (ORCA 4.0 V2, Hamamatsu Photonics, Hamamatsu City, Japan) was used. Microtubule dynamics was visualized at the same microscope using interference reflection microscopy (Mahamdeh and Howard, 2019). Movies were acquired for 20 min with a 5 s

time difference using NIS-Elements Advanced Research software v5.21 (Laboratory Imaging, Prague, Czechia). Analysis was done in FIJI using NanoJ-Core and Multi Kymograph plugins.

***In vitro* tubulin turbidity assay**

Porcine brain tubulin (final concentration 25 µM), FLAG-tagged GFP-CRMP2A purified from HEK293T cells (final concentration 1.25 µM), and GST-FKBP12 purified from bacteria (final concentration 4.5 µM) were used for tubulin turbidity assay. To inhibit FKBP12, we used FK506 (final concentration 40 µM; InvivoGen, tlrl-fk5).

The assay was performed in 96well plates with glass bottom (Invitrogen, M33089) in a final volume of 100 µl. All reagents were mixed on ice in BRB80 buffer with 25% glycerol, 1 mM DTT, and 1 mM GTP), and the absorbance at 350 nm was measured every 15 seconds (for 1 hour, 37°C) using BioTek Cytation3.

EB3 +tip tracking assay

IMCD3 cells were transduced with lentiviral particles carrying vector pTRIP overexpressing GFP-EB3 with or without overexpression of CRMP2A/CRMP2A S27A. For FKBP12 knockdown, a second lentiviral transduction with a pGhU6-mCherry vector carrying shRNA for FKBP12 was performed. Only cells holding both vectors (with mCherry and GFP signal) were selected. For FKBP12 overexpression, cells were transduced by pTRIP EB3 with or without overexpression of FKBP12. Transduced cells were then transfected by the mCherry-CRMP2A carrying vector. Only cells holding both vectors were captured. Live cell imaging was performed using a fluorescent microscope CARV II/Nikon Ti-E at 37°C, 5% CO_2 (CFI Plan Apo VC 100X Oil, each 2s, for 1min). The data analysis was performed in FIJI software using the plugin MTrackJ. The mean velocity of the growing microtubule ends on the periphery of the cell with no contact with other cells was counted. The data are represented in the form of kymographs using the FIJI plugin MultipleKymograph.

Primary neurons cultivation, transfection, and immunocytochemistry

Primary cortical neurons from CRMP2A knock-out (CRMP2A-KO) or WT embryos (E16.5-E17.5) were plated on coverslips (12 mm No. 1.5H; 0117520 – Paul Marienfeld) pretreated with Laminin and Poly-D-lysine (2 µg/ml and 50 µg/ml respectively) and cultured in Neurobasal media supplemented with B27 supplement, glutamine, and Penicillin/Streptomycin (ThermoFisher Scientific). Neuronal transfection was done at DIV1 using Lipofectamine 2000 in OptiMEM medium (ThermoFisher Scientific). Cells were fixed at DIV3-4 using 4% PFA and cold methanol unless stated otherwise. Cells were blocked with 0.1% BSA/PBS and incubated with primary (ON, 4°C), and secondary antibodies. Cells were visualized using a confocal scanning microscope Leica SP8 (PL FLUOTAR 25x/0.75 IMM or HC PL APO CS2 63x/1.40 OIL).

For correlation analysis, intensities of 100 pixels/cell (n=5) were measured and normalized (mean subtracted and divided by SD). Pearson correlation coefficient for CRMP2A and FKBP12/Pin1 signal was calculated. Differences between correlations were calculated according to Hypothesis tests for comparing correlations (Lenhard, 2014).

Microfluidic chambers were prepared from Sylgard 184 silicone (Dow) as described previously (Maimon et al., 2021) with modification of the wells prepared (4 x 7 mm diameter; Figure 5A). Neurons were plated on the “cell body part” of the chamber and four days after plating, neurons were stained using Cholera toxin Subunit B (ThermoFisher Scientific), and the “axonal part” of the chamber was captured for 40 hours (20-minute timeframe). Videos were then analyzed using FIJI plugin MTrackJ and average velocity was quantified.

Data analysis and presentation

GraphPad Prism was used for statistical analysis and graph illustration. Welch's t-test or Mann-Whitney test was used to compare two independent groups according to the data normality unless stated otherwise. Adobe Illustrator and FIJI were used for figures preparation.

Figures

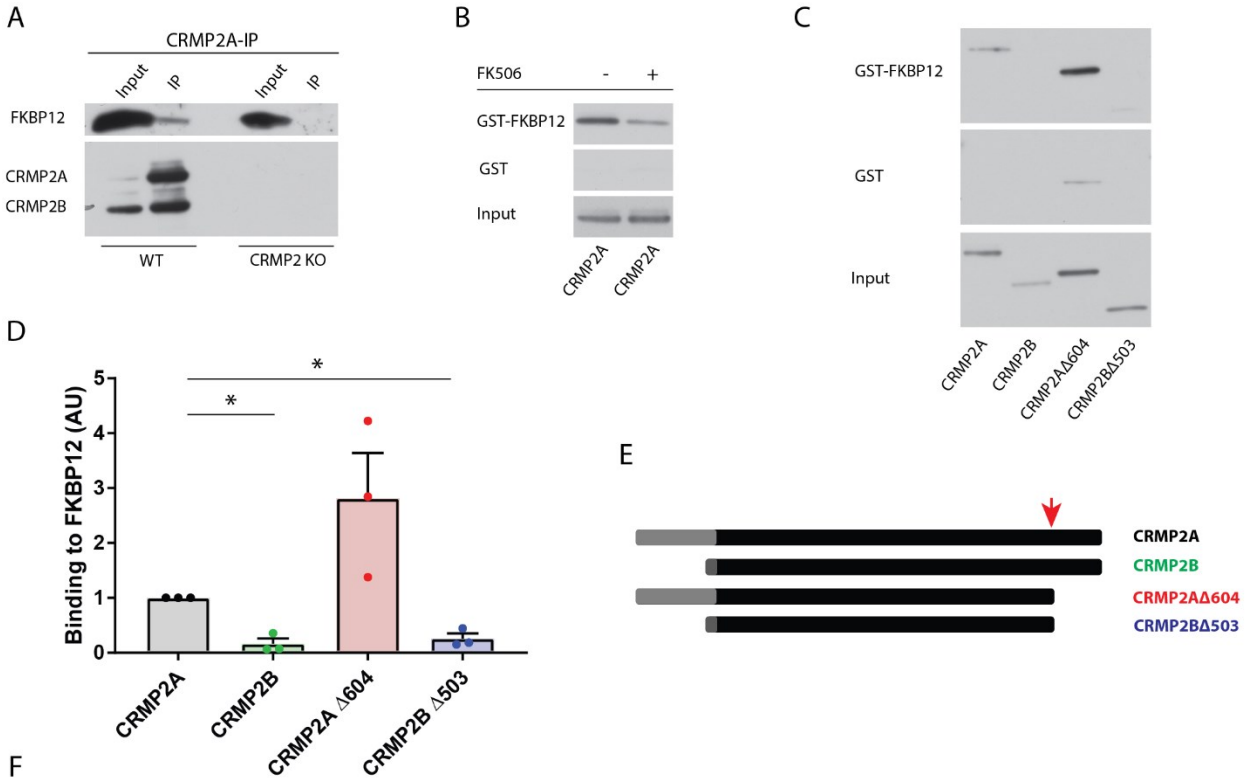

Fig. 1 – Prolyl isomerase FKBP12 interacts with CRMP2A *in vitro* and in axonal growth cones

A) FKBP12 co-immunoprecipitates with CRMP2A. Brains of young wild-type mice (WT) or CRMP2 knock-out mice (CRMP2-KO) were homogenized and used for immunoprecipitation using anti-CRMP2A antibody. FKBP12 co-immunoprecipitates with CRMP2A in WT but not in CRMP2-KO lysate which was used as a negative control. B) Pull-down of CRMP2A by GST-FKBP12 with or without FKBP12 inhibitor (FK506). The presence of FK506 reduces CRMP2A-FKBP12 interaction. C-E) FKBP12 binds preferably to CRMP2A isoform. E) Schematic representation of CRMP2A and CRMP2B isoforms and

their truncated forms (CRMP2AΔ604, CRMP2BΔ503) used for pull-down analysis (red arrow marking the deletion location, the alternative exon is shown in gray). C-D) Pull-down from HEK293T cell lysates with overexpressed CRMP2 isoforms or their truncated forms. FKBP12 binds the CRMP2A isoform more than the CRMP2B isoform regardless of its C-terminus presence. D) The quantification of the WB shown in C) normalized to the input (CRMP2A = 1 ± 0; CRMP2B = 0.16 ± 0.10; CRMP2AΔ604 = 2.82 ± 0.82; CRMP2BΔ503 = 0.26 ± 0.09; mean ± SEM, Welsch's t-test; *p < 0.05; n = 3 experiments). F) CRMP2A and FKBP12 are both abundant in primary cortical neuron cultures, particularly in axons and their growth cones (arrows). Neurons were stained at DIV4 with antibodies against FKBP12 and CRMP2A. Scale bar 10 µm.

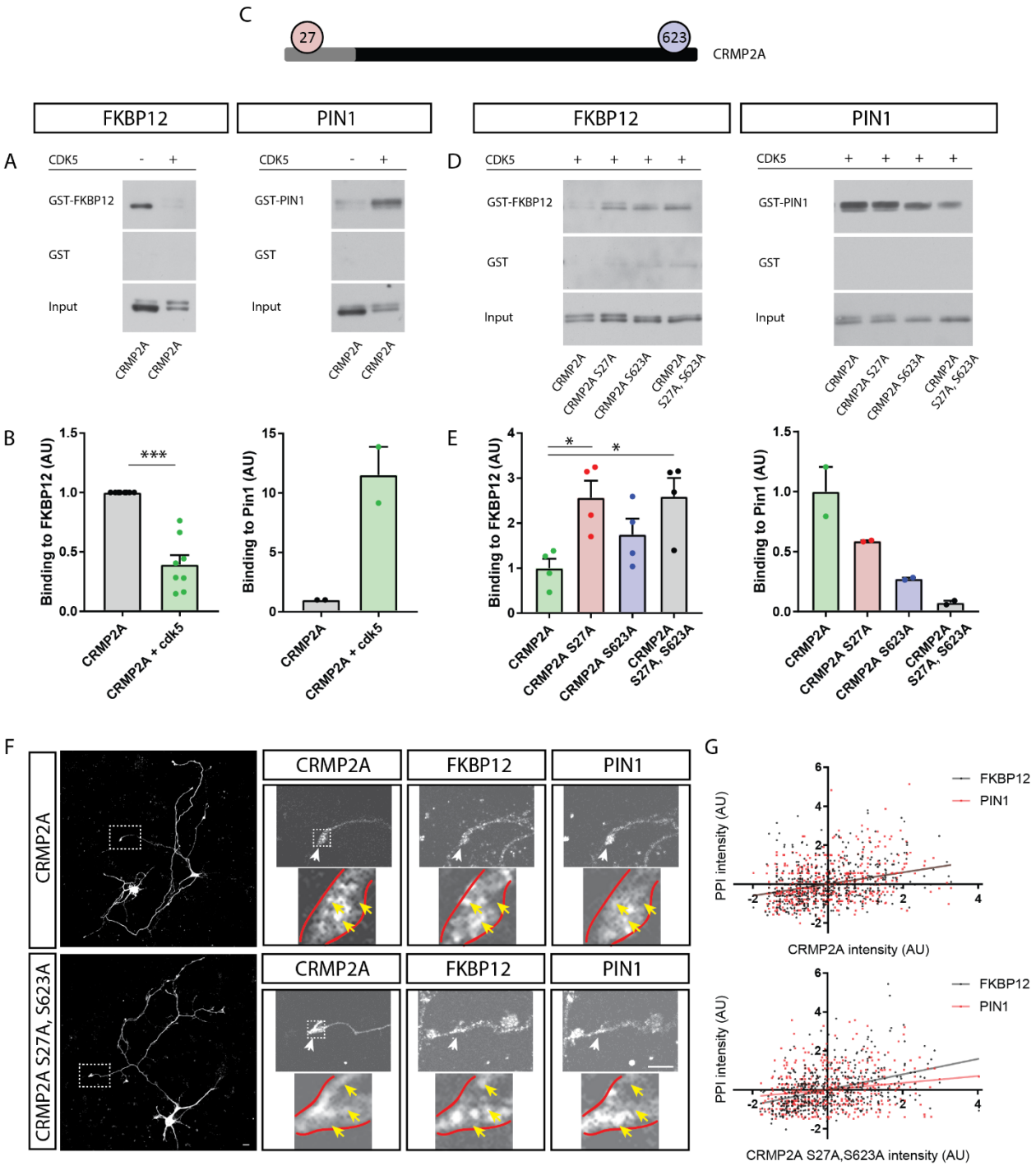

Fig. 2 FKBP12 binds preferentially unphosphorylated, while Pin1 phosphorylated CRMP2A

A-B) FKBP12 or Pin1 pull-down of Cdk5-phosphorylated CRMP2A. Phosphorylation of CRMP2A inhibits its binding to FKBP12 but promotes its binding to Pin1. A) Representative western blots and B) quantification normalized to the input (CRMP2A = 1 ± 0; CRMP2A + Cdk5 = 0.39 ± 0.08; mean ± SEM; Welsch's t-test; ***p = 0.0001; n = 8 experiments). C) Schematic representation of CRMP2A molecule and its two Cdk5 phosphorylation sites – S27 and S623. The alternative exon is shown in gray. D-E) Pull-down of CRMP2A and its dephospho-mimetic mutants (S27A, S623A, or S27A/S623A) by Pin1 or FKBP12 under high Cdk5 activity. S27A mutation increases the binding of FKBP12 to CRMP2A similarly to the double S27A, S623A mutant. S623A mutation shows a similar, non-significant trend (CRMP2A = 1 ± 0.21; CRMP2A S27A = 2.57 ± 0.38; CRMP2A S623A = 1.75 ± 0.35; CRMP2A S27A, S623A = 2.59 ± 0.41; mean + SEM; Welsch's t-test; *p < 0.05; n = 4 experiments). Pin1 preferentially binds to phosphorylated CRMP2A. F-G) Co-localization of di-dephospho-mimetic CRMP2A with FKBP12 or Pin1 in the growth cones. Primary CRMP2A-KO cortical neurons were transfected with mCherry-CRMP2A or di-dephospho-mimetic mCherry-CRMP2A S27A, S623A. F) Representative images of analyzed neurons and growth cones. Scale bar 10 µm. G) Correlations between the levels of mCherry signal (corresponding to CRMP2A or its mutated variant) and levels of FKBP12 or Pin1 (immunostained) are presented as scatter plots with linear regression. Both FKBP12 and Pin1 correlate similarly with CRMP2A, while FKBP12 correlates significantly more and Pin1 correlates significantly less with CRMP2A S27A, S623A.

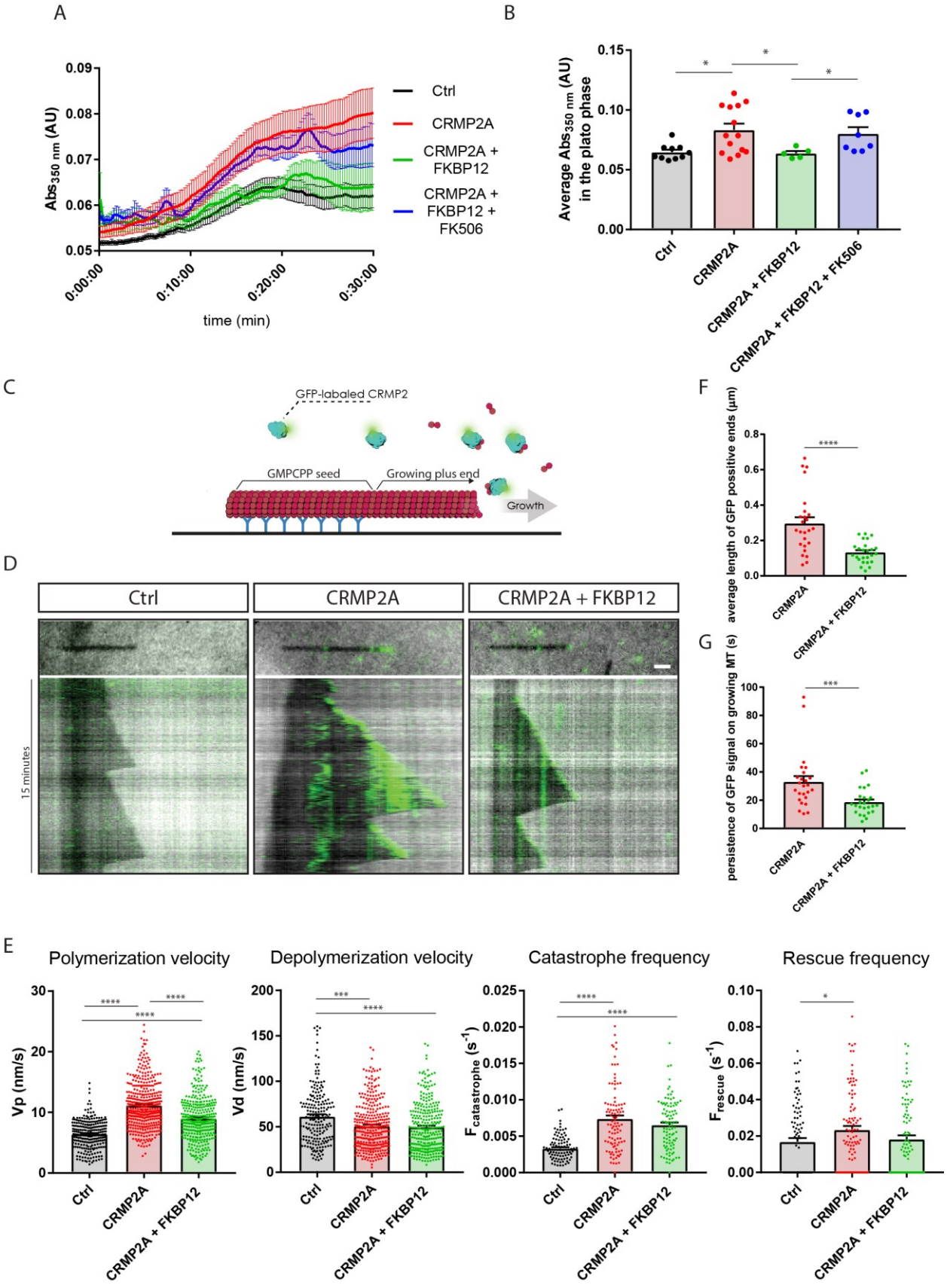

Fig. 3 FKBP12 negatively regulates microtubule dynamics *in vitro*

A-B) CRMP2A increases microtubule polymerization in tubulin turbidimetry assay *in vitro*, and FKBP12 abolishes this effect. Application of FKBP12 together with its inhibitor (FK506) rescues the CRMP2A effect on tubulin polymerization. B) Quantification of the turbidity assay, values in the plateau phase are shown (Ctrl = 0.065 ± 0.002; CRMP2A = 0.083 ± 0.005; CRMP2A + FKBP12 = 0.064 ± 0.002; CRMP2A + FKBP12 + FK506 = 0.080 ± 0.005; mean ± SEM; Mann-Whitney test; *p < 0.05; n = 10, 14, 5, 8 experiments). C-E) CRMP2A increases microtubule polymerization in *in vitro* microtubule polymerization assay, and FKBP12 abolishes this effect. C) Schematic representation of the *in vitro* microtubule polymerization assay. D) Representative kymographs demonstrating the effect of CRMP2A and FKBP12 on microtubule polymerization (dark – microtubules; green – GFP-CRMP2A). E) Quantification of the microtubule dynamics parameters. CRMP2A increases the microtubule polymerization rate, decreases the depolymerization rate, and increases the frequency of both catastrophes and rescues. FKBP12 inhibits the effect of CRMP2A mainly by reducing the polymerization rate (Polymerization velocity: ctrl = 6.45 ± 0.14; CRMP2A = 11.17 ± 0.19; CRMP2A + FKBP12 = 9.02 ± 0.19; mean ± SEM; Mann-Whitney test; *p < 0.05, ***p < 0.001, ****p < 0.0001; n = 259, 401, 350 polymerization events in 5 independent experiments; Depolymerization velocity: ctrl = 61.5 ± 2.2; CRMP2A = 51.0 ± 1.4; CRMP2A + FKBP12 = 49.7 ± 1.6; mean ± SEM; Mann-Whitney test; *p < 0.05, ***p < 0.001, ****p < 0.0001; n = 200, 326, 294 depolymerization events in 5 independent experiments; Catastrophe frequency: ctrl = 0.0033 ± 0.0002; CRMP2A = 0.0074 ± 0.0004; CRMP2A + FKBP12 = 0.0066 ± 0.0003; mean ± SEM; Mann-Whitney test; *p < 0.05, ***p < 0.001, ****p < 0.0001; n = 97, 100, 98 microtubules in 5 independent experiments; Rescue frequency: ctrl = 0.017 ± 0.002; CRMP2A = 0.023 ± 0.002; CRMP2A + FKBP12 = 0.018 ± 0.002; mean ± SEM; Mann-Whitney test; *p < 0.05, ***p < 0.001, ****p < 0.0001; n = 95, 99, 94 microtubules in 5 independent experiments). F) Quantification of average length of GFP-positive ends (CRMP2A = 0.2966 ± 0.03428 um, CRMP2A+FKBP12 = 0.1329 ± 0.01207 um; mean ± SEM; ****p<0.0001; Mann-Whitney test; n = 25 microtubules in 5 independent experiments). G) Quantification of the persistence of GFP signal on the growing microtubules (CRMP2A = 33.07 ± 3.955 s, CRMP2A+FKBP12 = 18.69 ± 1.844 s; mean ± SEM; ***p<0.001; Mann-Whitney test; n = 25 microtubules in 5 independent experiments). Scale bar 1 µm.

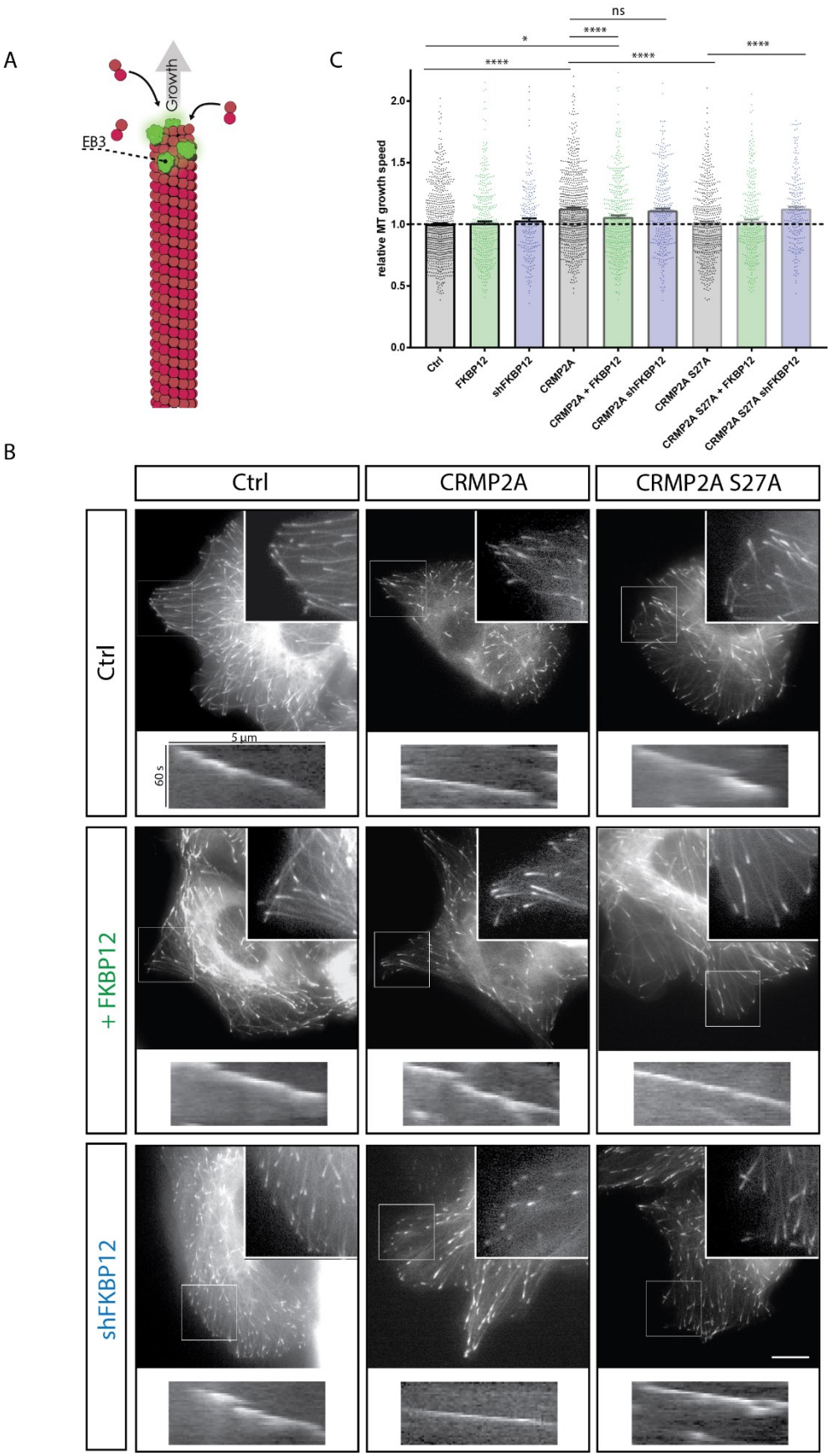

Fig. 4 FKBP12 negatively regulates microtubule growth in cells

GFP-EB3 was used to track the dynamics of growing microtubule ends in cells. A) Schematic representation of GFP-EB3 binding to growing ends of microtubules. B-C) FKBP12 inhibits CRMP2A-mediated increase of microtubule growth in IMCD3 cells. B-C) GFP-EB3 and CRMP2A or its mutated form (CRMP2A S27A) were expressed in IMCD3 cells together with a vector either expressing or silencing FKBP12. CRMP2A (but not CRMP2A S27A) expression increases the velocity of microtubule growth and this effect can be abolished by the expression of FKBP12. Knockdown of FKBP12 has no effect in combination with CRMP2A expression, but it increases microtubule growth in the presence of CRMP2A S27A. B) Representative images of analyzed cells and representative kymographs. C) Quantification of relative microtubule growth rate (ctrl = 1 ± 0.01; FKBP12 = 1.01 ± 0.02; shFKBP12 = 1.03 ± 0.02; CRMP2A = 1.13 ± 0.01; CRMP2A + FKBP12 = 1.06 ± 0.02; CRMP2A shFKBP12 = 1.11 ± 0.02; CRMP2A S27A = 1.01 ± 0.01; CRMP2A S27A + FKBP12 = 1.02 ± 0.02; CRMP2A S27A shFKBP12 = 1.12 ± 0.02; mean ± SEM; Mann-Whitney test; ns = not significantly different, **$p < 0.01$, ***$p < 0.001$, ****$p < 0.0001$; n = 761, 390, 235, 746, 462, 330, 550, 300, 235 microtubules in at least 7 independent experiments). Scale bars 10 µm.

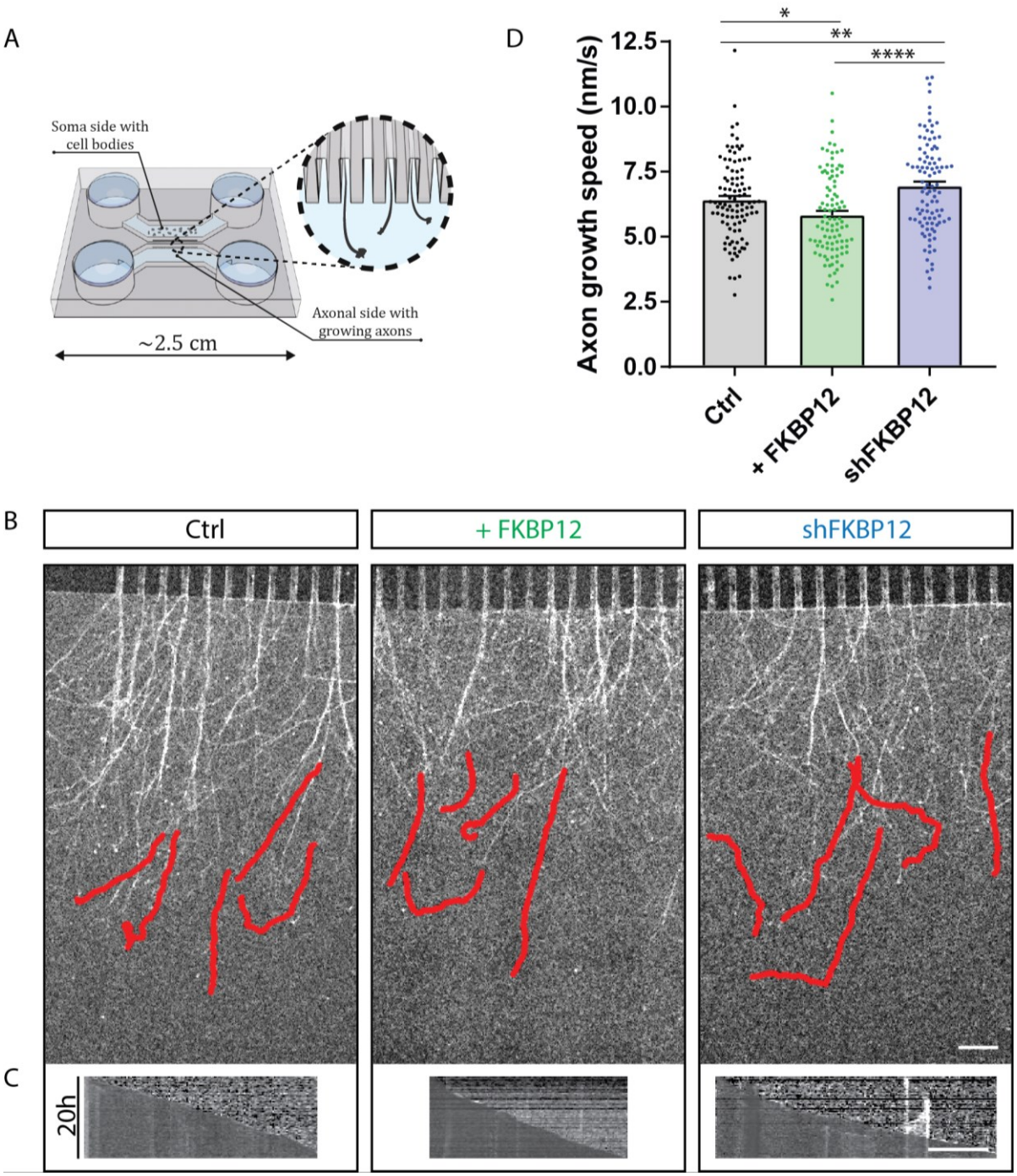

Fig. 5 FKBP12 modulates axonal growth in cultured neurons

A) Schematic representation of microfluidic chambers used in the experiments. B) Primary embryonic cortical neurons were grown in microfluidic chambers, stained using Cholera toxin Subunit B (Alexa 647), and their growth rate was analyzed. Knockdown of FKBP12 (shFKBP12) increases and expression of FKBP12 (+FKBP12) decreases the axon growth rate. B-C) Representative images with the trajectory of growing axons for 20 hours (B) and representative kymographs corresponding to the trajectories (C). D) Quantification of average axon growth rate in nm/s (ctrl = 6.41 ± 0.15 nm/s, +FKBP12 = 5.83 ± 0.16 nm/s, shFKBP12 = 6.94 ± 0.18 nm/s; mean ± SEM; Mann-Whitney test; *$p < 0.05$, **$p < 0.01$, ****$p < 0.0001$; n=100 axons in 4 independent experiments). Scale bars 100 µm, 10h.

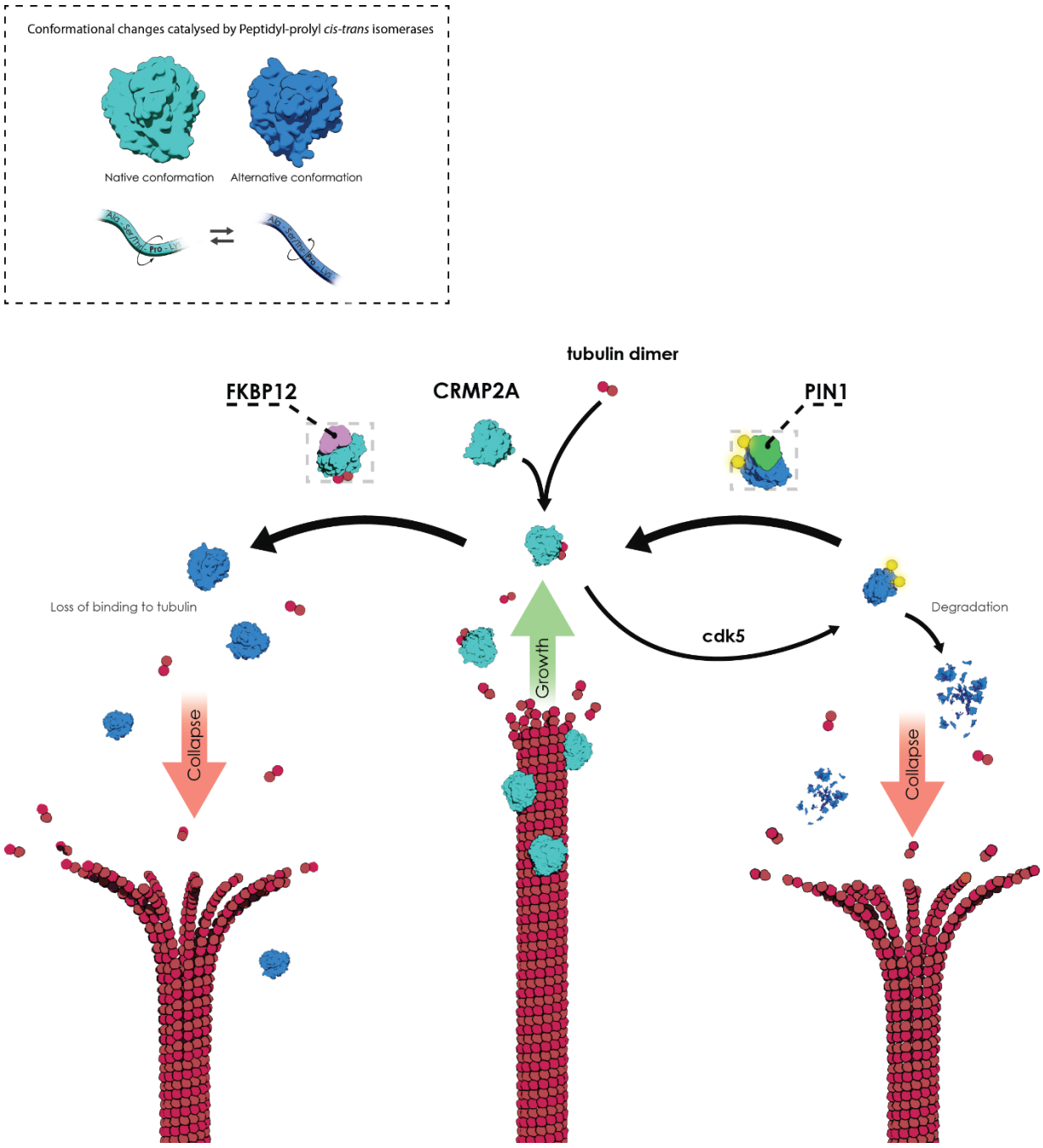

Fig. 6 Schematic representation of the model for the function of prolyl isomerases and CRMP2A on microtubules

Peptidyl-prolyl cis/trans isomerases can change the conformation of peptide bond affecting the conformation of proteins switching between native and alternative conformation (upper left corner). CRMP2A in its native conformation (light blue) binds to tubulin dimers (red) and to growing microtubules promoting microtubule growth and stability. After phosphorylation by Cdk5, CRMP2A is more prone to adopt an alternative conformation (dark blue) which is directed to proteolysis. The phosphorylated CRMP2A can be bound by prolyl isomerase Pin1 (green) which prevents degradation of phosphorylated CRMP2A and allows its return to the native conformation. Non-phosphorylated CRMP2A is bound by prolyl isomerase FKBP12 (pink) which inhibits CRMP2A by promoting the conformational change into alternative conformation and thus prevents microtubule polymerization and stabilization.

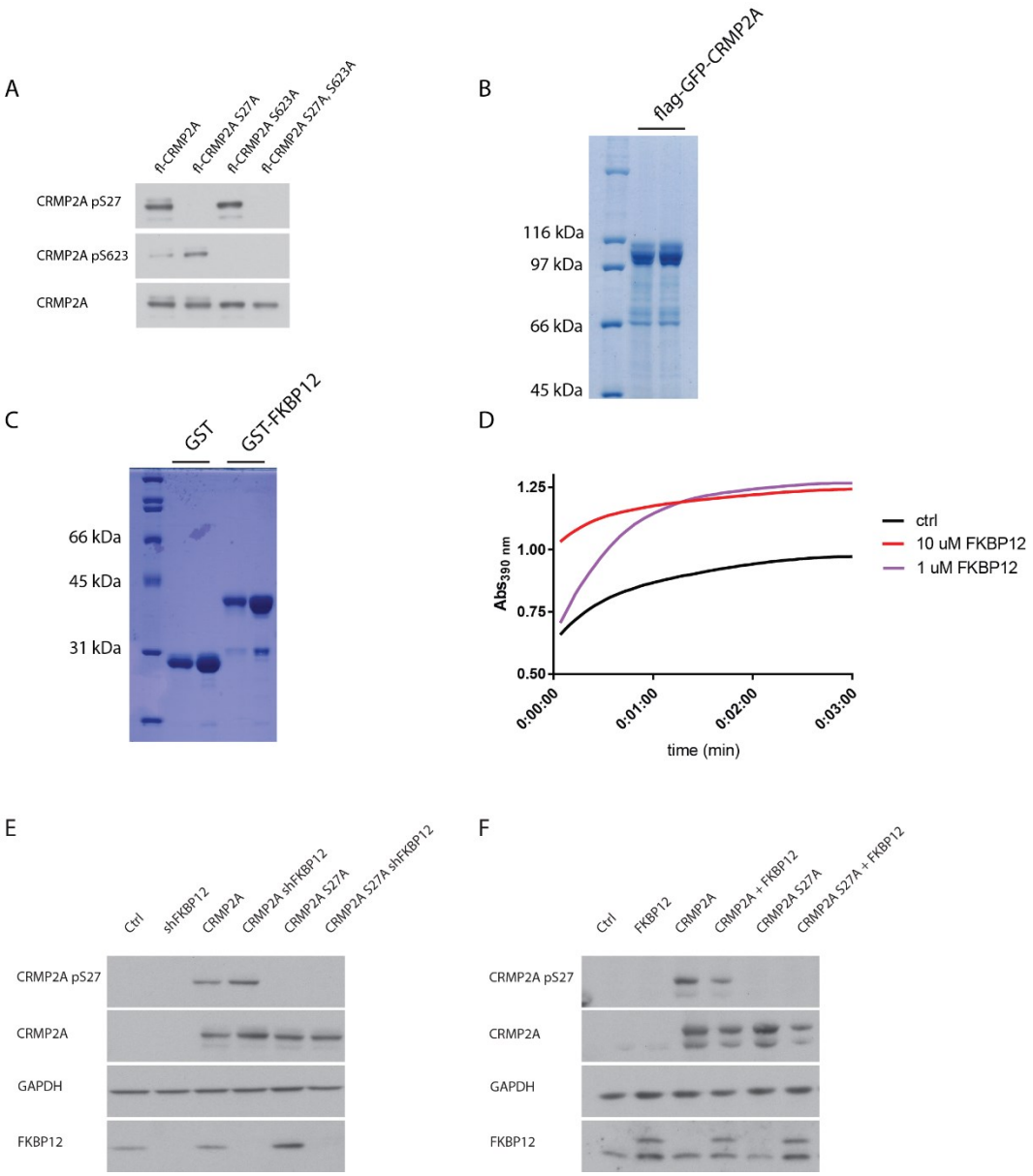

Supplementary figures

A) Dephospho-mimetic mutations used for pull-down experiments (Figure 2D-E). Dephospho-mimetic mutants are not recognized by phospho-specific antibodies while they are recognized by CRMP2A antibodies. Phospho-specific antibodies anti-CRMP2A pS27 and anti-CRMP2 pS522 (corresponding to pS623 on CRMP2A) were used.

B) SDS-PAGE gel showing purified FLAG-GFP-CRMP2A protein used for microtubule polymerization assays stained with coomassie brilliant blue.

C) SDS-PAGE gel showing purified GST-FKBP12 and GST (used as a control) used for pull-down and microtubule polymerization assays stained with coomassie brilliant blue.

D) PPI activity assay. Two different concentrations of FKBP12 (1 μM and 10 μM) were used to promote the digestion of a colorimetric substrate by chymotrypsin.

E-F) Western blots of cells used for GFP-EB3 assay, showing knockdown (E) or overexpression (F) of FKBP12 and overexpression of CRMP2A or CRMP2A S27A.

Acknowledgments

We acknowledge the Imaging Methods Core Facility at BIOCEV, supported by the MEYS CR (LM2023050 Czech-BioImaging) and IPHYS Bioimaging Facility, supported by MEYS CR (Large RI Project LM2018129 Czech-BioImaging) and ERDF (project No. CZ.02.1.01/0.0/0.0/18_046/0016045).

This work was supported by The Czech Science Foundation (GACR 16-15915S) and Charles University Grant Agency (GA UK 524218).

Author contributions

RW experiments, methods, experimental design, funding, results interpretation

JS experiment

DEC material supply, methods

JZ methods, results interpretation

PB graphic representation, methods

SB material supply

CJ material supply

MBr results interpretation, funding

ZL results interpretation, funding

MBa funding, experimental design, results interpretation

Competing interests

The authors declare no competing interests.

References

Aghdasi, B., K. Ye, A. Resnick, A. Huang, H.C. Ha, X. Guo, T.M. Dawson, V.L. Dawson, and S.H. Snyder. 2001. FKBP12, the 12-kDa FK506-binding protein, is a physiologic regulator of the cell cycle. *Proc Natl Acad Sci U S A*. 98:2425-2430.

Balastik, M., X.Z. Zhou, M. Alberich-Jorda, R. Weissova, J. Ziak, M.F. Pazyra-Murphy, K.E. Cosker, O. Machonova, I. Kozmikova, C.H. Chen, L. Pastorino, J.M. Asara, A. Cole, C. Sutherland, R.A. Segal, and K.P. Lu. 2015. Prolyl Isomerase Pin1 Regulates Axon Guidance by Stabilizing CRMP2A Selectively in Distal Axons. *Cell reports*. 13:812-828.

Blair, L.J., J.D. Baker, J.J. Sabbagh, and C.A. Dickey. 2015. The emerging role of peptidyl-prolyl isomerase chaperones in tau oligomerization, amyloid processing, and Alzheimer's disease. *J Neurochem*. 133:1-13.

Bretin, S., S. Reibel, E. Charrier, M. Maus-Moatti, N. Auvergnon, A. Thevenoux, J. Glowinski, V. Rogemond, J. Premont, J. Honnorat, and C. Gauchy. 2005. Differential expression of CRMP1, CRMP2A, CRMP2B, and CRMP5 in axons or dendrites of distinct neurons in the mouse brain. *The Journal of comparative neurology*. 486:1-17.

Caminati, G., and P. Procacci. 2020. Mounting evidence of FKBP12 implication in neurodegeneration. *Neural Regen Res*. 15:2195-2202.

Castoldi, M., and A.V. Popov. 2003. Purification of brain tubulin through two cycles of polymerization-depolymerization in a high-molarity buffer. *Protein Expr Purif*. 32:83-88.

Crews, L., R. Ruf, C. Patrick, W. Dumaop, M. Trejo-Morales, C.L. Achim, E. Rockenstein, and E. Masliah. 2011. Phosphorylation of collapsin response mediator protein-2 disrupts neuronal maturation in a model of adult neurogenesis: Implications for neurodegenerative disorders. *Mol Neurodegener*. 6.

Dilworth, D., G. Gudavicius, X. Xu, A.K.J. Boyce, C. O'Sullivan, J.J. Serpa, M. Bilenky, E.V. Petrochenko, C.H. Borchers, M. Hirst, L.A. Swayne, P. Howard, and C.J. Nelson. 2018. The prolyl isomerase FKBP25 regulates microtubule polymerization impacting cell cycle progression and genomic stability. *Nucleic acids research*. 46:2459-2478.

Fischer, G., H. Bang, and C. Mech. 1984. [Determination of enzymatic catalysis for the cis-trans-isomerization of peptide binding in proline-containing peptides]. *Biomed Biochim Acta*. 43:1101-1111.

Fukata, Y., T.J. Itoh, T. Kimura, C. Menager, T. Nishimura, T. Shiromizu, H. Watanabe, N. Inagaki, A. Iwamatsu, H. Hotani, and K. Kaibuchi. 2002. CRMP-2 binds to tubulin heterodimers to promote microtubule assembly. *Nat Cell Biol*. 4:583-591.

Gell, C., V. Bormuth, G.J. Brouhard, D.N. Cohen, S. Diez, C.T. Friel, J. Helenius, B. Nitzsche, H. Petzold, J. Ribbe, E. Schaffer, J.H. Stear, A. Trushko, V. Varga, P.O. Widlund, M. Zanic, and J. Howard. 2010. Microtubule dynamics reconstituted in vitro and imaged by single-molecule fluorescence microscopy. *Methods Cell Biol*. 95:221-245.

Gell, C., C.T. Friel, B. Borgonovo, D.N. Drechsel, A.A. Hyman, and J. Howard. 2011. Purification of tubulin from porcine brain. *Methods Mol Biol*. 777:15-28.

Gerard, M., A. Deleersnijder, J. Demeulemeester, Z. Debyser, and V. Baekelandt. 2011. Unraveling the role of peptidyl-prolyl isomerases in neurodegeneration. *Mol Neurobiol*. 44:13-27.

Gold, B.G., K. Katoh, and T. Storm-Dickerson. 1995. The immunosuppressant FK506 increases the rate of axonal regeneration in rat sciatic nerve. *J Neurosci*. 15:7509-7516.

Gold, B.G., M. Zeleny-Pooley, M.S. Wang, P. Chaturvedi, and D.M. Armistead. 1997. A nonimmunosuppressant FKBP-12 ligand increases nerve regeneration. *Exp Neurol*. 147:269-278.

Hanes, S.D. 2015. Prolyl isomerases in gene transcription. *Biochim Biophys Acta*. 1850:2017-2034.

Harper, S., and D.W. Speicher. 2011. Purification of proteins fused to glutathione S-transferase. *Methods Mol Biol*. 681:259-280.

Hellal, F., A. Hurtado, J. Ruschel, K.C. Flynn, C.J. Laskowski, M. Umlauf, L.C. Kapitein, D. Strikis, V. Lemmon, J. Bixby, C.C. Hoogenraad, and F. Bradke. 2011. Microtubule stabilization reduces scarring and causes axon regeneration after spinal cord injury. *Science*. 331:928-931.

Hoeffer, C.A., W. Tang, H. Wong, A. Santillan, R.J. Patterson, L.A. Martinez, M.V. Tejada-Simon, R. Paylor, S.L. Hamilton, and E. Klann. 2008. Removal of FKBP12 enhances mTOR-Raptor interactions, LTP, memory, and perseverative/repetitive behavior. *Neuron*. 60:832-845.

Chambraud, B., H. Belabes, V. Fontaine-Lenoir, A. Fellous, and E.E. Baulieu. 2007. The immunophilin FKBP52 specifically binds to tubulin and prevents microtubule formation. *FASEB journal : official publication of the Federation of American Societies for Experimental Biology*. 21:2787-2797.

Chambraud, B., E. Sardin, J. Giustiniani, O. Dounane, M. Schumacher, M. Goedert, and E.E. Baulieu. 2010. A role for FKBP52 in Tau protein function. *Proc Natl Acad Sci U S A*. 107:2658-2663.

Ikura, T., and N. Ito. 2013. Peptidyl-prolyl isomerase activity of FK506 binding protein 12 prevents tau peptide from aggregating. *Protein Eng Des Sel*. 26:539-546.

Jeong, J.Y., H.S. Yim, J.Y. Ryu, H.S. Lee, J.H. Lee, D.S. Seen, and S.G. Kang. 2012. One-step sequence- and ligation-independent cloning as a rapid and versatile cloning method for functional genomics studies. *Appl Environ Microbiol*. 78:5440-5443.

Jiang, L., P. Chakraborty, L. Zhang, M. Wong, S.E. Hill, C.J. Webber, J. Libera, L.J. Blair, B. Wolozin, and M. Zweckstetter. 2023. Chaperoning of specific tau structure by immunophilin FKBP12 regulates the neuronal resilience to extracellular stress. *Sci Adv*. 9:eadd9789.

Jinwal, U.K., J. Koren, 3rd, S.I. Borysov, A.B. Schmid, J.F. Abisambra, L.J. Blair, A.G. Johnson, J.R. Jones, C.L. Shults, J.C. O'Leary, 3rd, Y. Jin, J. Buchner, M.B. Cox, and C.A. Dickey. 2010. The Hsp90 cochaperone, FKBP51, increases Tau stability and polymerizes microtubules. *J Neurosci*. 30:591-599.

Kamata, T., M. Subleski, Y. Hara, N. Yuhki, H. Kung, N.G. Copeland, N.A. Jenkins, T. Yoshimura, W. Modi, and T.D. Copeland. 1998. Isolation and characterization of a bovine neural specific protein (CRMP-2) cDNA homologous to unc-33, a C. elegans gene implicated in axonal outgrowth and guidance. *Brain Res Mol Brain Res*. 54:219-236.

Khan, Z., G. Ferrari, M. Kasper, D.A. Tonge, J.P. Steiner, G.S. Hamilton, and P.R. Gordon-Weeks. 2002. The non-immunosuppressive immunophilin ligand GPI-1046 potently stimulates regenerating axon growth from adult mouse dorsal root ganglia cultured in Matrigel. *Neuroscience*. 114:601-609.

Kimura, T., K. Tsutsumi, M. Taoka, T. Saito, M. Masuda-Suzukake, K. Ishiguro, F. Plattner, T. Uchida, T. Isobe, M. Hasegawa, and S.I. Hisanaga. 2013. Isomerase Pin1 stimulates dephosphorylation of tau protein at cyclin-dependent kinase (Cdk5)-dependent Alzheimer phosphorylation sites. *J Biol Chem*. 288:7968-7977.

Lenhard, W., Lenhard, A. . 2014. Hypothesis Tests for Comparing Correlations. *Psychometrica*.

Lin, C.H., H.Y. Li, Y.C. Lee, M.J. Calkins, K.H. Lee, C.N. Yang, and P.J. Lu. 2015. Landscape of Pin1 in the cell cycle. *Exp Biol Med (Maywood)*. 240:403-408.

Lyons, W.E., E.B. George, T.M. Dawson, J.P. Steiner, and S.H. Snyder. 1994. Immunosuppressant FK506 promotes neurite outgrowth in cultures of PC12 cells and sensory ganglia. *Proc Natl Acad Sci U S A*. 91:3191-3195.

Lyons, W.E., J.P. Steiner, S.H. Snyder, and T.M. Dawson. 1995. Neuronal regeneration enhances the expression of the immunophilin FKBP-12. *J Neurosci*. 15:2985-2994.

Mahamdeh, M., and J. Howard. 2019. Implementation of Interference Reflection Microscopy for Label-free, High-speed Imaging of Microtubules. *J Vis Exp*.

Maimon, R., L. Ankol, T. Gradus Pery, T. Altman, A. Ionescu, R. Weissova, M. Ostrovsky, E. Tank, G. Alexandra, N. Shelestovich, Y. Opatowsky, A. Dori, S. Barmada, M. Balastik, and E. Perlson. 2021. A CRMP4-dependent retrograde axon-to-soma death signal in amyotrophic lateral sclerosis. *Embo J*. 40:e107586.

Mason, M.R., A.R. Lieberman, D.S. Latchman, and P.N. Anderson. 2003. FKBP12 mRNA expression is upregulated by intrinsic CNS neurons regenerating axons into peripheral nerve grafts in the brain. *Exp Neurol*. 181:181-189.

Nakamura, F., T. Ohshima, and Y. Goshima. 2020. Collapsin Response Mediator Proteins: Their Biological Functions and Pathophysiology in Neuronal Development and Regeneration. *Front Cell Neurosci*. 14:188.

Patrick, G.N., L. Zukerberg, M. Nikolic, S. de la Monte, P. Dikkes, and L.H. Tsai. 1999. Conversion of p35 to p25 deregulates Cdk5 activity and promotes neurodegeneration. *Nature*. 402:615-622.

Perrucci, G.L., A. Gowran, M. Zanobini, M.C. Capogrossi, G. Pompilio, and P. Nigro. 2015. Peptidyl-prolyl isomerases: a full cast of critical actors in cardiovascular diseases. *Cardiovasc Res*. 106:353-364.

Radomska, H.S., M. Alberich-Jordà, B. Will, D. Gonzalez, R. Delwel, and D.G. Tenen. 2012. Targeting CDK1 promotes FLT3-activated acute myeloid leukemia differentiation through C/EBPα. *Journal of Clinical Investigation*. 122:2955-2966.

Ruschel, J., F. Hellal, K.C. Flynn, S. Dupraz, D.A. Elliott, A. Tedeschi, M. Bates, C. Sliwinski, G. Brook, K. Dobrindt, M. Peitz, O. Brüstle, M.D. Norenberg, A. Blesch, N. Weidner, M.B. Bunge, J.L. Bixby, and F. Bradke. 2015. Systemic administration of epothilone B promotes axon regeneration after spinal cord injury. *Science*. 348:347-352.

Sengottuvel, V., M. Leibinger, M. Pfreimer, A. Andreadaki, and D. Fischer. 2011. Taxol Facilitates Axon Regeneration in the Mature CNS. *Journal of Neuroscience*. 31:2688-2699.

Shaw, P.E. 2007. Peptidyl-prolyl cis/trans isomerases and transcription: is there a twist in the tail? *EMBO Rep*. 8:40-45.

Schmid, F.X. 2001. Prolyl isomerases. *Adv Protein Chem*. 59:243-282.

Siekierka, J.J., S.H. Hung, M. Poe, C.S. Lin, and N.H. Sigal. 1989. A cytosolic binding protein for the immunosuppressant FK506 has peptidyl-prolyl isomerase activity but is distinct from cyclophilin. *Nature*. 341:755-757.

Steiner, J.P., T.M. Dawson, M. Fotuhi, C.E. Glatt, A.M. Snowman, N. Cohen, and S.H. Snyder. 1992. High brain densities of the immunophilin FKBP colocalized with calcineurin. *Nature*. 358:584-587.

Sugata, H., K. Matsuo, T. Nakagawa, M. Takahashi, H. Mukai, Y. Ono, K. Maeda, H. Akiyama, and T. Kawamata. 2009. A peptidyl-prolyl isomerase, FKBP12, accumulates in Alzheimer neurofibrillary tangles. *Neuroscience letters*. 459:96-99.

Suzuki, Y., S. Nakagomi, K. Namikawa, S. Kiryu-Seo, N. Inagaki, K. Kaibuchi, H. Aizawa, K. Kikuchi, and H. Kiyama. 2003. Collapsin response mediator protein-2 accelerates axon regeneration of nerve-injured motor neurons of rat. *J Neurochem*. 86:1042-1050.

Tanaka, E., T. Ho, and M.W. Kirschner. 1995. The Role of Microtubule Dynamics in Growth Cone Motility and Axonal Growth. *J Cell Biol*. 128:139-155.

Theuerkorn, M., G. Fischer, and C. Schiene-Fischer. 2011. Prolyl cis/trans isomerase signalling pathways in cancer. *Curr Opin Pharmacol*. 11:281-287.

Tong, M.M., and Y. Jiang. 2016. FK506-Binding Proteins and Their Diverse Functions. *Curr Mol Pharmacol*. 9:48-65.

Uchida, Y., T. Ohshima, Y. Sasaki, H. Suzuki, S. Yanai, N. Yamashita, F. Nakamura, K. Takei, Y. Ihara, K. Mikoshiba, P. Kolattukudy, J. Honnorat, and Y. Goshima. 2005. Semaphorin3A signalling is mediated via sequential Cdk5 and GSK3beta phosphorylation of CRMP2: implication of common phosphorylating mechanism underlying axon guidance and Alzheimer's disease. *Genes to cells : devoted to molecular & cellular mechanisms*. 10:165-179.

Yaffe, M.B., M. Schutkowski, M. Shen, X.Z. Zhou, P.T. Stukenberg, J.U. Rahfeld, J. Xu, J. Kuang, M.W. Kirschner, G. Fischer, L.C. Cantley, and K.P. Lu. 1997. Sequence-specific and phosphorylation-dependent proline isomerization: a potential mitotic regulatory mechanism. *Science*. 278:1957-1960.

Yoshida, H., A. Watanabe, and Y. Ihara. 1998. Collapsin response mediator protein-2 is associated with neurofibrillary tangles in Alzheimer's disease. *J Biol Chem*. 273:9761-9768.

Yoshimura, T., Y. Kawano, N. Arimura, S. Kawabata, A. Kikuchi, and K. Kaibuchi. 2005. GSK-3beta regulates phosphorylation of CRMP-2 and neuronal polarity. *Cell*. 120:137-149.

Zhang, H., E. Kang, Y. Wang, C. Yang, H. Yu, Q. Wang, Z. Chen, C. Zhang, K.M. Christian, H. Song, G.L. Ming, and Z. Xu. 2016. Brain-specific Crmp2 deletion leads to neuronal development deficits and behavioural impairments in mice. *Nature communications*. 7.

Zhou, X.Z., O. Kops, A. Werner, P.J. Lu, M.H. Shen, G. Stoller, G. Küllertz, M. Stark, G. Fischer, and K.P. Lu. 2000. Pin1-dependent prolyl isomerization regulates dephosphorylation of Cdc25C and tau proteins. *Mol Cell*. 6:873-883.

Zhu, L.Q., H.Y. Zheng, C.X. Peng, D. Liu, H.L. Li, Q. Wang, and J.Z. Wang. 2010. Protein Phosphatase 2A Facilitates Axonogenesis by Dephosphorylating CRMP2. *J Neurosci*. 30:3839-3848.

Ziak, J., R. Weissova, K. Jerabkova, M. Janikova, R. Maimon, T. Petrasek, B. Pukajova, M. Kleisnerova, M. Wang, M.S. Brill, P. Kasparek, X. Zhou, G. Alvarez-Bolado, R. Sedlacek, T. Misgeld, A. Stuchlik, E. Perlson, and M. Balastik. 2020. CRMP2 mediates Sema3F-dependent axon pruning and dendritic spine remodeling. *EMBO Rep*. 21:e48512.